

THIN-SKINNED DEFORMATION AND PLATE DRIVING FORCES
ASSOCIATED WITH CONVERGENT MARGINS

by

Daniel Michael Davis

A.B. Princeton University
(1978)

SUBMITTED TO THE DEPARTMENT OF
EARTH AND PLANETARY SCIENCES
IN PARTIAL FULFILLMENT
OF THE REQUIREMENTS
FOR THE DEGREE OF
DOCTOR OF PHILOSOPHY

at the

MASSACHUSETTS INSTITUTE OF TECHNOLOGY

August 2, 1983

© Massachusetts Institute of Technology 1983

Signature of Author [Handwritten Signature]
Department of Earth and Planetary Sciences

Certified by [Handwritten Signature]
Sean C. Solomon
Thesis Supervisor

Accepted by [Handwritten Signature]
Theodore R. Madden
Chairman, Department Committee

WITHDRAWN
FROM MASSACHUSETTS INSTITUTE
OF TECHNOLOGY
MIT LIBRARIES
LIBRARIES

THIN-SKINNED DEFORMATION AND PLATE DRIVING FORCES
ASSOCIATED WITH CONVERGENT MARGINS

by

Daniel Michael Davis

Submitted to the Department of Earth and Planetary Sciences
on August 2, 1983
in partial fulfillment of the requirements
for the degree of Doctor of Philosophy

ABSTRACT

This thesis consists of an investigation of several aspects of convergent margin mechanics and includes two main parts. The first of these is an extension of the model of Davis et al. (1983) for the mechanics of thin-skinned fold-and-thrust belts and accretionary wedges. The second part is an investigation of the absolute motions of the major plates since the late Cretaceous, building on the work of Davis and Solomon (1981), with the aim of applying these motions to tests of possible plate boundary forces. Both main parts of the thesis lead to constraints on the magnitude of stresses in the lithosphere near convergent margins.

I present a simple model for the overall mechanics of fold-and-thrust belts and their marine analogues, accretionary wedges. These thin-skinned, wedge-shaped loci of thrust faulting are regarded as mechanically analogous to soil being pushed by a bulldozer, at or very close to horizontal compressive failure. There exists a "critical taper", dependent upon the properties of the wedge and its base, for any wedge in compression. Any wedge with a taper which is narrower than this critical value cannot override its base without undergoing internal deformations which cause its taper to increase. The emphasis of this "Coulomb Wedge" model upon the compressive nature of thrust belts, and its accounting for the importance of topography in the deformation, have precedent in the work of Hubbert and Rubey (1959), Elliott (1976) and Chapple (1978). An important distinguishing characteristic of this model is the degree to which it permits the prediction of the overall cross-sectional shapes of active thrust belts, using parameters which are either directly observed or reasonably surmised. This model is tested in four ways. First, measured tapers of and slip-plane geometries in sand wedges in a laboratory sandbox experiment match those predicted by the theory. Second, the known thrust fault geometries, pore-fluid

pressures, and taper of the fold-and-thrust belt of western Taiwan are shown to be consistent with the theory, assuming that the wedge is roughly 20% stronger than its décollement. It is concluded that some deformation within the wedge takes the form of either fracture (as opposed to sliding), or sliding along sub-optimally aligned slip planes. Third, the wedge and décollement strengths derived for the well constrained Taiwan wedge are used to estimate the magnitudes of pore pressures in other thrust belts and accretionary wedges. These predictions are consistent with fragmentary well data. Narrow wedge tapers are invariably associated with either very high pore pressures or a very weak salt décollement. Finally, towards the back of some of the larger wedges, where wedge thickness exceeds roughly 15 km, an abrupt decrease in topographic slope is observed. This is in accord with the predicted behavior as the base of the wedge attains the depth of the brittle-ductile transition. It is concluded that deformation in many thrust belts probably involves shear stresses of nearly a kilobar at depth.

Submarine accretionary wedges differ from subaerial thrust belts in several ways. The surface slope must be higher for a submarine wedge because of the lower density contrast at the upper boundary of such a wedge; an abrupt decrease in slope of roughly 1° is, in fact, observed where the eastern Taiwan wedge emerges from the sea. Because erosion is typically less active than sedimentation on their upper surfaces, submarine wedges typically have a somewhat greater than critical taper, and thus undergo much less internal deformation away from the toe. Apparently, it is for this reason, and because sediments accreted at the toe may be incompletely lithified and highly overpressured, that submarine wedges are much less seismically active than are subaerial thrust belts. Evidence of overpressures, rapid flow of warm water from depth, and borehole collapse at the DSDP sites in the Barbados wedge are all consistent with such a model.

I present alternative velocity histories for each of the major plates since the late Cretaceous, based upon the assumption that all basal drag torques (assumed to be linear with speed) sum to zero. Such a representation has three interesting properties: 1) it permits the definition of an absolute reference frame for plate motions, while obviating the need to depend upon the assumed fixity of hotspots, 2) it is mathematically equivalent to a statement that there has been no true polar wander, and 3) in order for torques applied to the lithosphere to be properly balanced, it requires that all torques contributed by forces at plate boundaries must sum to zero. A tendency for the fastest-moving plates since the Cretaceous to be those which are subducted along a significant fraction of their boundary suggests that plate boundary forces are very important in

driving the individual plates. A trend toward globally faster plate motion is observed before roughly 50 m.y. ago. This faster motion may be related to the worldwide marine transgression at that time. A comparison of a paleomagnetically observed polar wander curve for any plate with the equivalent curve for a no-net-drag-torque reference frame serves to test the assumptions implicit in these calculations. Virtually all of the North American polar wander curve of Irving (1979) can be attributed to the motion of that continent, as opposed to true polar wander. The apparant lack of true polar wander is, at face value, at variance with the estimated imbalance in the driving torque due to ridge topography in the Pacific Ocean. There are two possible explanations for this result. Either shear stresses beneath the faster moving plates are well in excess of 1 MPa, or the net torques due to ridge-push and trench-pull approximately cancel. In that case, the net trench-pull torque would be approximately 9×10^{18} N·m, which corresponds to a mean difference, across a 100 km thick lithosphere, of 15 MPa between the stresses applied to the two plates.

The types of sediments found in the trench at a convergent margin are shown to be able to influence such diverse phenomena as underplating and back-arc spreading. Tectonic styles thus appear closely related to climate, which can play a major role in controlling erosion and sediment supply.

The results described above, as well as other observations concerning deformation near convergent margins, suggest that stresses in the overlying plate at convergent margins may be quite high; the shear stresses are probably near a kilobar.

Thesis Suprvisor: Sean C. Solomon
Title: Professor of Geophysics

ACKNOWLEDGEMENTS

Both as a graduate student and as an undergrad, I have been fortunate to be surrounded by very nice people and excellent scientists. I would particularly like to thank Sean Solomon for giving me a good example of how science should be done. Sean has been very patient with my dabbling and occasional floundering. While giving me the breathing room I needed, he was always available as a sounding board for my most recent musings. I was very fortunate to also have John Suppe to work with, putting me in the enviable position of having excellent 'advisors' to span the range of my main interests. My numerous trips to Princeton were a joy, thanks to the hospitality of Barbara, Ben, and Annie. The benefits to this thesis (and to my education) of my long-standing collaboration with John cannot be overstated.

Life in the room 521 grad student hovel was a constant reminder that graduate students, if they are lucky, learn primarily from their fellow students. Paul Okubo has proven to be a great addition to the old gang. I thank Mark Willis for introducing me to the joys of boreholes and Barbados, Rob Comer for his ideas on accretionary wedge tsunamicity and for being a constant (and to me unattainable) example of good work habits, and Jim Muller for impromptu minilectures on earthquake location and Civil War battles in which the South won moral victories. If you ever need an easygoing officemate from whom you can learn all about about planetary interiors, tidal interactions, numerical methods, continental convergence, convection or sailing, I recommend Roger Buck

very highly. Gerardo Suárez was a great help when I was first trying to make sense of the literature on plate motions. I greatly enjoyed our long discussions of the Andes, plate motions, nuclear disarmament and the Celtics.

Both Guy Consolmagno and Lynn Hall have been a big part of what has made grad school bearable and sometimes even fun. My fellow hoopsters, Roger (primal scream) Buck, Cliff Thurber, and Dave Friedman are also to be thanked for whatever remains of my sanity.

I thank Tony Dahlen for his help, particularly for clarifying problems John and I had run into with the critical taper derivation. Gerardo Suárez, David Elliott, Graham Westbrook, Donald Seely, and Jason Morgan all made good suggestions about material which wound up in the thesis. Dave Smith and Jane Bialkowski made the profiles of Peru and the Himalayas, respectively, and Casey Moore gave me the Barbados cross-section. Thea Paneth provided much-needed help with typing, and Sharon (money mogul) Feldstein and Jan (word wizard) Nattier-Barbaro provided gratefully appreciated help, both material and spiritual.

I thank Sarah for having put all of this into perspective. I haven't nearly the room to thank Léo for all of her contributions of time, effort, encouragement, patience and love. She knows.

Financial support for this thesis was provided by the National Science Foundation under grant EAR-7812936 and by the National Aeronautics and Space Administration under contract NAS 5-27339.

TABLE OF CONTENTS

	<u>page</u>
ABSTRACT	2
ACKNOWLEDGEMENTS	5
CHAPTER 1. INTRODUCTION	
1.1 Overview of convergent margins	9
1.2 Overthrust problem	14
1.3 Plate motions and driving forces	19
1.4 Stresses in the lithosphere	24
1.5 Organization of thesis	28
CHAPTER 2. WEDGE THEORY	
2.1 Introduction	34
2.2 Properties of the wedge model	38
2.3 Theoretical estimation of critical taper	41
2.4 Experimental verification with a laboratory model	51
2.5 Effects of isostasy and erosion on taper	55
2.6 Effects of fluctuations in basal friction	56
2.7 Possible complications	58
2.8 Realm of the theory	60
CHAPTER 3. MECHANICS OF THRUST BELTS	
3.1 Introduction	80
3.2 Tectonics of Taiwan	81
3.3 Comparison of the theory with Taiwan geology	88
3.4 Fault step-ups	92
3.5 Erosion and isostasy in Taiwan	96
3.6 Weak décollement	100
3.7 Himalayas and the brittle-ductile transition	104
3.8 Conclusions about thrust belts	106

CHAPTER 4. MECHANICS OF ACCRETIONARY WEDGES

4.1	A model for accretionary wedges	128
4.2	Barbados tectonics	129
4.3	Barbados as a complicated-rheology wedge	131
4.4	Barbados fault geometries	137
4.5	Leg 78A temperature data	142
4.6	Implications of high temperatures near Barbados	145
4.7	Leg 78A borehole instability	147
4.8	Barbados and the tectonics of a sediment-rich wedge	152
4.9	Other accretionary wedges.....	154
4.10	Overview of accretionary wedge mechanics.....	157

CHAPTER 5. ABSOLUTE VELOCITIES AND NET TORQUES

5.1	Introduction	182
5.2	A no-net-torque calculation	184
5.3	Calculated absolute velocities	194
5.4	Rates of spreading and marine transgressions	199
5.5	True polar wander	202
5.6	Thoughts on absolute magnitudes of plate driving forces	213
5.7	Conclusions concerning the absolute velocity models	219

CHAPTER 6. SUBDUCTION RESISTANCE AND ANOMALIES

6.1	Shallow resistance to subduction	241
6.2	Strength anomalies	242
6.3	Trench sediment balance	250
6.4	Summary	256

CHAPTER 7. DISCUSSION AND CONCLUSIONS

7.1	Thin-skinned deformation	266
7.2	Forces which drive plates	271
7.3	Lithospheric strength and stresses	276
7.4	Parting thoughts	278

REFERENCES	281
------------------	-----

BIOGRAPHICAL NOTE	306
-------------------------	-----

CHAPTER 1 INTRODUCTION

1.1 OVERVIEW OF CONVERGENT MARGINS

The theory of plate tectonics describes the surface of the earth as divided up into a small number of essentially rigid blocks, or plates (Wilson, 1965; Morgan, 1968; Le Pichon, 1968). These plates move separately from each other at relative speeds on the order of a few centimeters per year. Because there are divergent plate boundaries, at which new lithosphere is created, in order to conserve the surface area of the earth there must also be convergent boundaries at which lithosphere is destroyed.

In this thesis, I shall investigate several aspects of the mechanics of these convergent margins. Specifically, I shall present 1) a quantitative model for the mechanics of thin-skinned deformation in accretionary wedges and thrust belts, and 2) a test of plate driving forces, including those at convergence zones, against the absolute velocities of the plates since the late Cretaceous. Both of these parts of the thesis also provide constraints which shall be used to draw conclusions about the state of stress in the lithosphere. I begin with the basic background and terminology associated with these two main areas of investigation, subduction-related shallow deformation and plate driving forces.

SUBDUCTION-RELATED SHALLOW DEFORMATION

Subduction is the process by which lithosphere is

removed from the surface of the earth as it is underthrust beneath the margin of another plate and descends into the mantle. The convergence between the two plates which are colliding at a subduction zone is not entirely localized along the dipping boundary between the plates. In particular, a great deal of deformation typically takes place within the overlying plate for distances of up to several hundred kilometers from the trench. There is a great deal of variability between the styles of deformation observed at convergent margins around the world, but there are a number of features which are often observed to be associated with such regions. Figure 1.1 depicts some of these features of an idealized Cordilleran collision zone, a convergent margin possessing a series of long, linear mountain ranges. One important aspect of this collision process is the fact that shallow thrust faulting can take place in two widely separated areas (Dickinson, 1977). One of these is located immediately landward of the trench, where sediments, originating from both the deep ocean and the continent itself, are peeled off the downgoing oceanic crust and lifted from the trench, building up a large structure called an accretionary wedge. However, in some cases the sediment supply is insufficient to allow the construction of an accreted sediment wedge, and granitic continental rocks reach all the way to the trench.

A linear mountain belt can be a second locus of shallow thrusting associated with a convergent margin (Figure 1.1).

Some, but not all, such mountain belts deform in a thin-skinned manner, such that most of the deformation is confined to the part of the crust above a thrusting horizon, often stratigraphically controlled, which is called a *décollement*.

Although considerable natural variation exists among the many fold-and-thrust belts and accretionary wedges of the earth, there are several common properties which occur in cross section and which might form the basis of a successful theory of their mechanics. Chapple (1978) emphasized that fold-and-thrust belts and accretionary wedges exhibit three fundamental characteristics: (1) a basal surface of detachment or *décollement*, below which there is little deformation, and which dips toward the interior of the mountain belt, (2) large horizontal compression in the material above the basal *décollement*, and (3) a characteristic wedge shape of the deformed material, tapering toward the margin of the mountain belt (see Figure 1.2). These fundamental characteristics of thin-skinned thrusting have been the focus of much of the study of the mechanics of overthrusting, a review of which is presented in section 1.2.

PLATE DRIVING FORCES

A great deal of effort has been expended in trying to determine the mechanisms which drive the plates across the face of the earth. There is little debate that the ultimate source of the energy for these motions is the heat, both

primordial and radiogenic, which is contained within the earth. However, it is not clear how this heat is converted into plate motions. Plate recycling through sea-floor spreading and subduction can be viewed as the lithospheric expression of convection within the earth. Thermally-driven mantle convection should be expected to cause a shear stress to be resolved along the base of the lithosphere which might drive the plates. However, it is difficult to imagine a characteristic scale for such convection which would be small enough to drive individual, adjacent small plates, yet which would not be so much smaller than the largest plates that several such cells would cancel each other out.

Topography on the surface of the earth generated by thermal expansion of the lithosphere, particularly at mid-ocean ridges, produces potential energy which is thus available to drive the plates. However, plate speeds are not always very closely related to the apparent availability of such thermally-generated potential energy.

Forces generated at plate boundaries, particularly as a result of the negative bouyancy of subducted oceanic lithosphere, have been suggested as a plate-driving mechanism (McKenzie, 1969). However, small plates with a relatively large ratio of boundary length to surface area are not observed to move appreciably faster than do larger plates (McKenzie, 1969), a fact which can also be used to argue against the importance of basal drag forces (Chapple and Tullis, 1977). It would appear that the mechanism for

driving the plates is more complex than any one of these forces acting alone.

Any shallow frictional resistance to subduction will be resolved as a component of the boundary force acting upon both plates. An understanding of this subduction resistance could permit the quantification of a potentially important component in plate torque balances. It is also the compression associated with this resistance which must be overcome in order to permit back-arc spreading. Therefore, the quantification of this resisting force is important in the study of back-arc spreading and asthenospheric counterflow.

An idea which has proven useful in the study of the mechanics of plate tectonics is the concept of an 'absolute' reference frame for plate motions, with which it should become possible to draw stronger conclusions about the forces which drive those motions than would be possible by considering only relative plate motions. With the assumption that the locations of the earth's magnetic poles are (on average) fixed, paleomagnetism makes it possible to constrain changes in latitude. Another way in which to fix a suitable reference frame is to balance the torques applied to the lithosphere as a whole. This can be done by assuming that an element of the torque balance (presumably a basal drag force) depends upon absolute velocity. Given complete knowledge of plate boundaries and relative motions, such an approach to the problem permits the complete resolution of

absolute motions. However, the result is sensitive to the assumed rheology governing drag beneath the plates, as well as to the reconstruction. Finally, hotspot tracks provide a natural absolute reference frame, assuming that hotspots are truly fixed with respect to each other.

A review of published work dealing with the relationship between plate motions and their driving forces is given in section 1.3.

1.2 OVERTHRUST PROBLEM

The zones of folding and thrusting that lie along the margins of many mountain belts (for example, Figure 1.2) constitute one of the most widely recognized and best understood deformational features of mountain belts, worldwide. The Carpathians (Burchfiel, 1976), eastern Andes (Audebaud et al., 1973), Himalayan foothills (Gansser, 1964) and the Zagros Mountains (Stocklin, 1968) are well-known examples (Rodgers, 1972). The better known North American examples include the Rocky Mountain fold-and-thrust belt along the east side of the Cordilleran Mountain belt in Canada (Figure 1.2a) (Bally et al., 1966; Price, 1981), the United States (Royse et al., 1975), and Mexico (De Cserna, 1956) and the Valley-and-Ridge province in the central and southern Appalachian Mountain belt (Figure 1.2b) (Gwinn, 1970; Roeder et al., 1978; Tegland, 1978), along with its southwestern continuation as the Ouachita-Arbuckle fold-and-thrust belt (Viele, 1979). Previous models and theories of the mechanics of fold-and-

thrust belts have been based largely on observations of belts that are no longer tectonically active, simply because there has been more geological exploration of these inactive areas (for example, Figures 1.2a and 1.2b). Additional insight may be gained by examining the relatively few active fold-and-thrust belts, such as the Himalayan foothills and western Taiwan. Furthermore a great deal of geophysical information is now available for the oceanic analogue of fold-and-thrust belts, namely the accretionary wedges in front of island arcs (for example, Beck and Lehner, 1974; Seely et al., 1974; Hamilton, 1979; Nasu et al., 1979).

A variety of mechanical models have been developed for the mechanics of fold-and-thrust belts and for individual thrust sheets (for example, see Voight, 1976; McClay and Price, 1981), some of which were discussed in detail by Chapple (1978). One class of models assumes that the orogenic mass already exists. The marginal zone of thrusting is then produced through gravitational sliding or slumping of large rock sheets off the topographic high or by gravitational spreading of the orogenic mass under its own weight, much like the plastic spreading of a glacier or ice sheet. Large-scale gravity slides and slumps are known to exist (Voight, 1976), particularly in deltaic continental margins such as the U.S. Gulf Coast and the Niger Delta (Evamy et al., 1978; Mandl and Crans, 1981). The gravity sliding and spreading theories (e.g., Hubbert and Rubey, 1959; Price, 1973; and Elliott, 1976) may

satisfactorily explain structures in these settings, but they are unsatisfactory for explaining the deformation observed in ordinary fold-and-thrust belts and accretionary wedges. These gravitational mechanisms require important horizontal extension within the interior of the mountain belt, a requirement which is in conflict with observations in many mountain belts that show major compression throughout. For example, the measured shortening of the active fold-and-thrust belt of western Taiwan is substantially greater than the width of the mountain belt (Suppe, 1980a). Furthermore, the setting of fold-and-thrust belts and accretionary wedges along compressive plate boundaries easily explains the large compressive strain within these structures. In fold-and-thrust belts, both the thrust faults and the associated seismicity are readily observed. Accretionary wedges also show evidence of thrust faulting in both seismic profiles (Beck and Lehner, 1974; Hamilton, 1979) and tsunamicity (Fukao, 1979; Comer, 1982). The compressive wedge or bulldozer model produces the topographic mass as a result of thrusting, whereas in gravitational sliding, slumping, or spreading the thrusting is a response to the topographic mass.

Seismic reflection studies (e.g., Oliver et al., 1976; Brown et al., 1979; Brewer et al., 1981) have permitted the resolution of structure at great depths. COCORP studies of the Wind River Mountains (Smithson et al., 1979; Brewer and Turcotte, 1980) have traced the Wind River Thrust to a depth

of at least 24 km. Brewer and Turcotte (1980) point out that such a fault can be interpreted as a slip plane in a pervasively fractured rock mass, and its dip analyzed according to the Anderson (1951) theory of faulting. They show that the mean dip to 15 km depth ($\delta = 35^\circ$) corresponds to a coefficient of friction $\mu = \arctan (90^\circ - 2\delta) = 0.36$, ($\phi = 20^\circ$), and a shear stress along the thrust (at 10 km depth) $\tau \approx 90$ MPa. The dip of the thrust increases below 15 km. It is interesting to note that a similar analysis for the dip below 15 km (35° to 45°) leads to a lower value of $\mu = \arctan \phi$ and smaller shear stresses, in accordance with the idea that the strength of the crust decreases markedly below 15 km, possibly as a result of thermal weakening at depth.

These, or any other conclusions about the state of stress associated with overthrusting are difficult to prove. In some cases (Lambert, 1978), the orientation of paleo-stresses can be determined using microfractures. However, in general, the state of stress at depth in thrust belts is very difficult to determine even for belts which are undergoing active deformation. Solutions based upon a variety of rheological assumptions have been obtained for the stresses in overthrusts with geometries which are both idealized (Hafner, 1951; Müller and Hsü, 1980; Mandl and Shippam, 1981) and real (Müller and Hsü, 1980). A single question is at the core of many discussions of thrusting. That is, are stresses and strengths low (5-20 MPa), so that

gravitational driving forces can be important (Ramberg, 1973, 1981; Price, 1973, 1981; Elliott, 1976, 1981) or high (> 40 MPa), so that plate-tectonics-generated horizontal compression is dominant (Hubbert and Rubey, 1959; Chapple, 1978; Wiltschko, 1979; Müller and Hsü, 1980).

The primary objection to moving thrust sheets by horizontal compression has been the perception that the frictional resistance along the base would be excessive (Hubbert and Rubey, 1959; Voight, 1976). This problem was overcome in part by Hubbert and Rubey who showed that elevated pore-fluid pressures substantially reduce the frictional resistance; nevertheless, the required fluid pressures appeared to be excessively high for a general explanation of such a common phenomenon as fold-and-thrust belts. It is now apparent through the work of Chapple (1978), Davis and Suppe (1980; 1981), Stockmal and Chapple (1981), Davis et al. (1983), and Stockmal (in press) that the problem of excessive frictional resistance is largely an effect of an assumed rectangular geometry to thrust sheets and thrust belts. Once the geometry is modified to the observed slightly tapered wedge of sedimentary basins and fold-and-thrust belts, the frictional resistance of the basal décollement is no longer excessive for reasonable fluid pressures and rock properties.

The "Coulomb wedge" model of Davis et al. (1983) is presented in Chapter 2. In Chapter 3, it is used as the basis of a discussion of the mechanics of the fold-and-thrust

belt of western Taiwan, and a comparison of that mountain belt with the Zagros and the Himalaya. This analysis allows us to set constraints upon the likely magnitudes of differential stresses associated with thin-skinned deformation near convergent margins. In Chapter 4, this analysis is extended to accretionary wedges.

The study of thrust mechanics is closely related to the question of the strength of the crust. Section 1.4 gives an overview of the literature related to this question.

1.3 PLATE MOTIONS AND DRIVING FORCES

The velocities of the plates with respect to each other and to the underlying mantle have served to test a variety of simply parameterized models for the driving mechanism (e.g., McKenzie, 1969; Solomon and Sleep, 1974; Harper, 1975, 1978; Kaula, 1975; Solomon et al., 1975; Forsyth and Uyeda, 1975; Chapple and Tullis, 1977; Davis and Solomon, 1981; Jurdy, 1981; Schult and Gordon, in press).

Solomon and Sleep (1974) calculated absolute velocities of all the present-day plates for each of several models for plate driving forces. All models considered produced absolute velocities similar to those deduced from hotspot tracks (Morgan, 1971, 1981). Unfortunately, the results of these models were sufficiently similar that it was deemed impossible to differentiate among them in order to reliably determine a most likely plate tectonics driving mechanism.

Solomon et al. (1975) calculated absolute velocities and

horizontal deviatoric stresses in the plates for a wider range of driving force models. Their results suggest that ridge push and net trench pull are of roughly equal importance. In addition, a clear separation of plates into fast oceanic and slow continental crust, also noted by Minster et al. (1974), was taken to suggest that resistance to plate motion is concentrated beneath continents. Unlike absolute velocities, stresses were found to be sufficiently sensitive to the plate driving forces as to be a very useful test of alternative driving force models. It was further noted that the root-mean-squared (rms) equatorial absolute velocity is maximized for a pole which is essentially coincident with the earth's geographic pole. This was interpreted to suggest some relationship between plate motions and the earth's rotation. A similar relation between latitude and depth of ridge crests was observed by Menard and Dorman (1977).

Jurdy (1974) and Jurdy and Van der Voo (1974, 1975) reconstructed plate displacement fields for three time intervals since the early Cretaceous and determined that true polar wander during the Tertiary, if any, has been small in magnitude ($2^\circ \pm 4^\circ$) over the past 115 m.y. It was further suggested that hotspots do not provide a reliable, fixed reference frame.

Solomon et al. (1977a) combined the 55 m.y. reconstruction of Jurdy and Van der Voo (1974) with the analysis of Solomon et al. (1975), in order to determine whether or not

the conclusions drawn concerning plate driving forces based upon present-day plate distributions and motions would hold in the early Tertiary. In general, they did not. A slight latitude dependence to rms plate velocity was observed, as for the present. However, the effect was neither as marked nor as precisely centered upon the pole as for the present, suggesting that the present relation between plate motions and the earth's spin axis is purely coincidental. In addition, the separation of the lithosphere into fast (primarily oceanic) and slow (primarily continental) plates was shown not to hold.

Given the assumption that all plate boundary forces are symmetric, a lithospheric basal drag resistance located only beneath continents was found to be unlikely for two reasons. First, such a continental drag model requires a greater true polar wander than that suggested by the results of Jurdy and Van der Voo (1974). In addition, it predicts some rather unlikely-appearing plate motions, including motion, in an absolute sense, of the Farallon plate away from the trench at which it subducted beneath South America.

Forsyth and Uyeda (1975) solved for the relative magnitudes of a wide range of potential driving forces for the present-day plates, and using the hotspot framework of Morgan (1972) they minimized the torques on each of 12 plates in a least-squares sense by varying the magnitudes of weighting factors which describe the relative importance of each driving force. Their results suggest that plate motions

are essentially governed by a balance between a slab-pull force and forces resisting subduction. In addition, they suggest that a rate-dependent mantle resistance to the downgoing slab results in a plate "speed limit" of roughly 7 cm/yr.

Chapple and Tullis (1977) calculated the relative magnitudes of a suite of candidate driving forces, scaled their magnitudes to a calculated slab pull force, and reached conclusions similar to those of Forsyth and Uyeda (1975). They concluded that plate motions are dominated by a balance between a strong trench pull force and a strong rate-dependent resistance to convergence. They estimated this resistance to be 9 MPa/(cm/yr). For typical values of subduction dip and convergence rate, the shear stress is on the order of a few tens of megapascals. Drag on the base of the lithosphere was found to be negligible beneath oceans and small but significant beneath continents. Both hotspots and transform faults were found to be unimportant in the plate torque balance. Because of the tendency for the overlying plate at a subduction zone to move toward the trench (previously noted by Elsasser, 1971; Morgan, 1972; and others), Chapple and Tullis (1977) concluded that there is a net trenchward force acting on the overlying plate. This "trench suction" force must be quite strong, as it must overcome the force resisting the collision between the two plates. Jurdy (1978) pointed out that absolute motion schemes for the early Tertiary are strongly dependent upon

the assumptions made about the history of Antarctica. As the single link between the Pacific Ocean basin and the rest of the plates, the Antarctic region is the most important unresolved reconstruction problem for the Cenozoic.

Jurdy (1981) used relative motion reconstructions, paleomagnetic data, and hotspot tracks to calculate true polar wander since the early Tertiary. She concluded that there has been no significant motion of the pole relative to the lithosphere (1° - 5°), but a great deal of motion with respect to the mean hotspot reference frame.

Schult and Gordon (in press) tied the relative motions of all the major plates to a reference frame in which Africa is fixed with respect to hotspots. They found a high velocity for the Indian plate in the late Cretaceous and early Tertiary which they believe to be incompatible with a lithospheric drag force concentrated beneath continents. They conclude that oceanic and continental lithospheres are mechanically similar at depth. They state that the observed tendency for largely oceanic plates to move more rapidly than largely continental plates is not related to their drag properties. Rather, they suggest that subduction tends to be more long-lived for oceanic plates, statistically biasing them toward higher speeds.

Chapter 5 presents the reconstruction of the absolute velocities of the major plates since the Late Cretaceous of Davis and Solomon (1981), based on the assumption of no net torque due to basal drag. These absolute motions are used to

draw conclusions about the forces which drive plate motions. A comparison of plate motions predicted by the no-net-drag-torque model with paleomagnetic data is used to set constraints upon the magnitude and causes of true polar wander.

1.4 STRESSES IN THE LITHOSPHERE

The magnitudes of stresses in the earth's lithosphere is a subject of considerable debate. Direct measurements of the stress in the earth are limited to the uppermost few kilometers, so it is not clear that they can be safely extrapolated to great depth. However, down to a depth of 3 to 5 km, the maximum shear stresses measured appear to increase monotonically with depth, with no indication of a decrease in the gradient of the maximum shear stress (McGarr, 1980). Simple analyses of dips of thrust faulting in the Wind River range (Brewer and Turcotte, 1980) and normal faulting in the Basin and Range province (Zoback and Zoback, 1980) suggest shear stresses at 10 km depth of, respectively, approximately 90 MPa and roughly 70 MPa, assuming hydrostatic pore pressures. Many laboratory measurements have been made to determine rock behavior under crustal temperature and pressure conditions (Hoshino et al., 1972; Barton, 1976; Byerlee, 1978; Zoback and Zoback, 1980; McGarr, 1980), although such measurements are made at strain rates many orders of magnitude greater than for most crustal deformation (Pfiffner and Ramsay, 1982). Strengths have been surmised to

reach values well above 100 MPa (Stetsky, 1976; Kirby, 1980). Stresses at least this high have been invoked to explain both regional compensation of oceanic topography (McNutt, 1980), and shear heating on the Alpine fault (Scholz et al., 1979). Lithospheric flexure seaward of trenches may suggest such high stresses in the oceanic lithosphere (Hanks, 1979; Watts and Talwani, 1974; Turcotte et al., 1978), but modest strengths are also possible (Parsons and Molnar, 1976; Chapple and Forsyth, 1979).

Laboratory measurements of rock strength carried out at high temperatures and confining pressures have permitted the identification of thermally activated deformation mechanisms. The results of such studies suggest that while the upper part of the lithosphere is governed by relatively strong frictional behavior modified by the effects of pore pressures (Hubbert and Rubey, 1959; Healy et al., 1968), below a certain depth it becomes weaker due to the activation of time-dependent deformation mechanisms (Barton, 1976; Brace and Kohlstedt, 1980; Kirby, 1980; Caristan, 1982). The location of this brittle-ductile transition is controlled by the deformation of minerals which are common in the crust, such as quartz (Brace and Kohlstedt, 1980) and feldspar (Caristan, 1982). At the top of the mantle, deformation is thought to be controlled by the flow laws for olivine (Goetze, 1978), which is much stronger than most crustal minerals at high temperatures. As a result, the strength of the crust and uppermost mantle can be considered crudely

analogous to that of a jelly sandwich, with air above and a large vat of jelly beneath. It has been noted that earthquakes away from plate boundaries are strongly concentrated where sufficiently high stresses can be supported, namely in the two slices of "bread" (upper crust and uppermost mantle; Chen and Molnar, 1983; Molnar and Chen, 1982).

Additional factors, including frictional heating along faults (Scholz, 1980; Lachenbruch, 1980) and the possible presence of weak clays (Byerlee, 1978) as fault-gouge in faults, can greatly reduce the stresses which can be supported. The lack of an identifiable thermal anomaly associated with the San Andreas fault (Brune et al., 1969; Lachenbruch and Sass, 1973, 1980; Raleigh and Evernden, 1981) has been used to argue that average ambient shear stresses in the crust near such plate boundaries are small (less than 15 MPa). The close juxtaposition of normal and thrust faulting has led Dalmaryrac and Molnar (1981) to conclude that the average stress difference in the Andean crust is less than 50 MPa. The frequently small magnitudes of seismic stress drops for intraplate earthquakes (generally a few MPa; Richardson and Solomon, 1977), can be an argument for small shear stresses in the lithosphere, assuming total stress drop (Raleigh and Evernden, 1981).

Although there exists a great deal of evidence about the strength of the lithosphere, it has not yet been unequivocally constrained to be within any range smaller than roughly an order of magnitude. Within this thesis, an

attempt shall be made to keep an open mind on whether differential stresses in the crust are high (in excess of 100 MPa), low (10 MPa or less), or somewhere in between. Several pieces of evidence, particularly the success of the model for thrust belt mechanics presented in Chapter 2, lead to the conclusion that differential stresses of roughly 100 MPa can be supported in the middle of the continental crust near convergent margins.

1.5 ORGANIZATION OF THESIS

This thesis represents an investigation of the mechanical processes which take place at convergent margins, and how they relate to both the local geology and the driving forces of plate tectonics.

Chapter 2 presents a simple theoretical model which can be used to better understand the overall mechanics of fold-and-thrust belts and accretionary wedges. The motivation for this chapter is the same as for the work of Smoluchowski (1909), Hubbert and Rubey (1959), Elliott (1976), and Chapple (1978), all of which sought to understand what Hubbert and Rubey referred to as "the paradox of overthrusts". The work presented in Chapter 2 is almost entirely from Davis et al. (1983). It draws heavily from the insights of Chapple (1978), but differs from his work in several ways, particularly with regard to the assumed rheology, the way in which the problem is formulated, and most importantly, the degree in which the results can be

easily applied to the observed geology of fold-and-thrust belts and accretionary wedges.

Chapters 3 and 4 examine the thin-skinned mechanics of, respectively, thrust belts and submarine accretionary wedges. In Chapter 3, the subaerial mountain belt of western Taiwan is used to exemplify many aspects of thin-skinned thrusting. A few other thrust belts (the Zagros, the Himalaya, and the Salt Range of Pakistan) are briefly discussed in order to point out likely mechanical rationales for the ways in which they differ from the Taiwan example. In Chapter 4, the very well studied Barbados accretionary wedge is examined in light of the latest results from DSDP Leg 78A. Reflection seismic, downhole temperature, stratigraphic, bathymetric, fluid pressure and borehole stability data are all shown to be consistent with a conceptually simple and geologically reasonable picture of the regional mechanics. Other accretionary wedges (the Makran, Aleutian, and Japan Trench wedges) are very briefly discussed in comparison with the Barbados wedge.

Chapter 5 consists primarily of the development of a history of absolute plate motions since the late Cretaceous. This is accomplished by defining an absolute reference frame for plate motions in which all torques due to basal drag are balanced. The determination of such absolute reference frames is not new (Solomon and Sleep, 1974; Solomon et al., 1975, Jurdy and Van der Voo, 1975; and others). However, the work presented in Chapter 5 (much of which was published

by Davis and Solomon, 1981) is different in two particularly important ways. First, these results are cast in terms of velocity histories for each major plate, making it possible to discern relatively rapid changes in plate velocities and relate them to plate-boundary phenomena. Second, by comparing the apparent polar wander curve for North America predicted by a globally balance of all boundary-related torques with the observed polar wander (Irving, 1979), it is possible to draw some conclusions about the degree to which plate boundary torques may cancel out. It is thus possible to set some crude constraints upon the magnitudes of those plate boundary torques. A possible explanation is offered for the apparent lack of significant true polar wander during the Cenozoic. It is further suggested that this lack of true polar wander need not necessarily be typical of all of geological history.

Chapter 6 consists of a somewhat varied set of discussions concerning the fate of sediments at convergence zones, and the mechanical implications of their presence in the subduction process. It is suggested that the strength of shallow coupling at subduction zones and therefore the style of deformation in the overlying plate are highly sensitive to the sediment balance in the trench. The phenomenon of underplating is presented as a manifestation of the interplay between trench sediments and stresses.

Finally, Chapter 7 consists of an attempt to gather and synthesize the results of this thesis into a coherent

picture of the thin-skinned deformation associated with shallow resistance to plate convergence and the degree to which the resulting plate-boundary forces are important in controlling the motions of individual plates and the lithosphere as a whole. The results of the studies of thrust mechanics and plate driving forces are combined in order to cast some further light on the question of the magnitudes of stresses associated with convergent margins.

Figure Captions

Fig. 1.1 A schematic illustration of some tectonic elements of a hypothetical arc-trench system, with a great deal ($\approx \times 5$) of vertical exaggeration. Note the relative locations of the accretionary wedge and foreland thrust belt and their rough morphological similarity. Modified after Dickinson (1973).

Fig. 1.2 Highly simplified cross sections of two fold-and-thrust belts: (a) Canadian Rockies (after Bally et al., 1966), and (b) southern Appalachians (after Roeder et al., 1978).

Figure 1.1

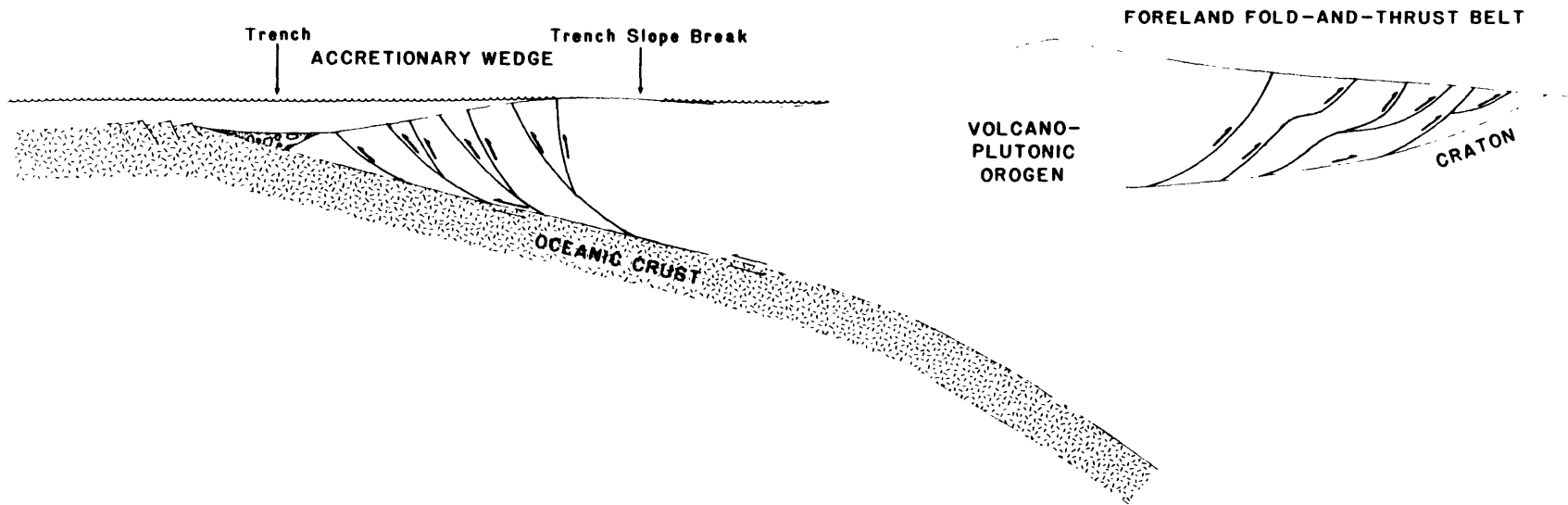
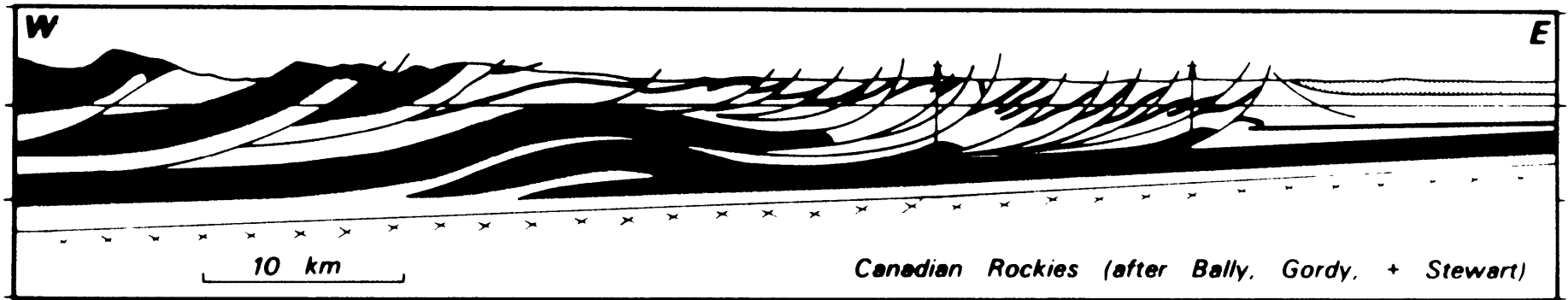
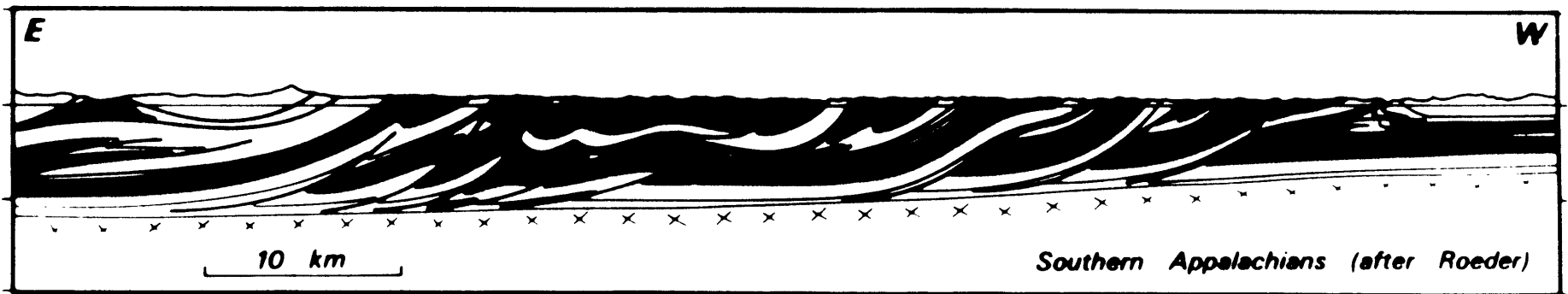


Figure 1.2

a)



b)



CHAPTER 2 WEDGE THEORY

2.1 INTRODUCTION

The overall mechanical behavior of fold-and-thrust belts and accretionary wedges along compressive plate boundaries can be considered to be analogous to that of a wedge of soil or snow in front of a moving bulldozer. The material within such a wedge deforms until a critical taper is attained, after which it slides stably, continuing to grow at constant taper as additional material is encountered at the toe. The critical taper is the shape for which the wedge is on the verge of failure under horizontal compression everywhere, including the basal décollement. A wedge which is more narrowly tapered than this critical taper will not slide when pushed but will deform internally, steepening its surface slope until the critical taper is attained. Common silicate sediments and rocks in the upper 10-15 km of the crust have pressure-dependent brittle compressive strengths which can be approximately represented by the empirical Coulomb failure criterion, modified to account for the weakening effects of pore-fluid pressure.

A simple analytical theory which predicts the critical tapers of subaerial and submarine Coulomb wedges (Davis and Suppe, 1980, 1981; Davis et al., 1983) is developed in this chapter. Its applications are confirmed quantitatively in four ways. First, in this chapter, laboratory model

experiments with dry sand are discussed. Observed tapers in the sandbox model match those predicted by the theory. Next, in Chapter 3, the known surface slope, basal dip, and pore-fluid pressures in the active fold-and-thrust belt of western Taiwan are used to determine the effective coefficient of internal friction within the wedge which is consistent with an assumed value of sliding friction on the base. The calculated excess of internal strength over basal friction suggests that although the Taiwan wedge is highly deformed by imbricate thrusting, it is not so pervasively fractured that frictional sliding is always possible on surfaces of optimum orientation. Instead, the overall internal strength apparently is controlled by frictional sliding along sub-optimally oriented planes and by the need to fracture some parts of the observed geometrically complex structure for continued deformation. Third, using calculated values of friction within and at the base of the wedge, I estimate in Chapters 3 and 4 the Hubbert-Rubey fluid-pressure ratios for a number of other active subaerial and submarine accretionary wedges based on their observed tapers, finding values everywhere in excess of hydrostatic. These predicted overpressures are reasonable in light of petroleum drilling experience in general and agree with nearby fragmentary well data in specific wedges where they are available. Finally, it is noted that the pressure-dependent Coulomb wedge theory developed here leads to the expectation that the theory

will break down if the décollement exhibits pressure-independent plastic behavior because of either temperature or rock type. The effects of this breakdown are observed in the abrupt decrease in taper where wedge thicknesses exceed about 15 km, which is the predicted depth of the brittle-plastic transition in quartz-rich rocks for typical geothermal gradients. On the basis of these successful tests of the theory, it is concluded that fold-and-thrust belts and accretionary wedges have the mechanics of bulldozer wedges in compression and that normal laboratory fracture and frictional strengths are appropriate to mountain-building processes in the upper crust, above the brittle-plastic transition.

This wedge behavior may be illustrated on the laboratory scale using a simple mechanical model (Davis, 1978). The model consists of sand contained in a bottomless box with transparent side walls that sits upon a sheet of Mylar, which in turn lies on a flat rigid base (Figure 2.1). In most sandbox deformational models, horizontal compression is induced by pushing one wall of the model. Here, the same effect is achieved by pulling the Mylar sheet upon which the sand rests; this pulls the sand against the back wall of the model, which serves as a rigid buttress. The apparatus mimics the process of plate subduction and allows large deformation with mechanical simplicity. Inhomogeneities are minimized by packing the sand evenly, and side-wall friction is greatly reduced by

coating the side walls with graphite.

A sequence of photographs of one experimental run is shown in Figure 2.2. As deformation progresses, the wedge thickens and the locus of active deformation moves away from the rigid buttress until the taper reaches its steady-state critical value. The wedge then slides stably. If sand continues to be accreted at the toe, the wedge continues to grow, maintaining its critical taper. Quantitative aspects of these experiments are discussed later in this chapter.

The wedge of homogeneous sand in the experiment is used to model fold-and-thrust belts and accretionary wedges as critically tapered deforming wedges. Such a model can only represent the gross macroscopic mechanics, and not the complex internal structural details or deformational histories of specific wedges. In the case of an accretionary wedge in front of an island arc, the bulldozer represents the lithospheric plate beneath which oceanic crust is being subducted, and in the case of a fold-and-thrust belt, it represents the inner, thicker part of the mountain range. It should also be noted that although a metal bulldozer is made of much stronger material than the material it pushes, this is not true in the Earth. Rigid, less easily deformed segments of the lithosphere are generally stronger largely because they are thicker.

2.2 PROPERTIES OF THE WEDGE MODEL

A fundamental premise of the model presented here is that rock deformation in the upper lithosphere is governed by pressure-dependent, time-independent Coulomb behavior, i.e., by brittle fracture (Paterson, 1978) or frictional sliding (Byerlee, 1978). Macroscopically, the empirical law describing both these modes of brittle behavior is the same, only differing in the numerical value of the cohesive strength S_0 and the coefficient of friction $\mu = \tan\phi$, which expresses the pressure dependence. The general Coulomb criterion for shear traction τ at failure is of the form

$$|\tau| = S_0 + \mu(\sigma_n - P_f) \quad (2.1)$$

where σ_n is the normal traction and P_f is the pore-fluid pressure (Figure 2.3).

Cohesion S_0 can be relatively unimportant in the mechanics of fold-and-thrust belts and accretionary wedges, which are composed predominantly of silicate sediments. Typical laboratory measurements of S_0 from fracture experiments on small samples of shales and sandstones range from 5 to 20 MPa (Hoshino et al., 1972). These measurements probably overestimate the cohesive strengths of in situ rock masses because they are commonly done on relatively pristine samples and because rock strength decreases with larger samples containing more flaws. At depths on the order of a few kilometers the effect of this relatively small cohesion is negligible compared to the pressure-dependent term in the failure equation. The

main effects of cohesion on wedge geometry will be observed near the toe of the wedge, where cohesion can add significantly to the total strength and produce a critical taper narrower than the corresponding cohesionless taper. Farther from the toe where the wedge is thicker the pressure-dependent term will dominate, and the critical taper will asymptotically approach the cohesionless value. For simplicity we shall temporarily ignore the effect of cohesion on toe shape in this discussion and employ instead of the cohesive relation of eq. 2.1 a non-cohesive failure law of the form

$$|\tau| = \mu \sigma_n^* \quad (2.2)$$

Here, as well as elsewhere in this discussion, an asterisk is used to denote the effective stress $\sigma_n^* = \sigma_n - P_f$.

Pore-fluid pressures P_f play a major role in the mechanics of thrust faulting (Hubbert and Rubey, 1959), and a proper accounting of their effect in both subaerial and submarine wedges requires some care. It is common in the subaerial case to assume that the water table is located at the rock surface (Figure 2.4a). In that case, the pore-water pressure is typically equal to the hydrostatic pressure for shallow depths. However, below some point whose location is stratigraphically controlled (Chapman, 1980; Gretener, 1981), it often rises well above the hydrostatic pressure, typically attaining a constant gradient somewhere in the range between the hydrostatic and the lithostatic gradient (Fertl, 1976). This gradient is

commonly described in terms of Hubbert and Rubey's dimensionless parameter λ , the ratio of pore-fluid pressure P_f to the vertical normal traction exerted by the lithostatic overburden. Although it tends to obscure the true variability of pore pressures with depth, λ is a convenient measure for use in a macroscopic model of deformation.

In many regions the water table may be located below the upper surface of the rock (Figure 2.4b). Fluid pressures are in that case reduced, and the rock will be relatively stronger. A third circumstance is that which arises in dealing with accretionary wedges: the rock surface in that case is submerged below sea level (Figure 2.4c). Rocks just below the seafloor will generally be quite weak, since the effective lithostatic pressure there always vanishes. To deal with this submarine case it is necessary to introduce a slight generalization of Hubbert and Rubey's subaerial λ , and that is done below; see eq. 2.6.

The lower limit of applicability of the present brittle wedge theory is the middle or lower crust where pressure and temperature become sufficiently high that common rocks begin to display temperature-dependent plastic behavior, deforming by motion of dislocations and other pressure-independent mechanisms. The expected effects of this brittle-plastic transition on the geometry of large wedges are discussed further at the end of this Chapter.

2.3 THEORETICAL ESTIMATION OF CRITICAL TAPER

Consider a homogeneous and isotropic wedge composed of a deformable non-cohesive Coulomb material being compressed by a push from its thick end, sliding along a rigid base (Figure 2.5). Let α be the local angle of topographic relief and β be the local dip angle of the rigid base, as shown. In the analysis of Davis et al. (1983), a system of local Cartesian coordinates is employed, having x parallel to the base in the segment of the wedge between x and $x+dx$, with z increasing upwards, and with the y -axis being the direction pointing into the page in Figure 2.5. The local thickness of the wedge, measured along the z axis, is denoted by H . In the case of a submarine wedge, the local thickness of the overlying water, measured vertically, is denoted by D .

The critical taper of such a horizontally compressive wedge is primarily controlled by the balance of forces in the x direction. Let us enumerate these forces acting on the segment of unit length along strike (i.e., in and out of the page) lying between x and $x+dx$. There is, first, a gravitational body force whose component in the x -axis direction is $-\rho g H dx dy \sin\beta$, where ρ , assumed constant, is the density of the rocks in the wedge and g is the acceleration of gravity. Second, in the case of a submarine wedge there is another force arising directly from gravity, namely the pressure of the water overburden, which has an x component equal to $-\rho_w g D dx dy \sin(\alpha+\beta)$,

where ρ_w is the density of water. For greater generality we shall consider explicitly the case of a submarine wedge in the analysis that follows. The corresponding result for the subaerial case may be recovered at any point in the argument by setting ρ_w equal to zero (or more precisely to the density of air, which is negligible). The third force, which acts on both subaerial and submarine wedges, is the frictional resistance to sliding along the basal décollement. In terms of the basal shear traction τ_b this force is $-\tau_b dx dy$, the minus sign arising because the force acts to resist sliding. Finally, let σ_x be the normal traction acting across any face perpendicular to the x axis, with compression being reckoned positive. The fourth force acting on the segment between x and $x+dx$ is then the resultant compressive push of these normal tractions acting on the two sidewalls. In contrast to the first three forces, this resultant is in the $+x$ direction, for two reasons: not only is the x face larger in area than that at $x+dx$ but, because the push is coming from a greater depth H , $\sigma_x(x,z)$ exceeds $\sigma_x(x+dx,z)$. Balancing forces requires in the limit $dx \rightarrow 0$ that

$$\rho g H \sin \beta + \rho_w g D \sin(\alpha + \beta) + \tau_b + \frac{d}{dx} \int_0^H \sigma_x dz = 0 \quad (2.3)$$

The thin-skinned nature of actual wedges permits, with very little error, the use of a small-angle approximation in which $\sin \alpha \approx \alpha$ and $\sin \beta \approx \beta$. With this substitution eq. 2.3 reduces to the simpler form

$$\rho g H \beta + \rho_w g D (\alpha + \beta) + \tau_b + \frac{d}{dx} \int_0^H \sigma_x dz = 0 \quad (2.4)$$

The vertical normal traction, σ_z , at any point in the wedge will be assumed to be solely that due to the lithostatic and hydrostatic overburden, i.e.

$$\sigma_z = \rho_w g D + \rho g (H - z) \quad (2.5)$$

This assumption also depends for its validity on a small angle approximation. By defining a dimensionless quantity

$$\lambda = \frac{P_f - \rho_w g D}{\sigma_z - \rho_w g D} \quad (2.6)$$

we may write the effective normal traction $\sigma_z^* = \sigma_z - P_f$ in the form

$$\sigma_z^* = (1 - \lambda) \rho g (H - z) \quad (2.7)$$

Eq. 2.6 provides the appropriate generalization of the pore-fluid pressure ratio $\lambda = P_f / \sigma_z$ of Hubbert and Rubey for the case of a submarine wedge. In essence, the hydrostatic pressure at the seafloor, $\rho_w g D$, has been adopted as a reference level; inspection of Figures 2.4a and 2.4c make it clear that this is a logical procedure.

The traction τ_b resisting frictional sliding on the base will be written as

$$\tau_b = \mu_b \sigma_z^* = \mu_b (1 - \lambda_b) \rho g H \quad (2.8)$$

where $\mu_b = \tan \phi_b$ is the basal coefficient of friction and λ_b is the generalized Hubbert-Rubey ratio from eq. 2.6, evaluated on the base. In introducing the basal values μ_b and λ_b we allow explicitly for the fact that the basal décollement will usually be a zone of weakness, either

because of a lower intrinsic strength or because of elevated fluid pressures. For a wedge with uniform internal properties μ and λ , we must necessarily have $(1-\lambda_b)\mu_b < (1-\lambda)\mu$ for the base of the wedge to be a throughgoing décollement.

To determine the remaining unknown quantity σ_x in the force-balance eq. 2.4 we must consider the state of stress within the wedge in more detail. A Mohr-circle representation of the stress at an arbitrary point is shown in Figure 2.6a. The maximum and minimum effective compressive stresses have been denoted by σ_1^* and σ_3^* , respectively. The local angle between the axis of maximum compressive stress and the x axis will be denoted by ψ (see Figure 2.5). Since a critically tapered wedge is assumed to be on the verge of shear failure throughout, there will be at every point two planes oriented at angles $\pm(\pi/4 - \phi/2)$ with respect to the σ_1^* axis on which the failure criterion $|\tau| = \mu\sigma_n^*$ is satisfied (Jaeger and Cook, 1969). By inspection of triangle BCD in Figure 2.6a we see that

$$\frac{1}{2}(\sigma_x^* - \sigma_z^*) = \frac{1}{2}(\sigma_1^* - \sigma_3^*)\cos 2\psi \quad (2.9)$$

whereas from triangle OAC we find

$$\frac{1}{2}(\sigma_1^* - \sigma_3^*) = \frac{1}{2}(\sigma_x^* + \sigma_z^*)\sin\phi \quad (2.10)$$

Combining these expressions we find the stress difference

$$\frac{1}{2}(\sigma_x - \sigma_z) = \frac{1}{2}(\sigma_x^* - \sigma_z^*) \text{ to be}$$

$$\frac{1}{2}(\sigma_x - \sigma_z) = \frac{\sigma_z^*}{\csc\phi \sec 2\psi - 1} = \frac{(1-\lambda)\rho g(H-z)}{\csc\phi \sec 2\psi - 1} \quad (2.11)$$

This equation, together with the corresponding result for the shear stress

$$\tau_{xz} = \frac{1}{2} (\sigma_x - \sigma_z) \tan 2\psi = \frac{(1-\lambda) \rho g (H-z) \tan 2\psi}{\csc \phi \sec 2\psi - 1} \quad (2.12)$$

completely define the state of plane stress within a non-cohesive critical Coulomb wedge in terms of a single parameter, the stress orientation angle ψ .

Upon combining equations 2.5 and 2.11 we are now able to write the integral appearing in the force balance equation 2.4 in the form

$$\int_0^H \sigma_x dz = \rho_w g D H + \frac{1}{2} \rho g H^2 + 2 \rho g \int_0^H \frac{(1-\lambda)(H-z)}{\csc \phi \sec 2\psi - 1} dz \quad (2.13)$$

Invoking the small-angle approximation once again we set

$$dH/dx = -(\alpha + \beta) \quad (2.14)$$

$$dD/dx = \alpha \quad (2.15)$$

so that

$$\begin{aligned} \frac{d}{dx} \int_0^H \sigma_x dz = & \rho_w g H \alpha - \rho_w g D (\alpha + \beta) - \rho g H (\alpha + \beta) \\ & - 2 \rho g (\alpha + \beta) \int_0^H \frac{(1-\lambda)}{\csc \phi \sec 2\psi - 1} dz \end{aligned} \quad (2.16)$$

In writing eq. 2.16 we have assumed that all of λ , ϕ and ψ are independent of x , but they may all in general still depend upon depth z . For simplicity, however, we shall henceforth consider both λ and ϕ to be strictly constant, regarding them as the averaged or effective values for the wedge as a whole. Even in a wedge with uniform properties, the angle ψ will vary appreciably with depth, particularly

if $\lambda_b \approx \lambda$ and $\mu_b \approx \mu$.

For convenience, after removing the factor of $(1-\lambda)$ from under the integral sign in eq. 2.16, let us define a dimensionless quantity

$$K = 2H^{-1} \int_0^H \frac{dz}{\csc\phi \sec 2\psi(z) - 1} \quad (2.17)$$

When eqs. 2.8 and 2.16 are substituted into eq. 2.4, we find the theoretical critical taper $\alpha+\beta$ of a noncohesive Coulomb wedge to be

$$\alpha+\beta = \frac{(1-\lambda_b)\mu_b + (1-\rho_w/\rho)\beta}{(1-\rho_w/\rho) + (1-\lambda)K} \quad (2.18)$$

This equation contains no explicit dependence on x , so that in the small-angle approximation, wedge with uniform properties and a planar base should have a constant surface slope. Note, in addition, that in the limit $\lambda_b \rightarrow \lambda \rightarrow 1$, eq. 2.18 reduces to $\alpha \rightarrow 0$, which is the expected result for a wedge composed of material having negligible strength. For future reference, let us note that eq. 2.18 defines a linear relationship between α and β of the form

$$\alpha + R\beta = F \quad (2.19)$$

where

$$R = \frac{(1-\lambda)K}{(1-\rho_w/\rho) + (1-\lambda)K} \quad (2.20)$$

$$F = \frac{(1-\lambda_b)\mu_b}{(1-\rho_w/\rho) + (1-\lambda)K} \quad (2.21)$$

To determine the quantity K exactly we must know the angle $\psi(z)$ at every depth in the wedge $0 < z < H$ and this cannot be found entirely analytically. It is possible

(Dahlen et al., 1982) for $\psi(z)$ to be found numerically by a very straightforward and rapid procedure, in both the case of a non-cohesive wedge as well as one with a finite cohesion S_0 . In this chapter, it is sufficient to develop instead a simple analytical approximation to K , which has been tested extensively and found to be extremely accurate. To develop this approximation we shall, for the moment, assume that $\lambda_b = \lambda$; the wedge existence condition is in that case simply $\mu_b < \mu$ and the critical taper equation (eq. 2.18) reduces to

$$\alpha + \beta = \frac{(1-\lambda)\mu_b + (1-\rho_w/\rho)\beta}{(1-\rho_w/\rho) + (1-\lambda)K} \quad (2.22)$$

Note that for a subaerial wedge, $\rho_w = \rho_{\text{air}} = 0$. If there is any cohesion whatsoever, permitting nonzero stresses at the top of the wedge, then σ there must be parallel to the local topography so that $\psi_t = \psi(H) = \alpha + \beta$. In the small-angle approximation the integrand in eq. 2.17 near the top of the wedge can thus be replaced by

$$\frac{1}{\csc\phi \sec 2\psi_t - 1} = \frac{\sin\phi}{1 - \sin\phi} \quad (2.23)$$

The angle $\psi_b = \psi(0)$ near the base of the wedge can be found from the specification that frictional sliding governed by a coefficient of friction μ_b is occurring there; a Mohr-circle representation of the basal stress state in the case $\lambda_b = \lambda$ and $\mu_b < \mu$ is shown in Figure 2.6b. By applying the law of sines to the triangles OAC and OBC, with $S_0 = 0$, we have

$$\frac{\sin \phi}{1} = \frac{\frac{1}{2}(\sigma_1^* - \sigma_3^*)}{\frac{1}{2}(\sigma_1^* + \sigma_3^*)} = \frac{\sin \phi_b}{\sin[\pi - 2\psi_b - \phi_b]}$$

$$\frac{\sin \phi_b}{\sin \phi} = \cos \left[\frac{\pi}{2} - 2\psi_b - \phi_b \right]$$

or (2.24)

$$\psi_b = \frac{\pi}{4} - \frac{\phi_b}{2} - \frac{1}{2} \arccos \left(\frac{\sin \phi_b}{\sin \phi} \right)$$

Simplifying terms and using a trigonometric angle-sum relation, we have

$$\cos 2\psi_b = \cos\left(\frac{\pi}{2} - \phi_b\right) \left(\frac{\sin \phi_b}{\sin \phi}\right) + \sin\left(\frac{\pi}{2} - \phi_b\right) \sin\left[\arccos\left(\frac{\sin \phi_b}{\sin \phi}\right)\right]$$

$$\sec 2\psi_b = \frac{\sin \phi}{\sin^2 \phi_b + \cos \phi_b (\sin^2 \phi - \sin^2 \phi_b)^{1/2}} \quad (2.25)$$

$$\frac{1}{\csc \phi \sec 2\psi_b - 1} = \frac{\sin^2 \phi_b + \cos \phi_b (\sin^2 \phi - \sin^2 \phi_b)^{1/2}}{\cos^2 \phi_b - \cos \phi_b (\sin^2 \phi - \sin^2 \phi_b)^{1/2}} \quad (2.26)$$

In the limiting case $\phi_b \rightarrow \phi$

$$\frac{1}{\csc \phi \sec 2\psi_b - 1} \rightarrow \tan^2 \phi_b \quad (2.27)$$

and if the basal layer is very weak, i.e. $\phi_b \ll \phi$,

$$\frac{1}{\csc \phi \sec 2\psi_b - 1} = \frac{\sin \phi}{1 - \sin \phi} \quad (2.28)$$

To obtain an approximate expression for K, we approximate the integrand in the interval $0 < z < H$ by a linear function passing through the two endpoints (eqs. 2.23 and 2.26). This leads to

$$K \approx \frac{\sin\phi}{1-\sin\phi} + \frac{\sin^2\phi_b + \cos\phi_b(\sin^2\phi - \sin^2\phi_b)^{1/2}}{\cos^2\phi_b - \cos\phi_b(\sin^2\phi - \sin^2\phi_b)^{1/2}} \quad (2.29)$$

Eq. 2.29, together with eq. 2.22, can be used to find the theoretical critical taper $\alpha+\beta$ of an actively deforming Coulomb wedge with prescribed physical properties μ , μ_b and $\lambda_b = \lambda$. The nature of the variation of K with μ and μ_b is illustrated in Figure 2.7. An increase in basal friction increases the critical taper because of the factor μ_b in the numerator of eq. (2.22), but an increase in the effective internal friction leads to a decrease in the critical taper since K is an increasing function of μ for fixed μ_b . An internally stronger wedge can be narrower and still undergo stable sliding without deforming. In order to obtain an approximation valid in the case $\lambda_b \neq \lambda$, it becomes necessary to replace ϕ_b in eq. 2.29 by the function $\arctan [\phi_b(1-\lambda_b)/(1-\lambda)]$. In all of the specific comparisons with laboratory and field observations considered below we have in fact assumed that $\lambda_b = \lambda$, so that the simpler forms (eqs. 2.22 and 2.29) are pertinent.

Before considering any applications of the critical taper formulae (eqs. 2.22 and 2.29) it is of interest to point out another more fundamental form of the force balance in a critical wedge, obtained by inserting eqs. 2.16 and 2.17 into eq. 2.4. This leads to a formula for the basal shear traction τ_b , namely

$$\tau_b = (\rho - \rho_w)gH\alpha + (1-\lambda)K\rho gH(\alpha+\beta) \quad (2.30)$$

This equation shows that the frictional sliding resistance on the base is counteracted by two terms, both of which may be thought of as driving forces responsible for the tectonic deformation and overthrusting. The first term is due to gravity acting on the sloping top surface of the wedge, and is the same as that which causes a glacier to slide in the direction of its surface slope regardless of the attitude of its bed. This term has been discussed in the context of gravity sliding or spreading models of overthrust tectonics by Elliott (1976). The effective density $\rho - \rho_w$ appears naturally in eq. 2.30 in the case of a submarine wedge, as expected on intuitive grounds. The second term depends on the taper $\alpha + \beta$, and is a consequence of the horizontally compressive push assumed to be acting from the rear of the wedge. For typical silicate sedimentary accretionary wedges with geologically reasonable values of μ , μ_b and $\lambda = \lambda_b$, this second term is several times larger than the first. This implies that basal shear tractions in compressive, critically tapered wedges are correspondingly larger than those estimated by Elliott (1976).

At this point in our discussion it is also appropriate to indicate the relationship between our analysis and the well-known Hubbert and Rubey (1959) analysis of the maximum possible lengths of thrust sheets. To illustrate the effect of fluid pressure on thrust faulting, they computed the maximum length of a rectangular body ($\alpha = -\beta$), of a given

thickness, that can be pushed along a basal decollement without undergoing internal Coulomb failure. Their analysis is appropriate to the immediate vicinity of the toe of a deforming wedge, where flat-lying sediments are being accreted. A thrust sheet longer than the Hubbert-Rubey maximum deforms by thrusting and thickening towards its rear until its geometry is that of a critically tapered wedge. The once perplexing mechanical problems posed by the existence of large-scale thrust sheets and fold-and-thrust belts are, in a sense, an artifact of imposing a fixed rectangular geometry; this point has also been emphasized by Chapple (1978). Whereas Hubbert and Rubey calculated the maximum length overthrust attainable without a taper, Coulomb wedge theory makes it possible to calculate the critical taper required for the emplacement of a thrust sheet of any length (Figure 2.8).

2.4 EXPERIMENTAL VERIFICATION WITH A LABORATORY MODEL

In the sandbox experiment described above (Figures 2.1 and 2.2) the sand was dry ($\lambda=0$), therefore the equation for the critical taper (eq. 2.22) reduces to

$$\alpha + \beta = \frac{\mu_b + \beta}{1 + K} \quad (2.31)$$

Loosely packed dry sand is a Coulomb material exhibiting negligible cohesion and an angle of internal friction near $\phi = 30^\circ$, corresponding to $\mu = 0.58$ (Lambe and Whitman, 1979). The coefficient of friction of sand on Mylar was measured to be $\mu_b = 0.30$ by experimentally observing the

inclination required to initiate gravitational sliding of a confined cylinder of sand resting on a Mylar surface. From equation 2.29 we find the value of K corresponding to $\mu = 0.58$ and $\mu_b = 0.30$ to be $K = 1.92$. The relation between α and β predicted by the theory is then

$$\alpha = 5.9^\circ - 0.66\beta \quad (2.32)$$

This prediction is confirmed by the experimentally determined result that (Figure 2.9)

$$\alpha = (5.7^\circ \pm 0.2^\circ) - (0.66 \pm 0.14)\beta \quad (2.33)$$

Experiments using graphite and sandpaper on the base produced substantially smaller and larger tapers (Davis, 1978; Goldberg, 1982), which is also in accord with the theory.

By examining triangle OAC in Figure 2.6 (a or b), we see that the preferred orientations of Coulomb fractures or slip planes should be inclined to the direction of the maximum compressive stress, σ_1 , by an angle θ given by the simple relation

$$\theta = \frac{\pi}{4} - \frac{\phi}{2} \quad (2.34)$$

Thus, the takeoff angle of a fault along the basal décollement is inclined to the décollement by the sum of this angle plus the inclination ψ_b of the σ_1 direction into the wedge (Figure 2.10). The absolute value of ψ_b is given by eq. 2.24. Assuming that $\phi = 30^\circ$ and $\phi_b = \tan \mu_b = 16.8^\circ$ (see above), we find that ψ_b should be 9.3° .

The predominance of forward thrusting in fold-and-thrust belts (see Figure 1.2) is probably related to the

difference in takeoff angles between forward and backward verging thrust faults. A backward verging thrust should step up from the décollement at an angle $\delta_b' = \theta + \psi$, which is considerably steeper than a forward (oceanward) verging thrust, which should step up at an angle $\delta_b = \theta - \psi$ (Figure 2.10). A shallow dipping thrust (and thus a forward, oceanward verging one) is probably favored for two reasons. First, a thrust with a shallow dip requires a smaller increase in potential energy for a given amount of convergence. In addition, a shallower dipping thrust is more likely to ride for more of its length along stratigraphically controlled planes of weakness, since the overall dip of the thrust is closer to bedding.

The sand in the apparatus is mechanically isotropic (the marker beds are identical to the rest of the sand, except for color). Therefore, it is not surprising that most of the deformation in the sandbox takes place in horst-like pairs of forward and backward vergent thrusts. Note the lack of resemblance between deformation in the sandbox (Figure 2.2) and in mountain belts (Figure 1.2).

It is easily seen (Figure 2.2) that forward verging sand-faults are, as expected, more shallowly dipping than their backward verging counterparts. Measurements were made of the overall dips of the most reliably measured 26 forward and 18 backward thrusts occurring during 12 runs of the sandbox apparatus under a variety of starting conditions. The dips averaged, respectively, roughly 22°

and 38° . These two data can be used to invert for an independent estimate of the magnitudes of the two determining parameters, ϕ and ψ_b . Note that the angle θ (eq. 2.34) should be equal to the average of the dips of the forward and backward slip planes, $\theta = 1/2 (\delta_b + \delta_b')$. Thus $\theta \approx 1/2 (22^\circ + 38^\circ)$, or 30° , and $\psi_b \approx 1/2 (38^\circ - 22^\circ)$, or 8° . Thus, eq. 2.34 yields an internal friction angle $\phi \approx 30^\circ$, in perfect agreement with the value assumed above.

We assume for simplicity that the angle ψ between the base of the wedge and the σ_1 direction within the mass of the sand above varies linearly with distance above the base of the sand. Thus, we approximate the mean value of ψ in the wedge by $\bar{\psi} = 1/2 (\psi_b + \alpha + \beta)$. Using the results of eq. 2.24, we have

$$\bar{\psi} = \frac{\pi}{8} - \frac{\phi_b}{4} - \frac{1}{4} \arccos \left(\frac{\sin \phi_b}{\sin \phi} \right) + \frac{1}{2}(\alpha + \beta) \quad (2.35)$$

For the experiment described above, with $\beta = 3^\circ$, and thus (eq. 2.32) $\alpha = 3.9^\circ$, this yields $\bar{\psi} \approx 8.1^\circ$, somewhat fortuitously close to the value determined above based upon observed fault step-ups in the sandbox experiment.

Neither eq. 2.18 nor eq. 2.29 contains any length scale; therefore the theory for non-cohesive Coulomb wedges is inherently scale-independent. The success of the theory in describing the behavior of our controlled laboratory model encourages us to consider applications to more complicated geological cases, despite the fact that they are many orders of magnitude larger.

2.5 EFFECTS OF ISOSTASY AND EROSION ON TAPER

Isostatic adjustment in response to the overburden that is added by growth of the wedge (Jordan, 1981; Beaumont, 1981) can result in some degree of reinitiation of deformation within the wedge. The greater stacking of thrust sheets toward the back of the wedge will tend to result in a greater degree of downward isostatic adjustment there than in the front. This results in an increase $\delta\beta$ in the dip of the basal décollement. Because total wedge taper is conserved in the isostatic process, i.e., $\delta\alpha + \delta\beta = 0$, the topographic slope α is correspondingly reduced.

The critical taper equation (eq. 2.19) shows that the criticality of a wedge depends on how its taper is partitioned between topographic slope α and basement dip β . Because the coefficient R given by eq. 2.20 is always less than one for rocks which are denser than water, each degree of α in the wedge taper is less effective in attaining critical taper than is a degree of β . Therefore, the exchange of α for β during isostatic adjustment causes the wedge to become subcritical and encourages renewed deformation within the wedge until a new critical taper is attained (Figure 2.11a).

Erosion also acts to induce deformation within the wedge by reducing the topographic slope while leaving the décollement dip unaltered, thus producing a subcritical taper (Figure 2.11a). In an active fold-and-thrust belt, the processes of erosion and internal deformation should be

consistently occurring at rates sufficient to counteract each other, as they are in western Taiwan (Suppe, 1981).

Erosion at the upper wedge surface is not likely to be important in a submerged accretionary wedge. Accretion at the front of the wedge should in that case be the major source of continued wedge deformation. The addition of extra mass at the front of an already critical wedge must result in a taper-preserving series of deformations, which enlarge the wedge by propagating toward the back. The addition of sediments on top of the wedge may make it supercritical. For these reasons, in addition to any differences in slip rates and rock strengths, the kinematics of subaerial and submarine wedges should be substantially different.

2.6 EFFECTS OF FLUCTUATIONS IN BASAL FRICTION

In the preceding discussion we have ignored possible time variations in the physical properties of either the wedge (μ and λ) or the décollement (μ_b and λ_b). Time variation in basal shear traction is most likely in long-lived, slowly accreting submarine wedges which have a high rate of subduction of the underlying oceanic plate. This could result in relatively rapid changes in the types of sediment fed into the trench. It is less likely in steady-state subaerial wedges. The complex nature of the thermal, geochemical, and mechanical factors which control fluid pressures (Fertl, 1976; Moore and von Huene, 1980), makes it difficult to characterize the circumstances under

which they might change in a manner likely to affect wedge mechanics.

Consider a submarine wedge initially at critical taper. If this wedge experiences a drop in basal friction, perhaps by encountering a stratigraphic change in décollement material, the critical taper will decrease and the previously critical wedge now will be at supercritical taper (Figure 2.11b). In contrast, if the wedge experiences a modest increase in basal friction, the critical taper will increase and the now subcritical wedge will deform until the new critical taper is attained (Figure 2.11b). If the new basal material has properties such that $(1-\lambda_b)\mu_b > (1-\lambda)\mu$, it cannot form a décollement, and a new décollement must form higher within the existing wedge. Under these conditions the wedge undergoes tectonic erosion along its base.

We might expect, from the above considerations, to find some submarine wedges that are at supercritical taper, recording a past period of higher basal friction. If a wedge is currently supercritical, the fluid-pressure ratio $\lambda = \lambda_b$ which we infer from its taper will be an underestimate. Oceanic sediments can be subducted beneath a supercritical wedge without offscraping and accretion. We might also expect, from the above considerations, to find some submarine wedges that are undergoing subduction-erosion or loss of material from their base because of a recent increase in basal friction above the value

$\mu_b = \mu(1-\lambda)/(1-\lambda_b)$. Non-accreting and negatively accreting wedges are being increasingly recognized along plate margins (for example, von Huene et al., 1980a; Aubouin et al., 1982b).

2.7 POSSIBLE COMPLICATIONS

Thus far, we have not discussed the implications of two of our fundamental assumptions, namely, that the wedge is made of a Coulomb material, and that this material has an insignificant cohesive strength. The final section of this chapter will discuss some of the implications of non-Coulomb behavior along the basal décollement. The implications for the Taiwan thrust belt of rock cohesion shall be discussed in Chapter 3. Evidence for and the importance of a perfectly plastic, normal-stress independent rheology near the toe of the Barbados wedge is discussed in Chapter 4. However, at this point in our discussion, it is appropriate to make certain general statements about the implications of these possible alternative wedge behaviors.

Cohesion within the wedge would make the wedge stronger, and therefore easier to push, even with a narrower taper. Therefore, one should expect that wherever there is a significant amount of cohesive strength, the wedge taper should be somewhat less than its value for the cohesionless case. The cohesion can be considered significant when it is at least comparable in magnitude to

internal friction (eq. 2.1). Thus, cohesion is important in controlling the taper of a thrust belt near its toe where the wedge thickness is smallest (Davis and Suppe, 1980; Davis et al., 1983). By strengthening the wedge, cohesion reduces the value of the critical taper near the toe of a wedge. At a greater distance back into the wedge, the taper increases, asymptotically approaching the value predicted with an assumption of cohesionless behavior. In our Cartesian coordinate frame we have an expression essentially identical to eq. 2.22, with the only addition being a dimensionless cohesive term, $C_0/\rho gH$, multiplied by a constant, Q (Dahlen et al., 1982):

$$\alpha + \beta = \frac{(1 - \rho_w/\rho)\beta + (1 - \lambda)\mu_b}{(1 - \rho_w/\rho) + K(1 - \lambda) + Q(C_0/\rho gH)} \quad (2.36)$$

where and K and Q are given by:

$$K \equiv \frac{2}{H} \int_0^H \frac{dz}{\cos\phi \sec 2\psi - 1} \quad (2.37)$$

and

$$Q \equiv \frac{1}{H} \int_0^H \frac{(\csc\phi - 1)dz}{\cos\phi \sec 2\psi - 1} \quad (2.38)$$

A cohesionless wedge at its critical taper for $\alpha=4^\circ$ and $\beta=6^\circ$ would be stable for much narrower tapers near its toe with $C_0 > 0$ (Figure 2.12). Note in eq. 2.36 that for small values of $C_0 = K_p S_0 = \left(\frac{1 + \sin\phi}{1 - \sin\phi}\right) S_0$, the taper-reducing effect of cohesion is limited to the toe region. Beyond the toe region, as the dimensionless ratio between cohesion and internal friction near the bottom of the wedge

approaches zero, then the taper of the wedge should asymptotically approach the cohesionless value.

If the wedge material consists of a material which is perfectly plastic and does not have any pressure dependence in strength, then it is still possible to have it deform under horizontal compression, as long as one hypothesizes a basal layer which is considerably weaker than the wedge as a whole (Chapple, 1978; Stockmal, in press). An assumption of such material behavior has several advantages, including computational simplicity. However, it is very difficult to relate such a model to most experimental data on rock strengths in the uppermost crust, which, as discussed earlier, suggest that frictional sliding is important. Also, the importance of pore pressures cannot be as clearly dealt with by a failure criterion which depends only on differential stresses (unaffected by pore pressures), and not, at least in part, upon the absolute magnitude of the stress.

2.8 REALM OF THE THEORY

One unusual aspect of this theory is that it appears to apply equally well to both thrust belts and accretionary wedges. Although the strengths of rocks in these two settings may be different, equally important differences between these two types of compressive wedges are related to the presence of a water overburden and the lack of subaerial erosion in the case of accretionary wedges (Davis

and Suppe, 1981). The differences resulting from the role of the water overburden, especially for small values of β , are shown in Figure 2.13.

A further method of testing the validity of the Coulomb-wedge theory is to examine natural cases in which the theory would be expected to break down in some expected way. Two situations will be considered: (1) the basal décollement exhibits pressure-independent plastic rather than Coulomb behavior because of rock type and (2) the thickness of the wedge exceeds the depth to the brittle-plastic transition so that the base no longer displays Coulomb friction because of high temperature.

The principal situation in which a relatively thin, low-temperature wedge might be expected to exhibit basal plasticity is a décollement composed of evaporites, as observed in some ancient fold-and-thrust belts, as well as in the Zagros Mountains (Stocklin, 1968), the unusually small surface slope and taper of which are discussed further in the next chapter.

As an accretionary wedge or fold-and-thrust belt grows, its basal décollement may become sufficiently deep that the assumption of brittle behavior is no longer valid because thermally activated deformation processes prevail. Below such depths sliding resistance along the basal décollement should drop rapidly and become independent of pressure. The Coulomb wedge theory is not expected to be valid toward the interior of very wide mountain ranges and

accretionary wedges. Such wedges should therefore show an abrupt drop in surface slope toward their interior, as the surface expression of the brittle-plastic transition along the base. Some possible examples of this phenomenon are discussed in Chapters 3 and 4.

In summary, an approximate theory has been derived for the minimum or critical taper required for a Coulomb wedge to slide stably along its basal décollement rather than deform internally. If the basal friction increases then the taper also does so, whereas an increase in the internal strength of the wedge decreases the critical taper. In addition to likely differences in the strengths of sediments near the toe, two important differences exist between subaerial and submarine wedges. (1) The horizontal gradient in buoyancy caused by the sloping rock-water interface gives rise to a term involving ρ_w/ρ in the critical taper eq. 2.22. This term discontinuously disappears as the wedge emerges above sea level and should produce about a 1° drop in surface slope. (2) Erosion requires continued deformation throughout a subaerial wedge to maintain the critical surface slope over the length of the wedge. In contrast, submarine wedges should deform mostly in the toe where new material is encountered, and they may be supercritical away from the toe because of sedimentation and fluctuations in basal friction. Observed instances of subduction without accretion or subduction-erosion in some submarine wedges may also be effects of

fluctuation in basal friction.

The Coulomb wedge theory is expected to break down where the wedge thickens to the depth of the brittle-plastic transition, below which the basal resistance to sliding should drop abruptly with increasing temperature. In the next two chapters, we shall discuss some specific wedges which display this predicted drop in taper where they reach a thickness of about 15 km, a depth which is in good agreement with the depth of the brittle-plastic transition in quartz for typical geothermal gradients.

In this chapter, it has been suggested that fold-and-thrust belts and accretionary wedges have the overall mechanics of a bulldozer wedge at failure in horizontal compression. Later in this thesis, this theory shall be tested and its implications shall be further explored on a variety of levels. These include 1) possible implications for plate tectonics driving forces, 2) some implications for the state of stress in and overall strength of the upper crust, and 3) the meaning of this theory with respect to observations of thrusting in specific convergence zones.

Figure Captions

- Fig. 2.1 Schematic diagram of laboratory sandbox model of Coulomb wedge. Underlying Mylar sheet is pulled out beneath buttress at left.
- Fig. 2.2 Photographic side view of stages in deformation of sand during an experimental run. Initially undeformed sand mass is increasingly compressed and deformed by thrusting until the critical taper is attained. Black sand layers are passive markers. Photograph is approximately 1/4 scale.
- Fig. 2.3 Typical rock strengths in the brittle regime for (a) granite, and (b) sedimentary rocks. The solid circles are fracture strengths (after Hoshino et al., 1972) and the open circles are frictional strengths (after Byerlee, 1967, 1978).
- Fig. 2.4 Relationship between fluid pressure P_f and vertical normal traction σ_z in three cases: (a) water table at surface; (b) water table below surface; (c) rock submerged. In all three cases the Coulomb shear strength is proportional to the difference $\sigma_z^* = \sigma_z - P_f$, shown by shading.
- Fig. 2.5 Schematic diagram of a wedge of material subject to horizontal compression and on the verge of Coulomb failure throughout. The force balance on an arbitrary column of width dx is shown, and the terminology used in deriving the equations of critical taper is indicated.

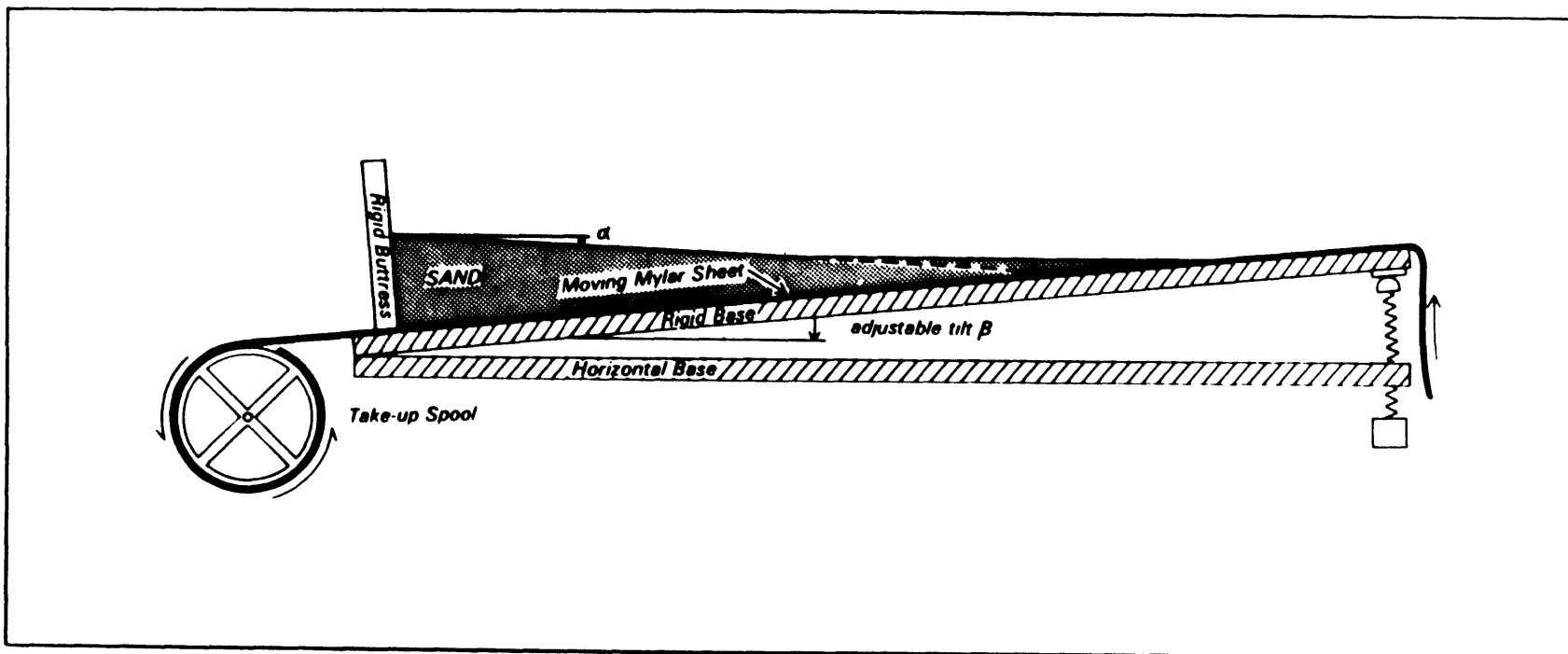
- Fig. 2.6 Mohr diagram illustrating the state of stress (a) at some point within the wedge and (b) at the base of the wedge. The quantities ϕ and ϕ_b are the angles of internal and basal friction, and ψ and ψ_b are the angles between σ_1 and the x axis within the wedge and at the base of the wedge. The basal shear traction τ_b is given by the intersection of the frictional failure law $|\tau| = \mu_b \sigma_n^*$ with the Mohr stress circle corresponding to the basal depth H.
- Fig. 2.7 Sensitivity of coefficient K to basal and apparent internal coefficients of friction μ_b and μ . If μ_b is small compared to μ , $K \approx \sin\phi / (1 - \sin\phi)$, but as $\mu_b \rightarrow \mu$, K decreases significantly and in fact $\partial K / \partial \mu_b \rightarrow -\infty$.
- Fig. 2.8 Comparison of Coulomb wedge mechanics with the well-known Hubbert-Rubey solution for a rectangular overthrust.
- Fig. 2.9 Mean surface slope measured by linear regression off photographs vs. dip of rigid base in sandbox experiments. Dots represent the average of a series of experimental runs with various values of β . The line is the theoretical prediction $\alpha = 5.9^\circ - 0.66\beta$.
- Fig. 2.10 Illustration of a) the sandbox experiment, b) the orientations of slip planes in the experiment, and c) their relationship to the state of stress.
- Fig. 2.11 a) Illustration of the effects on wedge geometry of surficial erosion and isostatic adjustment.

b) Illustration of the effect on the critical taper of changes in basal friction, either in λ_b or μ_b . Both erosion and isostatic adjustment drive a critical wedge into the subcritical regime, encouraging renewed deformation. A decrease in basal friction, on the other hand, gives rise to a supercritical wedge and possibly to subduction unaccompanied by accretion or wedge deformation. The sensitivity to changes in basal friction is quite pronounced. The case depicted here represents only a $\pm 2\%$ change in λ_b of a submarine wedge having $\lambda = \lambda_b = 0.8$ initially.

Fig. 2.12 Cross-sectional shapes of compressive wedges with $\lambda=0.7$, $\mu_b=0.85$, and $\mu=1.02$ with different values of cohesion C_0 : (a) Cohesionless, (b) 10 MPa, (c) 50 MPa, and (d) 100 MPa.

Fig. 2.13 Surface slope versus basal dip for cohesionless critical wedges as a function of fluid-pressure coefficient λ : (a) subaerial, and (b) submarine.

Figure 2.1



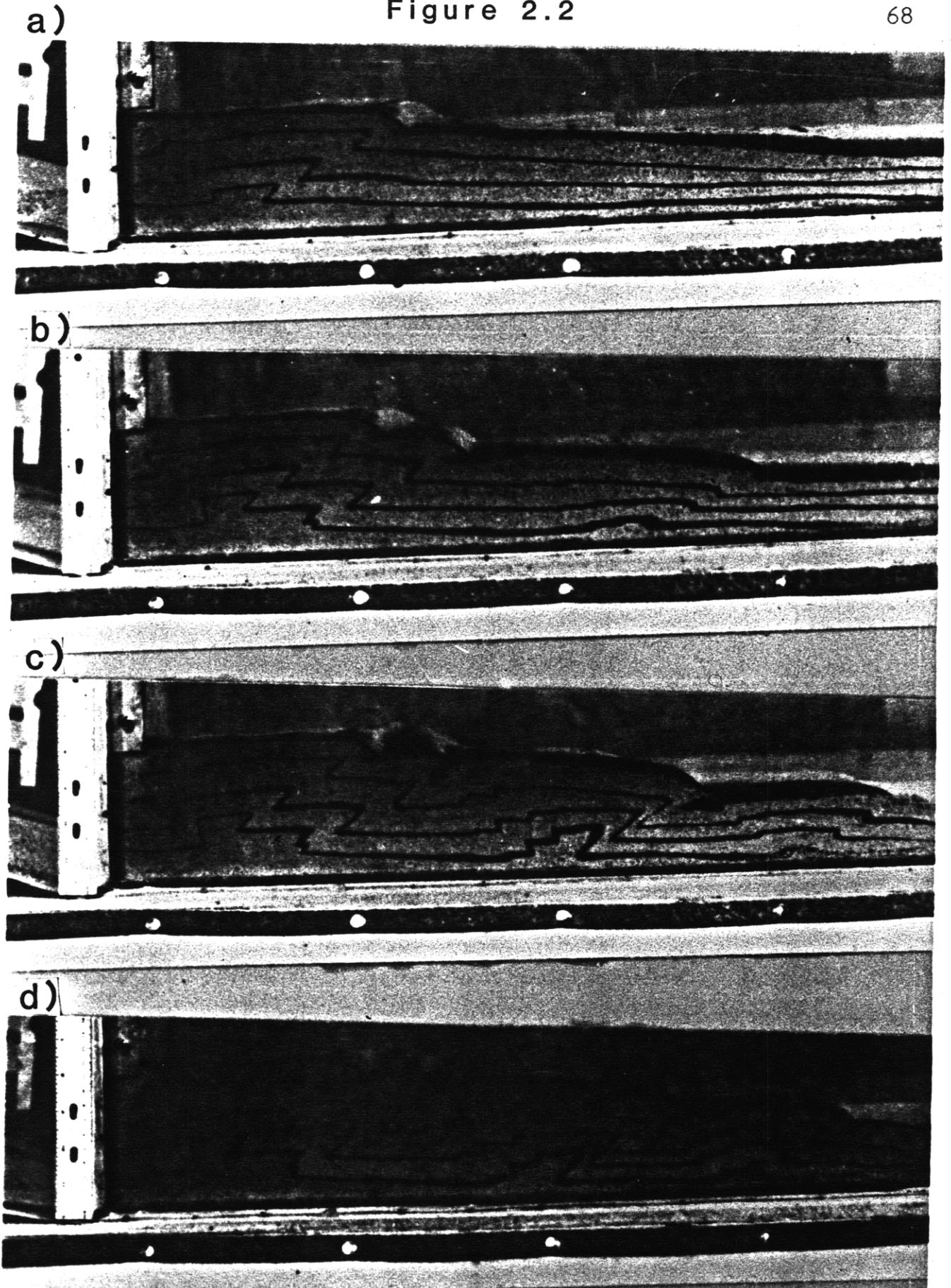


Figure 2.3

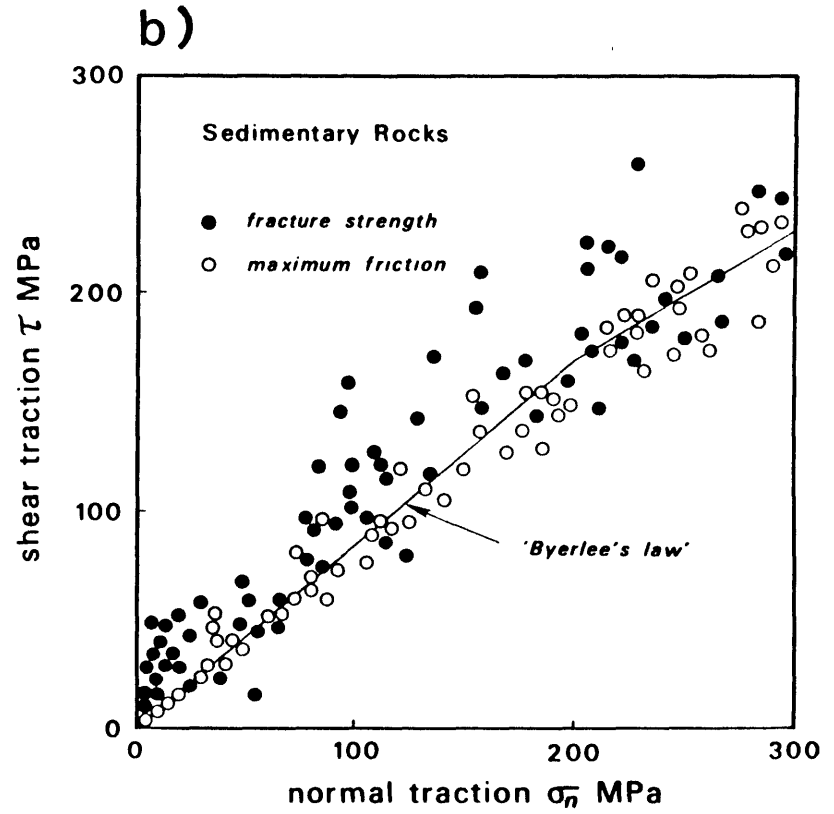
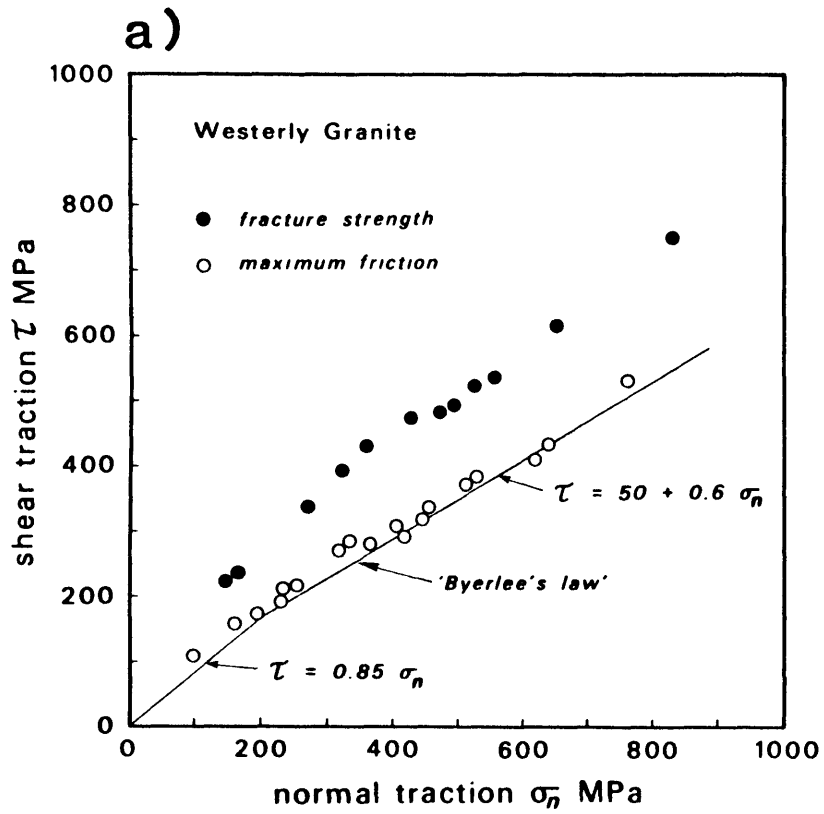


Figure 2.4

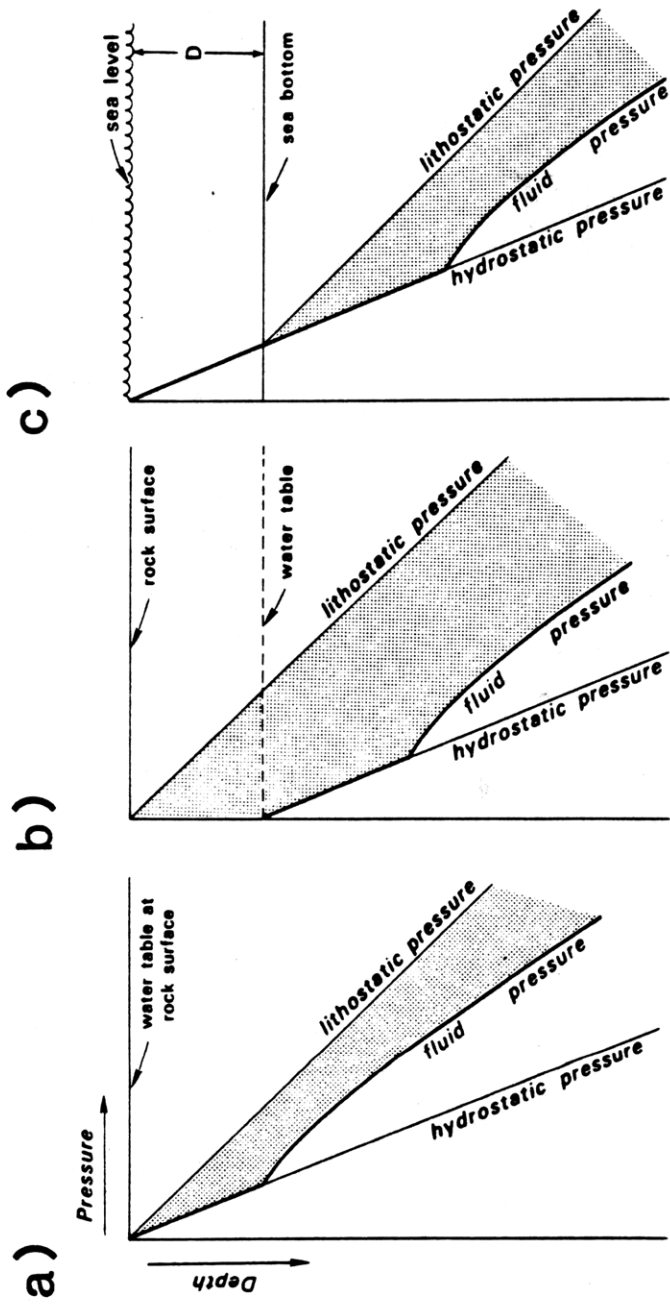


Figure 2.5

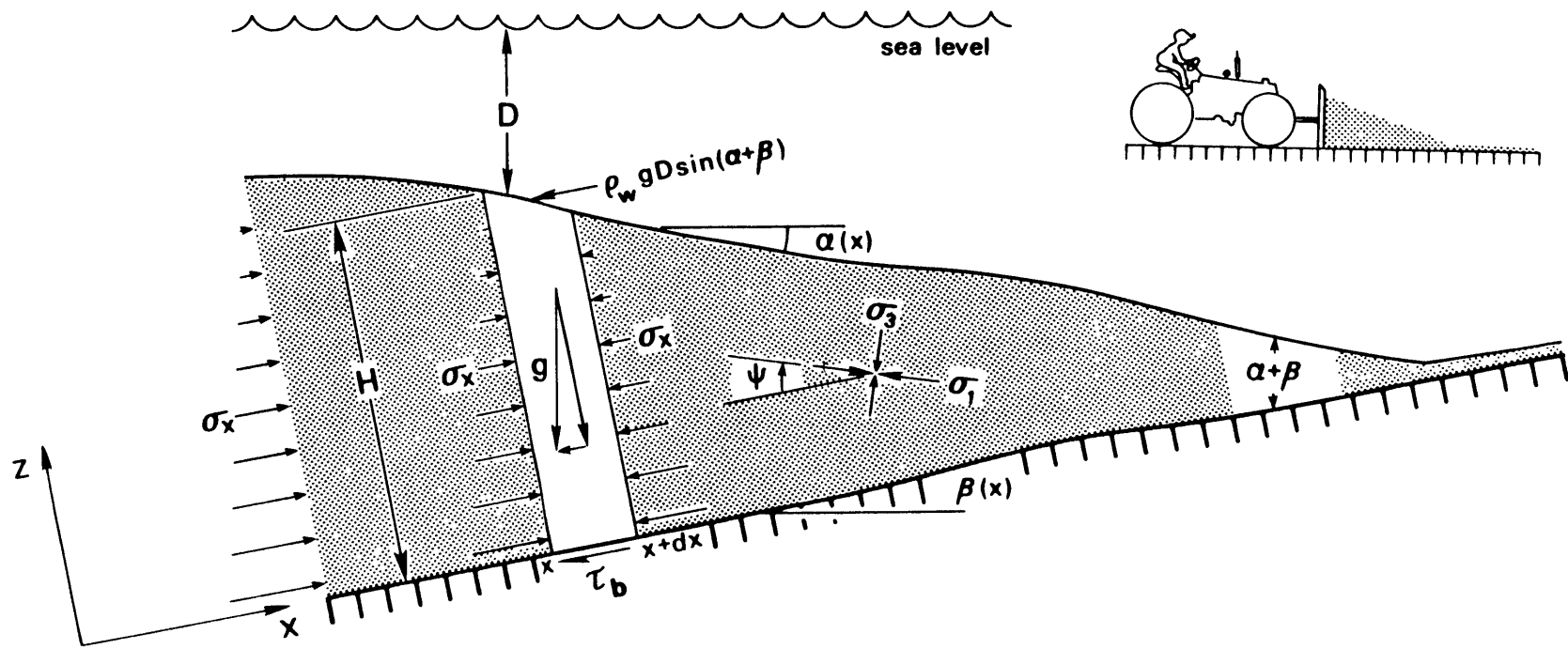


Figure 2.6

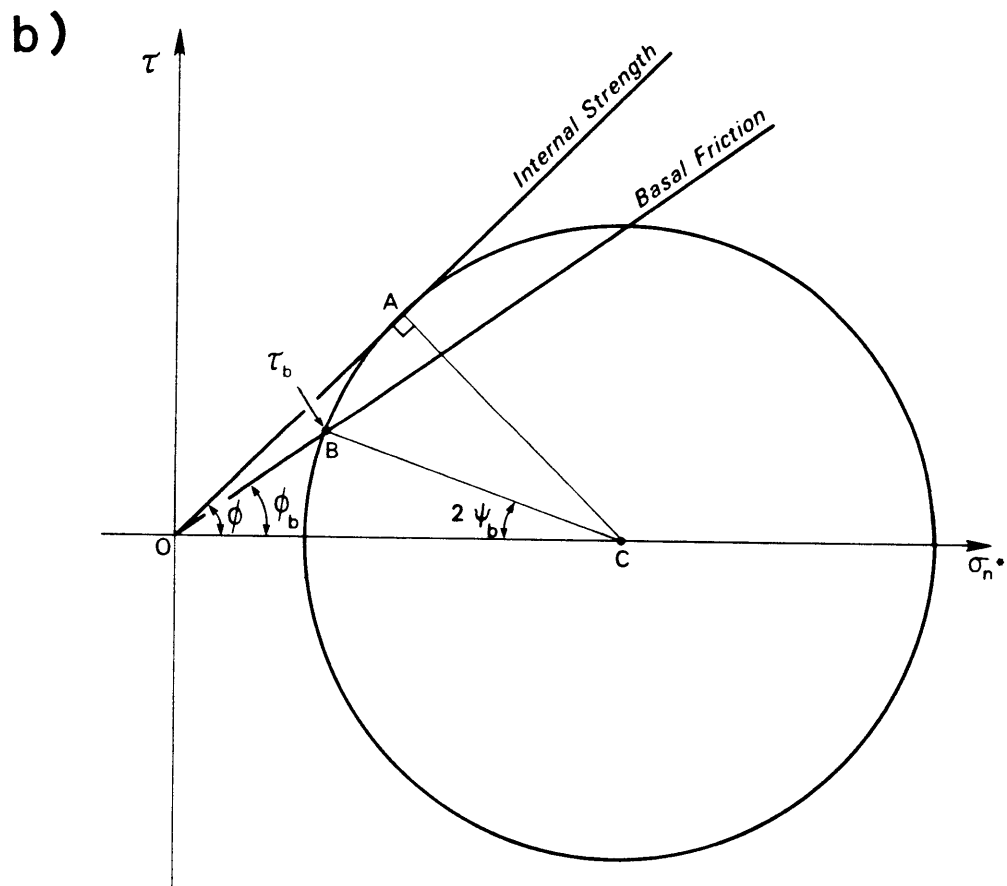
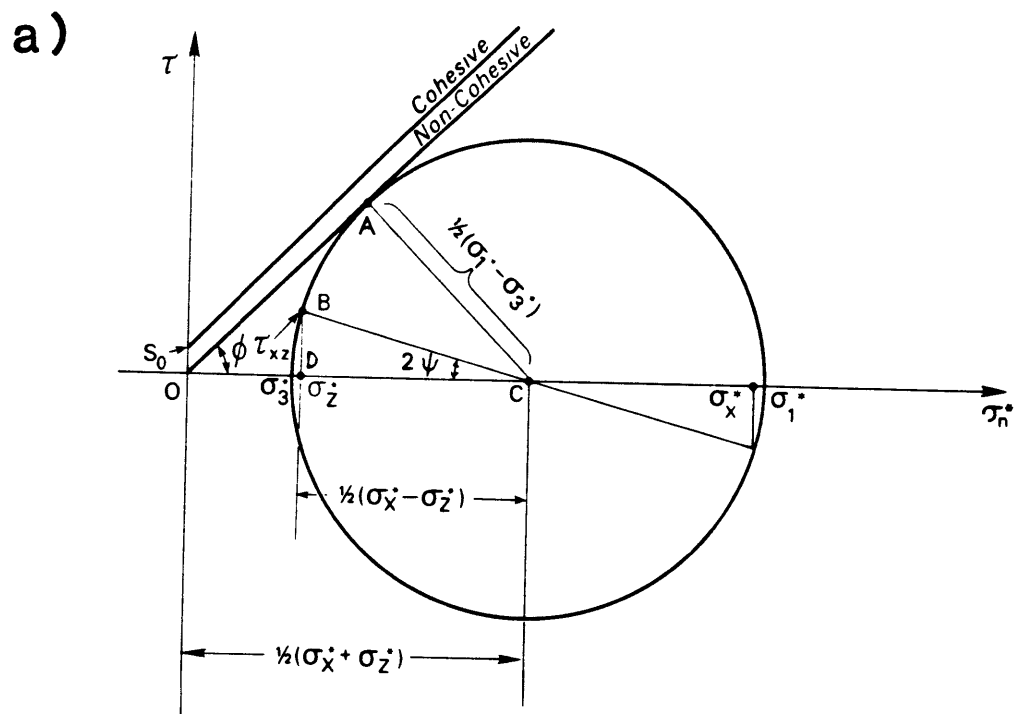


Figure 2.7

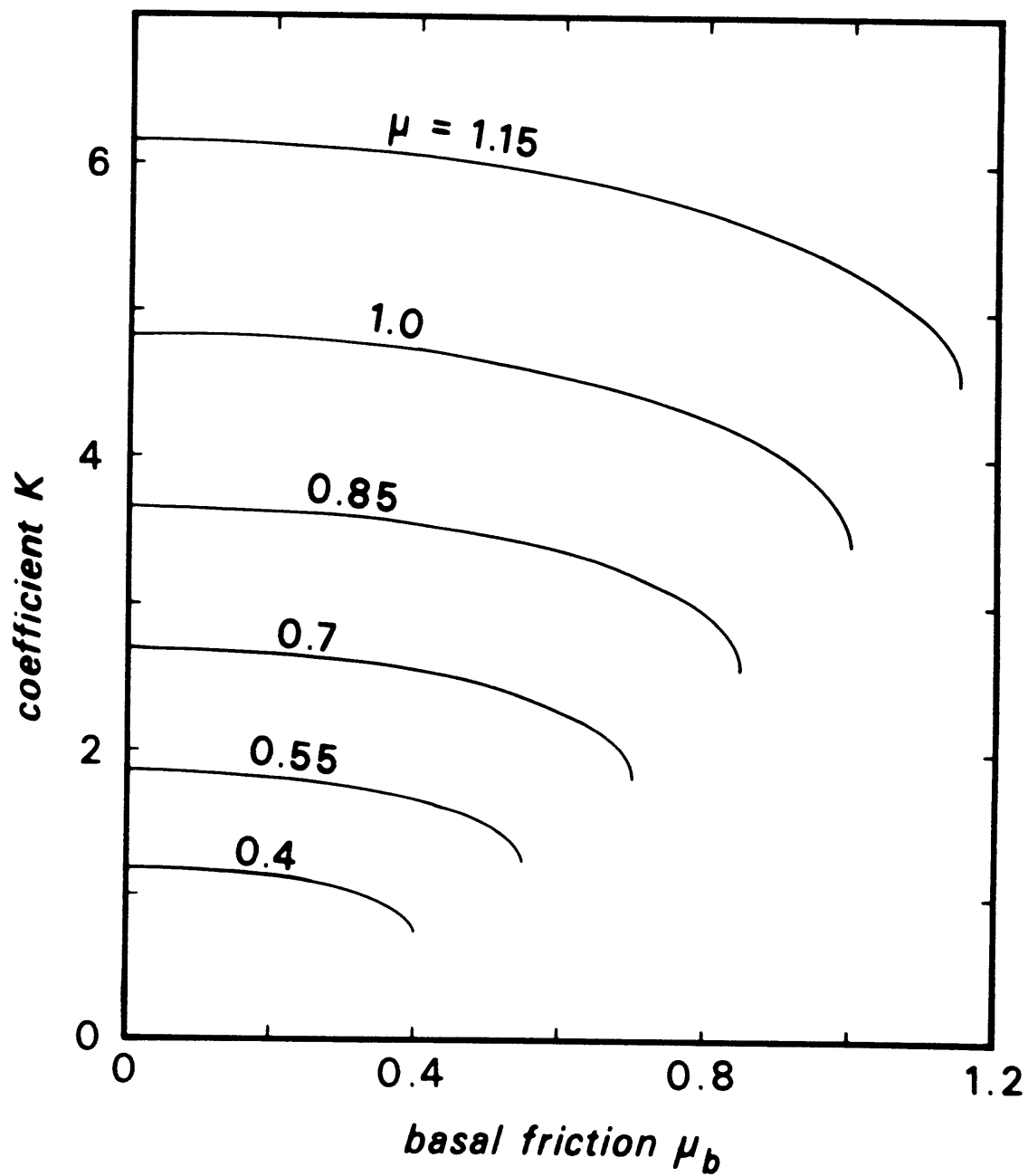


Figure 2.8

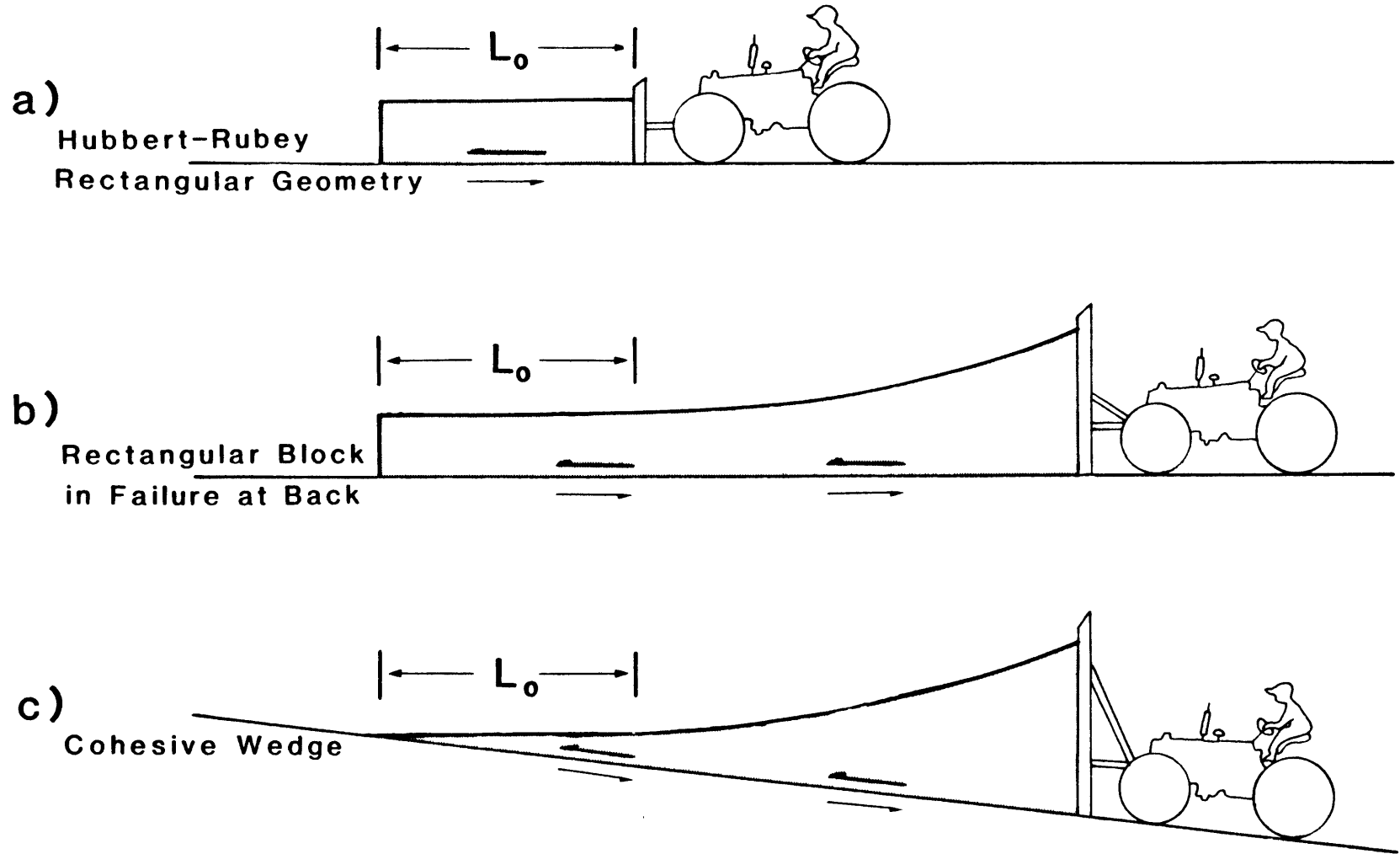


Figure 2.9

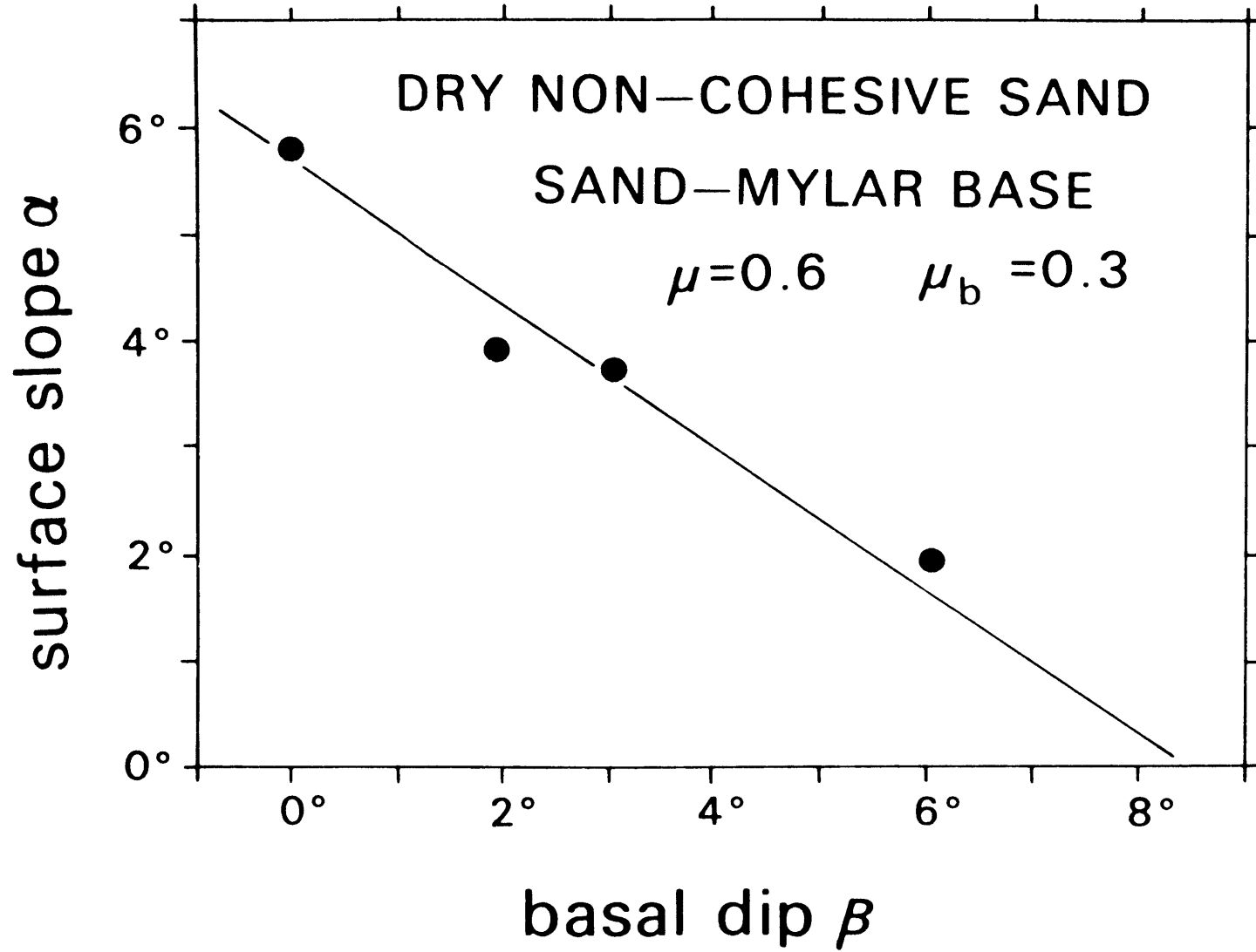


Figure 2.10

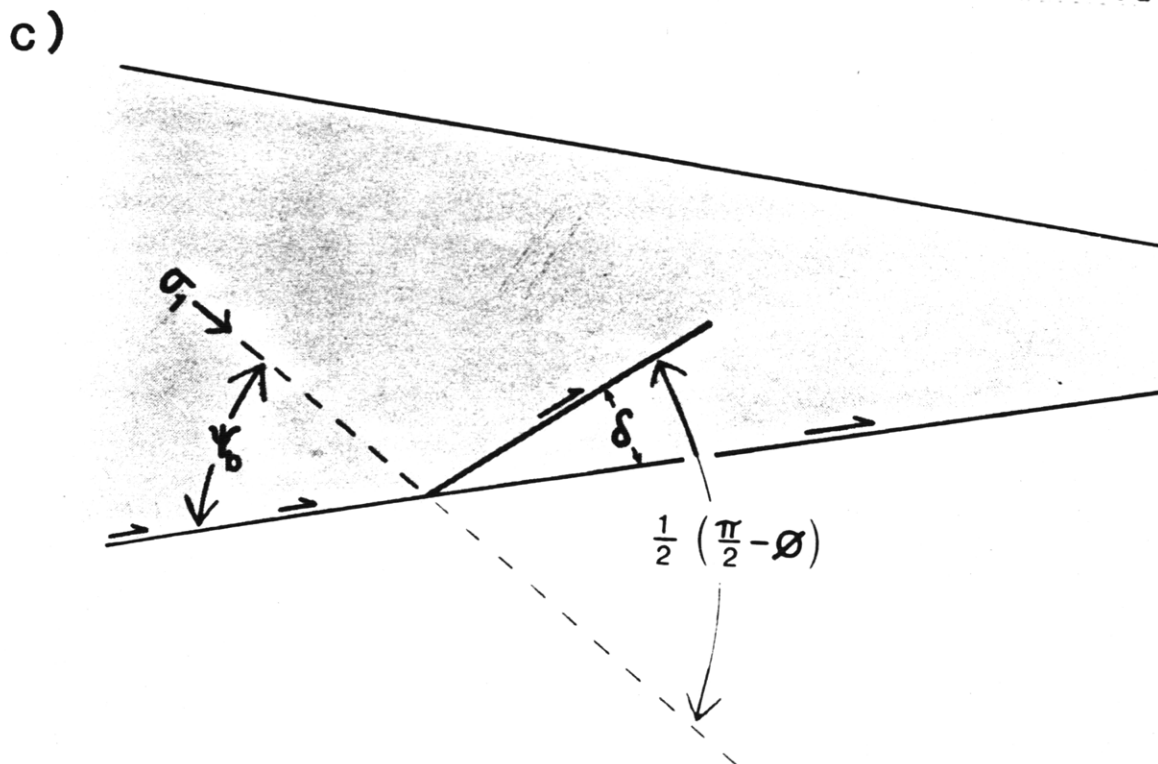
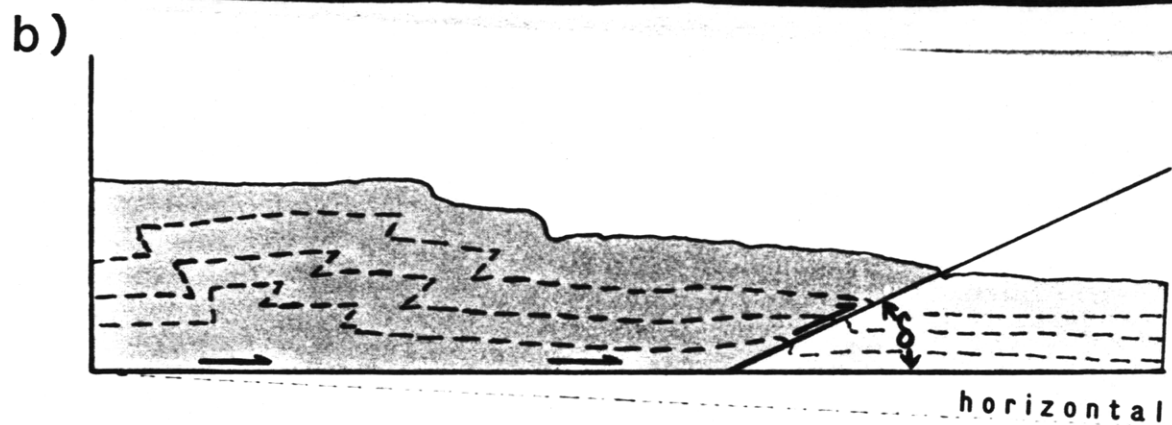
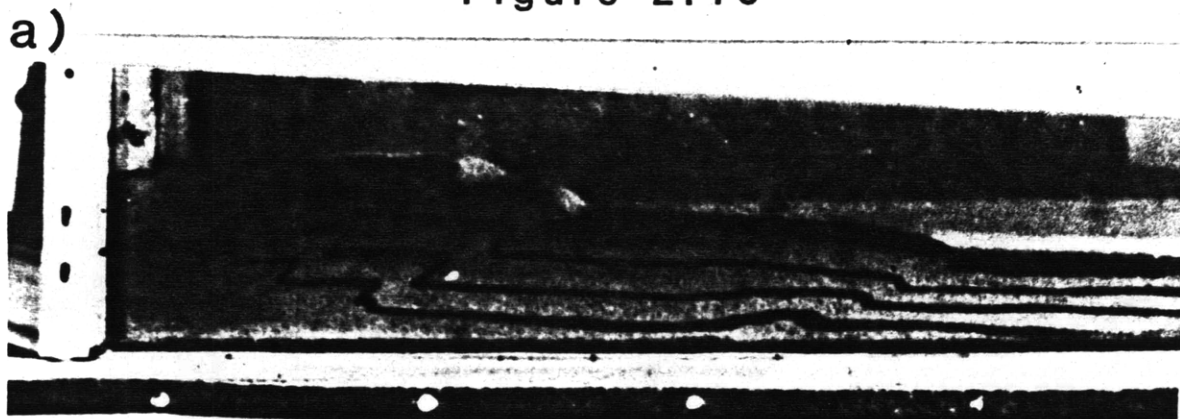


Figure 2.11

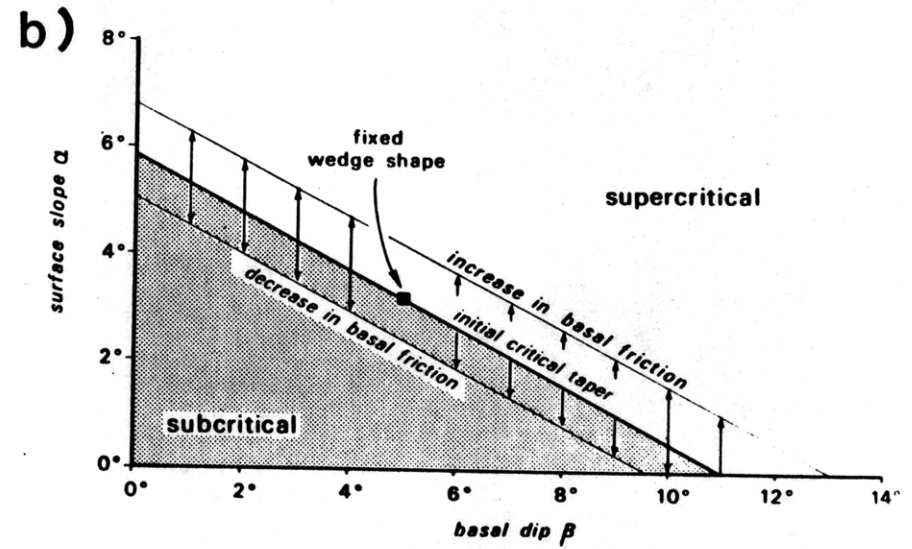
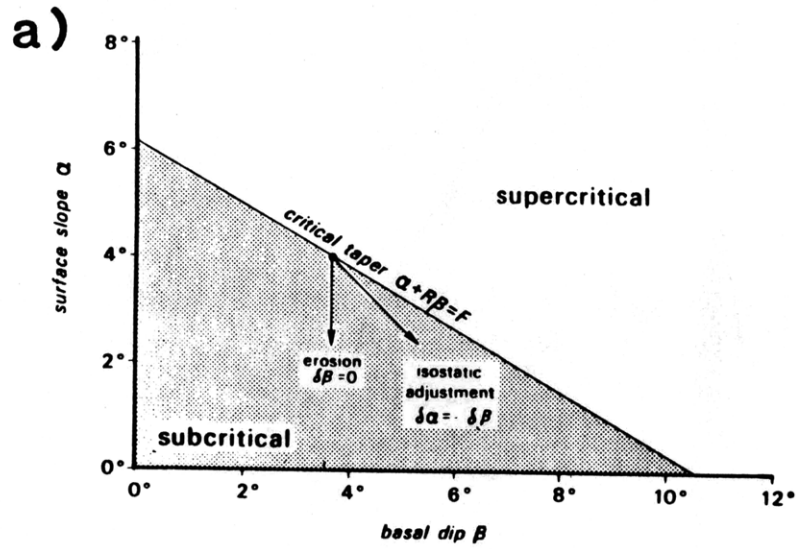


Figure 2.12

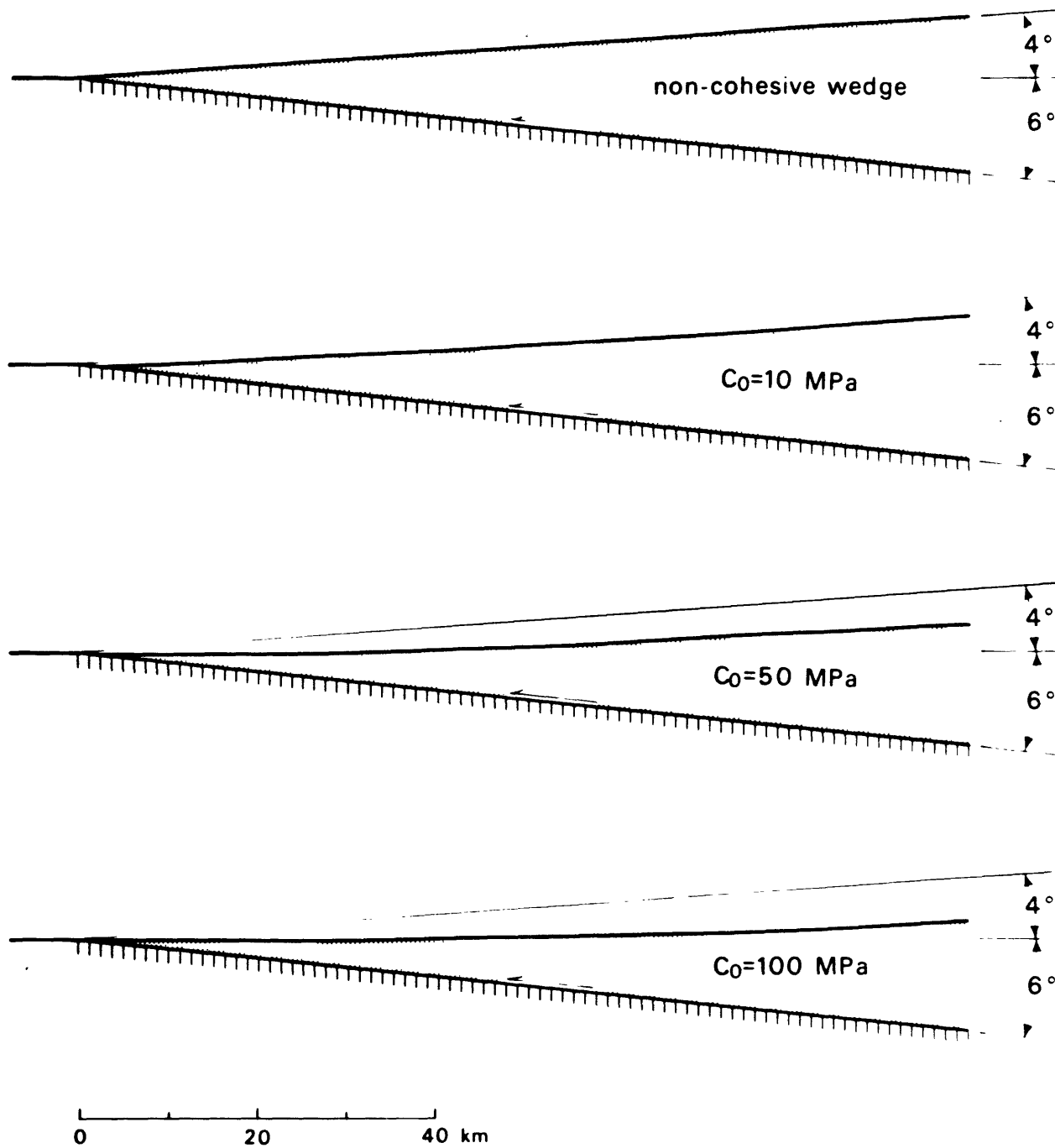
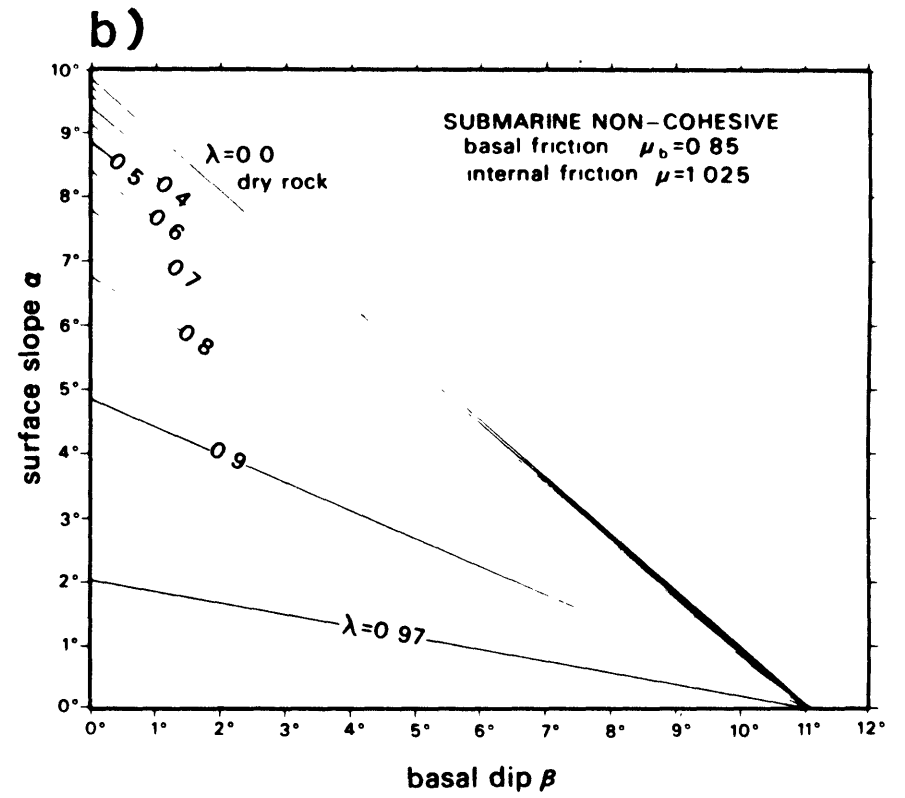
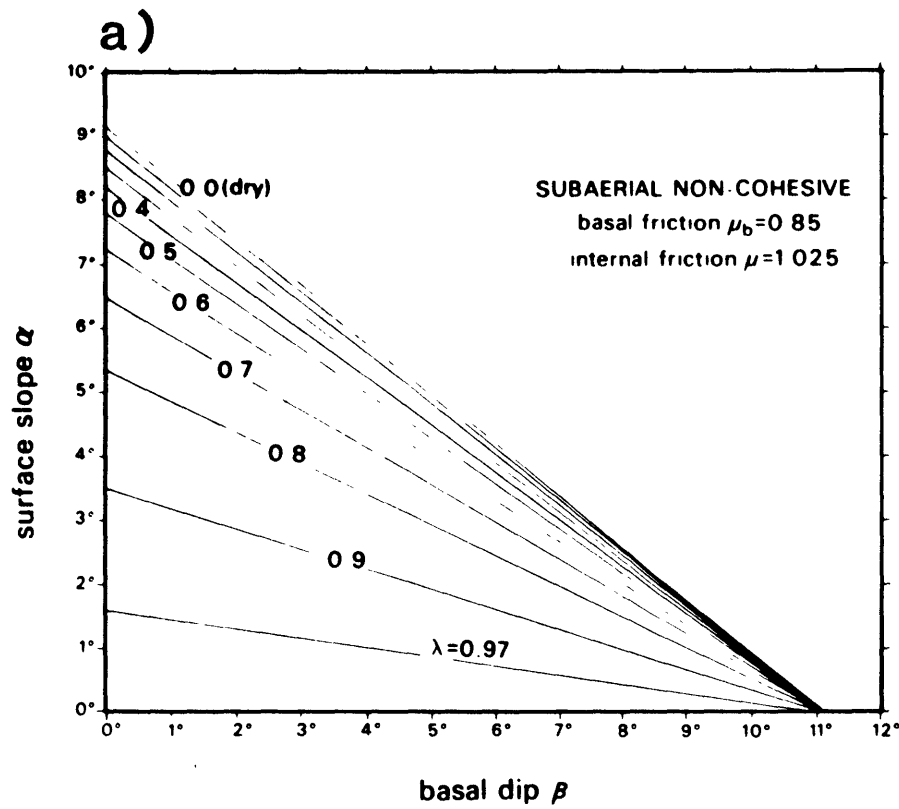


Figure 2.13



CHAPTER 3 MECHANICS OF THRUST BELTS3.1 INTRODUCTION

In this chapter, I shall discuss three modern mountain belts, each of which has undergone a considerable amount of crustal shortening associated with a convergent plate boundary. The manner in which the convergence has taken place in each of the mountain belts shall be used to illustrate aspects of the mechanical principles which govern them all.

Because it is one of the best understood of the currently active mountain belts, the fold-and-thrust belt of western Taiwan shall be considered at some length. Although it is located in a rather complicated plate tectonic setting, the Taiwan mountain belt is mechanically simple in two very important ways. First, it does not possess a basal décollement comprised of a material which is much weaker than the rocks of the bulk of thrust belt itself, such as salt. Second, the Taiwan mountain belt is quite small. At no point does it attain a depth at which temperatures are likely to be high enough for thermally activated flow mechanisms to significantly weaken the rock. These two simplifying attributes of the Taiwan example do not apply, respectively, to the Zagros and Himalayan mountain belts. These two examples are discussed in this chapter in an attempt to isolate the effects of a weak décollement and of high temperatures at great depths.

3.2 TECTONICS OF TAIWAN

Taiwan is an actively deforming mountain belt situated on the continental shelf of China at the western edge of the Philippine Sea plate (Figure 3.1). The relative motion between the Asian and Philippine Sea plates is relatively poorly constrained because the Philippine Sea plate, unlike all other plates of comparable size, is bounded only by consuming margins. Without any spreading margins to produce a magnetic record of its motions with respect to any other plate, the Philippine Sea plate cannot be reliably tied into the relative motion schemes which describe the motions of the other plates (Minster et al., 1974; Minster and Jordan, 1978). The best known estimate for the motions of the Philippine Sea plate is that of Seno (1977), made using fault-plane solutions along the Philippine Sea plate boundaries with the Pacific plate and with the Asian plate off Japan. Seno's solution for the relative motion in the plate collision in Taiwan yields a convergence rate of 7 cm/yr, and an instantaneous rotation vector for the two plates with a pole at 45.5°N and 150.2°E with an angular velocity of $1.20^{\circ}/\text{m.y.}$ There are large potential sources of error resulting both from the use of fault-plane solutions to constrain the plate closure velocity and from the implicit assumption of plate rigidity.

Along the Ryukyu trench to the northeast of Taiwan, the Philippine Sea plate subducts beneath Asia (Seno, 1977), but along the Manila trench to the south, the

polarity is reversed and oceanic crust attached to Asia subducts beneath the Philippine Sea Plate. The tectonics of the island of Taiwan are largely a manifestation of this changeover in polarity (Suppe, 1981).

It is noteworthy that the plate boundary in the Taiwan-Luzon region cuts across the continent-ocean boundary within the Asian plate (Figure 3.1); the Luzon Arc and Manila Trench are oriented north-south whereas the stable continental margin of China southwest of Taiwan is oriented northeast-southwest. This geometry results in an oblique collision between the Luzon Arc and the Chinese continental margin. The collision first began about 4 m.y. ago in northernmost Taiwan (Chi et al., 1981), is occurring now just south of Taiwan, and will occur in the future between Luzon and Hong Kong (Suppe, 1981). As the plate boundary impinges in turn on the thick sedimentary sequences on the Chinese continental rise, slope, and shelf the accretionary wedge expands continuously in width and height to become the Central Mountains of Taiwan rising nearly 4 km above sea level. Once the accretionary wedge rises above sea level it is no longer able to grow without bounds because of 5 to 6 km/m.y. erosion rates (Li, 1975); in fact the topography of the mountain belt in central Taiwan has reached a steady state in which tectonic compression is balanced by erosion (Suppe, 1981). Taiwan in this region is a presently active foreland fold-and-thrust belt with deformation extending into the toe, (Figures 3.2, 3.3) which suggests that the

interior of the mountain belt is at critical taper. Therefore the steady-state topography makes Taiwan a particularly appropriate place to study the critical taper of a subaerial wedge.

The fold-and-thrust belt of western Taiwan has the classic thin-skinned geometry (Rodgers, 1972; Chapple, 1978; Suppe, 1980b), as described in Chapter 2. The basal décollement dips eastward beneath the island. The topographically high spine of the island is, on the average, roughly 3 km high, and locally attains a height of 4 km. The thrust belt is composed of relatively young sedimentary rocks, with the Oligocene Wuchihshan Formation, roughly 5 km below the foothills, forming the base for much of the deformation (Suppe, 1980b). The present width of the mountain belt above sea level is a relatively small 80 km. A retrodeformed cross section (Suppe, 1980a) shows that the rocks have undergone a threefold compression of 160 to 200 km, which places the pre-collision position of the continental shelf far to the east, near the present western end of the Ryukyu Trench.

FLUID PRESSURES

The transition zone between normal (hydrostatic) and overpressured fluid reservoirs is stratigraphically controlled, probably due to a contrast in permeability between relatively permeable and impermeable shales (Suppe and Wittke, 1977). The transition zone is generally in or near the Miocene Chuhuangkeng Formation (Figure 3.4),

typically between 1 km and 4 km below sea level.

Fluid pressures are well-known within the western foothills and coastal plain of Taiwan as a result of formation tests and sonic log measurements obtained during petroleum exploration (Suppe and Wittke, 1977; Suppe et al., 1981; Namson, 1982). Typical fluid-pressure profiles at the western edge of the fold-and-thrust belt where there has been little erosion show an upper permeable zone of hydrostatic fluid-pressure gradients ($\lambda \approx 0.4$) overlying less permeable sediments exhibiting overpressured fluid-pressure gradients ($\lambda \approx 0.7$), as seen in the Tiehchanshan and Meilin wells in Figure 3.4. This overpressured gradient is very constant throughout western Taiwan. Very soon after the onset of deformation, the permeable Plio-Pleistocene sediments are eroded off the growing structures and overpressured fluid-pressure gradients are exposed essentially at the surface of the wedge, as for example in the Chuhuangkeng field in Figure 3.4, which has Miocene rocks at the surface (Suppe and Wittke, 1977). Furthermore, major décollement surfaces that are intersected by deep drilling in the foothill zone show the same overpressured fluid-pressure gradient as the overlying rocks (Suppe et al., 1981). On the basis of all information we have available, we adopt a constant fluid-pressure ratio $\lambda = \lambda_b = 0.675 \pm 0.05$ for both the wedge and the basal décollement. It should be noted, however, that direct fluid-pressure measurements are essentially restricted to

the western third of the wedge, so although the fluid-pressure data used are quite reliable, they require an assumption of regional homogeneity.

SURFACE SLOPE

The mean topographic slope is the most easily measurable of the important mechanical parameters. The island of Taiwan is divided into three distinct topographic provinces (Figure 3.5).

The southernmost quarter of the island is thought to be rising, not having yet attained an equilibrium between uplift and erosion. In the northern quarter of Taiwan, reduced topographic relief is attributed to a reduction in the activity of thrusting, which permits erosion to dominate. The central 150 km of the island is actively deforming, as evident from seismicity (Figure 3.3). Although the locus of the collision with the Chinese continental margin progresses southward at a rate of 90 km/m.y., making the island, in effect, a time cross-section of itself, the central third of the island shows no consistent north-south topographic variation. In this part of Taiwan, topographic profiles show very nearly constant surface slope, except for local ridges and drainage valleys on a scale of only a few kilometers. Best-fit linear regressions to the western slope of central Taiwan, vary between 2.5° and 3.4° (Figure 3.5) with the mean slope being $\alpha = 2.9^\circ \pm 0.3^\circ$. This is a remarkably constant surface slope over a fairly large area, suggesting that the entire area

has homogeneous material properties, fluid pressure, and décollement dip, well as being everywhere very close to its critical taper.

DECOLLEMENT DIP

The dip of the basal décollement in western Taiwan is of course not as easily measured as the regional surface slope, but it is fairly well determined in the frontal part of the wedge based on seismic reflection profiling, deep drilling, and the construction of retrodeformable geologic cross sections (Suppe, 1980a, 1980b, 1981; Suppe and Namson, 1979; Namson, 1982). The area of well-constrained regional dip extends from the deformational front located near Chiai to about 30 kilometers into the wedge; the measured dip is $\beta = 6^\circ$ at the stratigraphic level of the basal décollement near the base of the Neogene continental margin section. It is known, at least in northern Taiwan, that this single level of décollement exists under the entire width of Taiwan (Suppe, 1980a). We must extrapolate our 6° measurement in the toe region under the entire western slope of the mountains to obtain an estimate of the overall taper of the wedge. We believe that we know the décollement dip within $\pm 1^\circ$ everywhere, and within $\pm 0.25^\circ$ at many locations near the toe.

BASAL FRICTION

We have outlined the data on surface slope α , décollement dip β , and fluid-pressure ratio λ and λ_b in the

preceding sections. The remaining parameters that enter into the critical taper of the mountain wedge are the coefficient of friction on the basal décollement μ_b and μ' , the effective coefficient of internal friction. We define the effective internal friction coefficient as the ratio, at failure, between the shear and normal stresses. With no cohesion, there is no difference between the usual definition ($\mu = \tan\phi$) and this one. However, with the introduction of cohesion it is possible to have a value of the effective coefficient of internal friction

$$\mu' = \frac{\sigma_n^* \tan\phi + S_0}{\sigma_n^*} = \tan\phi + \frac{S_0}{\sigma_n^*} \quad (3.1)$$

with a value well above unity.

Neither μ' nor μ_b is known from direct measurements in Taiwan. Laboratory studies have shown sliding friction to be remarkably uniform for a wide variety of rock types. According to Byerlee (1978), frictional sliding is well described by the relation $|\tau| = 0.85\sigma_n^*$ for effective normal tractions in the range 5 to 200 MPa, which encompasses most rocks (Figure 2.3) for depths above the brittle-plastic transition, especially in overpressured environments. In view of this laboratory evidence, we shall adopt, on a provisional basis, Byerlee's empirical 'law' $\mu_b = 0.85$ on the basal décollement where it is reasonable to assume that essentially pure frictional sliding is occurring. We will then employ the critical Coulomb wedge theory, equations 2.22 and 2.29, to infer the effective coefficient of

friction within the wedge, μ' . This procedure yields our preferred model, but since there are many possible objections to the use of Byerlee's law on the base, we have in addition computed the complete range of values μ_b , μ' consistent with the measured Taiwan field parameters $\alpha=2.9^\circ$, $\beta=6^\circ$ and $\lambda = \lambda_b \approx 0.7$.

3.3 COMPARISON OF THE THEORY WITH TAIWAN GEOLOGY

Let us view the fold-and-thrust belt of western Taiwan as an example of the Coulomb wedge theory of Chapter 2 (see also Davis et al., 1983). Let us assume that we know both the basement dip $\beta=6^\circ$ and the strength of the basal décollement μ_b , for which we arbitrarily choose the Byerlee value of 0.85, while remembering that we are not committed to this high value. In analyzing the overall wedge taper (Figure 3.6a), we can fix the fluid pressure ratios $\lambda=\lambda_b=0.675$ and solve for the wedge taper as a function of the effective coefficient of friction μ' ; we assume that $S_0 = 0$, so $\mu = \mu'$ (Figure 3.6b). The best-fitting value for the strength within the wedge is then $\mu = \mu' = 1.03$, about 20% greater than the assumed strength of the basal décollement. Note that if we reverse the process and assume that $\mu = \mu' = 1.03$ then we find (Figure 3.6c) that the wedge taper in Taiwan is much less sensitive to the fluid pressure ratio $\lambda=\lambda_b$ than it is to the value of μ' .

The sensitivity of the result to uncertainty in $\lambda=\lambda_b$ and in β , the dip of the base of the wedge, is depicted in

Figures 3.7 and 3.8. Again assuming that $\mu_b = 0.85$, and $S_0 = 0$, μ is shown as a function of the uncertainties in λ and, respectively, α and β . The value of μ is constrained to be located within liberally sized error ellipses (for simplicity shown here as rectangles). Given the uncertainties in α , β and λ , and assuming that Byerlee's law is valid on the base, the uncertainty in μ is about ten percent so the inferred difference between μ' and μ_b is real. An effective internal friction identical to the basal friction $\mu_b = 0.85$ is definitely precluded, since it would give rise to a surface slope $\alpha = 5.9^\circ$, assuming that $\beta = 6^\circ$ and $\lambda = \lambda_b = 0.675$ (Figure 3.6b, 3.7b).

It should also be remarked that the inferred excess of effective internal friction over basal friction depends rather critically on the assumption that $\lambda = \lambda_b$. In fact, a solution having $\mu = \mu_b = 0.85$ with λ_b only 10% greater than $\lambda = 0.675$ is also consistent with the observed wedge geometry $\alpha = 2.9^\circ$ and $\beta = 6^\circ$. The essential requirement is that the interior of the wedge be slightly stronger than the base, for whatever reason. Since there is no evidence in any of the well data for even marginally greater overpressures on or below the *décollement*, we are led to conclude that $\mu' > \mu_b$.

The well-constrained values of μ obtained in this way still avoid the whole question of the validity of the Byerlee $\mu_b = 0.85$ assumption. Let us assume only those parameters of whose values we are most confident - those

which define the wedge shape, α and β . We can then determine the sensitivity of our calculated wedge strength, μ , to our assumption of a wedge base with a strength governed by Byerlee's law $\mu_b = 0.85$. We find that a range of solutions from $\mu_b = 0.20$ to $\mu_b = 1.75$ are consistent with the Taiwan data (Figure 3.9). Between those values, there exists a possible solution $\mu > \mu_b$ for any value of the basal friction μ_b . For most reasonable values of basal friction, wedge strength μ' is roughly 20% higher than the basal strength μ_b , given fluid pressures similar to those measured in Taiwan. The implication of this difference between μ and μ_b is that, on the average, slightly larger shear tractions are required to produce internal deformation within the wedge than to permit frictional sliding along its base, which is a through-going *décollement*. We interpret this to mean that the wedge material is not so extensively fractured that pre-existing slip planes of all possible orientations are available within it. Much of the internal deformation must be taken up by slip on sub-optimally oriented surfaces; it is also likely that the commonly observed complex geological structures within the wedge may require fracturing for the deformation to proceed. The ubiquitous presence throughout western Taiwan of fault-bend folds produced by the stepping up of faults from the basal *décollement* (Suppe, 1980b; Suppe and Namson, 1979; Namson, 1982) is consistent with

this interpretation.

The ambiguity in the absolute values of μ and μ_b can be resolved using other techniques. The basal friction coefficient $\mu_b = \tan\phi_b$ contains only a friction angle, ϕ_b , but the effective coefficient of friction in the wedge $\mu' = \mu + \frac{S_0}{\sigma_n^*} = \tan\phi + \frac{S_0}{\sigma_n^*}$ contains both a friction angle ϕ and a ratio of cohesion divided by the effective normal stress. This is simply a restatement of the Coulomb criterion (equation 2.1). For much of a typical wedge, the ratio $(S_0/\sigma_n^*) \ll \tan\phi$, so this term is ignored in the analyses of Davis et al. (1983) and Chapter 2.

The taper in Taiwan is fairly constant in east-west cross section, as well as along strike, suggesting that in most of that wedge, the internal friction predominates. This permits the assumption of eq. 2.2, in which we assumed that cohesion can, to the first order, be neglected. However, at the front of the Taiwan fold-and-thrust belt, where the depth to the basement is ~ 5 km, the wedge taper is roughly 1° less than its critical value toward the back of the wedge. Although, not unique, solutions for cohesion C_0 and wedge friction μ (Dahlen et al., 1982), assuming that $\mu_b = 0.85$, are particularly successful in fitting the wedge taper if they have $\mu = 0.95 \pm 0.05$ and $C_0 = 70 \pm 30$ MPa (Figure 3.10). It is important to note the great deal of uncertainty which exists in the way in which the wedge strength is partitioned between cohesion and stress dependent friction. A uniaxial compressive strength

$C_0 = 70 \pm 30$ MPa corresponds to a zero normal-stress shear stress at failure $S_0 \approx 13 \pm 6$ MPa.

3.4 FAULT STEP-UPS

Examination of slight deviations of the wedge from the predicted cohesionless taper is not the only way in which we can resolve the magnitude of cohesion in the wedge. It has been observed (Rich, 1934; Rodgers, 1950; Suppe and Namson, 1979) that there must be distortions in at least one fault block as such thrust blocks slip past each other on non-planar surfaces. Fault-bend folding theory (Suppe, 1976, 1979; Suppe and Namson, 1979), which relates the magnitudes of fault-bends to the resulting structure, permits the calculation of the effect upon geologic structures of many such folding distortions. The key to such quantification is the observation that observed structures in western Taiwan are compatible with a single fundamental angle for such fault step-ups. Let us consider the mechanical implications of the magnitude of the step-up angle of faults along the basal *décollement* in Taiwan, as determined by Namson (1982) using surface geology, well data, and fault-bend folding theory.

We shall assume that a step-up along the basal *décollement* occurs by breaking into the overlying rock. For the case of a cohesive wedge, we apply the law of sines to triangles $\triangle OBC$ and $\triangle DAC$ in Figure 2.6b in a manner analogous to that used in eq. 2.24 for a non-cohesive

wedge. Noting the appearance of the cohesive term, S_0 , we find that the angle ψ between the basal décollement and the direction of the maximum principal stress σ_1 is given by the following expressions:

$$\begin{aligned} \cos(\pi/2 - \phi_b - 2\psi_b) \left[\frac{1/2(\sigma_1^* - \sigma_3^*)}{\sin \phi_b} \right] &= \frac{1}{2}(\sigma_1^* + \sigma_3^*) = \\ &= \frac{1/2(\sigma_1^* - \sigma_3^*)}{\sin \phi} - S_0 \operatorname{ctn} \phi \end{aligned} \quad (3.2)$$

Combining terms, we have

$$\cos\left(\frac{\pi}{2} - \phi_b - 2\psi_b\right) = \frac{\sin \phi_b}{\sin \phi} - \frac{2S_0 \operatorname{ctn} \phi \sin \phi_b}{(\sigma_1^* - \sigma_3^*)}$$

or

$$= \frac{\sin \phi_b}{\sin \phi} - \frac{S_0 \operatorname{ctn} \phi \sin \phi_b (1 - \sin \phi)}{(\sigma_3^* + S_0 \operatorname{ctn} \phi) \sin \phi}$$

Rearranging terms and solving for ψ_b , the angle between the basal décollement and the direction of the maximum principal stress, σ_1 , we have

$$\psi_b = \frac{\pi}{4} - \frac{\phi_b}{2} - \frac{1}{2} \arccos \left[\frac{\sin \phi_b (1 + (S_0/\sigma_3^*) \cos \phi)}{\sin \phi (1 + (S_0/\sigma_3^*) \operatorname{ctn} \phi)} \right] \quad (3.3)$$

where $(S_0/\sigma_3^*) \approx (S_0/\rho g H(1-\lambda))$ is a dimensionless ratio which indicates the relative magnitudes of cohesion and the overburden at the depth of the step-up. The approximation may be improved by letting the overburden equal σ_z^* instead of σ_3^* , as the axis of the least principal stress is inclined to the z-axis at the base of the wedge by an angle ψ_b .

Namson (1982) produced cross-sections of western Taiwan, and calculated fault step-up angles. The distribution of the magnitudes of step-up angles observed near the toe is depicted in Figure 3.11. Namson's 58 observations have a mean value of 13.6° , with a standard deviation of 2.5° . Removal of three clearly spurious data points leaves a mean step-up angle of 13.8° .

It should be noted that some of the consistency of Namson's step-up angle results (Figure 3.11) may be spurious. In cases in which fault-bend folding theory clearly indicated two or more step-ups having taken place, he made the assumption, in the absence of further geological constraints, that those step-up angles were all equal in magnitude. This necessary assumption may lead to an artificial convergence of these results.

With the assumption that the step-up fractures pristine rock, we can determine orientation of a fault relative to the direction of the maximum principal stress. As pointed out in eq. 2.34, simple Mohr-Coulomb theory predicts fault planes inclined to the σ_1 -direction by an angle equal to $\pi/4 - \phi/2$. Along with eq. 3.3, which defines the orientation of the principal stresses, this relation allows us to calculate the magnitude of the step-up angle δ as a function of μ , μ_b and $S_0/\rho gH(1-\lambda)$, the ratio between cohesion and overburden. Assuming that $\mu = \mu_b = 0.85$, then Namson's observation that $\delta=13.8^\circ$ leads (Figure 3.12) to the conclusion that $S_0/\rho gH(1-\lambda) \approx 0.33$.

The insensitivity of the calculated S_0 to the wedge friction coefficient (Figure 3.12) suggests that $S_0/\rho gH(1-\lambda)$ for $\mu_b=0.85$ is determined to within a factor of less than 2. Near the toe, wedge thickness $H \approx 5$ km and $\rho \approx 2.4$ g/cm³. Thus, this method predicts that $S_0 \approx 12$ MPa, in excellent agreement with the previously mentioned rough estimates based upon wedge taper near the toe.

As previously mentioned, the assumption that $\mu_b = 0.85$ is not necessarily correct. If we assume that $\delta = 13.8^\circ$, then we can plot the relationship (Figure 3.13) between μ , μ_b , and $S_0/\rho gH(1-\lambda)$. The region above and to the left of the curved line in Figure 3.13 corresponds to cases in which the *décollement* would be stronger than the wedge. This line deviates from a simple $\mu=\mu_b$ curve to the extent that $S_0 > 0$, because cohesion permits wedges with μ somewhat less than μ_b . Solutions in the left part of Figure 3.13 ($\mu_b < .5$) cannot be unequivocally ruled out. However, such solutions require very low values of the cohesive strength, even when normalized by internal friction. Therefore, higher values of μ_b are considered to be most consistent with the presence of a large undeformed Hubbert-Rubey type toe in front of the Taiwan wedge. In addition, there is less fractional difference between wedge and *décollement* strengths for smaller values of μ_b . Thus, for smaller values of μ_b , thrust fault step-ups should take on an increasingly listric (sled-runner) geometry. There is no indication of highly listric fault geometries in the

fold-and-thrust belt of western Taiwan (Suppe, 1980a, 1980b; Namson, 1982). I therefore conclude that cohesive strengths compatible with the wedge taper are most consistent with the step-up data for high values of μ_b . These data suggest that $\mu_b > 0.55$, and are entirely consistent with a high-strength Byerlee 'law' friction of $\mu_b = 0.85$.

The most important result of the Coulomb-wedge analysis of western Taiwan is that the frictional and fracture properties commonly measured in rock mechanics experiments are consistent with the observed cross-sectional shape of western Taiwan, given the observed fluid pressures and décollement dip. This result suggests that the Coulomb wedge model is essentially correct as a first-order theory, particularly in light of the sensitivity of wedge taper to fluid pressure ratio. A slightly different fluid pressure ratio would predict a surface slope substantially different from that observed.

3.5 EROSION AND ISOSTASY IN TAIWAN

The omission of two additional factors from the analysis of Chapter 2, erosion and isostasy, can be justified by an examination of the behavior of the Taiwan wedge. Because erosion is known to take place in Taiwan at a rate of roughly 5mm/yr, it could be suggested that the taper should never reach its critical value, but should always be somewhat smaller. This could seriously affect our result, particularly if the erosion takes place in a geographically selective manner (i.e., with more erosion at

high altitude, even though the relief might not be any greater).

The effect of erosion upon the validity of this result is dependent upon the relative rates of operation of erosion and uplift. If erosion acts much more quickly to destroy topography than thrusting acts to restore it, then the wedge cannot attain its critical taper. However, if the state of stress in the wedge "senses" the reduction of taper due to erosion as the erosion is taking place, and the wedge responds by deforming on a time scale which is small compared to that which characterizes the erosion, then the wedge should not deviate appreciably from its critical taper.

The oblique nature of the arc-continent collision which builds the island of Taiwan gives us a convenient way in which to determine the relative time scales of erosion and the tectonic response to that erosion. As one walks from the southern end of the island of Taiwan towards the north, one walks through parts of the wedge which emerged from the sea at increasingly earlier times in the past as the oblique arc-continent collision propagated to the southwest at 90 mm/yr. The northernmost part of the island emerged from the sea roughly 4 million years ago, but the southern tip of the island is just now being lifted above sea level (Suppe, 1981). At the southern end of the island, where there is only a very limited amount of topographic relief, erosion cannot be a very important

factor. At the extreme northern end of Taiwan, the collision of the Luzon island arc with the continental margin of China is complete, so active thrusting has virtually ceased, and is no longer important.

Throughout the central part of the island, which constitutes half of its length and over three quarters of its surface area, the cross-sectional shape is remarkably constant (Figure 3.5). This has been interpreted (Suppe, 1981) to mean that for most of its history, any given cross-section through the island is in a state of topographic equilibrium. Thus, by looking at cross-sections starting in the south and proceeding northward, we can see that the history of any one of those cross-sections falls, in a general sense, into three stages. The southern end of the island is presently in stage 1 (which lasts slightly over 1 million years), during which thrusting associated with the new collision predominates, and the topographic profile rises with time. The middle of the island is currently in stage 2, which lasts ~ 2 m.y. During this period, thrusting acts just quickly enough to counteract the effects of continued erosion, and the island is in a sort of mass balance. During this stage, the island maintains a nearly constant width of 87 ± 4 km, and a cross-sectional area of 118 ± 24 km² (Suppe, 1981). In stage 3, which lasts somewhat less than 1 m.y., erosion finally wins out, as convergence ceases. This is currently taking place at the northern end of Taiwan.

It appears that as long as active convergence is under way, then the wedge remains on the verge of compressive failure everywhere, and thrusting acts to maintain the wedge taper just as fast as it can be destroyed by the effects of erosion. Therefore, it seems reasonably safe to assume that erosion does not appreciably affect the wedge taper whenever active thrusting is underway.

Isostasy can also be ignored without adversely affecting our results. The action of isostasy may, depending upon the rate of erosion, act either quickly or slowly compared to the rest of the wedge mechanical system. However, isostatic adjustment to accretion and overthrusting of sediments does not act to change the wedge taper. It merely tilts the wedge downward, exchanging a certain quantity of topographic slope for an equal amount of basal dip. Because the coefficient R in equations 2.19 and 2.20 is never greater than one, this can only act to make a previously critical wedge subcritical, thus leading to further thrusting. Thus, the calculation of critical taper, which is in reality a calculation of surface slope based upon a given dip of the basal décollement, is not affected by isostasy.

In other areas of active plate compression we have fewer constraints on décollement dip, fluid-pressure gradient, and fault geometry than in Taiwan. Therefore, as we explore the mechanics of other compressive wedges, we will keep in mind the insights learned from our well-

constrained Taiwan example.

3.6 WEAK DECOLLEMENT

We have seen that the mechanics of the Taiwan fold-and-thrust belt is best explained by assuming that the basal décollement is of a strength comparable to (only 15% to 20% less than) that of the wedge itself. However, not all rocks are strong. Given the presence of a relatively weak stratigraphic horizon, that horizon is likely to become the preferred décollement horizon.

Salt is a very weak rock, having a confining-pressure-independent strength of only 500 kPa for moderate ($10^{-13}/s$) strain rates even at temperatures as low as $100^{\circ}C$ (Carter et al., 1982). It is associated with thrust belts in the Zagros (Stocklin, 1968) and the Salt Range of Pakistan (Seeber and Armbruster, 1979; Seeber et al., 1981). Let us consider the effects which the presence of a salt décollement should have upon the mechanics of a thrust belt.

EFFECT OF A PRESSURE-INDEPENDENT YIELD STRESS

Let us replace the pressure-dependent resistance to sliding on the base of the wedge

$$\tau_b = \mu_b \sigma_z^* = \mu_b (1-\lambda_b) \rho g H \quad (2.8)$$

with a pressure-independent equation

$$\tau_b = \tau_Y \quad (3.4)$$

where τ_Y is the weak yield stress of salt described above. The corresponding subaerial critical taper equation is obtained by substituting $\tau_Y/\rho g H$ for $(1-\lambda_b)/\mu_b$ in eq. 2.18

and removing the submarine terms (ρ_w/ρ)

$$\alpha + \beta = \frac{(\tau_Y/\rho gH) + \beta}{1 + (1-\lambda)K} \quad (3.5)$$

where K is determined by the same method as used in Chapter 2 for a strong décollement. At the upper surface of the wedge, $\psi_t = 0$, so the integrand of the equation for K, eq. 2.17, is given by

$$\frac{1}{\csc\phi \sec 2\psi_t - 1} = \frac{1}{\csc\phi - 1} = \frac{\sin\phi}{1 - \sin\phi} \quad (3.6)$$

The corresponding expression for the base is somewhat more complicated. Following the analysis for a frictional ($\phi_b > 0$) décollement (Chapter 2), using simple trigonometric relations for triangles BCD and OAC in Figure 2.6a, we have

$$\frac{1}{2} (\sigma_x^* - \sigma_z^*) = \frac{\sigma_3^*}{\sec 2\psi (\csc\phi - 1)} \quad (3.7)$$

and

$$\sigma_3^* = \tau_b \csc 2\psi_b (\csc\phi - 1) \quad (3.8)$$

From eq. 2.12, we have

$$\frac{1}{\csc\phi \sec 2\psi_b - 1} = \frac{\tau_Y}{(1-\lambda)\rho gH} \cot 2\psi_b \quad (3.9)$$

Because of the extreme weakness of salt, $\tau_Y \ll (1-\lambda)\rho gH$ even at moderate depths. With $\rho = 2.4 \text{ g/cm}^3$, $\lambda = 0.7$, and $\tau_Y = 500 \text{ kPa}$, $\tau_Y/(1-\lambda)\rho gH = 0.1$ at 700m depth and 0.01 at 7 km. With a Byerlee law wedge, ψ_b would be only 1.6° or 0.2° , respectively. Therefore, we can make the approximation

$$\frac{1}{\csc\phi \sec 2\psi_b - 1} \approx \frac{\sin\phi}{1 - \sin\phi} \quad (3.10)$$

so, in eq. 3.5, $K \approx 2\sin\phi/(1-\sin\phi)$. Reviewing eq. 3.5, we see that a wedge with a salt *décollement* requires negligible amounts of both surface slope and overall taper, even in the absence of wedge cohesion. Although Eq. 3.5 does not strongly constrain β , in practice, a wedge with negligible topographic slope is unlikely to bow down to the basement which it overrides enough to produce a large β .

APPLICATIONS

The Zagros fold-and-thrust belt of southwestern Iran is located at the northeastern margin of the Arabian continental crust, folded during Plio-Pleistocene times (Berberian and Berberian, 1981). In addition to the Upper Cambrian Hormoz Salt, much of the Zagros area is underlain by evaporites of Triassic, Jurassic, Eocene and Miocene ages, often giving three separate layers of decoupling (Berberian, 1981). Despite its great length perpendicular to strike (roughly 300 km), the topography is rather subdued, reaching peaks of between 2 and 4 km (Kadinsky-Cade and Barazangi, 1982; U.S. Army Topographic Maps). Thus, the mean topographic slope, insofar as it can be defined, is considerably less than 1° , a value markedly smaller than that of the strong-*décollement* Taiwan thrust belt. Even this topography is irregular; this thrust belt does not truly possess a taper.

The fold-and-thrust belt of western Tadjikistan also has both a salt *décollement* and a marked lack of taper. The filling of the reservoir behind the Nurek dam has

been accompanied by induced seismicity (Simpson and Negamatullaev, 1981), the distribution of which is apparently dependent upon anisotropy of permeability (Leith et al., 1981). That induced seismicity occurs, even in regions favored by local structure, is interpreted to indicate that the thrust sheet within which the earthquakes occur slides atop its salt décollement at a state of stress within a few hundred kPa of horizontal compressive failure (W. Leith, personal communication, 1983). The apparent proximity of the stress state to horizontal compressive failure is required for a thrust belt at critical taper. The lack of taper of this critical wedge matches the prediction for a salt décollement.

The Salt Range of Pakistan is interpreted to be an upthrown block of a low-angle thrust fault along a salt horizon (Seeber and Armbruster, 1979), in which seismic deformation appears to be confined to the shallow-cover sediments (Molnar et al., 1973; McPowell, 1979). Like the Zagros, it has an extremely low surface slope. The entire Hazara-Salt Range area, at the extreme northwestern end of the Himalayan arc, is underlain by salt.

Seeber et al. (1981) have pointed out the close relationship between the geometry of the Himalayan syntaxis and the availability of a salt décollement. The Hazara thrust is essentially a southwestward extension from the northwestern end of the Himalayan Main Central Thrust. The front of the overthrusting deformation extends sharply

forward (southward), where it overrides a weak salt décollement, although Seeber et al. (1981) are not specific about whether the mechanism is associated with gravity gliding or a horizontal push. This forward projection of the basal thrust and the associated lower mean topographic slope of the thrust zone are, according to wedge theory, entirely consistent with the presence of a salt décollement. Because of its weaker décollement, the part of the thrust which is riding upon a layer of salt does not require as great a taper as the other parts of the thrust. Because only that part of the thrust which overrides a salt décollement can extend forward without appreciable taper, the surficial expression of thrusting responds directly to the presence of a discontinuous salt décollement.

In summary, mountain belts with salt décollement are observed to have very low mean topographic slopes, as predicted by theory. Despite the very low level of shear stress which can be resolved across such a décollement, the state of stress in the thrust sheet above appears to be very close to horizontal compressive failure.

3.7 THE HIMALAYAS AND THE BRITTLE-DUCTILE TRANSITION

In the preceding section, we have seen the effects of a weakening of the décollement of a thrust belt due to the presence of a weak rock such as salt. It is also possible for the décollement to become weak because it is so deep that thermally activated deformation mechanisms have become

important. Extrapolation of laboratory rock-deformation experiments (Brace and Kohlstedt, 1980) and analysis of the depths of earthquakes away from plate boundaries (Chen and Molnar, 1983) suggest that the brittle-ductile transition, at which rocks become weaker, is located at mid-crustal depths. The precise depth should be dependent upon rock type, strain rate, geothermal gradient, and pore pressure (Figure 3.14).

The Himalayan mountain belt, the site of some (but not all) of the closure associated with the Indo-Eurasian collision (Molnar et al., 1977) is one of the most important topographic features on earth, and it is the site of the highest topography on the planet. Its tectonics are very complex, probably involving at least some underthrusting of Indian crust and the piling up of slivers of Indian crust atop the Indian shield (Gansser, 1964; Le Fort, 1975; Lyon-Caen and Molnar, in press). The Indian plate is apparently flexed down under the weight of the Himalayas at a dip of approximately 3° beneath the Lesser Himalayas (Molnar, in press). Combined with the observed mean topographic slope of roughly 4° , and assuming that rock strengths are similar to those in Taiwan ($\mu \sim 20\%$ greater than μ_b) and that $\lambda_b = \lambda$, the wedge-taper equation (eq. 2.22) yields $\lambda \approx 0.76$ (Davis et al., 1983).

Passing from the Lesser Himalaya to the Greater Himalaya, décollement slip becomes increasingly more aseismic (Seeber et al., 1981), and as the dip of the Moho

increases to roughly 15° , the dips of the Main Boundary Fault and Main Central-Thrust also steepen (Molnar, in press). Rird (1978) and Molnar et al. (1977) have estimated upper limits to stresses in this region to be between 20 and 30 MPa. However, if we accept that the compressive wedge model of Chapter 2 permits somewhat higher stresses at moderate depths, then thermal weakening at the brittle-ductile transition should have major effects upon the mechanics of the wedge where its *décollement* reaches such depths. These effects are illustrated in Figure 3.15. Note the close match between the drop-off in topographic slope and the predicted depth (approximately 15 km) of weakening of the basal *décollement*. This correspondence is taken to be strong circumstantial evidence that the brittle-ductile transition has been resolved tectonically to occur at a depth in good agreement with that predicted by rock mechanics and seismological evidence. This transition is not observed in Taiwan for the simple reason that the Taiwan thrust belt is too small to attain such depths.

3.10 CONCLUSIONS ABOUT THRUST BELT MECHANICS

The idea that fold-and-thrust belts have the mechanics of bulldozer wedges at failure in horizontal compression has been verified quantitatively in this chapter. The observed taper of the western Taiwan fold-and-thrust belt can be matched by assuming that the coefficient of basal sliding

friction μ_b is 0.85, and that a somewhat higher effective internal friction applies near the toe, $\mu' \approx 1.03$. The difference between μ_b and μ' required to fit the observed taper of the fold-and-thrust belt in western Taiwan is interpreted in terms of two aspects of deformation within the wedge. First, the pre-existing fractures are sufficient only to allow frictional sliding on a limited number of generally sub-optimally oriented surfaces; second, it is frequently necessary to fracture locked geological structures for continued deformation. By using observations of taper near the toe of the wedge, the effective internal friction can be resolved into internal friction and cohesion terms with a range of possible solutions centered around $\mu \approx 0.95$ and $S_0 = 13$ MPa. The taper is maintained, despite the destructive effects of erosion, by sequential imbricate stacking of relatively coherent sediment sheets (Chapple, 1978; Mandl and Shippam, 1981).

The Coulomb wedge model has clearly defined conditions under which it can be expected to cease to explain satisfactorily the overall mechanics of a thrust belt. A wedge with a very weak plastic base, such as salt, should exhibit considerably lower surface slopes than most other wedges. The Zagros mountains have such a low mean surface slope. In addition, topographic slope is predicted to level out at the back end of a very large wedge, where the basal décollement becomes weak. This prediction appears to be confirmed in the Himalayas.

In conclusion, the brittle rock strengths commonly measured in laboratory experiments are consistent with the observed regional topographic slope and the geometry of faulting in the Taiwan fold-and-thrust belt. No extraordinary mechanical properties, such as extremely elevated fluid pressures or extremely weak basal layers, need be called on to explain the process of mountain building in either Taiwan or, except where there is independent evidence of their existence, in any of the other mountain belts discussed.

FIGURE CAPTIONS

- Fig. 3.1 Tectonic and bathymetric setting of Taiwan, with velocity triangle for the arc-continent collision, assuming the plate motions of Seno (1977). Note the switch in subduction polarity which leads to the construction of the island of Taiwan (after Davis et al., 1983).
- Fig. 3.2 Cross-section through the Taiwan fold-and-thrust belt (after Suppe, 1980b).
- Fig. 3.3 Toe of the active western Taiwan fold-and-thrust belt, showing hypocenters of microearthquakes near cross-section in foothills of southern Taiwan (after Suppe, 1980b; Wu et al., 1979; Davis et al., 1983). Seismicity at the toe is a good indication that the interior of the wedge is at or near its critical taper.
- Fig. 3.4 Observed fluid pressure/depth as a function of depth in three areas of western Taiwan (Suppe and Wittke, 1977; Suppe et al., 1981). The Tiehchanshan and Meilin areas are at the edge of the overthrust belt and have undergone little erosion. They display a permeable hydrostatic zone overlying the less permeable overpressured rocks. The Chuhuangkeng area is deeper in the fold-and-thrust belt, has undergone more erosion, and overpressured fluid pressure gradients reach essentially to the surface. It is considered

typical of the mountainous areas of western Taiwan. The overpressured values correspond to $\lambda = 0.7$ in these three areas and elsewhere in western Taiwan.

Fig. 3.5 Topographic profiles of western slope of central Taiwan in the region of steady state topography (see Suppe [1981] for locations). In all cases the topography can be well fit by a constant-slope regression. The mean slope of the set of profiles is $\alpha = 2.9^\circ \pm 0.3^\circ$.

Fig. 3.6 Regional tectonic cross section of south-central Taiwan near Chiai oriented N20°E, based on data of Suppe (1980b, 1981), Stanley et al. (1981) and Chi et al. (1981). The regional surface slope (a) of 2.9° in western Taiwan is well explained by (b) the critical Coulomb wedge theory with $\mu_b = 0.85$, $\mu = 1.03$, and $\lambda \approx 0.7$. This sensitivity to λ for fixed μ (c) is less than the sensitivity to μ with the fluid pressure ratio fixed at the observed value $\lambda = 0.675$.

Fig. 3.7 Surface slope α versus fluid pressure ratio λ for three basal dips $\beta = 5^\circ, 6^\circ, \text{ and } 7^\circ$, with Byerlee's law $\mu_b = 0.85$ assumed on the basal decollement. Shaded box shows measured values of α and uncertainties in α and $\lambda = \lambda_b$ in western Taiwan. The best fitting effective coefficient of internal friction (with $S_0=0$) is $\mu = 1.03$.

Fig. 3.8 Basal dip β versus fluid pressure ratio λ for the topographic slope observed in western Taiwan, $\alpha = 2.9^\circ$. The shaded box indicates the ranges of β and λ compatible with observations.

Fig. 3.9 Values of μ_b and μ consistent with the geometry of the western Taiwan thrust belt, having $\alpha = 2.9^\circ$ and $\beta = 6^\circ$, are illustrated. $S_0=0$ is assumed. For the measured fluid pressure ratio $\lambda \approx 0.7$, values between $\mu = \mu_b = 0.2$ and $\mu = \mu_b = 1.75$ can satisfy the data. With Byerlee's law $\mu_b = 0.85$ on the base, the effective coefficient of internal friction is $\mu = 1.03$. The set of possible solutions for $\lambda = \lambda_b$ is confined to the upper-left half of the figure ($\mu > \mu_b$) and is therefore limited to $0.2 < \mu_b < 1.75$ for $\lambda = 0.7$.

Fig. 3.10 Cross-sectional slice through the Taiwan wedge, illustrating variation in taper with distance from the toe for a cohesive wedge material (after Dahlen et al., 1982).

Fig. 3.11 Step-up angles of faults in northwestern Taiwan (after Namson, 1982).

Fig. 3.12 Step-up angle of a fault along the basal décollement as a function of dimensionless cohesion $[S_0/\rho g \bar{H}]$ and effective friction coefficient μ' , assuming that $\mu_b = 0.85$. \bar{H} is the effective depth to the décollement, equal to $(1-\lambda)$ times the depth.

Fig. 3.13 Dimensionless cohesion $[S_0/\rho gH]$ as a function of wedge and decollement friction coefficients μ and μ_b . The step-up angle is assumed to be 13.75° . Solutions are possible only below the curved line, corresponding to $\mu = \mu_b$. Note that for $[S_0/\rho gH] > 0.1$, then $\mu_b > 0.4$.

Fig. 3.14 Rock strength, as measured by the stress difference $\sigma_1 - \sigma_3$, versus depth in the earth, assuming frictional behavior $|\tau| = 0.85 \sigma_n^*$ for $\sigma_n^* < 200\text{MPa}$, and $|\tau| = 50 \text{ MPa} + 0.6 \sigma_n^*$ for $\sigma_n^* > 200 \text{ MPa}$ (Byerlee, 1978) near the surface and quartz plastic flow which is governed by $\dot{\epsilon} = 5 \times 10^{-6} (\sigma_1 - \sigma_3)^3 \exp(-0.19 \text{ MJ mol}^{-1}/RT)$, where $\dot{\epsilon}$ is in s^{-1} and $\sigma_1 - \sigma_3$ is in MPa (Brace and Kohlstedt, 1980) at depth. The plastic strength has been calculated for a range of geothermal gradients and geologically reasonable strain rates. The theoretical strength is greatest at the point of brittle-plastic transition, where the brittle and plastic strengths are equal.

Fig. 3.15 (a) Topographic profile across the Himalaya (south to left). Note flattening to the north. (b) Generalized cross-section of the central Himalaya, with interpretation of topographic flattening as an effect of plastic flow at depth (after Dahlen et al., 1982).

Figure 3.1

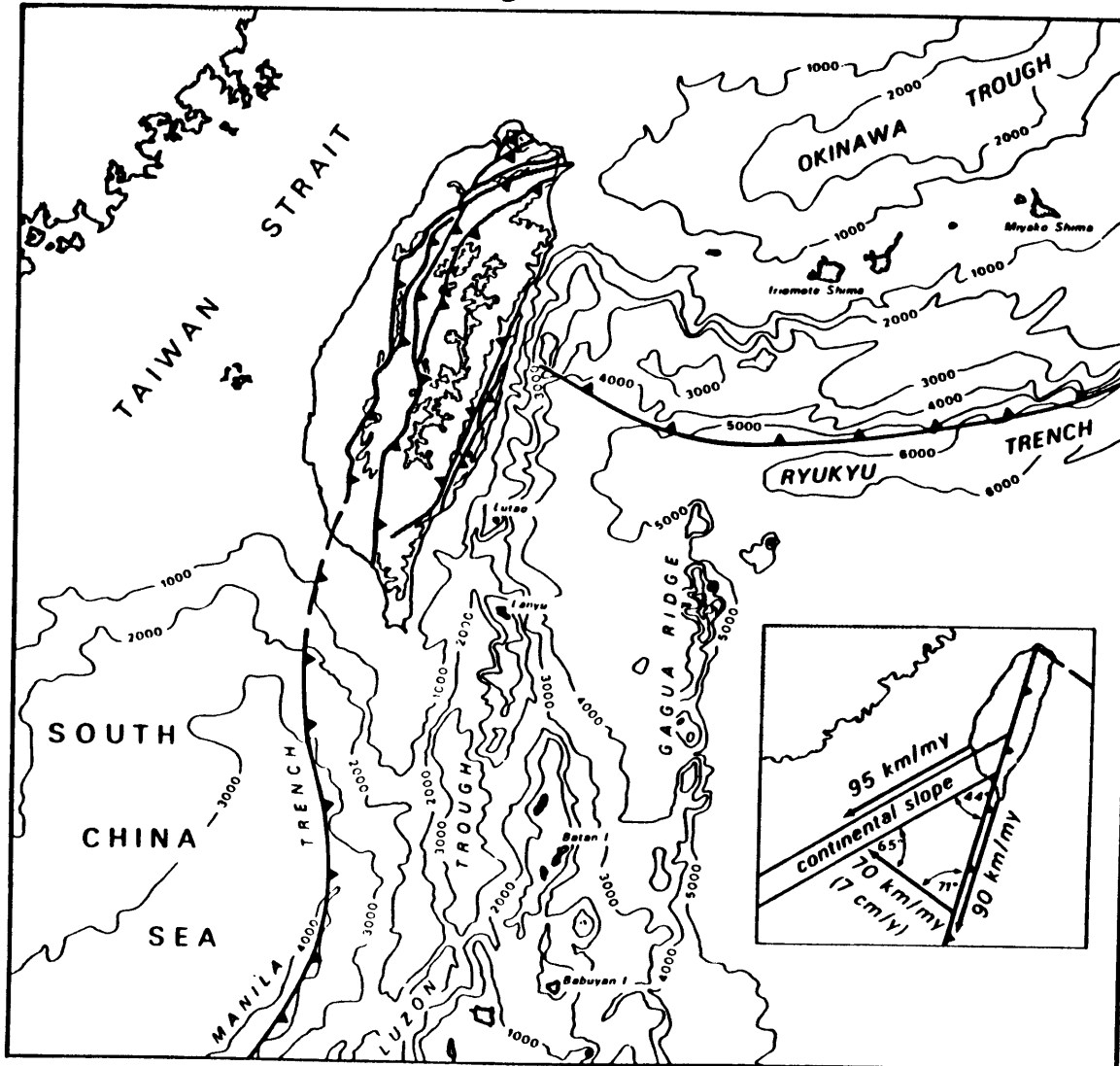


Figure 3.2

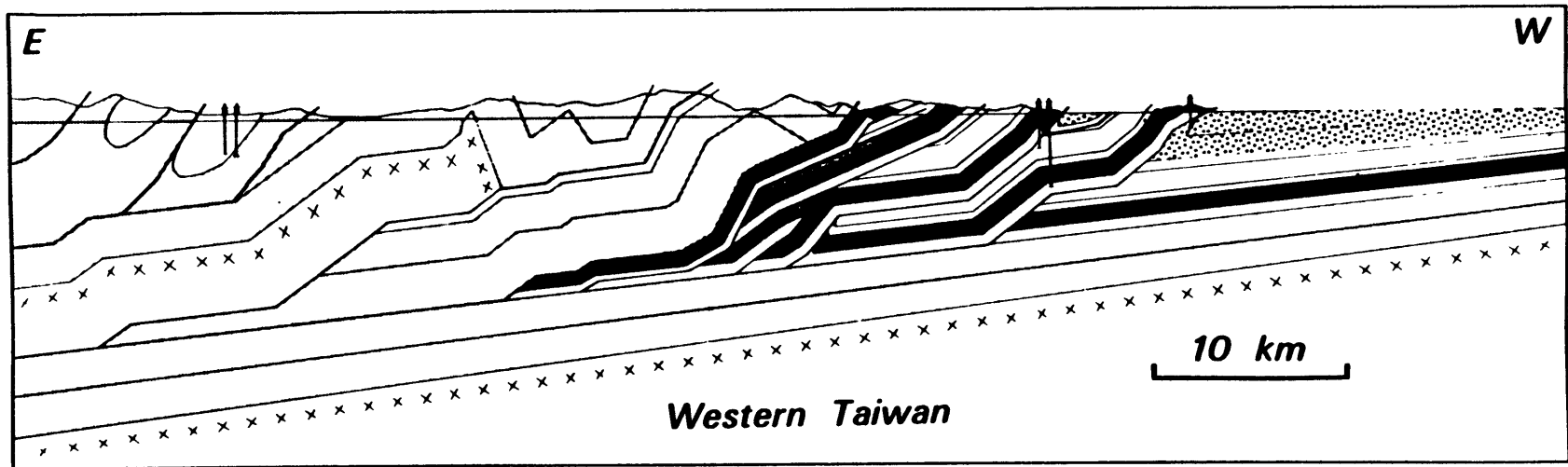


Figure 3.3

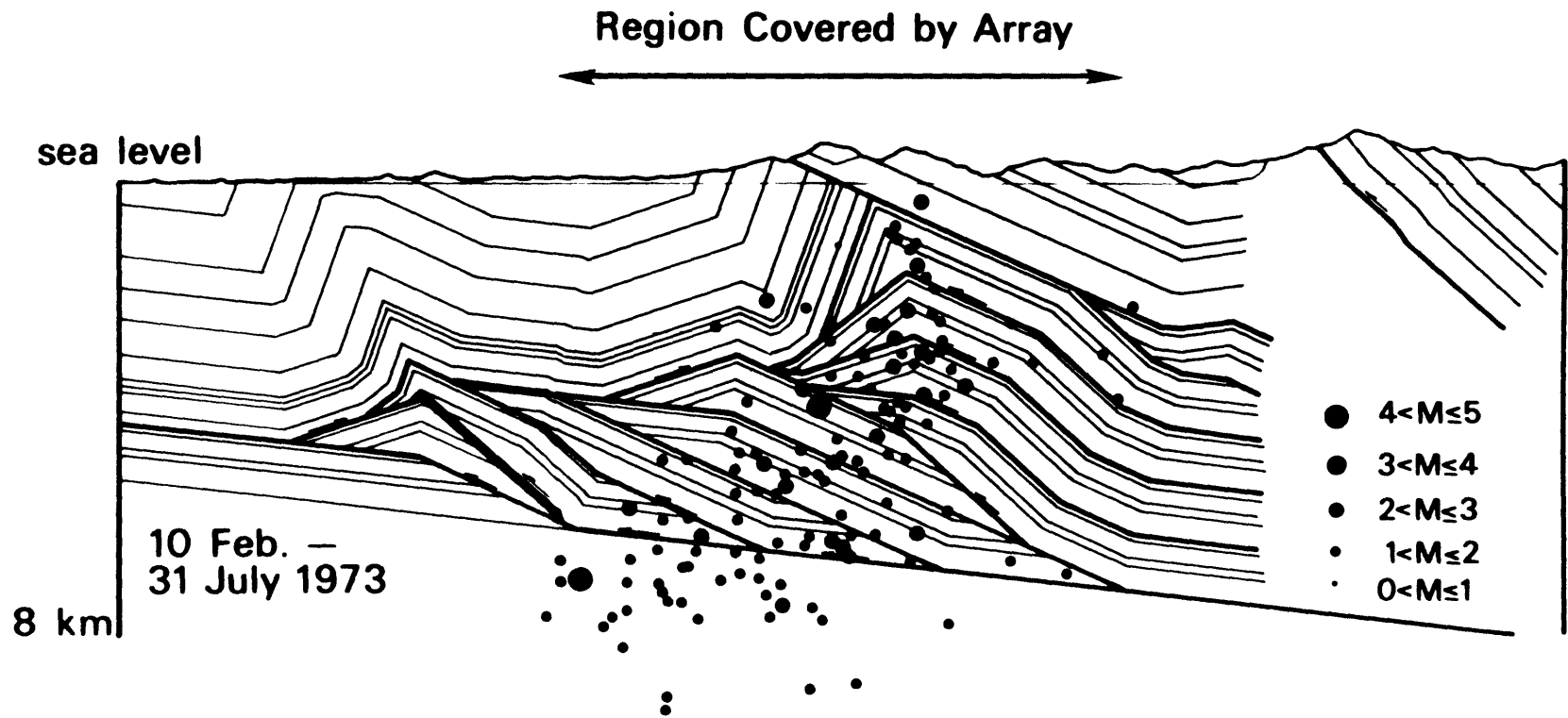


Figure 3.4

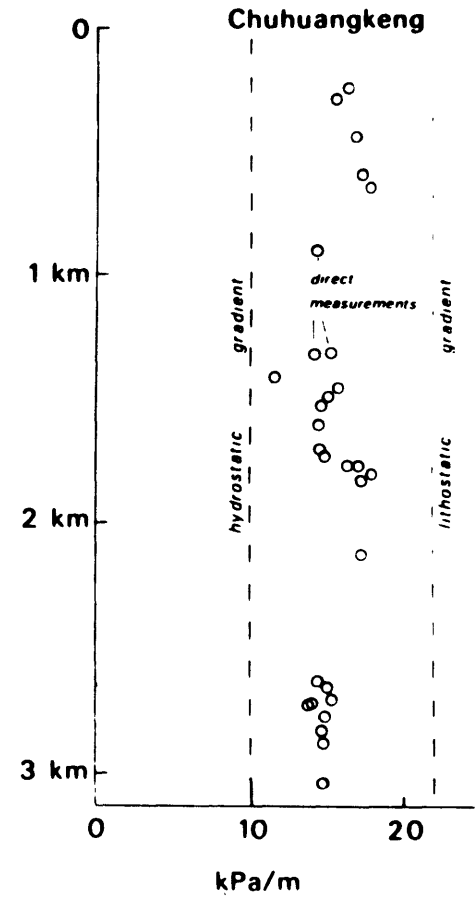
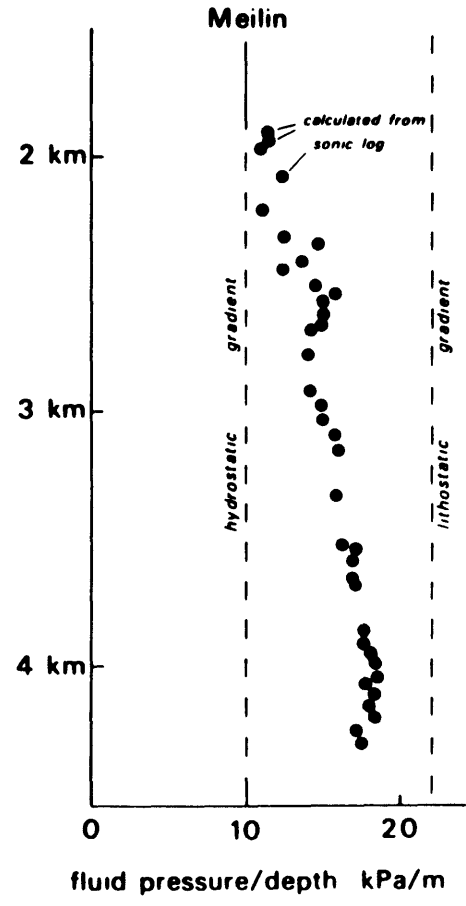
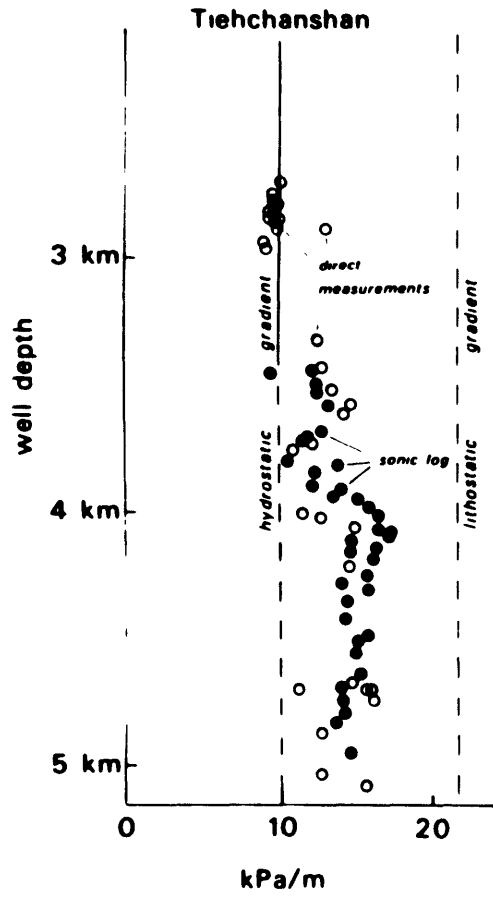


Figure 3.5

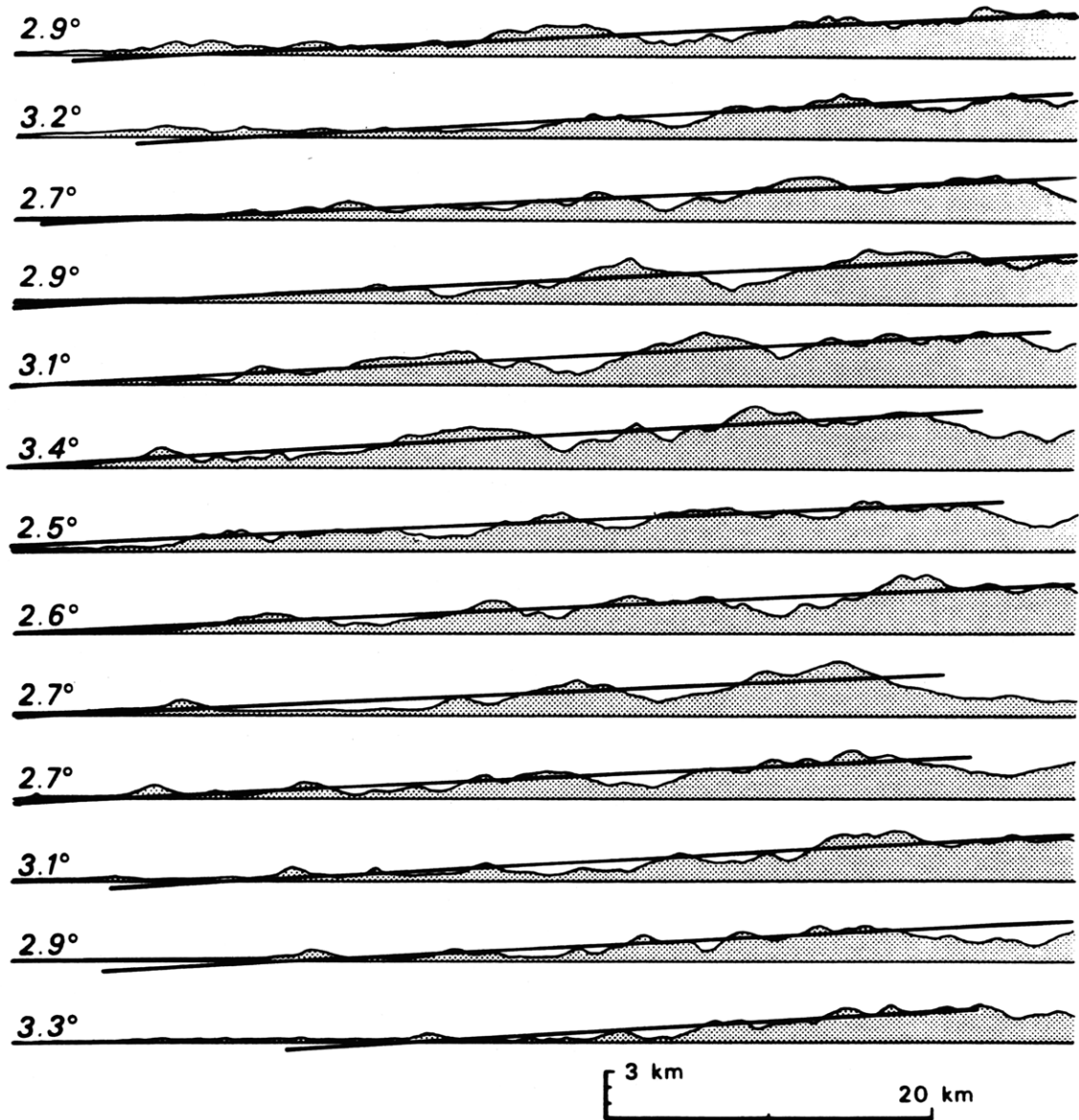
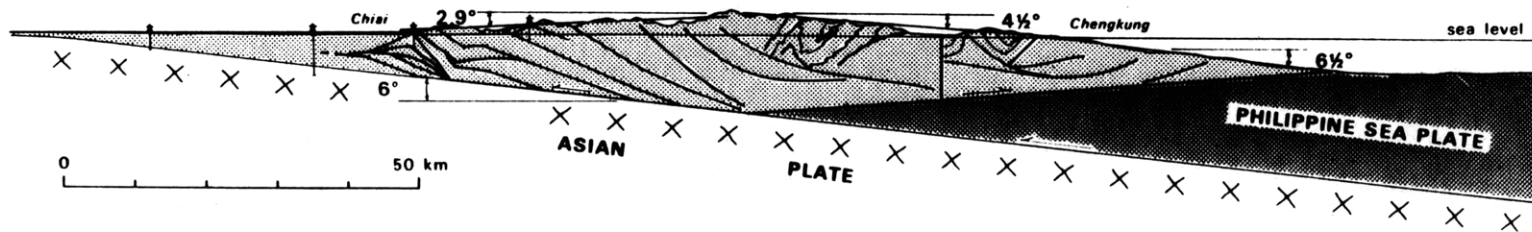
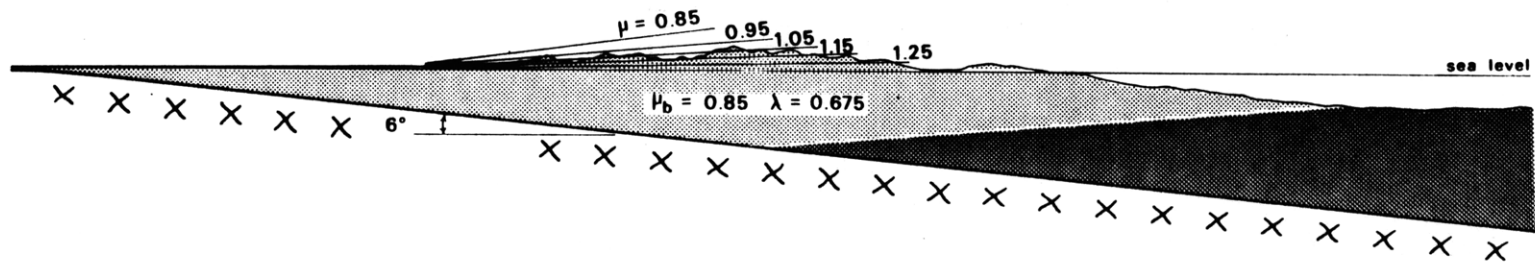


Figure 3.6

a)



b)



c)

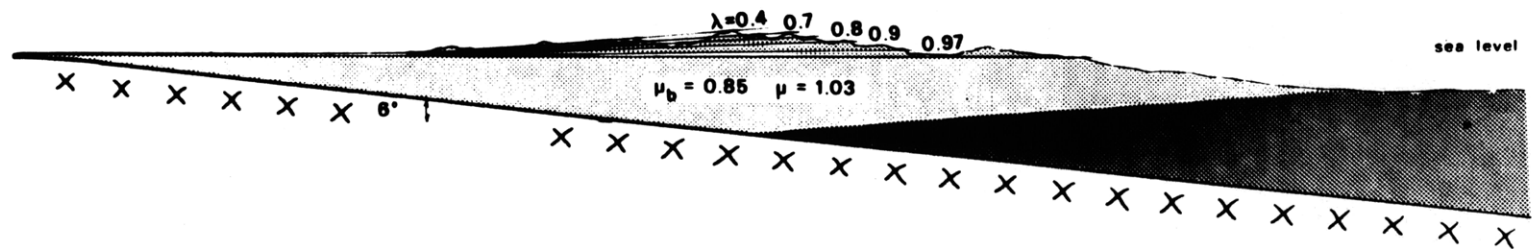


Figure 3.7

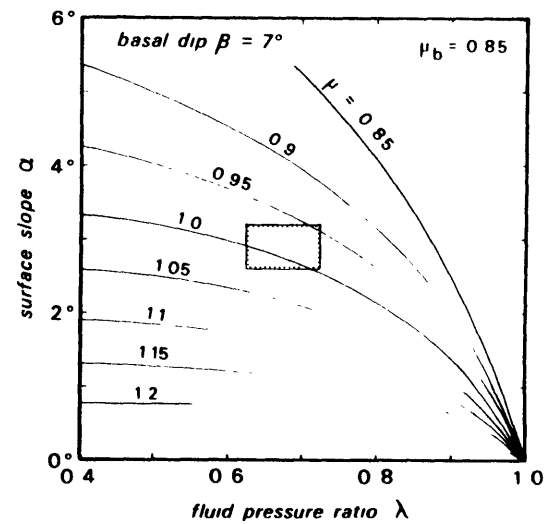
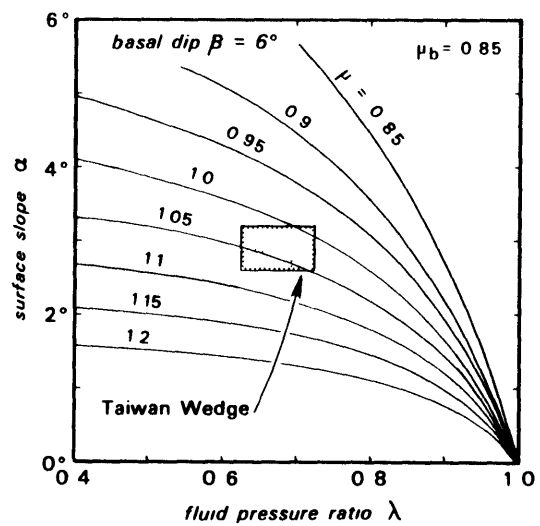
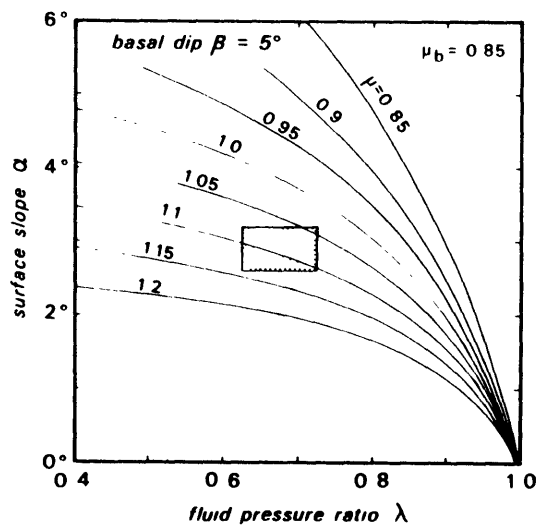


Figure 3.8

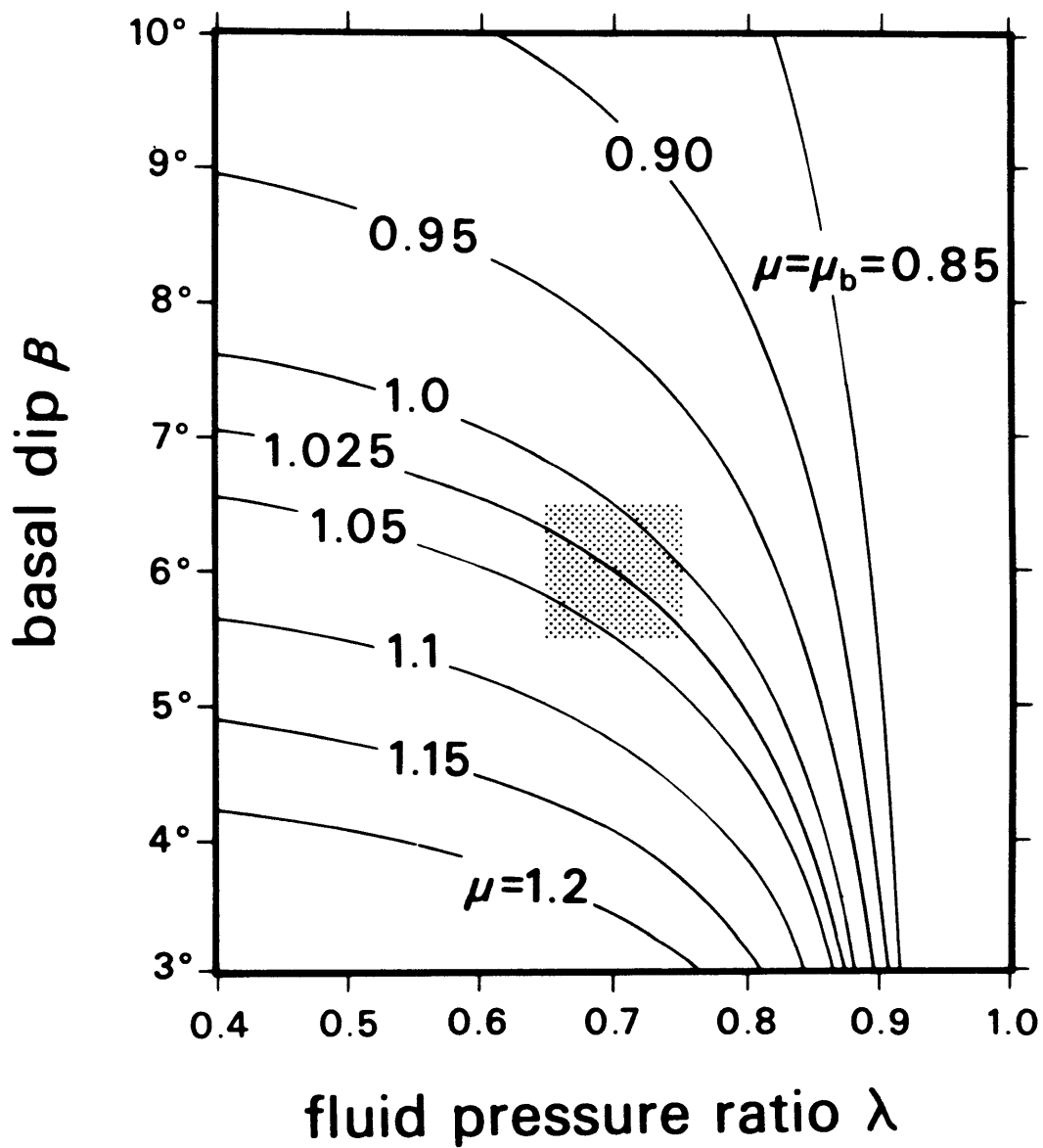


Figure 3.9

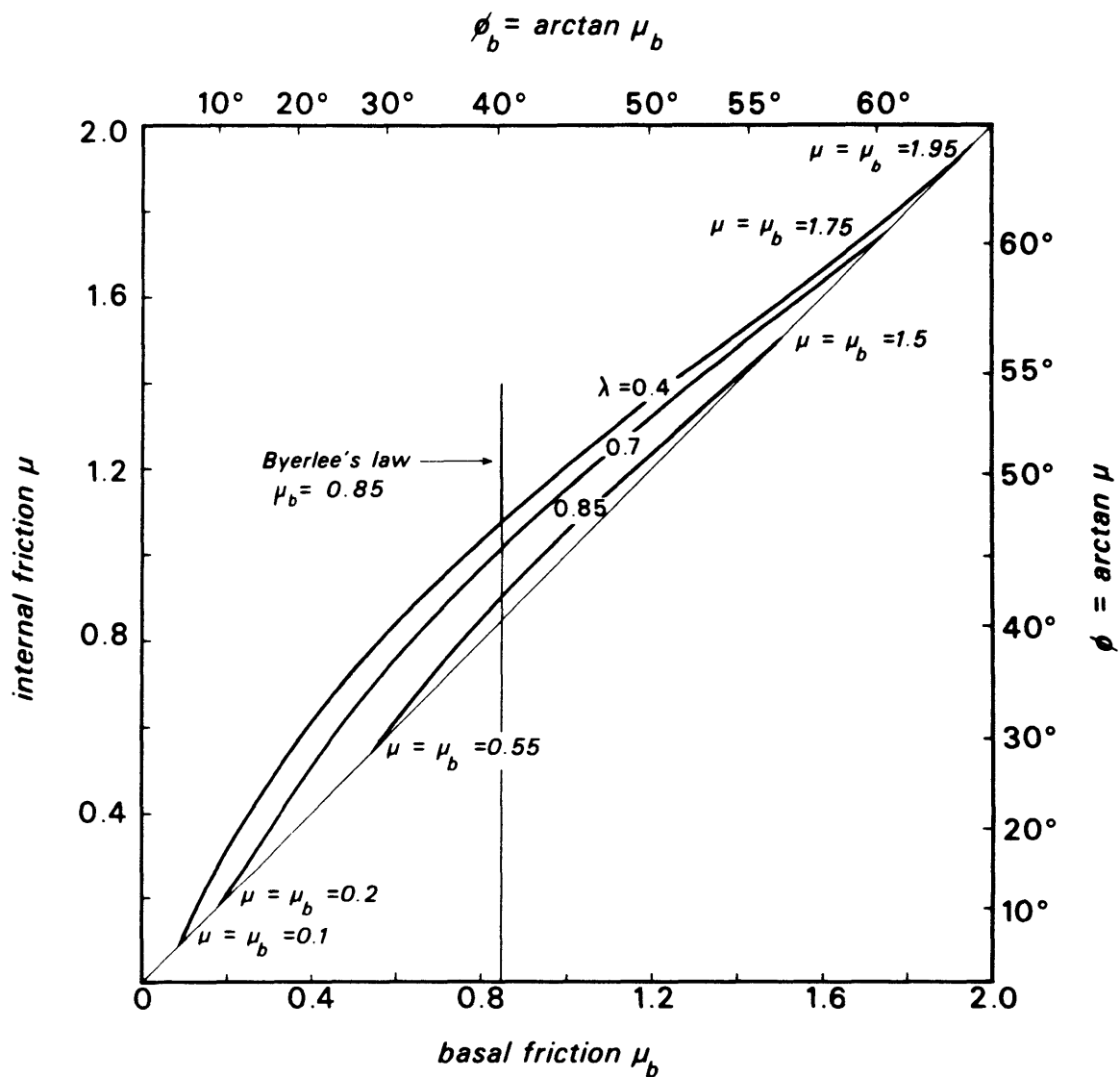
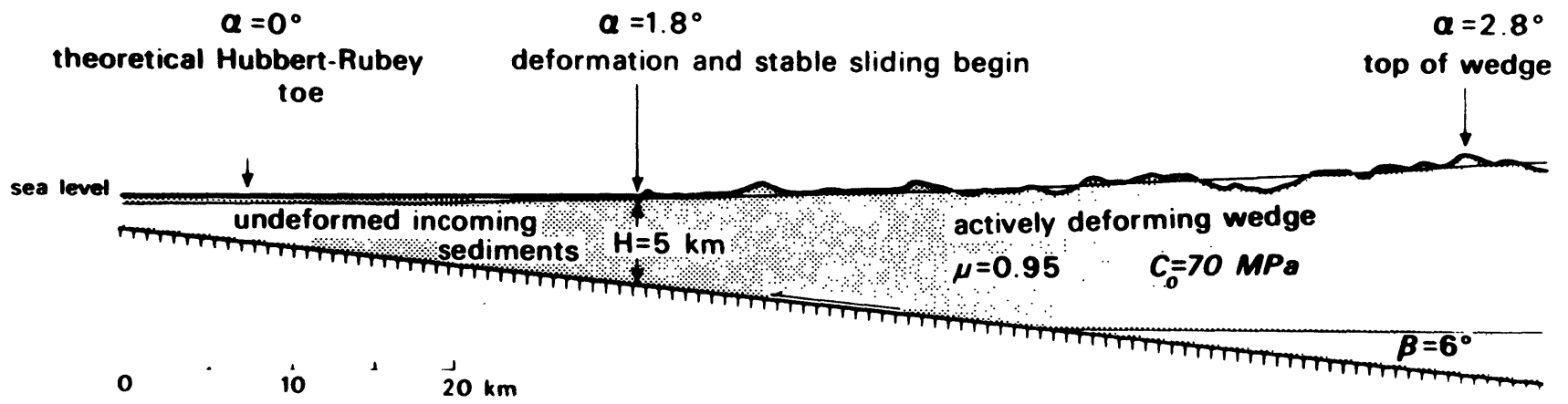


Figure 3.10



SOUTHERN TAIWAN

Figure 3.11

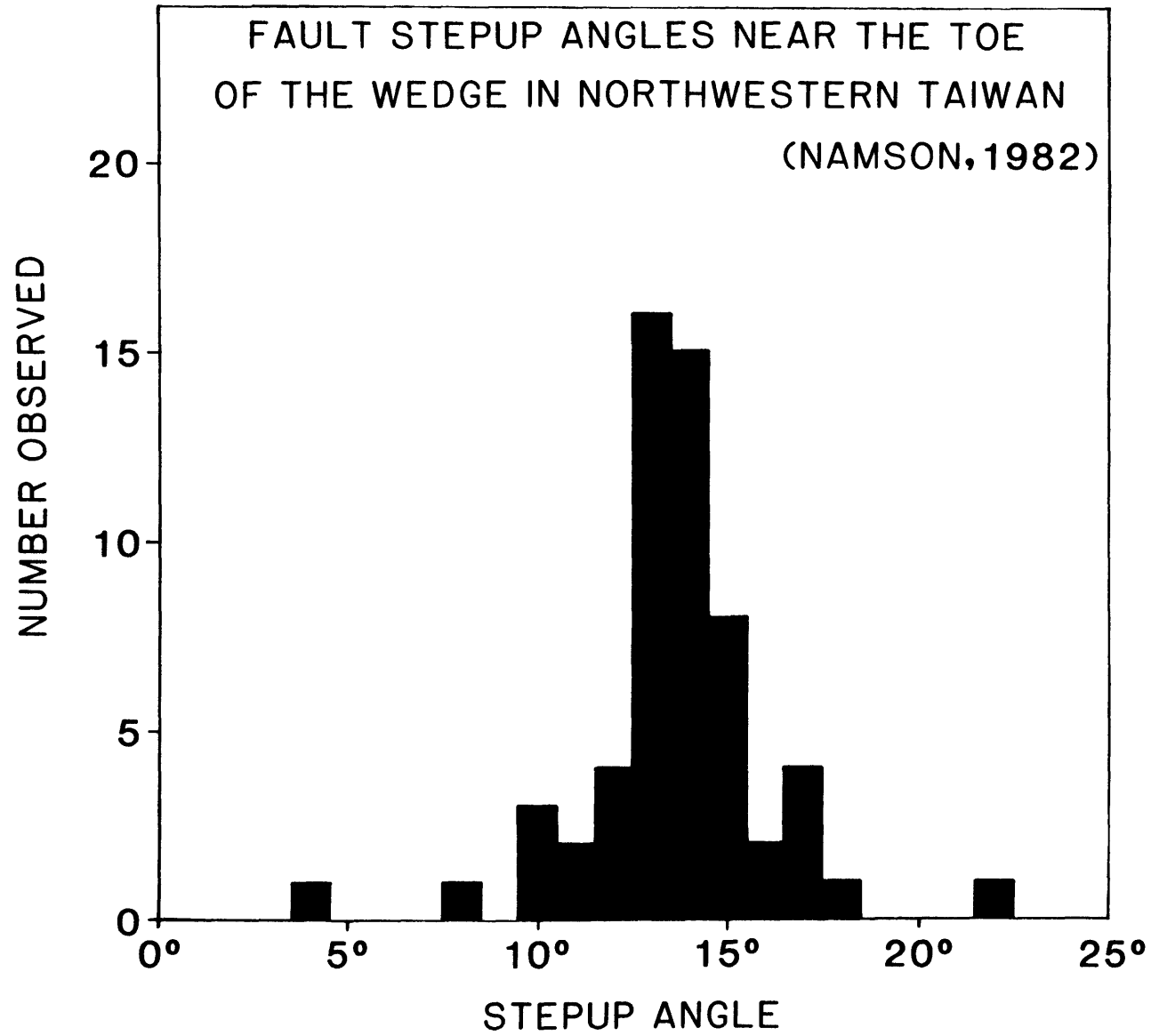


Figure 3.12

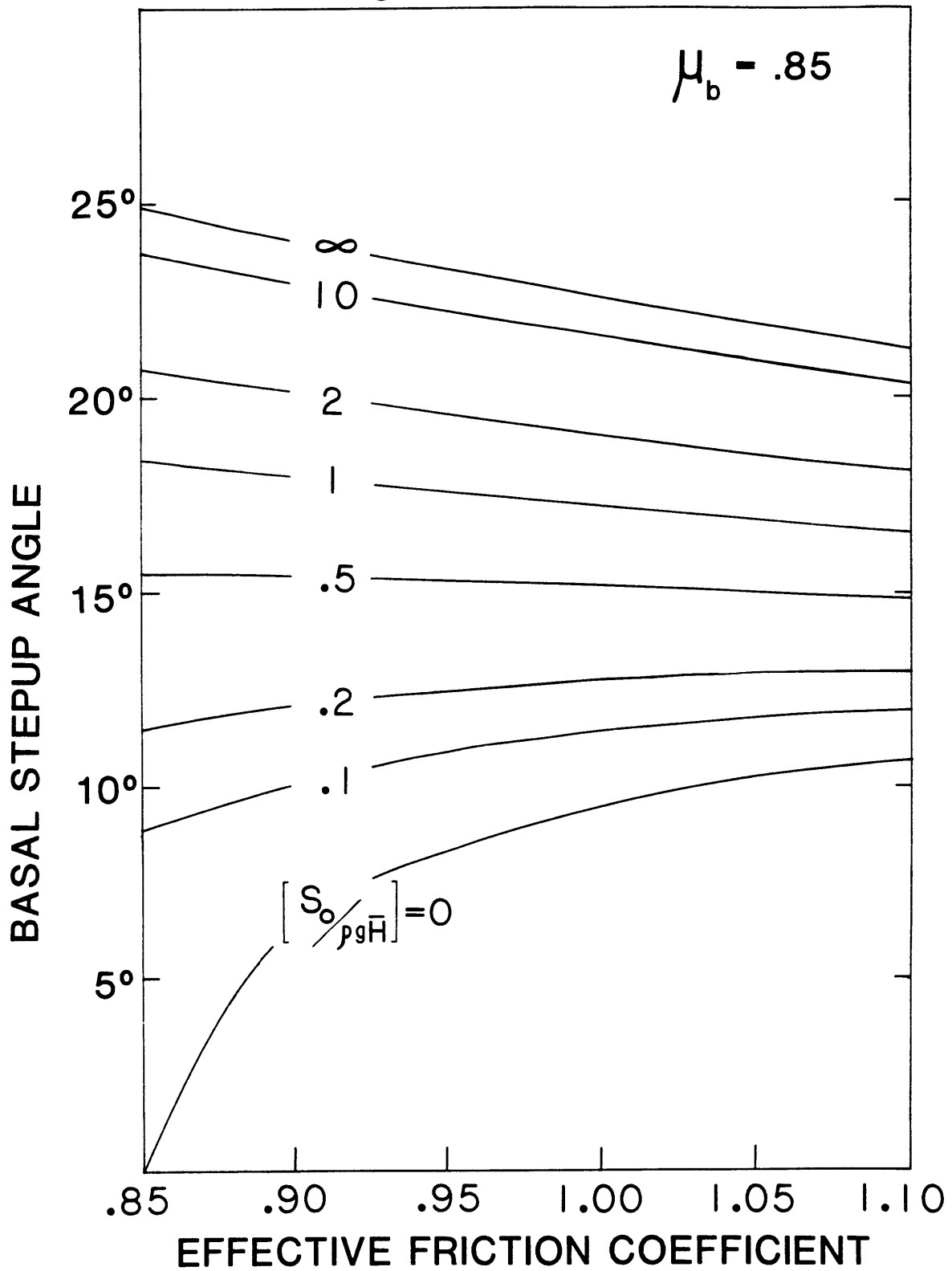


Figure 3.13

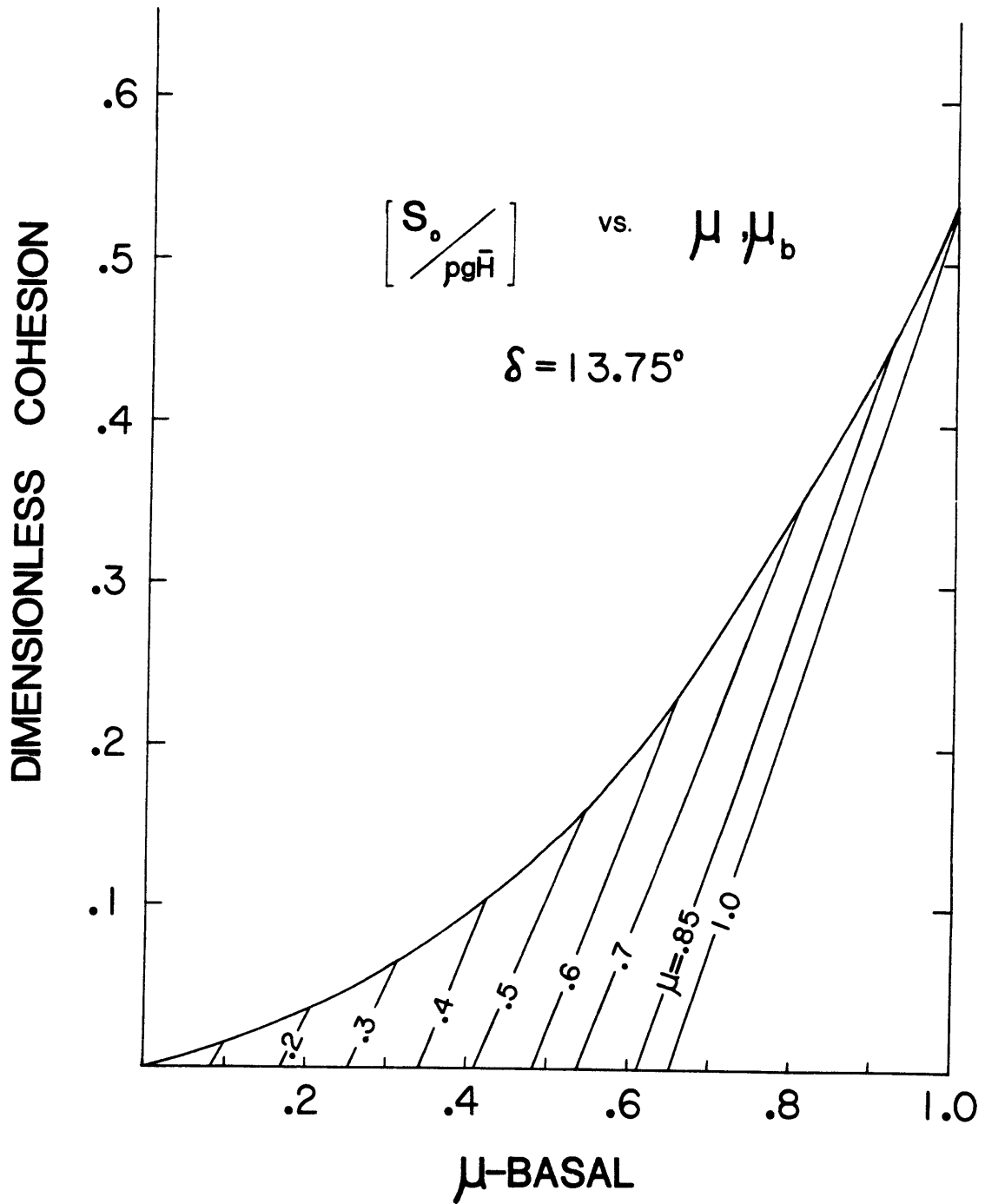


Figure 3.14

Strength MPa

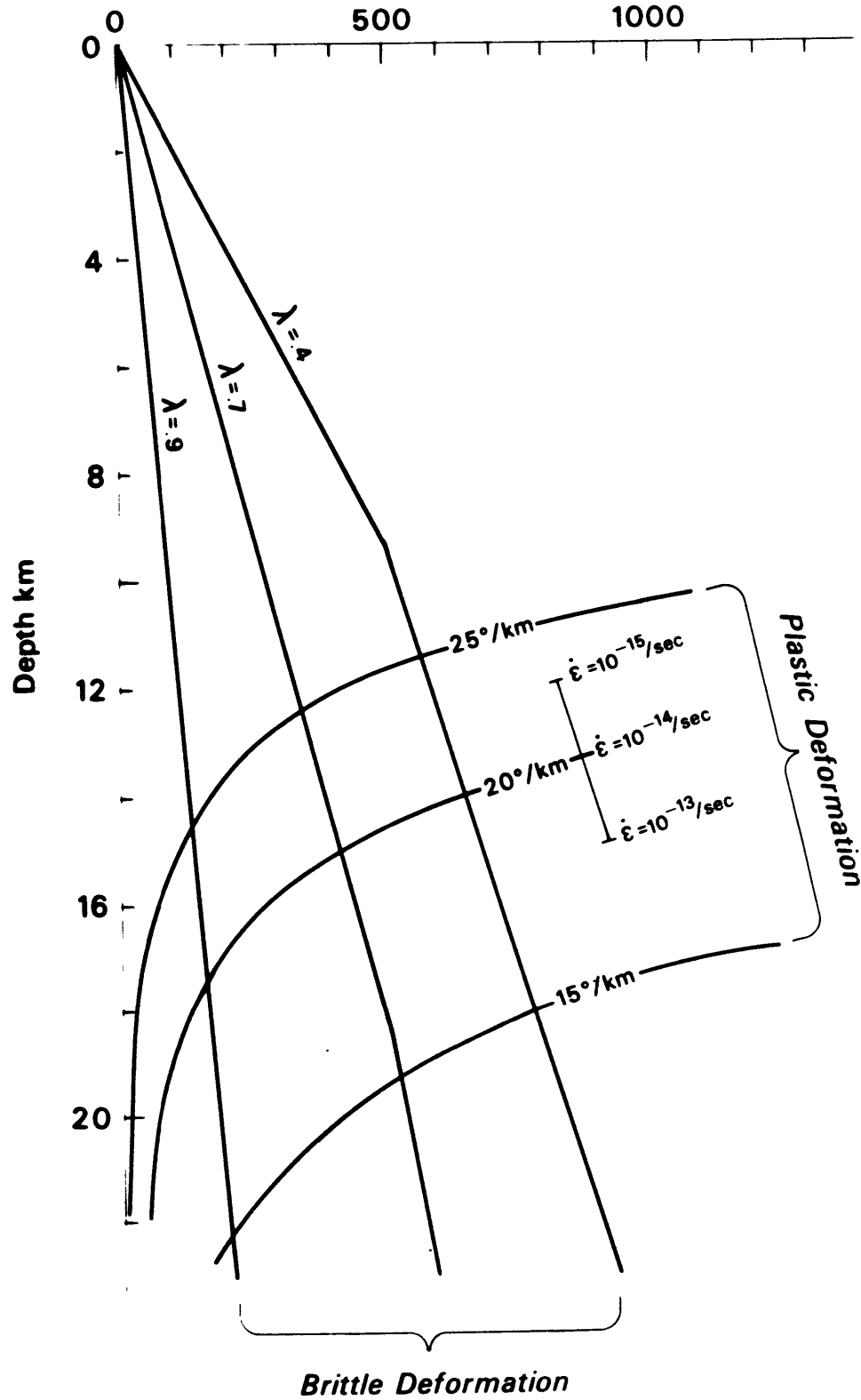
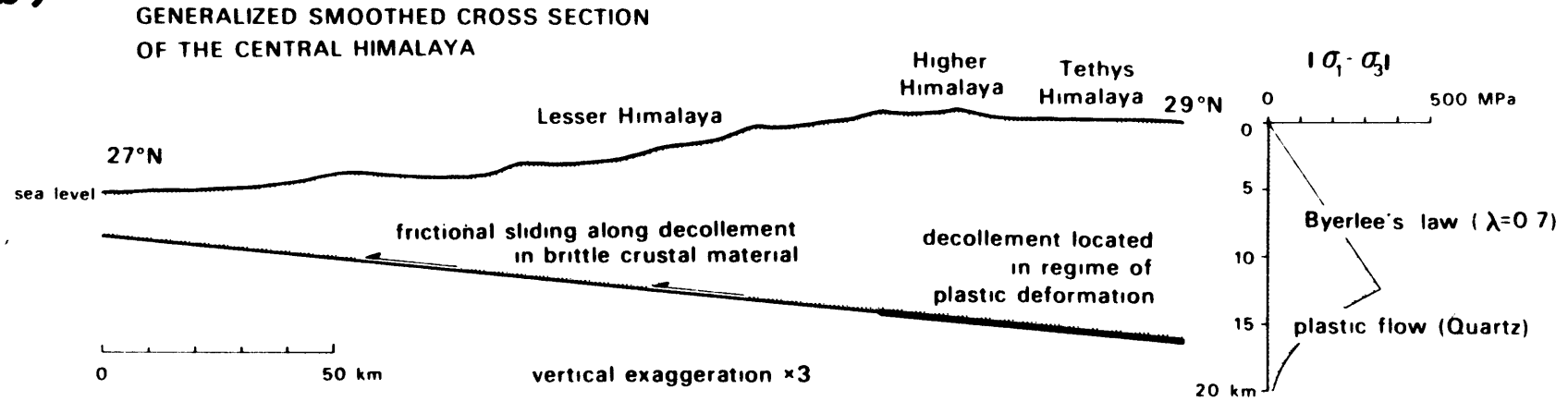


Figure 3.15

a)



b)



CHAPTER 4 MECHANICS OF ACCRETIONARY WEDGES

4.1 A MODEL FOR ACCRETIONARY WEDGES

The inner and outer walls of trenches are different in several ways. The outer wall is generally covered by only those sediments being rafted in atop the oceanic lithosphere, and its tectonics are typically dominated by the flexure of the oceanic lithosphere as it bends into the trench. However, the inner trench wall is typically the site of thrust faulting (Beck and Lehner, 1974), often within a large, wedge-shaped sedimentary body called an accretionary wedge or prism, although at a trench which is sediment-poor, such as part of the Peru-Chile trench, there may be little or no accumulated sediment (Schweller et al., 1981).

The accretionary wedge has been characterized by Seely et al. (1974) as being built up by a series of slivers of highly deformed accreted sediments, separated from each other by arcward-dipping thrust faults. As the process of accretion continues, new slivers are added to the front of the wedge, as older slivers are uplifted and rotated backward. The region apparently dominated by accretion and thrusting for sediments extends back to a topographic high, called the outer high or the trench slope break, which sometimes extends locally above sea level to form an island, such as Nias or Barbados. Behind the trench slope break, there is typically found a sedimentary basin, called the interdeep or the forearc basin (Seely et al., 1974; Karig and Sharman, 1975). Among the attributes of accretionary wedges

worth considering in this chapter are their variety, their relative aseismicity (Engdahl, 1977; Chen et al., 1982), and their frequently high pore pressures (Moore and von Heune, 1980). This chapter investigates several aspects of the mechanics of accretionary wedges (Figure 4.1), in light of the model of Davis et al. (1983) and Chapter 2.

4.2 BARBADOS TECTONICS

In this section, the mechanics of the wedge of accreting sediments at the eastern edge of the Caribbean plate, including the island of Barbados, are considered in light of the Coulomb-wedge hypothesis of Chapter 2. The narrow taper of the Barbados wedge is found to be consistent with the evidence which exists for high fluid pressures in the region. The hypothesis that the wedge is at or near compressive failure permits a description of the state of stress in the wedge. The borehole stability problems experienced at Sites 541 and 542 of DSDP Leg 78A are consistent with the view (Hottman et al., 1979) that boreholes act as stress concentrators, and that the stress concentration can lead to compressive failure of the borehole wall. This borehole instability comprises further evidence for a state of stress in which the wedge is on the verge of horizontal compressive failure.

Sites 541 and 542 of DSDP Leg 78A are located at the narrow frontal toe of the large accreting wedge of sediments located at the eastern edge of the Caribbean plate between

the plate boundary and the volcanic Lesser Antilles arc (Figures 4.2, 4.3). At this deformation front, oceanic crust of roughly 65 million year age is subducted to the west at a rate of 2.2 cm per year (Minster and Jordan, 1978). The sediments overlying the oceanic crust are partially accreted onto the overlying plate (Figure 4.4). This accretion and the subsequent compression of the sediments has resulted in the development of an imbricate-thrusting accretionary wedge (Seely et al., 1974; Westbrook, 1975). The wedge has grown outward to the unusually great length of roughly 200 km, and the trench has ceased to exist as a major bathymetric feature (Westbrook, 1982). Barbados, the only part of the wedge which is above sea level, is a local high point on the Barbados Ridge, which is near the back of the actively accreting wedge and which runs parallel to the deformation front (Westbrook, 1982; Speed and Larue, 1982). The relatively undeformed sediments of the Tobago Trough lie to the west of Barbados. Beneath the Tobago Trough and the Lesser Antilles the Benioff zone steepens to a dip of roughly 35° , but under most of the accretionary wedge the contact between the downgoing and overlying plates has a dip of only about 5° .

It has been shown that a sufficiently tapered wedge of Coulomb material can be pushed over a *décollement*, no matter how long it may be (Davis and Suppe, 1980; Davis et al., 1983). Let us investigate whether or not the available data concerning this accretionary wedge are consistent with a

tectonic setting dominated by horizontal compression.

Let λ be, in the manner of Chapter 2, the ratio of fluid pressure change divided by net increase in lithostatic overburden from the top surface of the wedge to any given depth within the wedge (eq. 2.6), and let λ_b be the corresponding ratio along the basal décollement. It has been observed (Fertl, 1976) that, in general, $\lambda_b > \lambda$. Unlike Taiwan (Suppe and Wittke, 1977; Davis et al., 1983), the Barbados wedge does not have very well-constrained pore pressures (Moore and von Huene, 1980). Therefore we shall, in general, make the conservative assumption that there is no sudden increase in the fluid pressure gradient at the basal décollement (which would greatly facilitate overthrusting) as we apply the theory presented in Chapter 2.

4.3 BARBADOS AS A COMPLICATED-RHEOLOGY WEDGE

Let us apply these results to the Barbados area. The crust of the overlying plate in this region is a narrowly tapered wedge showing a great deal of deformation. This deformation includes numerous thrust faults verging eastward, toward the deformation front (Westbrook, 1975, 1982). The basal décollement deepens westward at a dip of roughly 5° , and the mean bathymetric slope varies between 0° and 2° . These values are reasonably typical of sediment-rich accretionary wedges around the world, but the Barbados wedge has a somewhat narrower taper than most (Davis et al., 1983). The quantity of sediments available for accretion varies

considerably along strike, but, in general, a cross-section bears at least a superficial resemblance to the imbricated structure typical of accretionary wedges (Seely et al., 1974).

There is considerable north-south variation in the tectonics of the accretionary margin. The thickness of the incoming sediment pile atop the oceanic crust of the Atlantic varies by a factor of about 10; from 7 km near the South American continent to only 700 meters near the DSDP Leg 78A drill sites. Insofar as this affects the rate of accretion, it affects the amount of deformation required within the wedge in order to maintain the taper needed for overthrusting. The Tiburon and Barracuda rises (Figure 4.2) are lateral inhomogeneities which violate 2-dimensional assumptions made to simplify the problem of understanding the mechanics of the area. Also, the convergence direction becomes increasingly oblique to the north, presumably moving the direction of the greatest principal stress axis away from the direction perpendicular to the deformation, adding another 3-dimensional complication to the mechanics.

By making two assumptions, we can 'predict' the fluid pressure ratio in any part of the wedge which is above the brittle-ductile transition. First, we assume that the value of the fluid-pressure-gradient coefficient λ_b along the basal décollement is no larger than λ in the wedge. Because the onset of a zone of high fluid pressures is often controlled by a particular stratigraphic horizon (Fertl, 1976; Suppe and

Wittke, 1977) and the basal décollement is likely to be located in overpressured zones, this assumption is not necessarily correct. By assuming that $\lambda_b = \lambda$, we arrive at a value which is larger than that required for either λ or λ_b if the décollement is actually more overpressured ($\lambda_b > \lambda$) than the wedge (eq. 2.18). Thus, the assumption that $\lambda_b = \lambda$ gives a maximum value for the fluid pressure ratio required for the wedge to be at critical taper.

The second assumption which we make to predict the fluid pressure ratio is a result of the need to define the state of stress in the wedge which is close to failure. We assume that the wedge is highly fractured, so most deformation occurs along pre-existing faults. However, fractures do not exist in all possible orientations, so slip generally requires a somewhat larger stress difference $\sigma_1 - \sigma_3$ than would be needed for a slip plane at the optimal orientation. Occasionally, geometric locking of structures may require fracture instead of friction, bringing into play the relatively small cohesive strength of sedimentary rocks (Hoshino et. al., 1972). In Taiwan, where fluid pressures and wedge geometry are very well constrained, the wedge is about 20% stronger than the décollement (Chapter 3). This added wedge strength probably reflects sliding along sub-optimal slip planes due to a finite number of available slip planes, as well as occasional geometric locking. Pore pressures cannot be invoked to explain this strength difference in Taiwan, where $\lambda = \lambda_b$.

If the strengths of the Barbados wedge and *décollement* are similar to those in Taiwan, then the taper of this accretionary prism is consistent with relatively high values of $\lambda = \lambda_b$ ranging from ~ 0.85 in the wedge to ~ 0.97 near the toe. These estimates must be regarded as an upper bound; they would be reduced somewhat if the base of the wedge is weaker than expected. This can be the case either if the *décollement* is significantly 'lubricated' by weak clay minerals or if the fluid pressures there are higher than in the overlying rocks. Pore pressures are not known in great detail near Barbados. Because, unlike Taiwan, it is quite possible in the Barbados wedge that $\lambda_b > \lambda$, it is conceivable that there is no difference between the intrinsic strengths of the wedge and its base. Instead, the basal weakening, the existence of which is required by the narrow taper, may be a result of elevated fluid pressures.

Some scattered fluid pressure data exist for the region. Wells drilled on Barbados show elevated pore pressures (Figure 4.5), with λ at depth near 0.8 (Moore and von Heune, 1980). Also, an inadvertently performed packer experiment at Site 542 (Moore, 1983) gives indication of an approximately lithostatic fluid pressure ($\lambda \approx 1$) near the *décollement*. Using eq. 2.30 and assuming Byerlee friction and the fluid pressure ratios determined above, we find that shear stresses along the basal *décollement* are lower than for the Taiwan fold-and-thrust belt, remaining below 2 MPa throughout the wedge. Beneath Site 541, I find a value of τ_b 200 kPa.

At the deformation front near DSDP Sites 541 and 542, the depth to basement is so small (300-500 meters) that two complicating factors are introduced. First, the sediments may not have been buried at a sufficient depth for a sufficiently long time to have compacted and consolidated. This brings the Coulomb assumption into question in a wedge which is as thin at its toe as is the Barbados wedge. In addition, should the wedge material have a non-zero cohesive strength, it is at the narrow toe that the simplifying assumption that the material is cohesionless and that the first term on the right-hand side of eq. 2.1 can be ignored will be least appropriate. A cohesionless wedge is entirely scale-independent; it can be of any desired length and still be pushed from behind, as long as it has a sufficient taper. When the cohesive strength ceases to be much smaller than the effective normal strength at the base of the wedge (as may be the case near the toe), this assumption of scale-independence ceases to be appropriate.

Note that cross-sections of the Barbados wedge (Figure 4.4) show a very small degree of convexity in the upper surface of the wedge near the toe. It has been suggested (Dahlen et al., 1983; Davis, 1983) that this may be related to weak plastic behavior of the wedge material. Chapple (1978) assumed that the material in fold-and-thrust belts is governed by a single, normal-stress independent yield strength. Although inappropriate for most sediments, this assumption may be appropriate near the toe of the Barbados

wedge. However, unlike the rheology chosen by Chapple, this plastic behavior is not necessarily indicative of the intrinsic strength of the incompletely lithified near-toe sediments. The essentially lithostatic pore pressures observed during the Leg 78A inadvertent packer experiment (Moore, 1983) can effectively eliminate much of the depth-dependent component of strength in eq. 2.1. Therefore, particularly in light of the shallow depths involved, the mechanics of the toe of the Barbados wedge can be dominated even by the small shear strength of the material (Marlow and Lee, 1983) and an otherwise insignificant basal cohesion (Dahlen et al., 1983). Dahlen et al. (1983) have shown that both fault step-up angles and the convexity of the frontal 20 km of the Barbados wedge can be matched very closely by a plastic wedge behavior resulting from the essentially lithostatic pore pressure. Assuming that $\lambda = \lambda_b = 1$, $\mu = \mu_b = 0.7$, this analysis indicates that the décollement is only 5% to 10% weaker than the wedge, and that the wedge strength is between 300 and 500 kPa. These low values of the shear stress, and those determined above without the assumption of lithostatic pore pressures, are in close agreement with the cohesion as measured in samples from that site (Marlow and Lee, 1983). These measurements (which yield a lower limit to strength, due to the possibility of drilling-induced weakening), give laboratory strengths of 100 to 150 kPa.

These results suggest an important possible difference between fold-and-thrust belts and at least some accretionary

wedges. Apparently, the accretion of sediments may take place so rapidly in some accretionary wedges that the mechanics of the toe is governed by unlithified and nearly lithostatically overpressured sediments, with the extreme overpressures maintained by continued tectonic loading. In such a case, the normally negligible cohesive strength of the base of the wedge may become significant and the front of the wedge may be very weak. Such behavior may be resolved bathymetrically by the presence of a convex wedge taper.

4.4 BARBADOS FAULT GEOMETRIES

Given the mechanical properties of the wedge at its base, we can predict the takeoff angles of thrust faults as they step up from the base. In a non-cohesive wedge which is 20% stronger than its Byerlee frictional sliding base, eq. 3.3 gives a value of 12° for ψ_b , the angle between the base and the direction of greatest compressive stress. If this difference between the strengths of the wedge and its basal décollement becomes large, ($\phi \gg \phi_b$), then $\psi_b \rightarrow 0^\circ$. If $\phi \approx \phi_b$, then $\psi_b \approx 45^\circ - \phi/2$, giving a value of ψ_b ranging between 25° for Byerlee friction ($\phi \approx 40^\circ$) and 45° for an infinitely weak ($\phi \approx 0^\circ$) wedge. It was pointed out in Chapter 2 that the preferred orientations of Mohr-Coulomb fractures or slip planes are inclined to the σ_1 direction by an angle θ given by

$$\theta = \frac{\pi}{4} - \frac{\phi}{2} \quad (2.34)$$

and the takeoff angle of a forward vergent fault at the base of the wedge should be inclined to it at an angle $\delta_b = \theta - \psi_b$. For the case of a wedge and décollement of equal strengths ($\phi = \phi_b$), this means that $\theta = \psi_b$, so $\delta_b = 0^\circ$, and faults stepping up from the base of the wedge have a 'sledrunner' geometry, in which the dip of such a fault asymptotically approaches that of the basal décollement. At shallower depths in the wedge, where $\psi \rightarrow \alpha + \beta$, the dip of such a fault relative to the upper surface of the wedge, $\delta \rightarrow \theta$, or roughly 25° for Byerlee friction, even near the toe of the wedge, where extremely high pore pressures apparently cause it to be very weak. Westbrook (1982) has reported thrusts dipping at an angle of roughly 20° near the surface and shallowing out at depth, as required by the argument presented above. Because wedge taper is much less sensitive to absolute strength than to the relative strengths of the wedge and its base, the sensitivity of fault step-ups to the friction angle ϕ can provide a useful additional constraint, as used by Dahlen et al. (1983).

The front of the Barbados wedge complex accretes some but not all of the sediments brought into it by the subducting crust of the Atlantic Ocean. Near the Leg 78A sites, where the sediments overlying oceanic basement are 700m thick, all but the top third or so of the sediments which are of Miocene age and younger are subducted (Biju-Duval et al., 1982). There clearly must be some sort of mechanical segregation process occurring at the frontal thrust which selects only the upper part of the oceanic

sediment load for accretion and permits the remainder to subduct.

It is not always clear by what mechanical criteria it is determined that a particular stratigraphic horizon shall be the one at which the basal *décollement* is located. Lithology can be an important factor. Relatively recently deposited and incompletely lithified sediments are much more likely to be plowed up by the accreting wedge than are deeper and more competent sediments (Moore, 1975). In general, the horizon which allows sliding with the least resistance will become the *décollement* because of energy considerations.

The presence of a relatively impermeable stratigraphic horizon below which fluid pressures are higher than they are above should influence the location of thrusts in accretionary wedges much as in subaerial thrust belts. In this way, an intrinsically weaker *décollement* horizon could be bypassed in favor of a deeper level at which the fluid pressures are higher, so the bias toward the underthrusting of a large fraction of the oceanic sediments may no longer apply (Chapter 6). Thus, the observed underthrusting of most of the sediments at the trench in the Leg 78A area (Biju-Duval et al., 1982) does not necessarily mean that a similarly large fraction of the sediments are fully subducted. Underplating of sediments at depth further to the west is possible.

As new material is brought in by the convergence of the two plates, compression at the toe requires that a new

imbricate thrust slice be cut into the encroaching oceanic sediments. The slice is cut from the base of the existing basal thrust to the surface at an angle controlled by the mechanical properties of the sediments. As the new sedimentary slice is added to the accretionary wedge, faults directly behind that point undergo slip in response to the slightly changed stress state and a series of deformations occurs within the wedge as a result of which the wedge taper is maintained. The addition of a new active frontal thrust may require a vertical rotation of older, rearward thrusts, giving them a larger angle of dip than they originally had. Although these older thrusts become relatively inactive, they may still need to undergo some slip in order to maintain the critical taper of the wedge. However, as they rotate further from their optimal slip orientation, it becomes less likely that slip will occur entirely along the old slip planes. Instead, further imbrication along new thrusts becomes a more likely possibility. Westbrook and Smith (1983) point to mud volcanoes to the east of the deformation front as evidence for the rapid migration of pore waters. They suggest that the migration of overpressures toward the advancing diapirs serves to weaken the sediments in preparation for them to be accreted by the advancing wedge.

The nature and frequency of these internal deformations are very different for thrust belts and accretionary wedges. Most thrust belts undergo geologically rapid erosion (Suppe, 1981), reducing the wedge taper. This process requires

thrusting in order to restore wedge taper. In this way, deformation and seismicity can be triggered by erosion. Thus, the predominance of sedimentation over erosion on the surface of accretionary wedges contributes to making them less active than their subaerial counterparts.

At the very thick back end of an accretionary wedge, the wedge is sufficiently thick that its base is likely to be below the depth of the brittle-plastic transition (Figure 3.14), a depth which is dependent upon rock type, pore pressures, and the geothermal gradient. The weakening of the base of the wedge below the depth of transition to plastic behavior corresponds to a reduced value of τ_b in eq. 2.29. This in turn leads to a lower value of the critical taper ($\alpha+\beta$) on the right hand side of that equation. In other words, where the base of the wedge is weakened by high temperatures at depth, the wedge can stably ride over the downgoing plate even though it has a smaller taper than would otherwise be required. This effect of the brittle-plastic transition is consistent with the flattening out of the upper surface observed at the thick end of many large thrust belts and accretionary wedges.

The combination of plasticity at depth and a steepening of the dip of the base of the wedge should result in a western limit to the critically tapered region of the Barbados wedge. To the east of this limit, the accretionary wedge should be at or very near horizontal compressive failure, although the magnitudes of differential stresses

are moderated by high pore pressures.

4.5 LEG 78A TEMPERATURE DATA

Drilling at sites a short distance on either side of the deformation front during Leg 78A of the DSDP (Figure 4.2) afforded an exceptional opportunity to study the convergence process. Temperature measurements were attempted at all three sites of Leg 78A, using three separate instruments. These were the Tokyo T-probe (Uyeda and Horai, 1982), a Gearhart-Owen downhole logging instrument, and a temperature sensor attached to a downhole seismic instrument (Davis and Hussong, 1983). The results of these measurements for Sites 541 and 542 appear to be related to the state of pore pressures along the basal decollement.

SITE 541

Two apparently successful temperature measurements were made at the bottom of the hole drilled at Site 541 (Figure 4.6) using the T-probe during interludes in the drilling. The equilibrium temperatures measured at 48.5m and 95m are, respectively, $\sim 16.2^{\circ}\text{C}$ and $\sim 15.5^{\circ}\text{C}$. If correct, these measurements are indicative of astoundingly high temperatures for such depths. Although there is independent confirmation of very high temperatures at somewhat greater depths, these particular measurements must be considered unconfirmed and possibly suspect.

The preferred way in which to evaluate downhole temperatures is with a downhole logging instrument, such as

the Gearhart-Owen instrument used on Leg 78A. The inability of this logging device to measure temperatures more than a short distance past the end of the pipe makes it impossible to construct a true temperature profile for Site 541. The results of a logging trip which barely exits the pipe contain, at best, a single decipherable temperature-depth data point. Temperature measurements for this hole (Figure 4.7a) are dominated by pipe-related effects. The instrument recorded a sharp temperature increase from 2.5°C to roughly 5°C within 10 meters of the mudline. This apparently represents a boundary region (separating cold sea water and warmer water from below) located in the top few meters below the sea floor where the hole is considerably wider than the pipe diameter.

The relatively constant temperatures measured from 10 m BSF to the bottom of the pipe are probably related to upward flow of water outside the pipe, and are not directly indicative of the true undisturbed thermal gradient. The temperatures measured by the logging device increased by 10°C in the first 20 meters below the pipe. This would appear to be a boundary layer between the pipe, which had been cooled by the pumping of cold water during the deployment of the logging device, and the relatively unaffected parts of the hole a few tens of meters below the pipe which had not undergone circulation of cold water since several hours earlier. By the time the device hit an obstruction in the hole and could not proceed any further,

the temperature had reached 15°C. The fact that the logged temperature had slowed but not stopped its rapid increase with depth suggests that the logging device had passed most, but not all, of the way through the region of the hole disturbed by pipe-end thermal effects. Assuming that nothing else had happened to affect the temperature since the last circulation to total depth, we can use the analysis of Jaeger (1961) to determine what fraction of that temperature disturbance still remains. Such an analysis (Davis and Hussong, 1983) indicates that the temperature has recovered 70% of the way to its pre-disturbance value. Given a conservative estimate of 15.0°C for the temperature of the hole just beyond the influence of pumping in the pipe, this yields an undisturbed temperature of 20.4°C in the hole at a depth of roughly 170 m BSF. The total penetration depth of drilling in this hole is 459 m and there was evidently at least some upward movement of warm water within the hole. It is therefore not clear whether this temperature is indicative of the pre-drilling temperature at the depth at which the measurements were taken or, instead, whether it reflects in-hole convection of warm water from a more highly overpressured zone near the base of the hole.

SITE 542

When the drilling pipe became stuck in Hole 542B an explosive charge was detonated in the pipe to attempt to recover as much as possible of the Bottom Hole Assembly, but

instead it blew a hole in the drill string. A temperature log was run in the pipe (Figure 4.7b) down to the depth of the explosion, where the instrument was apparently stopped by shredded metal.

A rapid increase in temperature at the deepest point in the logging run suggests that the logging device had approached the explosion site, where it encountered warm water flowing up from below and then out of the hole which had been blown in the pipe. The maximum temperature recorded (9.8°C) can be regarded as an absolute minimum estimate of the temperature somewhere between the measurement depth and the bottom of the hole. Without better knowledge of the role of convection in the pipe and of the exact location of the hole blown in the pipe, no hard numbers can be attained for the thermal gradient at this site.

4.6 IMPLICATIONS OF HIGH TEMPERATURES NEAR BARBADOS

The front of an overthrusting margin is expected to have a lower thermal gradient than the nearby oceanic crust (Toksoz et al., 1971). Observations on the Japan Trench transect (Langseth and Burch, 1980) yield geothermal gradients of 24 to $36^{\circ}\text{C}/\text{km}$. Measurements on Leg 66 off the southwestern coast of Mexico (Shipley and Shephard, 1982) indicate gradients of 25 to $40^{\circ}\text{C}/\text{km}$.

The very limited data from Site 542 are not necessarily inconsistent with a thermal gradient comparable to those in

other accretionary prisms. However, Site 541 appears to be truly anomalous. A temperature of 20.4°C at 170 m BSF, if indicative of the undisturbed temperature at that depth, requires a mean thermal gradient of 104°C/km. If the temperature measured just below the bottom of the pipe actually reflects upward movement of warm water from somewhat closer to the bottom of the hole, then the undisturbed thermal gradient would be between that value and 40°C/km. The latter possibility appears to be inconsistent with the measurements taken with the Tokyo T-probe at this site, which suggest that most (roughly 13°C) of the temperature increase occurs in the top 50 meters below the seafloor.

However they are interpreted, these data from Leg 78A require abnormally high thermal gradients both at the toe of the accretionary prism (Figure 4.7a,b) and directly in front of the toe (Figure 4.7c). Exceptionally high fluid pressures (Moore, 1983) and geochemical evidence (Scientific Staff, 1983) are consistent with upward migration of warm waters as a heat transfer mechanism.

The source of the warm water at Sites 541 and 542 is not entirely clear. Volcanism can be ruled out because the nearest likely source, the Lesser Antilles Arc, is almost 300 km away. The low values for the shear stress near the toe of the wedge, as determined in this chapter, require that if these high temperatures are related to shear heating, then most of that heating must have taken place

farther back in the wedge. One possible source may be a region near the décollement shear zone somewhat to the west of the deformation front. Nearly lithostatic fluid pressures along this zone (Moore, 1983) could provide the fluid pressure head required to drive the migration of pore fluids. Because of the greater depth of the basal décollement farther to the west, these fluids should be warm. The intrinsic permeability of the sediments is quite low, so these fluids would most readily flow upward along fractures. Because of the westward dip of thrust faults in the area, this upward movement would tend to concentrate warm waters to the east, near the toe where Sites 541 and 542 are located (Davis and Hussong, 1983). Tectonic shortening, thickening, and piling up of overburden may provide a mechanism for the maintenance of the required fluid pressure head.

4.7 LEG 78A BOREHOLE INSTABILITY

Difficulties have often been experienced in drilling boreholes in accretionary wedges. These difficulties take the form of abnormal pore pressures (Moore and von Huene, 1980; Hottman et al., 1979; J.Harms, personal communication, 1982) and hole collapse. Both of the Sites of Leg 78A located on the accretionary wedge (Sites 541 and 542) showed signs of borehole instability.

The origin of abnormal pore pressures in accretionary wedges has been the subject of some debate. Proposed

mechanisms include methane generation, aquathermal pressuring, and phase changes, any of which might produce overpressures by increasing fluid volume (Moore and von Huene, 1980). Alternative mechanisms involve the loading of additional overburden atop sufficiently impermeable rock. This loading can result from either rapid sedimentation, as in the Louisiana Gulf Coast (Fertl, 1976), or from tectonically generated loading and horizontal compression. Thrust faulting in active accretionary wedges and in fold-and-thrust belts is well suited to producing such a tectonic loading. Considerable evidence exists for high fluid pressures beneath Barbados (Moore and von Huene, 1980), and at the DSDP Site 542 (Moore, 1983).

Borehole instability is a subject of considerable concern in drilling near the base of the trench slope (Moore and von Huene, 1980). Let us consider the borehole collapse problem in terms of the borehole acting as a stress concentrator in a marginally stable environment as implied by Coulomb wedge theory. We expect that the rock is close to compressive failure, and model the borehole as a vertical cylindrical hole drilled into an elastic half space (Timoshenko and Goodier, 1951). This hole acts as a stress concentrator, altering the state of stress in its vicinity (Hottman et al., 1979; Hubbert and Willis, 1957). We ignore edge effects (the borehole is much longer than it is wide) and fluid-flow effects (the high permeability observed at Site 542 was a fracture permeability and the sediments

themselves are highly impermeable). The results of eq. 3.6 allow us to assume that $\psi \approx 0$, so that one of the far-field principal stress axes (in this case σ_3) is vertical. The state of stress near the borehole, expressed in cylindrical coordinates and using the convention that compressive stresses are positive, is (Haimson, 1968)

$$\begin{aligned}\sigma_{rr} &= \left(\frac{\sigma_1 + \sigma_2}{2}\right)(1 - R^{-2}) + \left(\frac{\sigma_1 - \sigma_2}{2}\right)(1 + 3R^{-4} - 4R^{-2})\cos 2\theta + \frac{P_w}{R^2} \\ \sigma_{\theta\theta} &= \left(\frac{\sigma_1 + \sigma_2}{2}\right)(1 + R^{-2}) - \left(\frac{\sigma_1 - \sigma_2}{2}\right)(1 + 3R^{-4})\cos 2\theta - \frac{P_w}{R^2} \\ \tau_{r\theta} &= \left(\frac{\sigma_1 - \sigma_2}{2}\right)(1 - 3R^{-4} + 2R^{-2})\sin 2\theta \\ \sigma_{vv} &= \sigma_3 - 2\nu(\sigma_1 - \sigma_2)(R^{-2})\cos 2\theta\end{aligned}\quad (4.1)$$

for any point at a distance R borehole radii from the center of a borehole in a direction at an angle θ from the direction of undisturbed maximum compressive stress. The variables σ_{rr} , $\sigma_{\theta\theta}$, and σ_{vv} are the components of stress in the r , θ , and vertical axis directions, respectively, P_w is the water pressure in the borehole, and ν is Poisson's ratio. Note that the stress concentration effect is extremely localized near the hole. The effects of the drilling procedure on the sediments very close to the borehole may affect our ability to assume both a failure criterion and the elastic behavior required for this stress analysis. However, if calculations suggest that failure extends well beyond the immediate vicinity of the borehole wall, then we may feel safe in predicting that fracture of the sediments and collapse of the borehole will take place.

Assuming that we have a reasonable idea of the conditions in the borehole at Site 541, with a state of stress close to failure, let us consider the stability of the borehole against collapse. At the borehole wall (where $R=1$), the stress state becomes

$$\begin{aligned}
 \sigma_{rr} &= P_w \\
 \sigma_{\theta\theta} &= \sigma_1 + \sigma_2 - 2(\sigma_1 - \sigma_2)\cos 2\theta - P_w \\
 \tau_{r\theta} &= 0 \\
 \sigma_{vv} &= \sigma_3 - 2\nu(\sigma_1 - \sigma_2)\cos 2\theta
 \end{aligned}
 \tag{4.2}$$

It has been pointed out (Hottman et al., 1979) that changes in P_w , the pressure of the mud (in our case water) in the borehole can allow different types of borehole wall failure to occur. The most familiar of these is hydrofracture (Hubbert and Willis, 1957), which results when high mud weights in the hole make P_w large enough to reduce $\sigma_{\theta\theta}$ to the point of tensile failure at $\theta = 0^\circ$ and 180° . This produces a vertical fracture perpendicular to the borehole wall and σ_2 direction.

Other sorts of failure are possible in a borehole. The fact that the boreholes at DSDP Sites 541 and 542 were filled with water instead of mud makes P_w too small for the initiation of tensile failure in the borehole wall. Instead, we expect that the state of stress at all points on the wall of one of these boreholes should be such that the direction of least compressive stress is in the radial σ_{rr} direction. A short distance past the borehole wall, the vertical stress σ_{vv} attains its far-field status as the

least compressive stress and fractures rotate to a more nearly horizontal orientation. However, in the immediate vicinity of the borehole, the stress state is such that failure takes the form of tangential compression of the wall at $\theta = 90^\circ$ and 270° . If the hole is filled with water, then P_w (and thus σ_{rr} at $R=1$) can be small enough that the effective radial stress $\sigma_{rr}^* = \sigma_{rr} - P_f$ can become sufficiently tensile as to overcome the tensile strength of the material. The result, as described by Hottman et al. (1979) for a borehole drilled in the Gulf of Alaska, is an in-fall of wall material into the hole and the collapse of the hole in the direction of the far-field maximum compressive stress. Here, as in the Aleutian wedge, the σ_1 direction is roughly perpendicular to the trench or deformation front axis. For either a depth-dependent Coulomb or depth-independent plastic failure criterion, the stress concentration at and near a borehole wall will be sufficient to initiate failure (Figures 4.8a,b).

Given the near-failure state of stress which we expect to exist before drilling, collapse of the hole due to distortion of the stress field in the vicinity of the hole is to be expected for any reasonable failure criterion. Thus any possible non-Coulomb behavior of sediments which are either too deep and hot or extremely shallow and not fully lithified (as is largely the case at Sites 541 and 542) will not seriously affect this conclusion.

In an accretionary prism having the state of stress

predicted by the compressive wedge theory (eq. 3.2), borehole instability is very likely. One major exception to this rule would be holes drilled in ponded sediments which are partially decoupled from the thrusting mass of sediments beneath, in that they have not acquired the large horizontal stresses found in the wedge on which they have been deposited. Another locale in which boreholes in an actively accreting prism might be stable would be sites in a locale with supercritical taper. Such a supercritical wedge would, like a supercritical part of an otherwise critical wedge, have a state of stress different from that predicted using the assumption that the wedge is everywhere in compressive failure.

4.8 BARBADOS AND THE TECTONICS OF A SEDIMENT-RICH WEDGE

We can confirm that like Taiwan, the Barbados wedge has a gross taper which is consistent with a base weaker than the rocks in the wedge itself by only a small amount. In Taiwan, the strength difference is attributable to cohesion within the wedge, as pore pressures do not preferentially weaken the basal décollement to a significant degree. In the Barbados wedge, the sparse available pore pressure data leave open the likelihood that higher pore pressures along the base of the wedge play an important role. The observed taper is consistent (eqs. 3.2-3.4) with a wedge and décollement of the same intrinsic strengths as those in Taiwan, but with very high values of $\lambda = \lambda_p$ from ≈ 0.85 near Barbados to ≈ 0.97 near

the toe. This result suggests that the shear stress across the basal décollement is roughly 0.2 MPa near Site 541. Using a different formulation, a similar value has been obtained by Westbrook and Smith (1983).

A borehole drilled into an elastic half-space under horizontal compressive failure should have a tendency to be unstable, and tend to collapse. This is in accord with the observations made at DSDP Sites 541 and 542. This is interpreted to support a basic premise of the Coulomb wedge theory, namely, that the wedge is in a state of stress near horizontal compressive failure.

Unusually high temperatures measured at Sites 541 and 542 during DSDP Leg 78A may be related to the observed nearly lithostatic pore pressures and flow of water at depth. It is surmised that the rapid increase in tectonic overburden as the wedge grows may cause warm waters to migrate upward and forward toward the deformation front along fractures. If the high temperatures are generated by shear heating, then the results of the preceding sections, Davis (1983), Westbrook and Smith, (1983), and Dahlen et al. (1983) make it clear that shear stresses near the toe of the wedge are much too low for the shear heating to have taken place in that area. Instead, it must have taken place farther back into the wedge, where much higher shear stresses are predicted along the basal décollement.

An understanding of the mechanics of accretionary wedges based upon Coulomb-wedge theory permits quantifi-

cation of the relationships between pore pressures, states of stress, and the stability of boreholes in accretionary wedges. These relationships are consistent with the results of DSDP Leg 78A, and suggest that the Barbados accretionary wedge complex is deforming under horizontal compression resulting from shear stresses generated as it overrides its basal décollement (Figure 4.9).

4.9 OTHER ACCRETIONARY WEDGES

In accretionary wedges other than the Barbados-Lesser Antilles wedge, constraints upon décollement dips, fluid pressure gradients and the orientations of faults are, at best, sparse. However, some data on décollement dip are now available because of seismic reflection or refraction studies (e.g., Beck and Lehner, 1974; Seeley et al., 1974; and some others). Therefore, by assuming the same values of rock strength and function as found for Taiwan, namely, $\mu_b = 0.85$ and $\mu' = 1.03$, we may compute a predicted fluid pressure coefficient $\lambda_b = \lambda$, given the observed taper of the wedge (Figure 4.10 and Table 4.1). The assumption that $\lambda_b = \lambda$, as opposed to allowing for the fairly likely possibility that $\lambda_b > \lambda$, upwardly biases the estimates of the pore pressure ratios. In general, if either pore pressure value is constrained by well data, it is λ , the value in the wedge. Note further that such an indirect estimation of fluid pressures is least susceptible to errors in α or β for large values of $\lambda = \lambda_b$. This is apparent from

an examination of the spacing of the converging lines in Figure 4.11, which relates λ and β to the value of $\lambda = \lambda_p$.

By the method described above, seismic reflection modeling of the Peru Trench (Keller et al., 1979) yields $\lambda = 0.6$. In considering this profile, there are two points which deserve consideration. First, the broad range of rocks which have similar frictional properties (Byerlee, 1978) alleviates the necessity of worrying about the type of rock found above the dipping plate boundary, as long as particularly weak rocks (such as halites or clays) are not dominant. Therefore, possible tectonic erosion at the Peru Trench (Schweller et al., 1981) is irrelevant with regard to wedge taper. Second, accretionary wedges can display an abrupt drop in surface slope toward their interiors in a manner similar to subaerial mountain ranges (Chapter 3, Figure 3.15). Such a bathymetric break is observed in the Peru wedge (Figure 4.12) and is interpreted to be the surface expression of the brittle-ductile transition along the base of the wedge. The depth of the basal decollement is very similar to the corresponding depth in the Himalaya, roughly 15 km (Chapter 3).

The same sort of analysis using the well-known Beck and Lehner (1974) and Hamilton (1979) seismic section across the Java trench south of Bali corresponds to $\lambda = 0.7$. A relatively poorly constrained model (based upon gravity data) of the Sunda Arc (Kieckhefer et al., 1981) also yields $\lambda = 0.7$.

The Oregon margin seismic section of Snively et al. (1980) corresponds to $\lambda = 0.9$, a value in good agreement with fragmentary well data taken on the shelf, which indicates that $\lambda \approx 0.85$ (Moore and von Heune, 1980). The taper obtained from the eastern Aleutians section of von Huene et al. (1979) leads to the conclusion that $\lambda = 0.88$. A maximum fluid pressure ratio of $\lambda = 0.87$ was reported for nearby wells, located in shallow water to the north (Hottman et al., 1979).

A profile of the Makran wedge in the Gulf of Oman (White and Ross, 1979) shows virtually no taper (Figure 4.13). The existence of an extremely narrow taper ($\alpha + \beta < 4^\circ$), in the apparent absence of salt (White and Klitgord, 1976; Jacob and Quittmeyer, 1979; White, 1977, 1982) leads to the prediction that $\lambda = 0.98$. This is an extraordinarily high fluid pressure ratio, reminiscent of those typically invoked to explain non-tapered overthrusting (Hubbert and Rubey, 1959). However, there exist some indications that this result may be correct. White (1979) points out that rapid sedimentation in the Gulf of Oman provides an ideal setting for the generation of abnormally high pore pressure. The presence of mud volcanoes along the coast (Ahmed, 1979) is not necessarily a strong indication of high overpressures, but J. Harms, (personal communication, 1982), cites drilling just offshore of the south Makran coast which yield extremely high overpressures in fine-grained, very low permeability mudstones. No exact λ measurement is available, because the

"highly experienced" drilling crew considered the hole to be dangerous and out of their experience. However, rough mud weight data suggest that the pore pressures must have been nearly lithostatic.

4.10 OVERVIEW OF ACCRETIONARY WEDGE MECHANICS

We have considered the tectonics of one accretionary wedge (that beneath Barbados) in some detail. That wedge, as well as several others which have been considered in only the most cursory of ways, appear to have a taper consistent with fragmentary well data and the assumption that they deform in horizontal compression in a manner similar to the fold-and-thrust belt of western Taiwan (Chapter 3). There also appears to be a considerable degree of similarity between the drop-off in topography, attributed to ductile behavior at depth, which is observed in the backs of some thrust belts, and those found in the overlying plate at a subduction zone. Although they can, in many ways, be considered to be mechanically analogous, fold-and-thrust belts and accretionary wedges differ in several important ways.

Reflection seismic data (Beck and Lehner, 1974; and others) and field evidence (Byrne, 1982) suggest that much deformation in accretionary wedges takes place, as expected, in the form of thrust faulting. Fold-and-thrust belts are typically characterized by pervasive seismicity where they are active (Figure 3.3). However, it appears that there is

very little seismic activity within most accretionary wedges (Engdahl, 1977; Chen et al., 1982). Much of the difference in seismicity can be explained by the fact that unlike thrust belts, accretionary wedges do not have their upper surfaces eroded away. The action of erosion would, if not balanced by thrusting, cause decay of the topography in mountain belts over a period of time strongly dependent upon climate. In a moist climate, such as that in Taiwan, most topography could be removed in as little as one million years (Li, 1975). Thus, in a subaerial wedge, it is erosion which drives thrusting and, therefore, seismicity. In general, once a sediment packet is accreted at a trench, its history is quite tranquil compared to that of a similar sediment packet in a subaerial thrust belt. In fact, studies of structures and uplift rates in the Mid-America trench (Moore and Watkins, 1982; Moore et al., 1982) suggest that deformation is strongly concentrated in the region of the toe, near the trench. However, as we have seen in the case of the Barbados wedge, the rapid piling up of sediment slices can cause the wedge to consist of very highly overpressured and incompletely lithified sediments. Temperature data from the DSDP Leg 78A are best understood in terms of such a rapidly accreting, highly overpressured geologic setting. Although not necessarily indicative of extreme pore pressures themselves, these temperature observations are consistent with such observations in boreholes both on the island of Taiwan and at the DSDP Sites.

The Japan Trench accretionary wedge, which contains continentally derived as well as pelagic sediments (von Huene et al., 1981; von Huene and Arthur, 1982), displays the familiar combination of a basal décollement and arcward dipping thrust faults (Shiki and Misawa, 1982). The seismicity of this area is of interest. Low-angle thrust events occur (apparently along the basal décollement where the bulk of the convergence takes place) very close to flexure-associated normal faulting in the downgoing (Pacific) plate, although there are not many large thrust events within 50 km of the trench (Yamashina et al., 1978; Yoshii, 1979). The exceptions to this lack of large thrusting events are the so-called tsunamigenic earthquakes (Fukao, 1979; Nishenko and McCann, 1979). These events (Figure 4.14) appear to represent a stepping up of thrusting from the basal décollement into the wedge (Fukao, 1979; Comer, 1982), part of a family of low-frequency earthquakes (Utsu, 1980; Fukao and Kanjo, 1980). The combination of low frequency and low seismic (as opposed to tsunamigenic) magnitude of these events may suggest weakness of the wedge sediments.

The evidence of wedge seismicity and supposition based upon compressive wedge theory lead to the conclusion that there are fundamental differences between accretionary wedges and thrust belts. These appear to be related to differences in the activity of erosion, the presence of a water overburden, and intrinsic rheological differences.

Table 4.1 Geometries of active fold-and-thrust belts and accretionary wedges and the corresponding inferred fluid-pressure ratios $\lambda=\lambda_b$, compared with available direct fluid-pressure measurements. Qualitative bounds on the inferred values of $\lambda=\lambda_b$ due to uncertainties in α and β can be gauged from Figure 4.11.

	α	β	α, β source	predicted		λ source
				$\lambda=\lambda_b$	observed λ	
SUBAERIAL						
Taiwan	2.9°±0.3°	6.0°±0.5°	Davis et al. (1983), Suppe (1980b, 1981)	—	0.675±0.05	Extensive well measurements; Suppe and Wittke (1977), unpublished data
Himalayan	4.0°±0.5°	3.0°±1.0°	Ohta and Akiba (1973), Secber et al. (1981)	0.76	—	—
SUBMARINE						
Japan	4.5°±0.5°	5.4°±0.5°	Nasu et al. (1979)	0.5	—	—
Peru	3.8°±0.3°	5.9°±1.0°	Keller et al. (1979)	0.6	—	—
Java	3.1°±0.3°	6.6°±1.0°	Hamilton (1979)	0.7	—	—
Sunda	4.0°±1.0°	5.0°±1.0°	Kieckhefer et al. (1981)	0.7	—	—
Guatemala	5.7°±0.7	2.5°±1.0°	Seely et al. (1974)	0.7	high	indirect evidence; DSDP Leg 84 drilling; Aubouin, et al. (1982)
Aleutians	3.0°±0.5°	4.5°±1.0°	von Huene et al. (1979b)	0.88	-0.87	mud weight in a well in ponded sediments; Hottman et al. (1979)
Oregon	2.1°±0.5°	6.0°±1.0°	Snively et al. (1980)	0.90	0.85±0.03	mud weight in a well on the shelf; Moore & von Huene (1980)
Barbados						
overall taper	1.0°±0.5°	8.0°±0.8°	Westbrook (1975)	0.92	0.80±0.05	mud weight in a well on Barbados; Moore & von Huene (1980)
near toe	0.7°±0.2°	4.5°±0.5°	Scientific Staff, DSDP Leg 78A	0.97	-1	packer experiment in Hole 542; Scientific Staff, Sci. Staff
Makran	1.6°±0.3°	2.0°±1.0°	White and Ross (1979)	0.98	-1	mud weight in a well offshore Pakistan; Harms (private comm. 1982)

FIGURE CAPTIONS

- Fig. 4.1 Seismic reflection profile across the Java Trench, after Beck and Lehner (1974). Bulldozer added to illustrate compression generated by plate motions.
- Fig. 4.2 Map of the Lesser Antilles area showing the location of the DSDP Sites 541 and 542 and the island of Barbados with respect to the overthrust boundary between the Caribbean plate and the downgoing oceanic lithosphere of the North American plate.
- Fig. 4.3 Line drawing taken from seismic reflection profiles (from Shell Oil Co., courtesy of J.C. Moore), across the Barbados wedge near the DSDP Leg 78A sites. The letter 'B' indicates the approximate location of the island of Barbados (roughly 200 km south of this section).
- Fig. 4.4 Detailed cross-section of the area near the deformation front of the Barbados wedge (after Biju-Duval et al., 1982).
- Fig. 4.5 Pore pressure data from four wells on the island of Barbados. Upper and lower limits for pore pressure with depth are indicated by empty and filled circles, respectively (after Moore and von Huene, 1980).
- Fig. 4.6 (a) Plot of recorded temperature versus time for the Tokyo T-Probe at a depth of 48.5 m BSF (Below Sea Floor) in Hole 541.

(b) Plot of recorded temperature versus time for the Tokyo T-Probe at a depth of 95m BSF in Hole 541. Note the slow drop-off of temperature after the probe was lifted from the bottom of the hole. This is probably the effect of mud sticking to the instrument.

Fig. 4.7 (a) Temperature measured as a function of depth by Gearhart-Owen downhole logging device in Hole 541. The light dashed line indicates the minimum undisturbed thermal gradient calculated to be consistent with observations.

(b) Temperature measured as a function of depth by Gearhart-Owen downhole logging device in Hole 542B.

(c) Temperature measured as a function of depth by Gearhart-Owen downhole logging device in Hole 543A.

Fig. 4.8 The stability of the region near a borehole under conditions similar to those at DSDP Sites 541 and 542. It is assumed that the sediment density is 1.8 g/cm^3 , Poisson's ratio is 0.4, the borehole is filled with water, and that the far-field stress difference $\sigma_1 - \sigma_3$ at this point 300 meters below the the surface beneath 5 km of water is 80% of that required for failure. The far-field σ_1 direction is along $\theta = 0^\circ$ and 180° . The difference (in MPa) between maximum shear stress and that required for

failure (negative numbers indicating stability) are plotted for the region around the hole for (a) a Byerlee law failure criterion (with $\phi=40^\circ$), and (b), a perfectly plastic material with internal friction $\phi=0$.

Fig. 4.9 A schematic diagram (with a great deal of vertical exaggeration) illustrating the implications of the compression-dominated mechanics for the Barbados wedge.

Fig. 4.10 Cross-sectional profiles, with no vertical exaggeration, of various active submarine accretionary wedges. The Himalayan fold-and-thrust belt is included for comparison. Heavy dashed lines are best fitting linear profiles used to infer fluid pressure ratios $\lambda = \lambda_b$, which are shown. Sources of data are given in Table 4.1.

Fig. 4.11 Theoretical linear relationships $\alpha + R\beta = F$ for a) subaerial and b) submarine wedges, with various fluid pressure ratios $\lambda = \lambda_b$, assuming that $C_0 = 0$, $\mu_b = 0.85$ and $\mu = 1.03$. Boxes indicate observed geometries of active wedges, used to infer the fluid pressure ratios within them. Heavy outlines indicate those wedges for which some direct fluid pressure information is available. A rock density $\rho = 2.4 \text{ g/cm}^3$ was used in the submarine case; other values would yield very similar results as the sensitivity to ρ is slight.

Fig. 4.12 Surface slope of Peruvian continental margin along latitude 14°S as a function of distance from trench. The decrease in surface slope beyond 55 km is interpreted to reflect a reduced basal resistance where the base of the wedge extends below the brittle-plastic transition (after Davis et al., 1983).

Fig. 4.13 Map and cross-section of the Makran wedge (after White and Ross, 1979; Berberian, 1981) illustrating the narrow taper of the wedge, and the locations of mud volcanoes onshore and well-data suggesting extremely high pore pressures and diapirism.

Fig. 4.14 Illustration of the mechanism for tsunamigenic earthquakes located a) to the east of Japan (after Fukao, 1979; Comer, 1982). Note b) the throughgoing fault plane, stepping up from from the basal décollement to the surface. Shaded areas of ellipses are those parts which were surmised to have been uplifted.

Figure 4.1

SEISMIC REFLECTION PROFILE
ACROSS JAVA TRENCH

Beck and Lehner (1974)

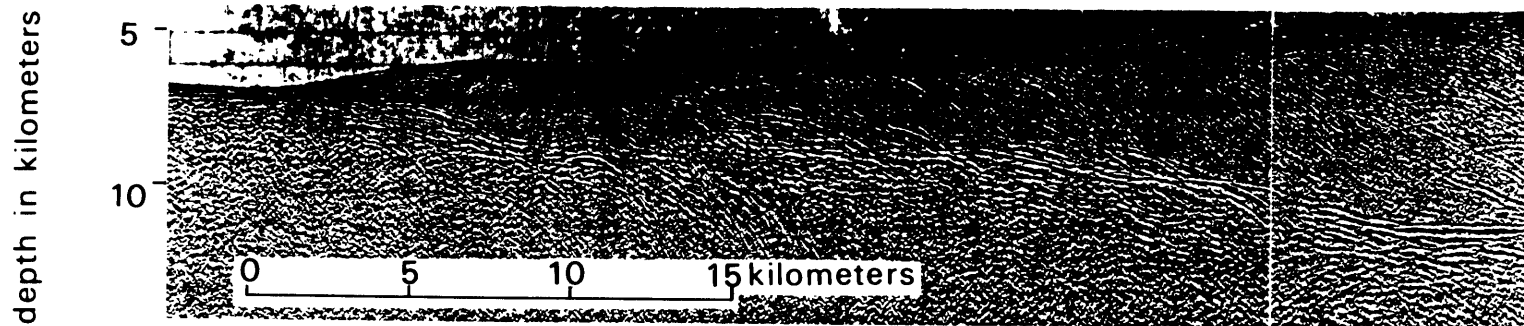
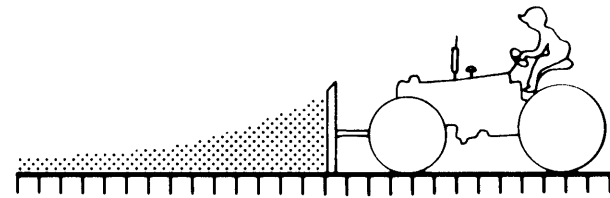


Figure 4.2

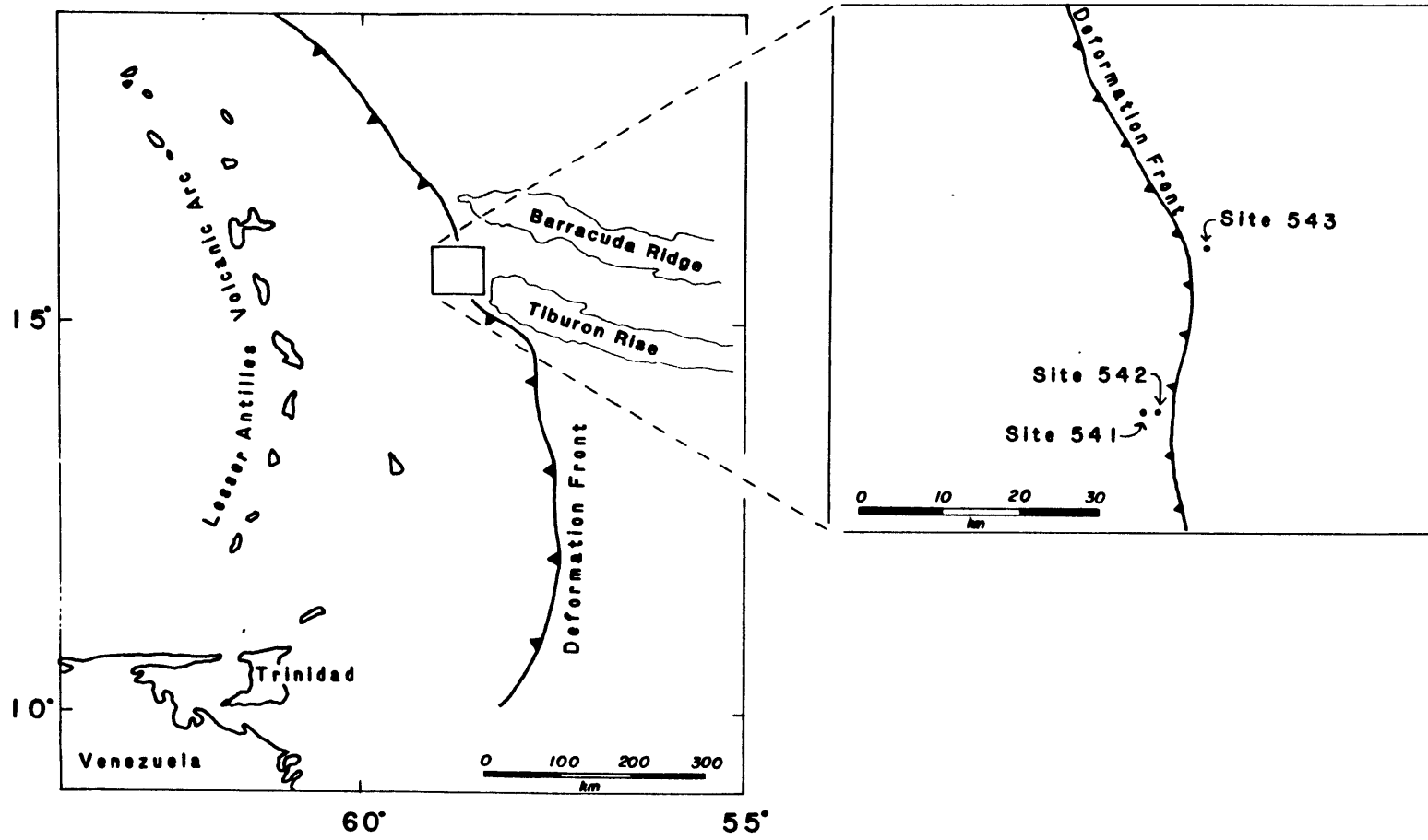
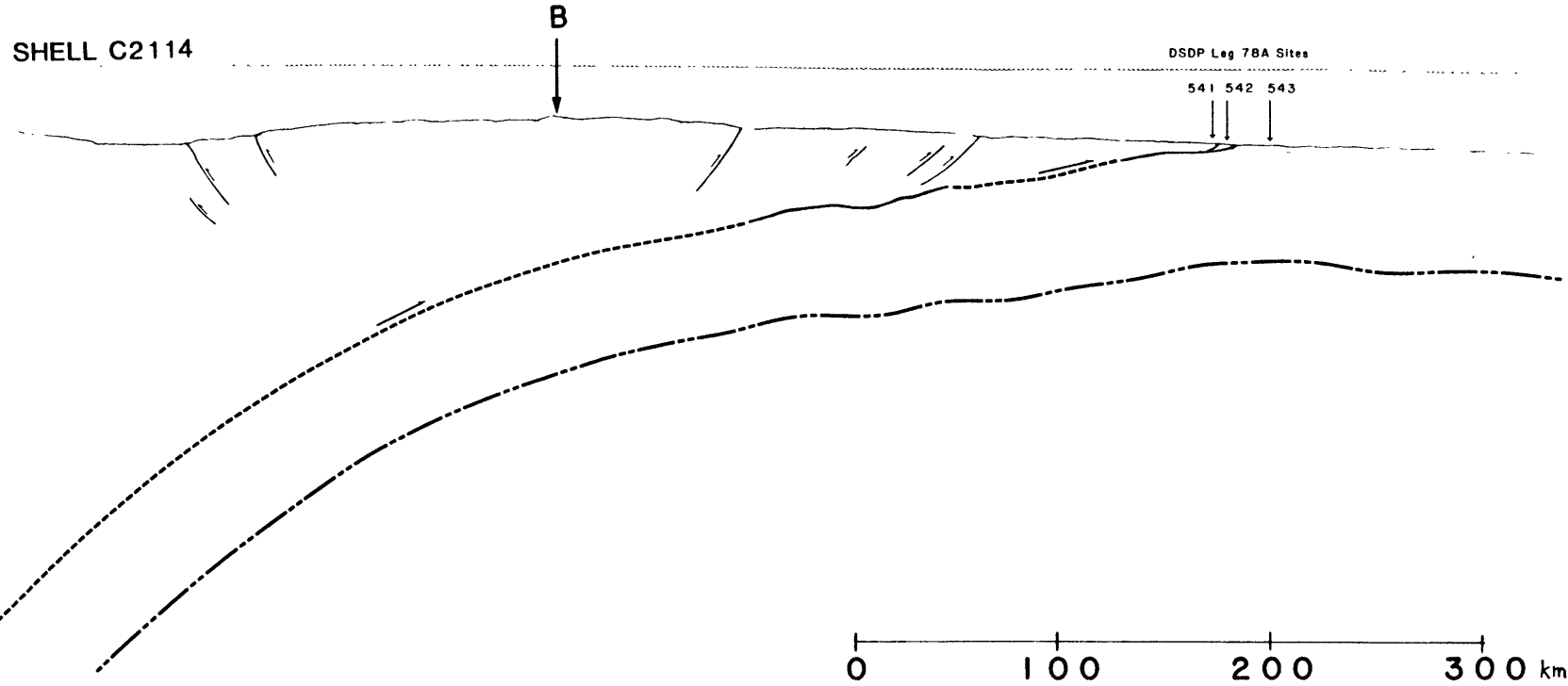
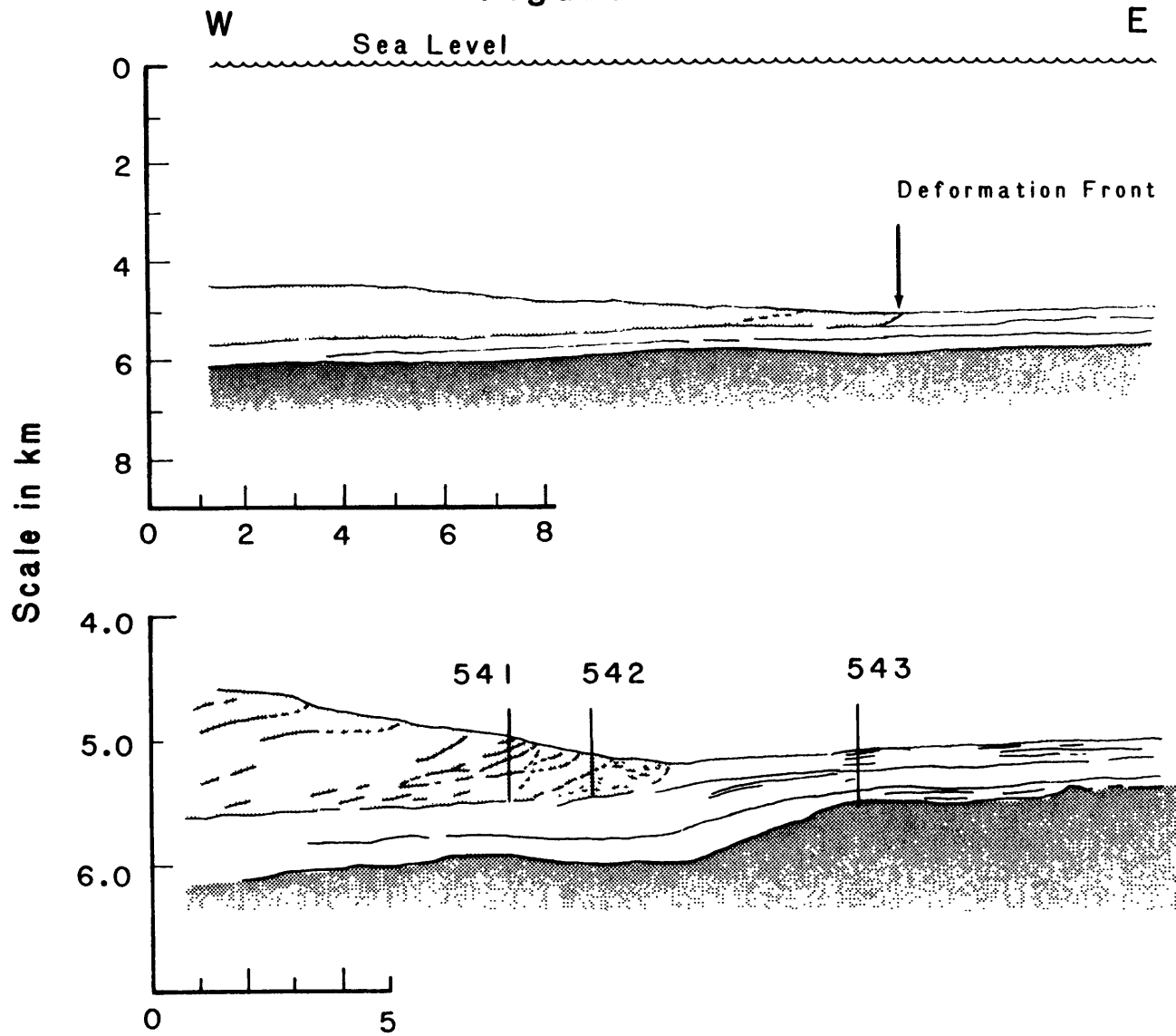


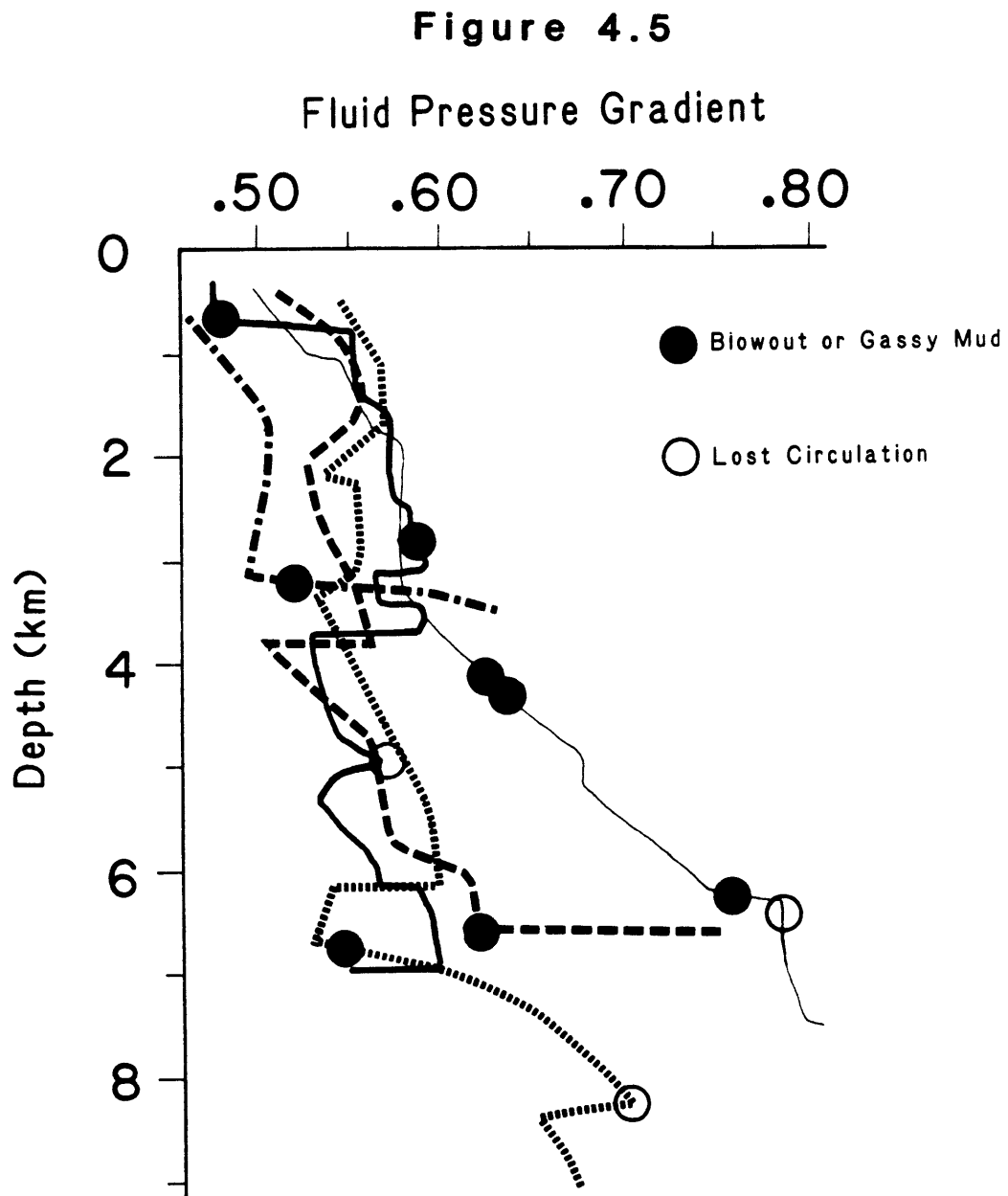
Figure 4.3



no vertical exagg.

Figure 4.4





(After Moore and von Huene, 1980)

Figure 4.6

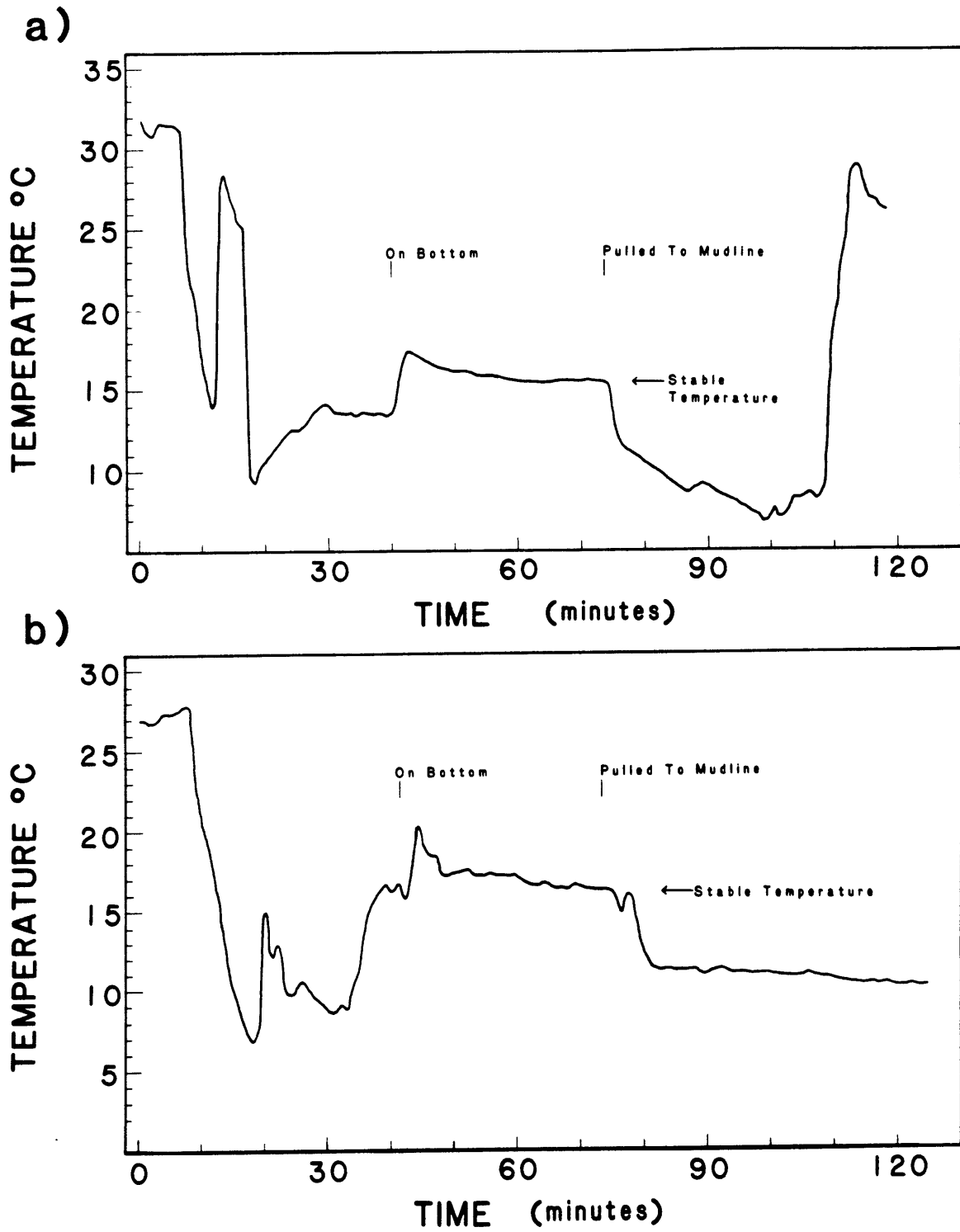


Figure 4.7a

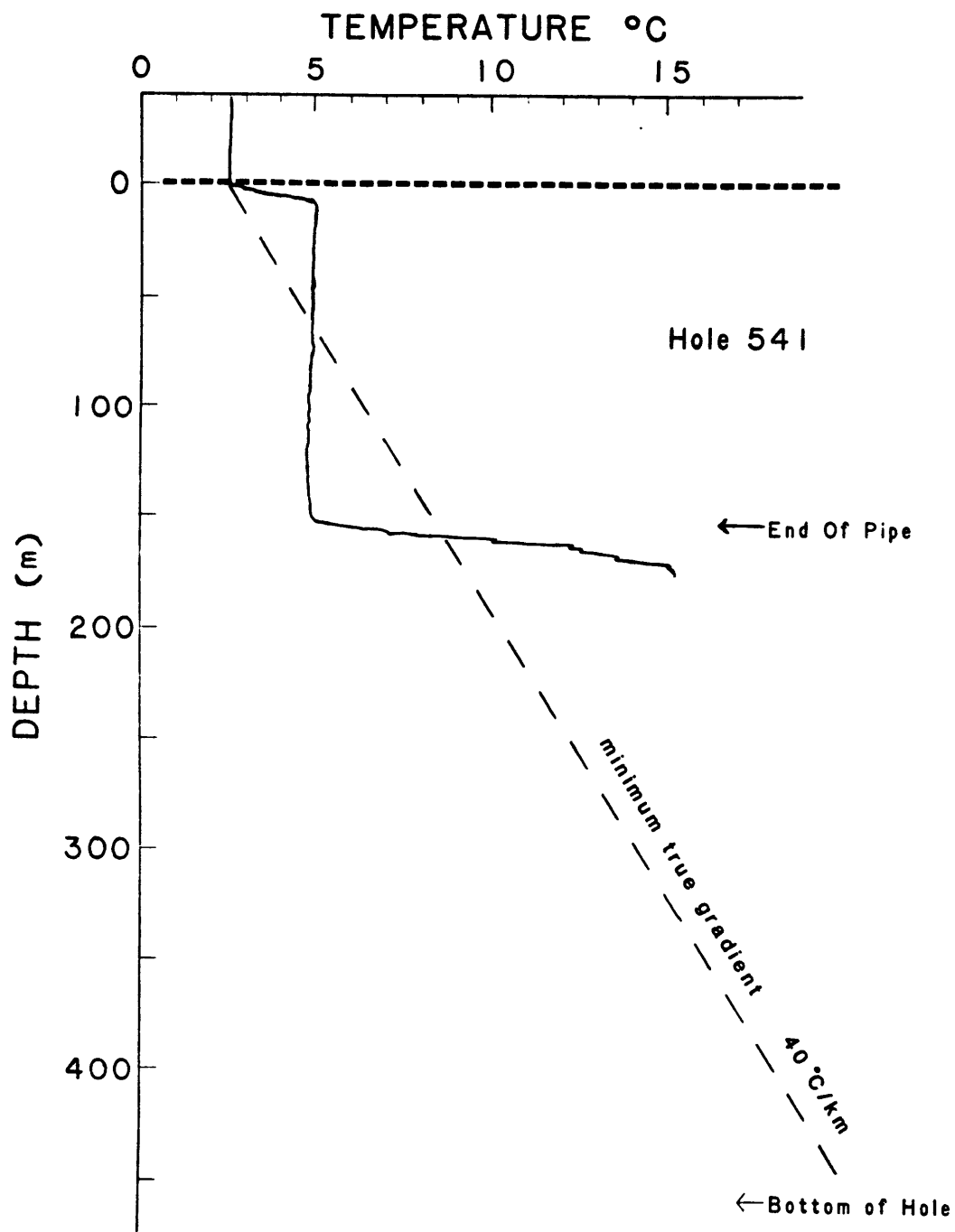
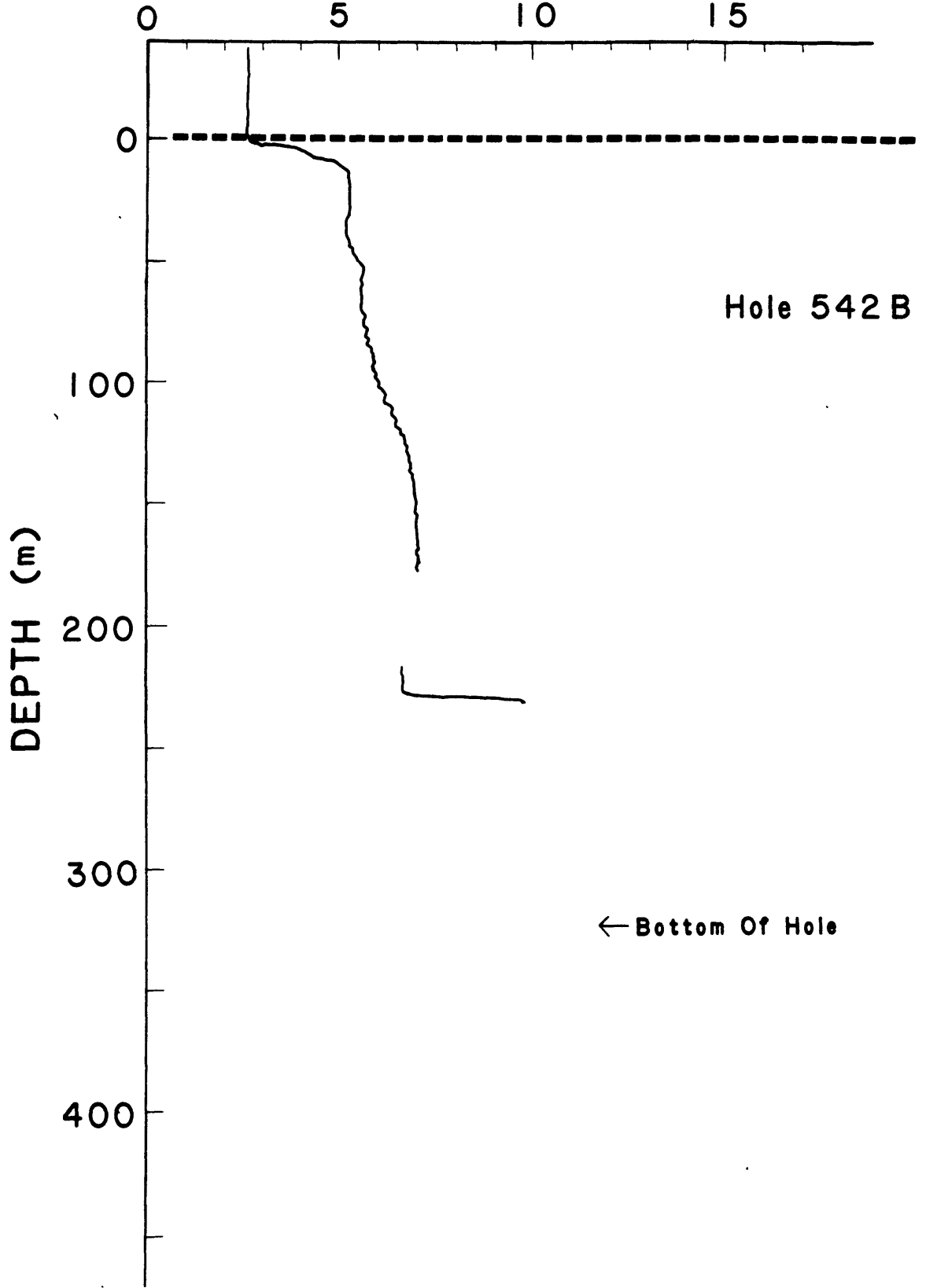


Figure 4.7b
TEMPERATURE °C



Hole 542 B

← Bottom Of Hole

Figure 4.7c
TEMPERATURE °C

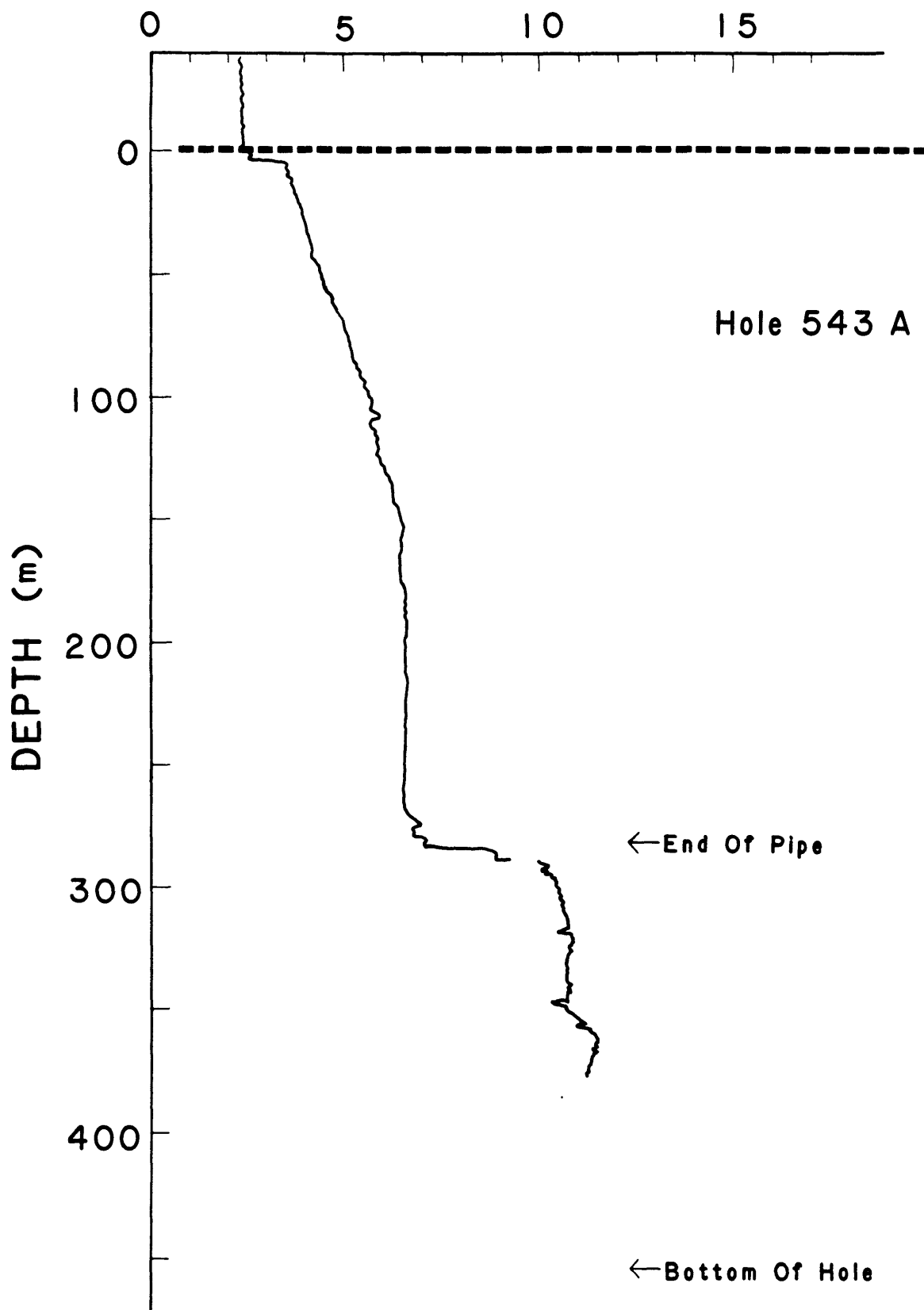


Figure 4.8a

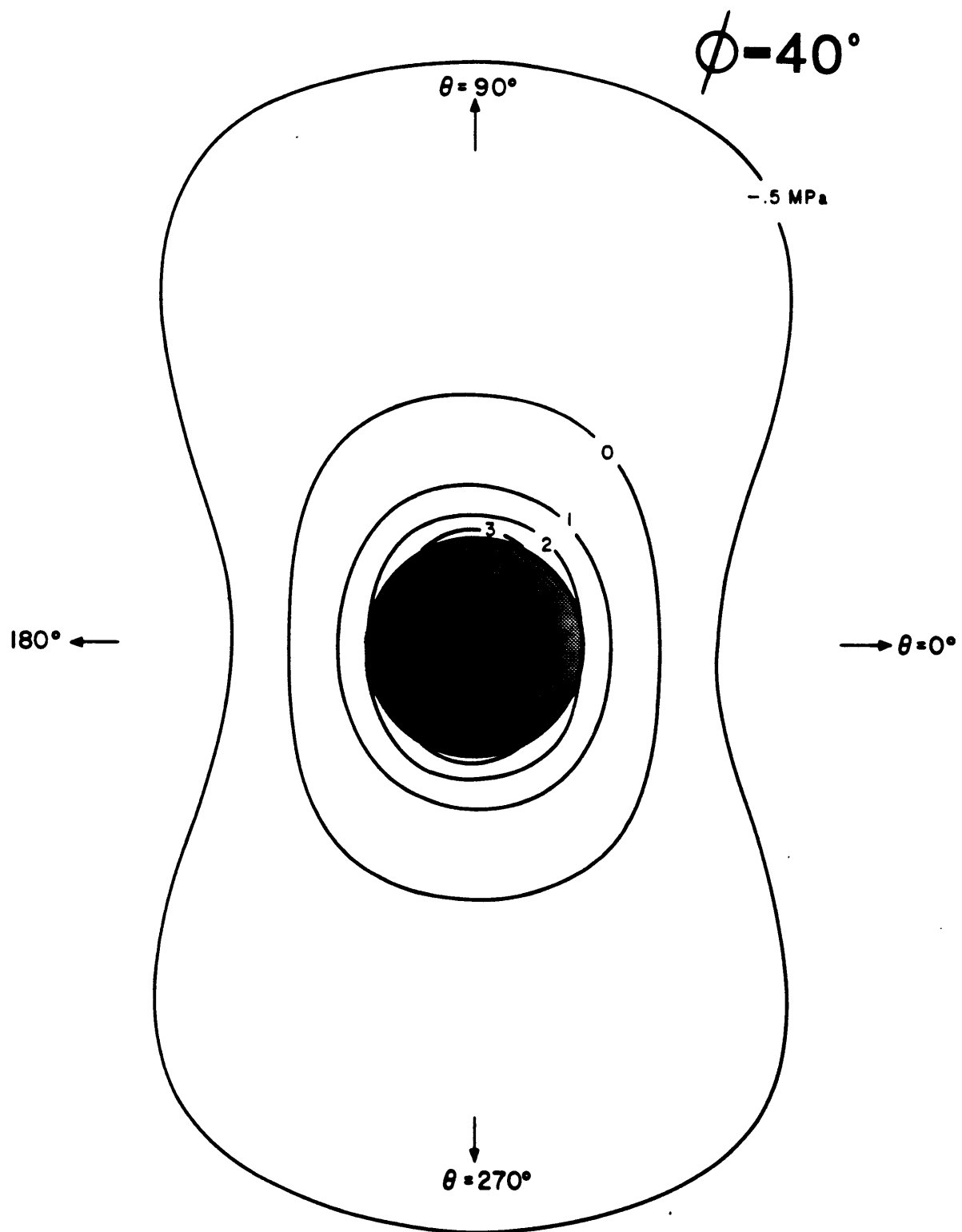


Figure 4.8b

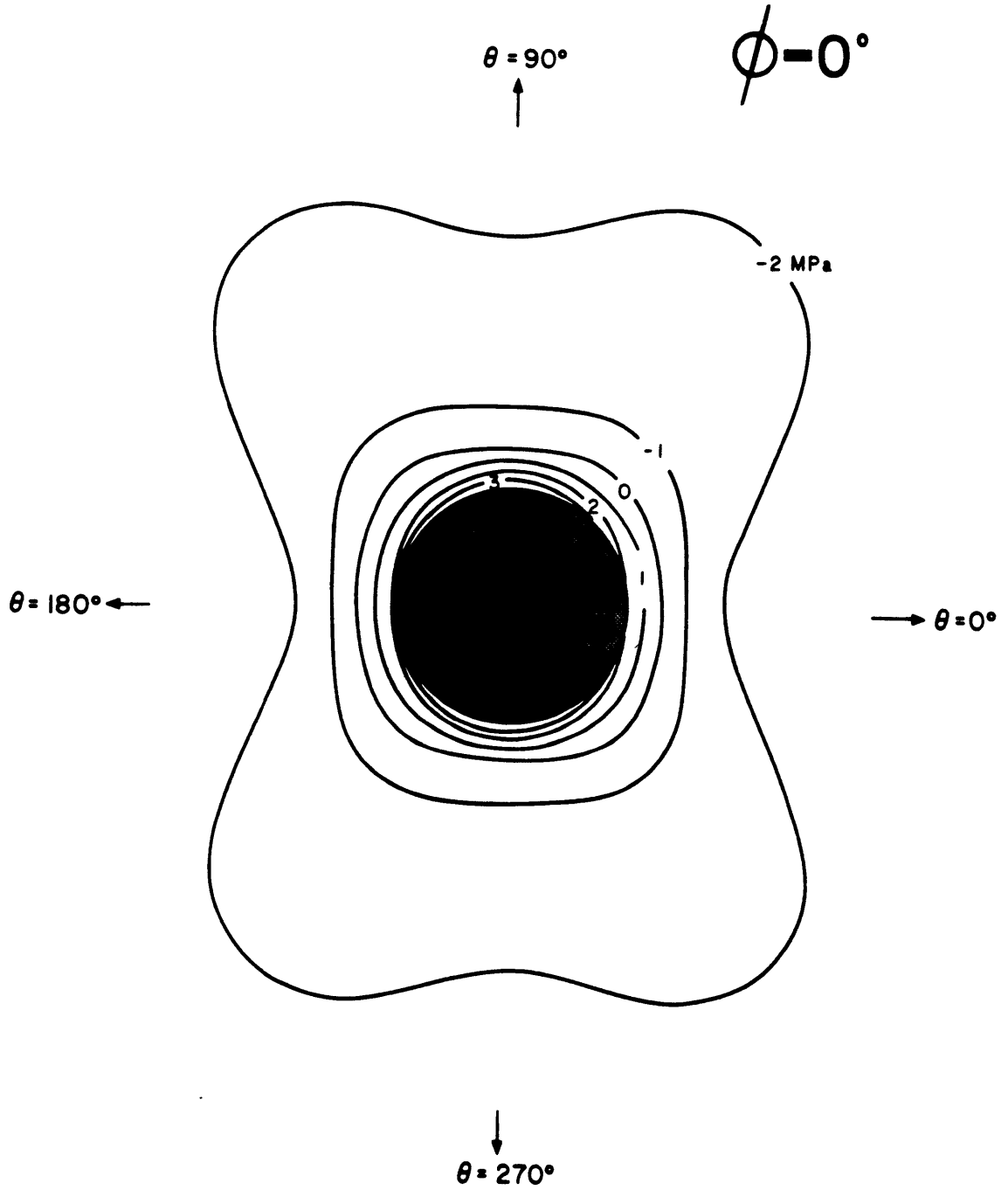


Figure 4.9

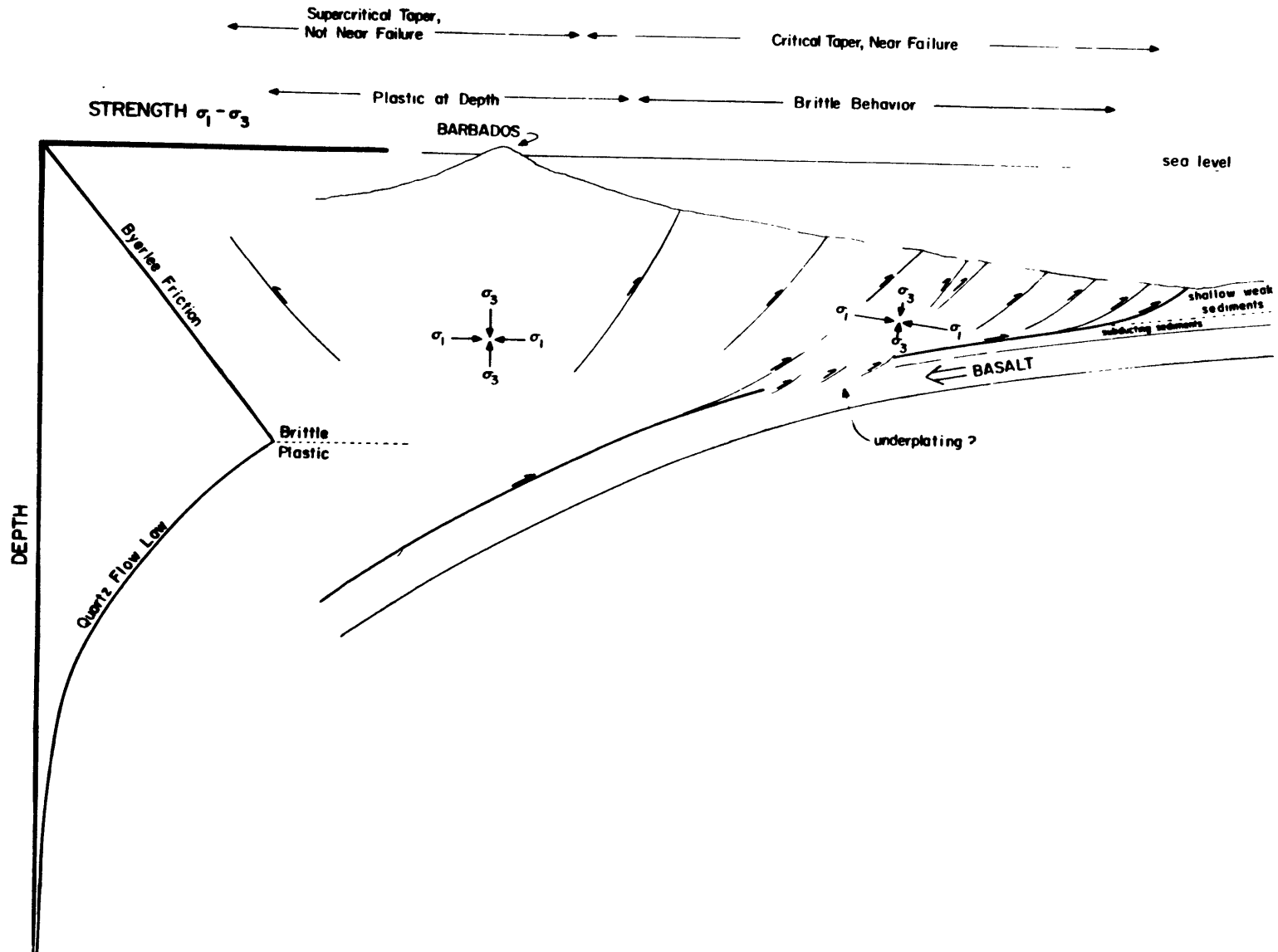


Figure 4.10

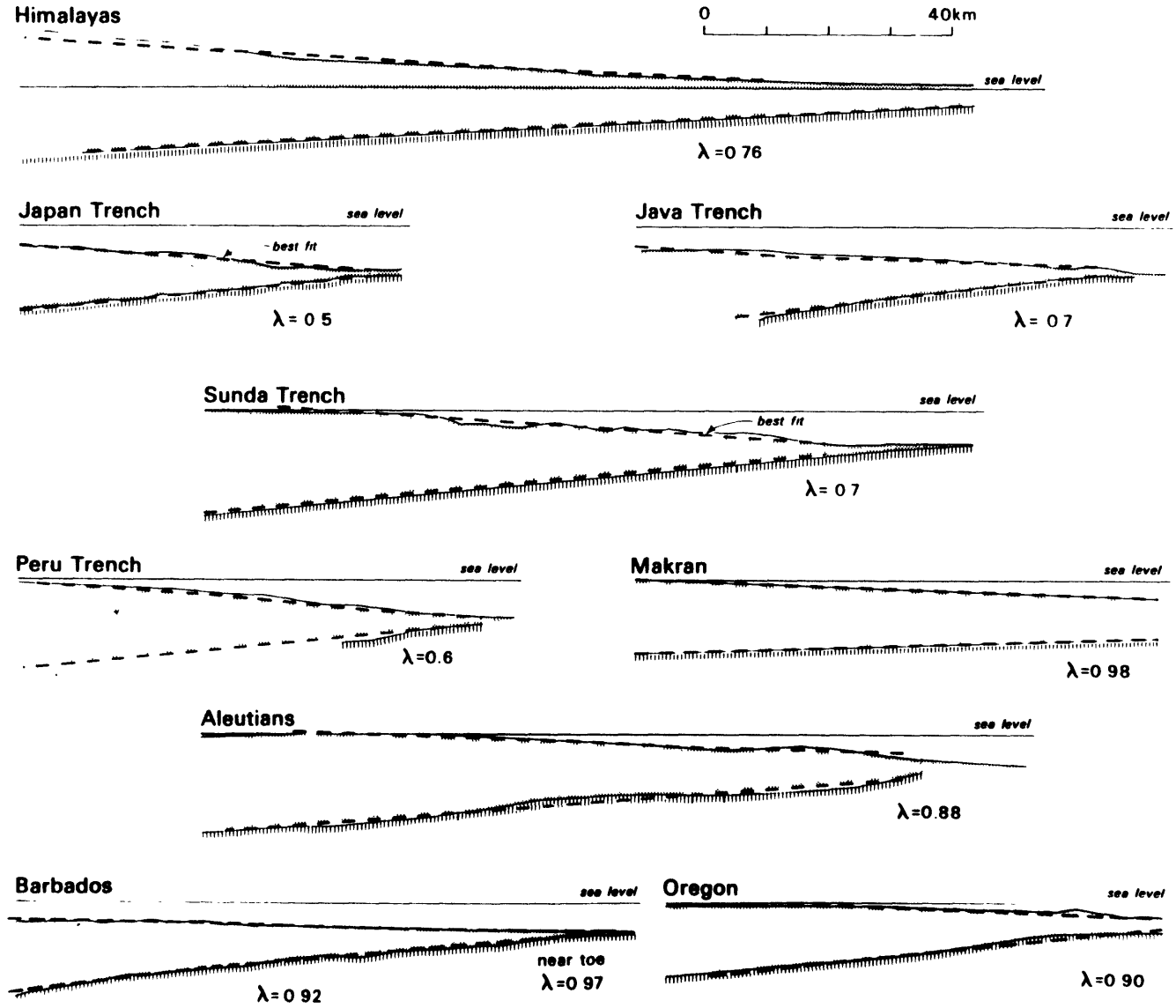
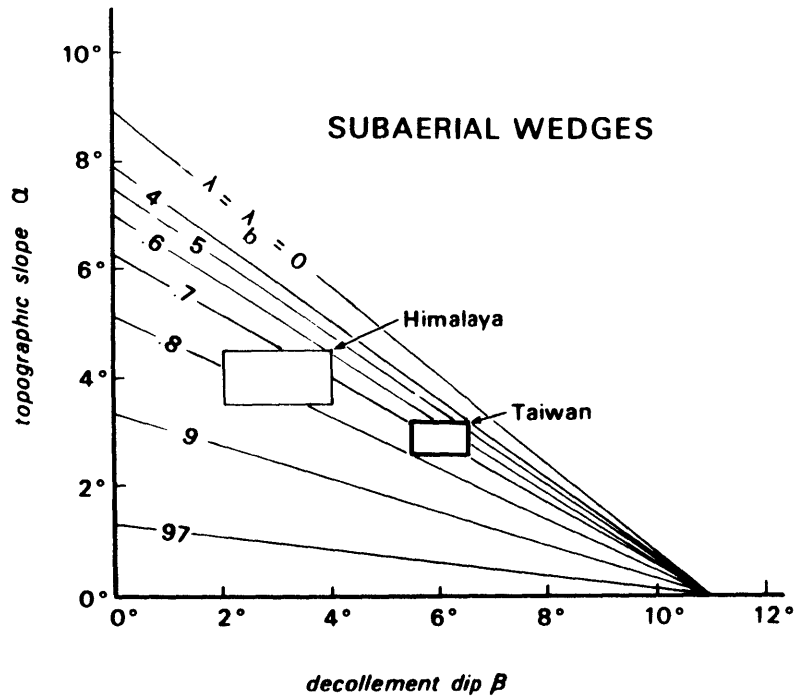


Figure 4.11

a)



b)

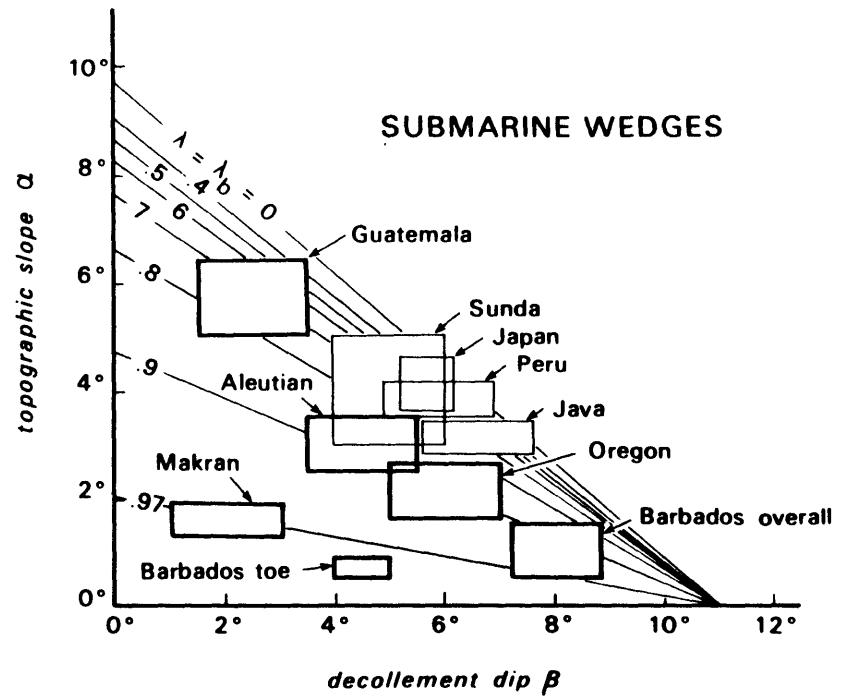


Figure 4.12

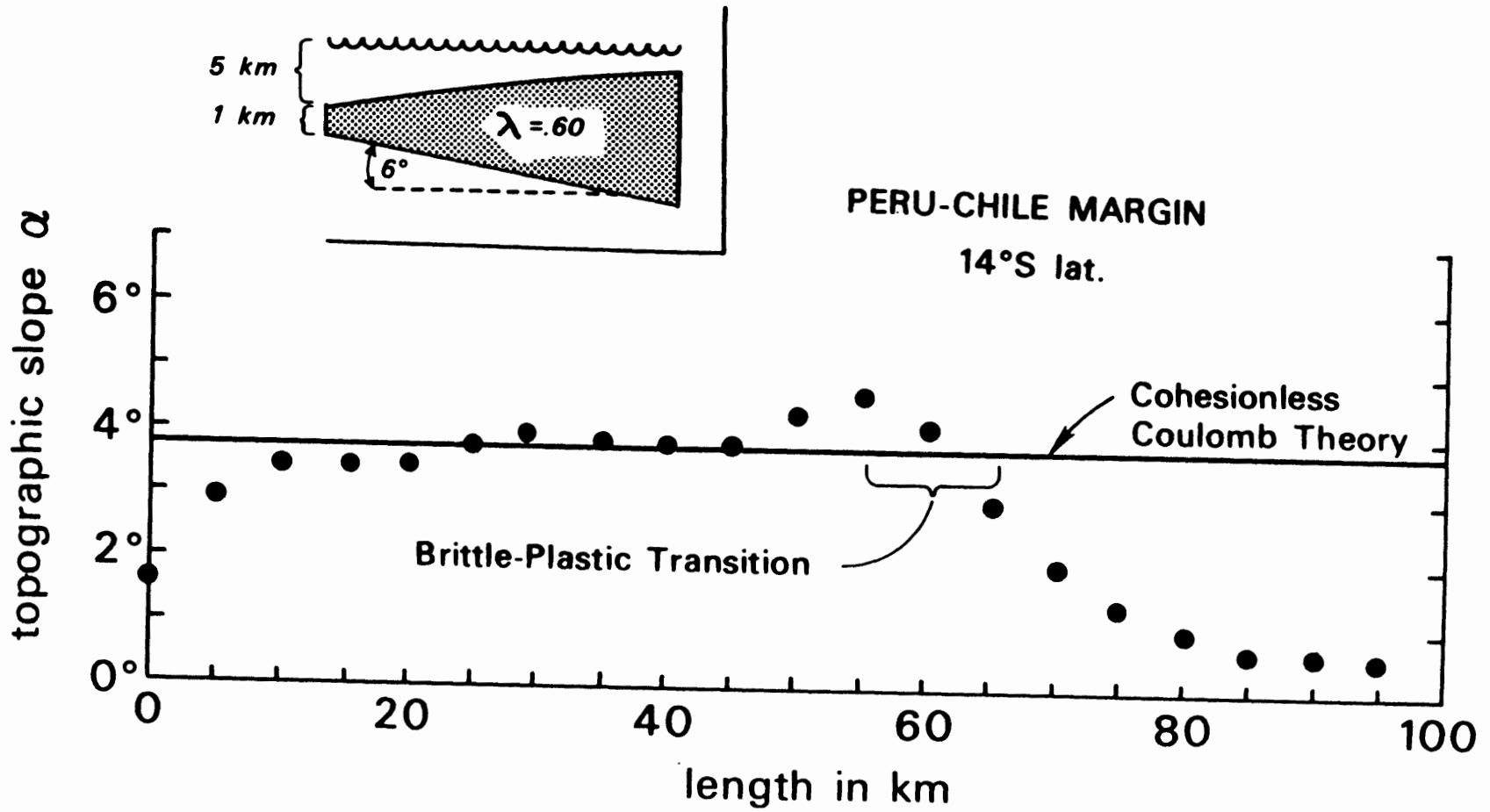


Figure 4.13

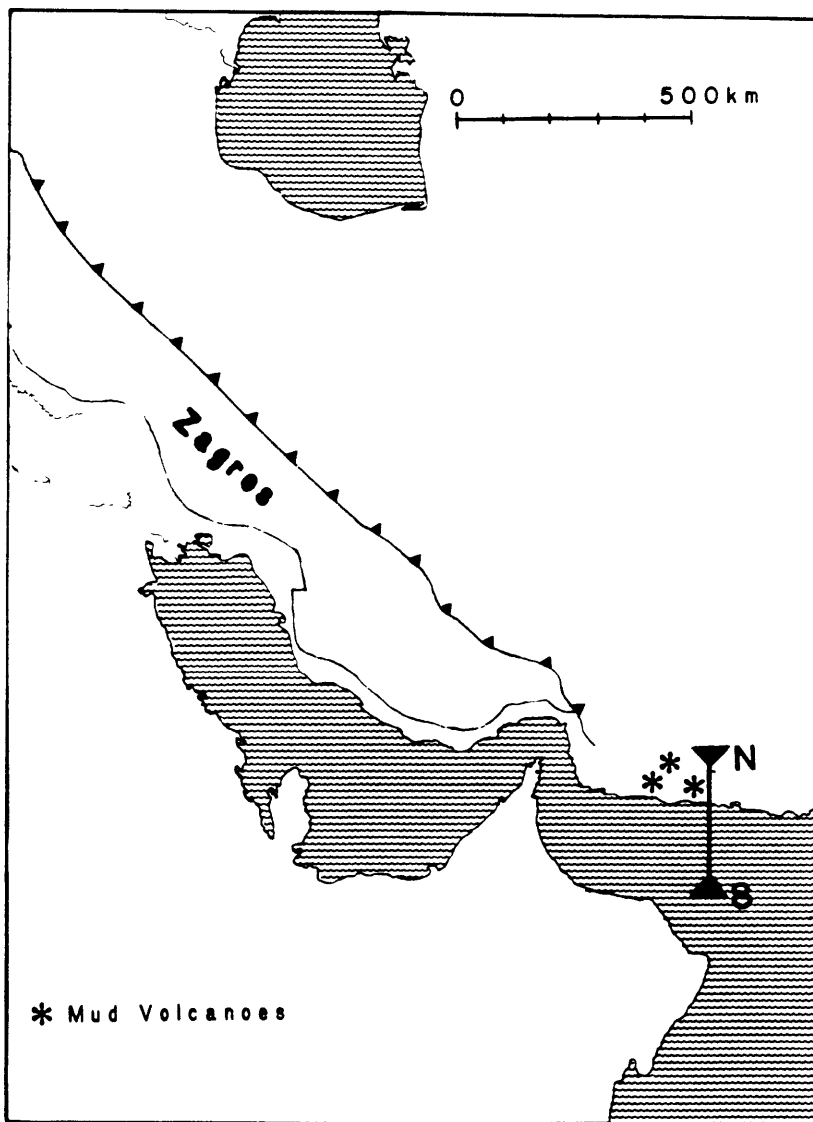
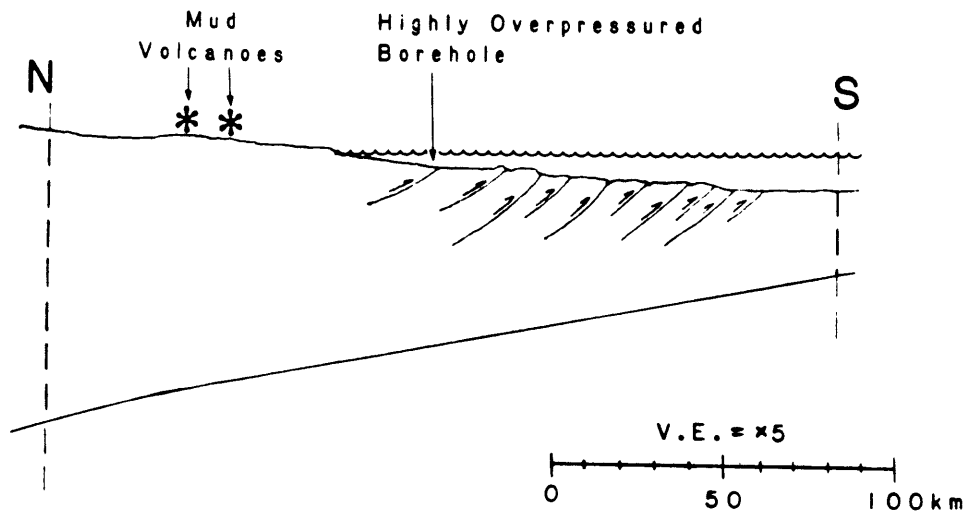
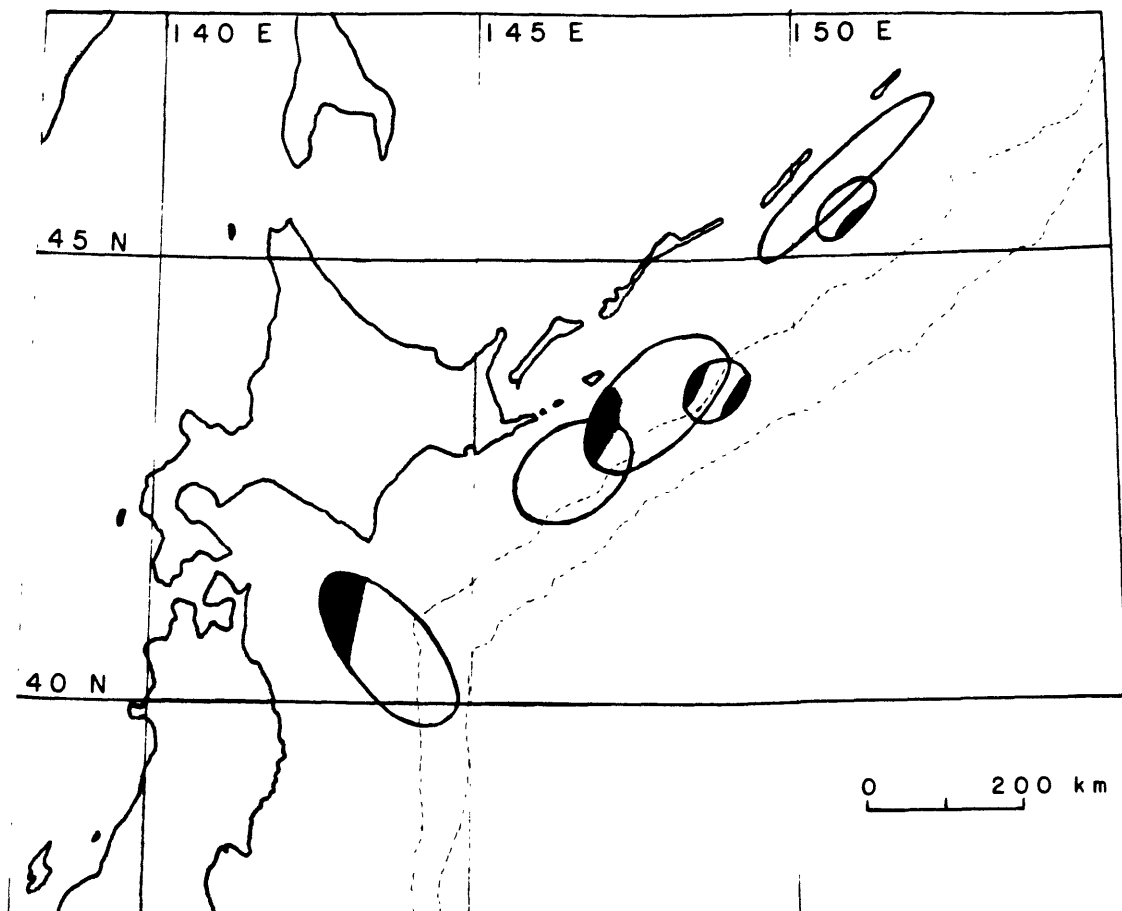
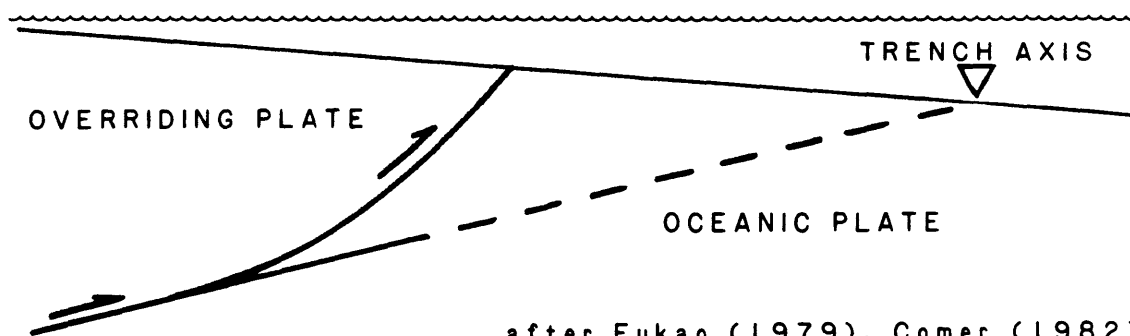


Figure 4.14

a)



b)



CHAPTER 5 ABSOLUTE VELOCITIES AND NET TORQUES5.1 INTRODUCTION

Among the reasons for studying the histories of absolute motion of the major plates are: 1) the characterization of relatively sudden changes in plate velocities and the relationships among the velocity histories of the different plates, 2) the discrimination among possible reference frames for "absolute" plate motions, and, as a long-term goal, 3) the development of a coherent model of the plate driving forces through time that can quantitatively account both for the global plate velocities and for rapid and large changes in the magnitude or direction of motion for individual plates. This chapter presents a determination of plate motions relative to a no-net-torque reference frame for the period 80 m.y. to the present. On the basis of these motions we address the above questions.

Because of the finite number of present plates and because of the uncertain dependence of the present characteristics of plate geometry and motion on the past evolution of plates and their boundaries, the amount of information on plate driving forces that one can obtain from the present plate velocities is limited (Chapter 1). Additional and independent information can be obtained from a study of the relationship of plate motions to driving forces at past times sufficiently distant from the present so that plate geometries or late velocities show significant differences.

Among the features of absolute velocity models which have been developed for the early Tertiary (Solomon et al., 1977a; Jurdy, 1978) were several that differ from solutions for present-day motions. Results of previous studies, described in Chapter 1, generally suggest that the clear separation of plates at present into fast oceanic plates and slow continental plates (Minster et al., 1974; Solomon et al., 1975; Forsyth and Uyeda, 1975) apparently did not hold 55 m.y. ago, and that subducted plates did not move much faster than those not subducted at 55 m.y., in contrast to the present (Solomon et al., 1975; Forsyth and Uyeda, 1975).

In this chapter, an expansion on work published by Davis and Solomon (1981), I shall examine these comparisons of plate speed with plate or plate boundary type for the entire period 80 m.y. ago to Present. One subject of interest is the question of whether there appears to be a definite limit to plate speeds, and whether any such limiting speed is higher for oceanic plates than for continental ones. Most importantly, we shall consider the role of plate boundary forces, particularly those associated with convergent margins, in determining plate speeds. This shall be done in two ways. First, we shall compare the calculated plate velocity histories with what is known about the histories of these plate boundaries. Second, the magnitude of the asymmetric torque applied to the lithosphere at a convergent margin shall be constrained by comparison of the observed polar wander curve for North America with the curve calculated on the assumption of no net torque.

5.2 A NO-NET-TORQUE CALCULATION

RECONSTRUCTIONS

The primary sources of data for reconstructing plate boundaries and for determining relative plate velocities are the finite plate rotations determined from magnetic anomalies in the various oceans and published in the literature. The major source of uncertainty in deriving global models of plate motions prior to 30 m.y. ago is the plate reconstruction in the south Pacific area. Proposed alternative models include separation of Antarctica into two plates for a period prior to that time (e.g., Molnar et al., 1975; Jurdy, 1978), internal deformation or plate segmentation within the Pacific plate (e.g., Suárez and Molnar, 1980; Gordon and Cox, 1980), and maintenance of plate integrity for both the Antarctic and Pacific plates (e.g., Weissel et al., 1977). Because of the importance of the southern Pacific plates (Pacific, Farallon, Kula) relative to the rest of the world, we consider the question of the correct reconstruction as open, and we have tested each of the proposed alternatives.

For each adopted set of reconstructions, the finite rotations are used to derive a globally consistent set of instantaneous relative angular velocity vectors (Solomon et al., 1977a) at 5 m.y. time intervals back to 80 m.y. ago. The total finite rotations for each plate in the model are then used to reconstruct plate positions at each 5 m.y. interval, using a digitized set of plate boundaries. Next,

the rotated positions of continents, ridges, trenches, transforms, and seafloor magnetic anomalies are used to produce a global map of plates and continents for each reconstruction time.

At each time for which the global set of relative angular velocities has been determined, there are several possible reference frames by which to define "absolute" plate motions. For this chapter we adopt a reference frame based on a global balance of torques on the lithosphere produced by plate driving forces (Solomon and Sleep, 1974), although alternative reference frames (e.g., fixed "hot spots") are possible. For each reconstruction and reference frame, the absolute plate motions through time are cast in terms of the rms plate speed. Changes in plate speeds with time provide a basis both for testing the assumptions and for defining tests of driving force models. The associated positions of the plates through time may also be tested against such independent information as paleomagnetic data which yield apparent polar wander.

PROCEDURE

The basic data set for determining the motions of the major plates in the past consists of a set of incremental rotations describing the finite relative motion between pairs of plates through time. The data set consists of the present positions of plate boundaries, prominent seafloor magnetic anomalies, and continental boundaries, along with one or more reference frames by which to define absolute velocity. From

the finite rotations we obtain, following the procedure of Solomon et al. (1977a), a self-consistent set of relative angular velocity vectors describing the "instantaneous" relative motions of all of the plates with respect to a single reference plate. We chose the North American plate as the reference because it is likely to be a slowly moving plate in most physically defined reference frames (Morgan, 1972; Solomon and Sleep, 1974). From the present plate boundaries and oceanic magnetic anomalies and the finite rotations we obtain maps of the plate boundaries for past times. For a given reference frame for absolute motions, we obtain the absolute angular velocities of the plates from their relative velocities.

A conceptually simple measure of the absolute speed of each plate as a function of time is the root-mean-squared (rms) velocity:

$$V_{\text{rms}} = \left[\frac{1}{A} \int_A (\vec{\omega} \times \vec{r})^2 dA \right]^{1/2} \quad (5.1)$$

where $\vec{\omega}$ is the absolute angular velocity vector at the appropriate time, \vec{r} is the radius vector from the earth's center to a point on the plate, and A is the total area of the plate over which the integration is performed. The rms speed of a plate is more physically meaningful than other possible scalar representations because of its close relation to the dissipation of energy by viscous drag at the base of the plates, assuming a linear drag law (Solomon et al., 1975).

To perform the integration in eq. 5.1, we first

define for each plate a Cartesian coordinate frame such that the z-axis is parallel to $\vec{\omega}$. Let θ be the colatitude in this reference frame. We divide the plate area into thin bands of constant colatitude θ_i and width $d\theta_i$. Let ϕ_i be the total length, in radians of longitude, of the segments of the i-th band within the plate. The rms velocity of the plate can then be expressed as:

$$\begin{aligned}
 V_{\text{rms}} &= \frac{\sum_i (\omega R \sin\theta_i)^2 \cdot R \sin\theta_i \phi_i \cdot R d\theta_i}{\sum_i R \sin\theta_i \phi_i \cdot R d\theta_i} \\
 &= \frac{\omega^2 R^2 \sum_i \sin^3\theta_i \phi_i d\theta_i}{\sum_i \sin\theta_i \phi_i d\theta_i} \quad (5.2)
 \end{aligned}$$

where R is the radius of the earth and ω is the scalar magnitude of $\vec{\omega}$.

As a framework for determining absolute plate motions in the past, we adopt the premise that no net torque has been exerted on the lithosphere. This premise, equivalent to a statement of conservation of angular momentum associated with tectonic motions for the earth's lithosphere, has provided a basis for the determination of present-day absolute motions of the plates in good agreement with data from paleomagnetism, paleosedimentation rates, and hot spot tracks (Solomon and Sleep, 1974; Solomon et al., 1975). With the further simplifying assumption that forces exerted on the lithosphere near plate edges are symmetric about the plate boundary, then only viscous drag at the base of the plates needs to be considered explicitly in the equation expressing

the balance of torque on the lithosphere. Departures from this last assumption are considered in a later section.

The torque contributed by viscous drag beneath each plate is assumed to be given by:

$$\vec{T} = - \int_A C(\vec{r}) \vec{r} \times (\vec{\omega} \times \vec{r}) dA \quad (5.3)$$

where C is a scalar drag coefficient with units of force per unit area per unit plate speed. Eq. 5.3 is based on the assumptions of: (1) a linear relationship between viscous drag (basal shear stress) and plate speed (strain rate); and (2) a purely resistive drag force that acts in a direction opposite to that of absolute plate velocity. Laboratory measurements of creep in mantle materials indicate that a nonlinear relationship between stress and strain rate is more likely than a linear one (e.g., Weertman, 1970), but the absolute velocities of the present plates are only weakly sensitive to the assumed rheology for the asthenosphere (Solomon et al., 1977b), so assumption (1) is retained here for computational simplicity. We will further assume, hereafter, that D is independent of lithosphere type and absolute velocity. Models of the asthenosphere "counterflow" needed to balance plate divergence and convergence indicate that assumption (2) is reasonable for the fast moving plates but may be incorrect for the slowly moving ones (Harper, 1978; Chase, 1979; Hager and O'Connell, 1979). Fortunately the slower moving plates make only a small contribution to the torque balance, so that assumption (2) is a reasonable

approximation for the purposes of this chapter in the absence of solutions for the full mantle flow problem.

We calculate the integral expression (eq. 5.3) for torque as follows. Define a Cartesian coordinate system for each plate as above with ω along the z-axis and let \vec{e}_x , \vec{e}_y , and \vec{e}_z be unit vectors along the respective axes. In such a coordinate frame, the local absolute velocity vector \vec{v} is given by:

$$\vec{v} = \vec{\omega} \times \vec{r} = \omega R \sin \theta (-\sin \phi \vec{e}_x + \cos \phi \vec{e}_y) \quad (5.4)$$

where θ is colatitude and ϕ is longitude ($\phi = 0$ along \vec{e}_x and $\pi/2$ along \vec{e}_y). The contribution to the torque vector from the drag acting on a unit area of the plate is:

$$\begin{aligned} d\vec{T} &= -C\tau \vec{x} \times \vec{v} \\ &= C\omega R^2 \sin \theta (\cos \theta \cos \phi \vec{e}_x + \cos \theta \sin \phi \vec{e}_y - \sin \theta \vec{e}_z) \end{aligned} \quad (5.5)$$

Dividing the plate area as above into bands of constant colatitude, let ϕ_{ij} and ϕ_{ij} be the length and central longitude of the j-th segment of the band of colatitude θ_i crossing the plate between longitudes ϕ_1 and ϕ_2 . Then, for the whole plate:

$$\vec{T} = \sum_i C\omega R^2 \sin \theta_i \left[\cos \theta_i \left(\sum_j \int_{\phi_1}^{\phi_2} (\cos \phi \vec{e}_x + \sin \phi \vec{e}_y) d\phi \right) - \phi_i \sin \theta_i \vec{e}_z \right] R \sin \theta_i \cdot R d\theta_i$$

or

$$\begin{aligned} \vec{T} &= -C\omega R^4 \sum_i \sin^2 \theta_i d\theta_i \left[\sin \theta_i \phi_i \vec{e}_z \right. \\ &\quad \left. - 2 \cos \theta_i \sum_j \sin \left(\frac{\phi_{ij}}{2} \right) (\cos \phi_{ij} \vec{e}_x + \sin \phi_{ij} \vec{e}_y) \right] \end{aligned} \quad (5.6)$$

The torque calculated from eq. 5.6 for each plate is then transformed into a standard Cartesian reference frame in

which the z-axis coincides with the earth's rotation axis. In this coordinate system the components of the torque vectors for each plate can be summed to yield the total net torque on the lithosphere for the reference frame in which the vectors $\vec{\omega}$ are prescribed.

In practice we first calculate \vec{T} for each plate from eq. 5.6 using the velocities given in the reference frame with North America fixed. The net torque \vec{T} with $C=1$ is numerically equivalent to the angular velocity of the lithosphere as a whole with respect to North America. If the negative of this angular velocity vector is added to the relative angular velocities of all plates with respect to North America, then the net torque due to drag is zero.

In this reference frame, the rms velocity of the lithosphere is minimized and the net rate of rotation of the lithosphere is identically zero. Within the constraint of our assumption that forces other than basal drag apply no net torque to the lithosphere as a whole, this method of calculating absolute plate motions should produce apparent polar wander curves for each plate which may be directly compared to paleomagnetically determined polar wander curves. Any difference between predicted and observed curves is likely to reflect a net torque applied to the lithosphere by unmodeled (e.g., plate boundary) forces and a resultant "true polar wander" (McElhinny, 1973; Jurdy and Van der Voo, 1974, 1975).

The finite rotation poles used to describe the relative

motions of the major plates since the ~~late~~ Cretaceous were taken from the literature. As far as possible, the rotations for closing any given ocean basin were derived from a single source. The rotations of Norton and ~~Slater~~ (1979) were used to close the Indian and South Atlantic Oceans and the Red Sea. In the North Atlantic, Africa and Greenland were closed to North America according to the rotations of Pitman and Talwani (1972), and the rotations for Eurasia with respect to North America are those of Sclater et al. (1977). The rotations used for relative motion of the Pacific and Antarctic plates are from Molnar et al. (1975). The motions of the Farallon and Kula plates with respect to the Pacific are, respectively, those of Pilger (1978) and Grow and Atwater (1970). Cocos plate motions were taken from Hey (1977). The motion of the Caribbean plate is from Malfait and Dinkelman (1973). Because it has no ridges along its boundaries, and knowledge of its motions is limited to less accurate techniques (Seno, 1977), no Philippine plate was included.

Schult and Gordon (in press) have pointed out some differences between their results and those of Davis and Solomon (1981) presented in this chapter, particularly a conclusion that Africa moved more slowly in the late Cretaceous than is indicated by our results. Of the differences between the reconstructions used in the two papers, only one appears to be significant. Schult and Gordon believe that Pitman and Talwani (1972) misidentified

anomaly 32 as anomaly 31, and they instead adopt the reconstruction of Cande and Kristoffersen (1977). If this criticism of Pitman and Talwani is valid, then the Africa-North America spreading rate used by Davis and Solomon (1981) for the period 80 to 63 m.y. ago is too fast. This would result in an erroneous additional westward motion of North America, and would affect conclusions on true polar wander for this period. This possible error has no impact, however, on the calculated plate motions since 63 m.y. ago.

Because of the uncertain history of the Antarctic and Pacific plates during the Cenozoic, three separate reconstruction models are considered here. In model A, the Antarctic and the Pacific are each assumed to have remained single plates throughout the Cenozoic (Figure 5.1). In model B, the Antarctic is treated as two separate plates (Figure 5.2). In model C, the Antarctic is considered as a single plate through the Cenozoic but the Pacific is divided into two plates in the early Tertiary (Figure 5.3). Rotation poles given in the concluding summary of Gordon and Cox (1980) are used for the split-Antarctic and split-Pacific models; relative motion in both cases is assumed to have lasted through the Paleogene (21 to 66 m.y. ago). In model B, West Antarctica is rotated 16° clockwise (forward in time) relative to East Antarctica, about a pole at 10° S, 72° W (Gordon and Cox, 1980); in Model C the North Pacific is rotated relative to the South Pacific 16° about a pole at 69° N, 57° W. Reconstructions between East and West Antarctica

present some serious difficulties. There is, at present, no clear seafloor evidence that relative motion on a scale as large as that proposed by Gordon and Cox (1980) has occurred. Further, the paleomagnetic evidence for two separate Antarctic plates indicates that any relative motion ceased by about 40 m.y. ago (Molnar et al., 1975; Suárez and Molnar, 1980) rather than continuing until 21 m.y. ago as in the reconstruction of Gordon and Cox (1980). If the relative displacement between East and West Antarctica proposed by Gordon and Cox (1980) occurred entirely prior to 40 m.y. ago, then the velocities of the Pacific Ocean plates relative to the rest of the world in model B for that time period would be higher than shown below. A final difficulty with the Gordon and Cox (1980) reconstruction arises from the fact that East Antarctica in their scheme is adjacent to the western edge of South America during the late Cretaceous. Because of a difference in our reconstruction of the circuit Antarctica-Africa-South America, the Gordon and Cox (1980) motion between the Antarctic plates results in some overlap between South America and the Antarctic Peninsula for the model B given here.

Maps of plate boundaries and continental shelf outlines were prepared at 5 m.y. increments in time back to 80 m.y. ago for each of the three plate reconstruction models. These maps were constructed from a digitized version of present plate and continent boundaries and from appropriate finite rotations of these boundaries in a self-consistent frame

(fixed North America). Growth and shrinkage of plates are handled routinely by this scheme. Changes in the shape of ridge and transform boundaries (primarily in the Pacific) were accommodated by keeping track of prominent seafloor magnetic anomalies. Magnetic anomalies were rotated with their underlying plate, and mid-ocean ridges were rotated according to the assumption of symmetric spreading. The plate boundaries determined for each time formed the basis for the calculations of rms velocity and torque given in eqs. 5.2 and 5.6.

5.3 CALCULATED ABSOLUTE VELOCITIES

The rms velocities of the major plates from 5 to 80 m.y. ago for the three alternative plate reconstruction models are given in Figures 5.4 to 5.7. The rms velocities for model A are shown for both the fixed-North-America frame (Figure 5.4) and for the reference frame with no net torque on the lithosphere exerted by basal drag (Figure 5.5). The latter frame is the basis for the rms velocities shown for the split-Antarctic model B (Figure 5.6) and the split-Pacific model C (Figure 5.7). The velocities at 5 m.y. ago in Figures 5.5 to 5.7 are in good agreement with the rms absolute velocities calculated for the present-day plates under the same assumptions (Solomon et al., 1975).

There are a number of noteworthy conclusions that may be drawn from Figures 5.4 to 5.7, both from common features of all models shown and from differences among the models for

the different assumptions concerning early Tertiary plate reconstructions. The plots of V_{rms} may be used to discern some types of errors in the reconstructions. One of the clearer examples is the case of the Farallon plate at 30 to 35 m.y. ago. The apparent slowness of the motion at 30 m.y. ago and the relatively rapid motion at 35 m.y. ago is likely to be an artifact of an incorrect time interval used to specify one or more of the finite plate rotations in the mid-Tertiary. Global analyses of plate speeds such as in Figures 5.4 to 5.7 will permit new constraints to be placed on plate reconstructions, and a review of the individual finite rotations with such figures as guides should result in the removal of anomalous accelerations and decelerations such as the one indicated for the Farallon plate.

A comparison of Figures 5.4 and 5.5 supports the view that the absolute motion of North America has been small since the late Cretaceous and that plate velocities calculated relative to a fixed North America are at least a fair approximation for the faster moving plates to the velocities calculated in another, more physically meaningful reference frame. It is worth noting that some of the small, shorter period fluctuations in the speeds of individual plates in Figure 5.4 (e.g., COC, SAM, IND) have been damped out in Figure 5.5, lending credence to a reference frame defined by lithospheric torque balance.

Models A, B and C yield generally similar curves for the rms velocities of the major plates since the late Cretaceous.

Compared to model A, the split-Antarctic model B gives higher speeds for the Kula and South American plates from 25 to 65 m.y. ago and somewhat different curves for the Farallon and Pacific plates with respect to the rest of the world for that same time period. Compared to model A, the split-Pacific model C differs primarily in the faster motion of the north Pacific and Kula plates during that time interval. For models B and C the areas of the Kula plate and of the northern portion of the Pacific plate are substantially larger in the late Cretaceous and early Tertiary than for model A.

It is difficult to choose among the three reconstructions the one which is most likely to be accurate. Model A gives the slowest lithospheric rms velocities during most of the early Tertiary, and gives the most stable and least erratic-looking velocity histories for the largest continental plates, but is inconsistent with Pacific ocean hotspot and pelagic sediment data (Suárez and Molnar, 1980; Gordon and Cox, 1980). Model B gives the highest lithosphere rms velocities, gives a clearly incorrect overlap of western Antarctica and southernmost Chile, and is based upon geologically unconstrained assumptions about the history of Antarctica. Model C with the Pacific plate split in the manner of Gordon and Cox (1980), is, by a small margin, the favored model, although none can be rejected outright.

At present, the fastest moving plates are the oceanic plates being actively subducted, and it has been proposed that the apparent upper limit of 8-10 cm/yr for the present

speeds of such plates is due to a natural regulation of subduction rate by a balance between forces of buoyancy and of resistance at subduction zones (Forsyth and Uyeda, 1975). As Figures 5.5 to 5.7 demonstrate, it is likely that V_{rms} has exceeded 10 cm/yr for the Indian and Kula plates by significant amounts for extended periods in the geologic past. The absolute speeds of 15 to 20 cm/yr for the Indian plate prior to 55 m.y. ago are particularly large. Such apparently rapid northward motion, predicted by the adopted reconstruction of Norton and Sclater (1979), deserves both careful scrutiny and, if found to be valid, an eventual physical explanation. The values shown for the late Cretaceous and early Tertiary velocity of India depend, in part, upon the determination of the time at which India separated from Madagascar. However, the time of this split is reasonably well constrained (Norton and Sclater, 1979), and paleomagnetic data from India (Pierce, 1978) yield a value for the northward speed of India of 14.9 ± 4.5 cm/yr, consistent with the values given in Figures 5.5 to 5.7. These results for the velocity history of India suggest that the range of speeds for the present plates might be a coincidence of present conditions rather than indicative of an inherent "speed limit" for plate motions.

The separation of the plates at present into fast oceanic and slow continental plates (Minster et al., 1974; Solomon et al., 1975; Forsyth and Uyeda, 1975) appears also to be approximately valid over the past 50 million years.

For times prior to 50 m.y. ago, however, this distinction is less appropriate. The most obvious counter-example is the exceedingly rapid motion of the partly continental Indian plate. The African plate, also, shows an rms velocity in the late Cretaceous comparable to or slightly greater than the velocities of the Pacific and Farallon plates (but note the discussion above on uncertainties in the North Atlantic reconstruction for this time period). Thus the notion that continental lithosphere intrinsically moves slowly with respect to the underlying mesosphere does not appear to be a general rule (Solomon et al., 1977a; Jurdy, 1978; Gordon et al., 1979). The sizeable decrease in the rms velocity of Africa between 65 and 60 m.y. ago is contemporaneous with the change to a much smaller rate of convergence between Africa and Eurasia (Dewey et al., 1973). This rapid change suggests that the high speed of the African plate before that time may have been related to a greater trench-pull driving force. For all of the reference frames and reconstructions used here, however, it remains true that the slowest moving plates are all largely continental.

A generalization that does appear to hold for the last 80 m.y. is that the fastest moving plates, whether oceanic or continental, are being actively subducted along a substantial fraction of their boundary. Plates moving at an rms velocity of 6 cm/yr or greater in Figures 5.5 to 5.7 are all in the process of being subducted.

5.4 RATES OF SPREADING AND MARINE TRANSGRESSIONS

There appears to be a distinct trend towards faster motions in the late Cretaceous compared to the Cenozoic. This tendency is displayed in Figures 5.4 to 5.7 for a number of individual plates and is not sensitive to the adopted plate reconstruction for the early Tertiary.

The rms velocity history of the lithosphere as a whole since the late Cretaceous, based upon the assumption of no net torque, is plotted in Figure 5.8. The rms speed of the lithosphere during the late Cretaceous was apparently nearly twice as large as during the middle and late Cenozoic, and should correspond to a major change in the rate of plate recycling. It is worth noting that the assumption of no net torque due to drag as used here, or equivalently of no net angular velocity of the lithosphere, yields the minimum value of rms velocity for the lithosphere as a whole for a given reconstruction. Thus relaxation of this assumption would give even higher rms velocities than those shown in Figure 5.8.

Mid-ocean ridges, at which new oceanic crust is generated, form the longest and most dramatic continuous topographic features on this planet. The strong correlation between the age and depth of the sea floor has been interpreted to be the result of cooling of the lithosphere as it moves away from the ridge (McKenzie and Sclater, 1969; Sleep, 1969). A number of empirical relationships between age, heat flow, and depth have been explored, and detailed

models proposed (e.g., Sclater et al., 1971). Subsidence is assumed to result from isostatic compensation, as the relatively dense oceanic lithosphere thickens as cooling causes the solidus to propagate downward. It has been shown (Davis and Lister, 1974; Parsons and Sclater, 1977) that for crust younger than roughly 80 m.y. of age this subsidence is proportional to the square root of age. The faster global seafloor spreading should result in generally younger seafloor, hotter and broader mid-ocean ridges, and therefore a greater volume displacement of ocean water and major marine transgressions (Hallam, 1971; Hays and Pitman, 1973). The likely relationship between fast motions and marine transgressions has been discussed as a mechanism for the Cretaceous transgressions (Hays and Pitman, 1973; Pitman, 1978, 1979).

It should be noted that the exact magnitude of the change in sea-level required to produce the Cretaceous marine transgressions has never been determined with any great deal of reliability. Estimates (Figure 5.9) vary from roughly 150 m to well over 300 m (Watts and Steckler, 1979; Vail and Mitchum, 1979). In addition, changes in the rate of creation of oceanic lithosphere are not necessarily required in order to produce such an effect. Parsons (1982) has pointed out that there are three major ways to vary the volume of the ocean basins. First, an increase in the rate of production of new sea floor can, as described above, increase the width of the topographic high associated with spreading ridges.

Second, the surface area of oceans may vary with time, particularly in the case of continent-continent collisions. Finally, selective consumption of sea floor at trenches can modify the age distribution of oceanic lithosphere in such a manner as to produce the same result as a change in the rate of production of ocean floor. Parsons (1982) argues that this third mechanism cannot be ignored, particularly in light of the migration toward the Americas of the East Pacific Rise-Farralon-Kula Ridge system through the late Cretaceous and early Tertiary.

Lithospheric rms velocities (Figure 5.8) are found to be only slightly higher than the present value since 60 million years ago. Higher velocities occur at earlier times when the uncertainties in our reconstructions are greatest. It is difficult to separate the effects of reconstruction errors from the actual rms velocity history, as it is a property of the reference frame chosen that any errors in reconstruction will tend to bias upward the calculated lithospheric rms velocity. Given the arbitrariness of all three models for the India-Antarctica-Pacific links before 60 m.y., the size of the plates of the Pacific ocean basin, and the "fulcrum effect" which causes small reconstruction errors in this link to cause large errors in calculated motions in the northern Pacific ocean, these velocities must be regarded with a healthy skepticism. In order to produce an effect large enough to eliminate the observed higher rms lithospheric velocity in the late Cretaceous, however, one must invoke

reconstruction errors much larger than are likely to be the case, as the difference in drag torque resulting from any error can be balanced by much smaller motions of the rest of the lithosphere. I conclude that plate rms velocities were higher in the late Cretaceous and early Tertiary than they are at present. There is strong circumstantial evidence that these higher plate speeds are closely related to the widespread marine transgressions at that time.

5.5 TRUE POLAR WANDER

Paleomagnetic poles through time for the major plates provide an independent check on the reconstructions and reference frames used in this paper. In particular, the reference frame used for Figures 5.5 to 5.7 is one in which there is no net rotation of the lithosphere and therefore no true wander of the magnetic pole with respect to the set of plates. Tests of true polar wander with respect to the lithosphere have been conducted by McElhinny (1973), by Jurdy and Van der Voo (1974, 1975), and by Jurdy (1981). In all cases, no resolvable wander of the pole with respect to the lithosphere as a whole has been discerned for the Tertiary. While these results lend credence to the reference frame for plate motions used here, small departures of predicted polar motion for individual plates from paleomagnetic observations may indicate that unmodeled plate forces produce a net torque on the lithosphere that has not been included in the present analysis.

In Figure 5.10, the apparent polar wander curves for North America for models A, B, and C, based upon a consistent reference frame with no net drag-related torque, are compared to Irving's (1979) geomagnetic poles at 25, 50 and 75 m.y. ago. At 25 m.y. ago the apparent North American poles of this paper match Irving's pole within its error circle. The match is still acceptable at 50 m.y. ago, but by 75 m.y. ago, all have diverged significantly from the paleomagnetic data, with the split-Pacific model C matching best (Figure 5.11). The sense of motion matches reasonably well (Figure 5.10), but the rate of apparent polar wander under the assumption of no net drag-related torque is slower than indicated by Irving's (1979) paleomagnetic poles.

The discrepancy between predicted and paleomagnetic poles for North America in the late Cretaceous suggests that while a global balance of torques may still provide a reference frame for plate motions, net torques on the lithosphere may be exerted by forces other than basal drag. The small magnitude of this discrepancy, however, suggest that such net torques are probably small in comparison to the typical contribution to the torque balance by drag beneath any of the larger plates.

Let us consider some possible sources of unbalanced torques which might act upon the lithosphere as a whole. Resistance to sliding along transform margins might be a very important factor in the balance of forces for an individual plate. Whatever the torque applied to a plate along a

transform boundary, however, an opposite and equal torque must be applied to the plate on the other side of that boundary. Therefore, no net torque is applied to the lithosphere as a whole at transform boundaries. Let us consider in some detail the torques which might be applied at the two other types of plate boundary.

RIDGE-PUSH FORCE

The magnitude of the contribution of mid-ocean spreading centers and their associated topographic relief to the set of forces which drive the plates is a subject of some uncertainty, with estimates typically ranging between 1.0×10^{12} and 4.2×10^{12} N per meter of ridge length (Hales, 1969; Frank, 1972; Artyushkov, 1973; Lister, 1975; Richardson and Solomon, 1977; Richardson, 1978; Turcotte, 1982). For a 100 km thick lithosphere, this yields net deviatoric stresses of from 10 to 36 MPa. It is even questioned whether subaerial topographic variations near continental margins might be more important as potential sources of driving forces than mid-ocean ridge topography (Frank, 1972; Chapple and Tullis, 1977).

Use of present-day plate motions to invert for driving mechanism (Forsyth and Uyeda, 1975; Chapple and Tullis, 1977) does not lead to the conclusion that the ridge-push force is a particularly important one. If the ridge-push is a plate boundary force, then it should be proportionally more important for smaller plates (such as the Cocos or Nazca plates) than for the Pacific plate. The fact that the speed

of oceanic plates does not appear to decrease appreciably with greater areal extent could thus be interpreted as an argument against the ridge-push force as an important factor for any plate (McKenzie, 1972). However, the ridge-push is the result of a gravitational body force, and not a boundary force (Lister, 1975), a distinction which alleviates much of the problem of area-independent speeds of oceanic plates.

Simple models for the cooling of oceanic lithosphere as it moves away from the spreading ridge have some interesting properties for driving forces (Lister, 1975; Hager, 1978). As the lithosphere ages, it cools, adding new, formerly asthenospheric, material to its base. However, its thermal boundary conditions remain the same and its mean temperature (and thus, its mean density) is conserved. In order to remain isostatically compensated, this strong, dense, and continually thickening lithosphere must subside.

Let us perform a simple calculation to illustrate some of the implications of the square-root-of-age relation for depth discussed above (Davis and Lister, 1974; Parsons and Sclater, 1977). Let the age-depth relation be

$$D = D_0 + K_1 \left(\frac{T}{\tau}\right)^{1/2} \quad (5.7)$$

where D is ocean depth, D_0 is the depth at zero age, T is the age of a given patch of oceanic lithosphere, K_1 is a length constant, and τ is a time constant. Define a dimensionless constant n such that

$$n = \frac{\rho_l - \rho_w}{\rho_l - \rho_m} \quad (5.8)$$

where ρ_w , ρ_l and ρ_m are, respectively, the mean densities of water, the lithosphere, and the asthenosphere. Then, assuming that the lithosphere has zero thickness beneath the ridge and that isostatic compensation holds for $T > 0$, the lithospheric thickness H must be given by the expression

$$H = (n-1)(D - D_0) \quad (5.9)$$

The material in this column of lithosphere slides downhill at a slope equal to that of the bathymetry (as opposed to that of the base of the lithosphere, which is n times larger), as the result of the addition of new material added with cooling at depth). This slope is given by the expression

$$\theta = \frac{\partial D}{\partial x} = \left(\frac{K_1}{\tau^{1/2}}\right) \frac{\partial}{\partial x} \left(\frac{x}{v}\right)^{1/2} = \left(\frac{K_1}{2}\right)(\tau v x)^{-1/2} \quad (5.10)$$

where x and v are, respectively, the distance from the ridge and the spreading half-rate. Equation 5.10 reduces to

$$\theta = \left(\frac{K_1}{2}\right)\left(\frac{T}{\tau}\right)^{1/2}(x)^{-1} \quad (5.11)$$

We can formulate a simple expression with which we can estimate the horizontal component of gravitational force acting upon a segment of the cooling lithosphere (Figure 5.12). Let the segment extend from the top to the base of the lithosphere, and be bounded by unit distances in the dx and dy directions (perpendicular and parallel to the ridge axis, respectively). Either by summing the forces which act on the lithospheric segment in Figure 5.12, or by considering the change in gravitational potential of the segment as it moves away from the ridge, we can estimate the horizontal driving force F_S acting upon the lithosphere beneath a unit

patch of sea floor, sliding on its own growing base, to be

$$F_S = (\rho_1 - \rho_w)H g \sin\theta \, dx \, dy \quad (5.12)$$

where g is the acceleration of gravity. With a small-angle assumption ($\sin\theta \approx \theta$), this reduces to

$$\begin{aligned} F_S &= \frac{(n-1)(\rho_1 - \rho_w)(K_1)^2}{2} \left(\frac{T}{\tau}\right) x^{-1} \, dx \, dy \\ &= \frac{(n-1)(\rho_1 - \rho_w)(K_1)^2}{2 \tau v} \, dx \, dy \end{aligned} \quad (5.13)$$

As has been pointed out by several authors (e.g., Lister, 1975; Hager, 1978), based upon somewhat different derivations, this relation has the surprising property that the incremental driving force is independent of distance from the ridge. This result is directly dependent upon the assumption of both a square-root of age relation for depth and complete isostasy. Parsons and Sclater (1977) give values of the parameters in the age-depth relation (eq. 5.7) for $\tau < 80$ m.y. as follows: $D_0 = 2500$ m, $K_1 = 350$ m, and $\tau = 1$ m.y. = 3.154×10^{13} sec. Combined with typical published estimates (Lister, 1975; Hager, 1978) for the other pertinent variables; $\rho_w = 1.0$ g/cm³, $\rho_1 = 3.36$ g/cm³, $\rho_m = 3.30$ g/cm³ (which yield $n \approx 40$), $g = 9.8$ m·s⁻², and $v = 70$ mm/yr we can find the horizontal force acting upon each unit area of sea floor, projected to the base of a patch of lithosphere which is less than 80 million years old. This force is a uniform 7.4×10^5 N per square meter of sea floor, in a direction away from and perpendicular to the ridge. Expressed as a total push per unit length of ridge, this gives a result (to 80 my) of 4.2 N/m which is close to or

slightly higher than most of the other estimates cited earlier. The most likely source of error in this estimate lies in the assumption of isostasy with a poorly constrained value of n (eqs. 5.8, 5.9, and 5.13).

In terms of a net global torque balance, the ridge-push can be ignored for any spreading ocean with a ridge which is truly mid-oceanic. Thus, all ridges in the Atlantic, Indian, and Arctic oceans can be assumed to provide negligible net torque. However, at present (Figure 5.13) and throughout the Tertiary (Figures 5.1-5.3), spreading centers have been located very close to the eastern edge of the Pacific ocean. This is the one area in the world in which the net torque due to a ridge-force may be important.

The bathymetry of the ocean floor flattens out considerably past 80 million years (Parsons and Sclater, 1977), so the gravitational driving force should be strongly concentrated in lithosphere younger than that age. We can carry out a calculation similar to that described above for younger ocean floor, using the empirical age-depth relation of Parsons and Sclater (1977) for age $T > 80$ m.y., $D = 6400m - 3200m \exp(-T/62.8 \text{ m.y.})$. We find $F_S (T > 80)$, the incremental driving force associated with a patch of lithosphere older than 80 m.y. old, is given by the expression

$$F_S (T > 80) = (\rho_l - \rho_w) H g \sin \theta \, dx \, dy$$

$$\approx (\rho_l - \rho_w) \left[(n-1) K_2 (1 - \exp(\frac{-T}{\tau_2})) \right] g \left(\frac{K_2}{\tau_2 v} \right) \exp(\frac{-T}{\tau_2}) \, dx \, dy \quad (5.14)$$

$$\approx (\rho_1 - \rho_w)g(n-1)\left(\frac{K_2}{\tau_2 v}\right)\left[\exp\left(\frac{-T}{\tau_2}\right) - \exp\left(\frac{-2T}{\tau_2}\right)\right]dx dy$$

where $K_2 = 3200$ m, $\tau_2 = 62.8$ m.y., and all other variables are the same as for eq. 5.13. This gravitational driving force is smaller than that for younger lithosphere, and decreases rapidly with age until for very old crust formed at the time of the Jurassic-Cretaceous boundary (anomaly M17), the incremental force per unit area is an order of magnitude less than for that of late Cretaceous (80 m.y.) age or younger.

We can divide the Pacific Ocean basin into "balanced" regions with lithosphere of matching age on the opposite sides of a spreading center and "unbalanced" regions which might contribute to create a net lithospheric torque. All such regions younger than 80 m.y. old are shown as shaded in Figure 5.13. The unbalanced part of the Pacific ocean younger than 80 m.y. (darker shading) has a total area of roughly 4×10^7 km². Because it is not oriented in such a manner as to maximize the resulting net torque, it acts in a manner equivalent to only 2.0×10^7 km² of optimally aligned sea floor. This is less than 10% as large as the total area of ocean floor younger than 80 m.y., which is 2.12×10^8 km² (Parsons, 1982). We can integrate the driving torque across this area by summing, in a vectorial sense, and according to a right-hand rule, the torque due to topography in each part of this area. The net torque about the center of the earth for that part of the Pacific ocean younger than 80 m.y. of age is 1.98×10^{26} N·m about a pole located at latitude 76.5°S,

longitude 99.8°W . The addition of lithosphere older than 80 m.y. makes only a very small difference in the net torque, changing it to 2.1×10^{26} N·m about a pole at 76.7°S , 105.8°W . The errors associated with this calculation, particularly with regard to the magnitude of the torque, are believed to be large compared to the additional contribution of lithosphere older than 80 m.y. The same calculation can be carried out for any chosen time in the past. Because of its susceptibility to errors in the reconstruction, no attempt was made to extend the calculation to the early Tertiary. However, largely due to the presence of the non-subducted Kula Ridge, the net torque at 30 m.y. ago due to lithosphere which was then younger than 80 m.y. was found to have a pole farther from the geographic pole (59.6°S , 76.7°W , with a magnitude of estimated to be 1.4×10^{26} N·m).

TRENCH-PULL FORCE

The negative buoyancy of a relatively cool subducted slab results in a plate driving force which presumably pulls the subducting plate into the trench. The magnitude of this driving force has been estimated by a number of authors. One essential factor is the thermal structure of the slab, which yields a negative buoyancy. Other important variables include the length and dip of the slab. The result, averaged across the thickness of the lithosphere (McKenzie, 1969; Jacoby, 1970; Turcotte and Schubert, 1971; Solomon and Paw U, 1975; Richardson, 1978), is typically between 100 and 400 MPa. Hager (1978) points out that while the horizontal mass

difference associated with a subducting slab (Schubert et al., 1975) is smaller than that for a spreading ridge, the much greater dip associated with the subducting slab gives it a much greater potential for driving plate motions. However, the stresses associated with the trench-pull force are probably much less than the several hundreds of MPa suggested by simple calculations, primarily due to local resistance to subduction at a variety of depths. Therefore, the relative importance of the trench-pull and ridge-push forces is not obvious a priori, either for a single plate or for the lithosphere as a whole.

Whatever the net pull acting upon the downgoing plate may be, it is not the value of this term which is of interest in calculating a net lithospheric torque. The observation that most overlying plates are moving toward the trench (Elsasser, 1971; Morgan, 1972) leads to the conclusion that there is a net trench "suction" force acting upon the upper plate which is large enough to overcome the shallow resistance near the trench (Forsyth and Uyeda, 1975; Chapple and Tullis, 1977). As both plates are pulled toward the trench, the net lithospheric torque must be calculated from the difference between these forces (Chapter 6). It is not entirely clear how the magnitude of the slab-pull force is scaled, particularly with respect to subduction velocity. Harper (1978) suggests that as slab thickness S is proportional to the square root of age T , then the time to thermal equilibrium ($\propto S^2$) is proportional to T , and the

downdip mass excess to VS^2 or VT , where V is the convergence rate. This leads him to conclude that total torque is proportional to VS^3 , or $VT^{3/2}$. However, given the ambiguity attached to this question, let us make the simplest possible assumption, namely that each unit length of trench provides an equal trench-pull force. We can thus sum up the torques associated with each trench-segment in the world (Figure 5.14) in the manner of Solomon and Sleep (1974) who show that the trench-pull torque T_t is given by

$$\vec{T}_t = C_t \int_{\text{line } t} \vec{r} \times (d\vec{l} \times \vec{r}) \quad (5.15)$$

where C_t is a constant, \vec{r} is a radius vector from the center of the earth, and $d\vec{l}$ is a tangent to the line t which the trench follows across the surface of the earth. This is reduced to

$$\vec{T}_t = C_t (\vec{r}_2 - \vec{r}_1) \quad (5.16)$$

where \vec{r}_1 and \vec{r}_2 are the radius vectors corresponding to the two ends of the trench. Carrying out this operation with $C_t = 1$ for all of the trenches in Figure 5.14, we find a net torque pole at 16.1°N , 84.1°E ; this location differs by only 20° of arc from the pole at 3.8°S , 82.3°E determined by Solomon and Sleep (1974). The magnitude of the torque is equal to that of 1.197 radians (7630 km) of optimally aligned trench. As there is a total length of 4.83×10^4 km of trench on the earth's surface (Parsons, 1982), this means that the orientation of trenches is sufficiently random (Figure 5.14) as to effectively eliminate 84% of their net-torque-applying ability. The remaining portion (16%)

which is calculated here is smaller than the 20-30% reported by Solomon and Sleep (1974). This "net torque efficiency" of 16% for the trench-pull force is similar to the value of 10% determined above for the ridge push force. This means that both potential driving forces are approximately equally inefficient at driving the lithosphere as a whole. The addition of continent-continent convergence zones causes the net torque pole to move to 20.8°N, 54.7°E, as compared to 11.1°N, 58.8°E for Solomon and Sleep (1974).

5.6 THOUGHTS ON ABSOLUTE MAGNITUDES OF PLATE DRIVING FORCES

LITHOSPHERIC VERSUS SINGLE-PLATE DRIVING FORCES

The balance of torques on the lithosphere as a whole is considerably different from a similar balance of torques for a single plate. A single-plate torque balance is dominated by boundary forces (trench-pull and possibly transform fault forces) and a pseudo-boundary force (the ridge-push force). Thus it would appear that an attempt to balance the relatively small basal drag torques is equivalent to the case of the tail wagging the dog. As stated earlier, it is a fundamental assumption for the analysis of this chapter that boundary torques around the world summed in a vector sense around the world have an absolute value much smaller than the sum of their individual magnitudes. In other words, it is assumed that they nearly cancel.

We are now in a better position to analyze this assumption. Torques related to transform faults can be assumed to

sum to zero. We have seen that the rough symmetry of the world's growing oceans greatly reduces their associated ridge-push forces from consideration in the global torque balance, despite their importance as driving forces for individual plates. Even in the Pacific Ocean, much of the ocean floor younger than 80 m.y. is balanced. In total, the ridge-push force balances roughly 90% of its own potential net torque, reducing its net global torque by a factor of roughly ten.

Forces related to trenches, dominant for individual plates, are even more severely reduced in importance on a global scale. First, we have shown that the orientations of trenches around the world reduce the net torque which they can apply to the lithosphere by roughly 84%. The torque applied to the downgoing plate is governed by the difference between the net slab-pull and the sum of deep and shallow resistances to subduction, while the torque applied to the overlying plate is opposite in sign, and is governed by the difference between the "trench-suction force" and that same shallow resistance to subduction. Thus, no matter how large it may be, the shallow resistance to subduction does not appear in the net global lithospheric torque balance. That balance is controlled by the difference between the slab pull force and the sum of the deep resistance to subduction and the trench suction force. As described earlier, in order to explain motions of overlying plates, this trench suction force must be even larger in magnitude than the shallow

resistance to subduction, which (Chapter 4) is quite large and is disproportionately important compared to the area over which it acts. Thus, in terms of the net lithospheric torque, not only is the trench-pull torque resolved only as 16% of the sum of net local torques associated with trenches, but because it must be partially offset by the trench "suction" force acting on the opposite plate, the local torque is itself considerably smaller than that which is applicable for a single-plate torque balance.

MAGNITUDES OF TORQUES

Close examination of Figure 5.11 shows that during the past 50 m.y., the paleomagnetic pole of Irving (1979) has not deviated from the poles calculated for any of three reconstruction models by more than 1.9°. Earlier than that time, the predicted and observed poles diverge, with the observed poles further toward the Pacific Ocean half of the world than predicted.

This is roughly the same direction of polar wander as that which would be expected to result from the ridge-push force, which has a pole at latitude 59.6°S, 76.7°W at 30 m.y. ago. We can decompose a net rotation of the lithosphere into its components (Ω_x , Ω_y , and Ω_z) about the x, y and z axes (located respectively on the Greenwich meridian at the equator, 90°E on the equator, and the north pole). Paleomagnetic data are sensitive to Ω_x and Ω_y , but totally insensitive to Ω_z . Therefore, a driving torque at such a high latitude as the present location of the ridge-push

torque (77°) is inefficient at generating an observable polar wander. Taking the 30 m.y. ridge-push torque as representative, to the first order, of that torque over the past 50 m.y., we can calculate the mean stress at the base of the lithosphere if that were the only non-basal torque applied to the lithosphere.

If the coefficient of basal drag is everywhere uniform, then the magnitude of the torque associated with a rotation of the whole lithosphere is given by

$$|\dot{T}| = \int_{-\pi/2}^{\pi/2} 2\pi\omega CR^4 \cos^3\theta \, d\theta = \frac{8\pi}{3} \omega CR^4 \quad (5.17)$$

where C is the drag force constant (a ratio of basal shear stress to speed), and R is the radius of the earth. Taking the observed true polar wander over the past 50 m.y. to be $< 1.9^\circ$, we find an angular velocity about a pole at the equator of $3.8 \times 10^{-8} \text{ }^\circ/\text{yr}$, although uncertainty in Irving's smoothed paleopoles permits as much as twice this motion. Making the assumptions described above, we find

$C = 4.3 \times 10^{14} \text{ kg}\cdot\text{m}^{-2}\cdot\text{s}^{-1}$, and the basal shear stress 90° from the torque pole associated with this mean lithospheric motion would be roughly 100 kPa. This value for C , however, would require (for a linear drag law) basal shear stresses beneath relatively fast moving plates equal to 2 or 3 MPa, stresses roughly an order of magnitude higher than that suggested by the calculations of Melosh (1977) and well above the single-plate estimates of Davies (1978).

It is unlikely that the ridge push force results in a

torque which is much larger than that contributed by the net trench-pull force, an assumption implicit in the preceding analysis. The trench-pull torque, which has an undetermined magnitude, has a pole calculated above to be located at latitude 16.1°N , longitude 84.1°E at present and 10.1°N , 66.1°E at 55 m.y. ago. Although separated from the ridge-push pole by only (very approximately) 130° , the trench-pull torque tends to produce a true polar wander curve (toward 174°E at present and toward 156°E at 55 m.y. ago) which is almost exactly opposite to that produced by the ridge-push torque (toward 16°W at present and toward 13°E 30 m.y. ago).

Ignoring for the moment the poorly understood period before roughly 60 m.y. ago, we can explain the lack of any clearly resolved true polar wander over the past 60 m.y. (particularly for model C) in any of three ways: 1) The assumptions of a uniform and linear drag torque might be fundamentally incorrect. However, as explained above, this appears to be a reasonable assumption, particularly for those plates which have the largest effect upon the torque balance. 2) All unbalanced torques might be too small to be resolved, due to the resulting true polar wander being obscured by basal drag. However, as shown above, this is likely to imply unacceptably high shear stresses at the base of fast-moving plates. Finally, 3) the motions of the pole resulting from the trench-pull and ridge-push torques might roughly cancel. The torques applied to the lithosphere by these two driving forces cannot sum to zero, but Ω_x and Ω_y can approach zero,

giving no polar wander. If the longitudes of the two torque poles are roughly 180° apart (they are shown above to be approximately 170° apart at present), and assuming a linear drag law, no polar wander requires that

$$T_{\text{RIG}} \cos \phi_{\text{RIG}} = T_{\text{TREN}} \cos \phi_{\text{TREN}} \quad (5.18)$$

where T_{RIG} and T_{TREN} are the magnitudes of, respectively, the ridge-push and trench-pull torques, and ϕ_{RIG} and ϕ_{TREN} are the latitudes of the corresponding poles. Making the assumptions about the ridge-push torque described above, eq. 5.18 gives a value of the trench-pull torque of approximately $T_{\text{TREN}} = 6.8 \times 10^{25} \text{ N}\cdot\text{m}$. Given the orientations and lengths of trenches described above, and assuming a lithospheric thickness of 100 km, this yields a net trench-pull associated stress in the two plates at the convergent margin of $1.5 \times 10^7 \text{ N/m}^2$, or 15 MPa. Considerable care must be exercised in the interpretation of this result, as it does not correspond directly to any simply measurable parameter. It may be best to describe this result in terms of the net torque, taking both plates into account, per unit length of trench. Defined in this way, we find the trench-pull torque to be equal to $9.0 \times 10^{18} \text{ N}\cdot\text{m}$ per meter of length of trench.

The fortuitous balance of torques described above would suggest that there might have been times in the past when plate geometries were not arranged such that the net ridge-push and trench torques nearly opposed each other in generating true polar wander. If this were the case, then

the negligible true polar wander during the Tertiary (Jurdy and van der Voo, 1974, 1975; Jurdy, 1981; Davis and Solomon, 1981) need not be indicative of other time periods. It is tempting to ascribe to a torque imbalance what appears to be rapid polar motion prior to 40 m.y. ago (Figure 5.11), as well as periods during which many of the major plates showed rapid motions, possibly associated with some polar wander, such as the late Jurassic (Schult and Gordon, in press). For example, subduction along the northern Tethyan margin before continental collision would produce a true polar wander in the direction observed in Figure 5.11. If the present-day ridge-push torque were to act in the same direction as an equally large trench-pull torque, then true polar wander could be as large as several cm/yr, if we accept the estimates of Melosh (1977) for the magnitude of the shear stress on the base of a lithospheric plate. However, possible errors in reconstructions during the late Cretaceous and earliest Tertiary, such as those pointed out by Schult and Gordon (in press), are too large to confirm any such hypothesis at this time.

5.7 CONCLUSIONS CONCERNING THE ABSOLUTE VELOCITY MODELS

Models for the configurations, positions and absolute motions of the major plates for the period 80 m.y. ago to the present have been presented in this chapter. The models have been based on three alternative reconstructions of the plates in the southern Pacific Ocean for the early Tertiary.

A number of conclusions can be drawn from the results of the work presented in this chapter: (1) The reconstruction model with two Antarctic plates in the early Tertiary gives speeds significantly higher for the Kula plate and somewhat higher for the Pacific plate for that time compared to a model with a single Antarctic plate. The magnitudes of these increased speeds depend on the detailed reconstruction. A reconstruction model with a split-Pacific plate for the early Tertiary yields similarly higher speeds for the North Pacific and Kula plates, although the range of possible reconstructions of this type is not well constrained. The split-Antarctic and (to a lesser extent) split-Pacific models result in much larger areas for the Kula and Farallon plates in the late Cretaceous, and therefore significantly faster subduction of those plates since that time.

(2) The absolute motion of India was anomalously fast (15-20 cm/yr) during the late Cretaceous, before the Indian and Australian plates had joined, and apparently disproves the hypothesis that a maximum speed of about 10 cm/yr is regulated by the subduction process (Forsyth and Uyeda, 1975). During this period, India moved at a speed 2 to 3 times faster than any other continent, and faster than any oceanic plate. This anomalous behavior is relatively insensitive to uncertainties in the Tertiary reconstruction of the Pacific and Antarctic plates, as well as to the effect of the disputed reconstruction of Pitman and Talwani (1972).

(3) The tendency at present for largely continental

plates to move much more slowly than oceanic plates (Forsyth and Uyeda, 1975; Solomon et al., 1975) has persisted for the last 50 m.y. in a reference frame based on balancing torque due to basal drag beneath the plates. This separation of plate speeds by lithospheric type does not appear to hold for the late Cretaceous, however, and should not therefore be regarded as a general rule (cf., Gordon et al., 1979). The fastest moving plates have consistently been those subducted along a substantial fraction of their boundary. Although errors in reconstruction may explain the fast motion of some of the continents, the motion of India is clearly too fast to be interpreted as anything but real.

(4) A distinct trend is observed toward globally faster plate motion in the late Cretaceous compared to the present. Since roughly 50 million years ago, there has been no significant change in the overall rate of plate motions. This estimate is sensitive to possible errors in plate reconstructions, but it is not strongly controlled by any single plate. While the exact magnitude of the velocity change is subject to some uncertainty, the presence of significantly higher speeds appears to be the most plausible explanation of the result. The end of this period of fast motion was followed about 20 m.y. later by the termination of a major worldwide marine transgression (Hays and Pitman, 1973). The faster global plate motion also implies that the heat flow in the late Cretaceous contributed by oceanic lithospheric recycling was significantly greater than at

present (Turcotte and Burke, 1978; Sprague and Pollack, 1980).

(5) The apparent polar wander curve for North America based on a reference frame defined by a balance of torques arising from basal drag lies close to published paleomagnetic poles. The difference between the paleomagnetically observed motion of North America with respect to the spin axis and that defined by the torque-balance requirement may be attributable to a small net torque on the lithosphere exerted by plate boundary forces.

(6) That the magnitude of the net torque contributed by plate boundary forces is inferred to be small can be explained in any of three ways. First, there may be a fundamental error in the assumption of linear drag, although for reasons described earlier this is considered the least likely possibility.

Second, all net torques may, as originally assumed, be small compared to basal drag. This would be possible if the basal drag associated with true polar wander is as small as 100 kPa, assuming that the net trench-pull torque is also small (not appreciably larger than the calculated net ridge-push torque of roughly 2.1×10^{26} N·m). However, this implies that the drag stress on the base of a relatively fast ($V \approx 10$ cm/yr) plate is as large as 2 or 3 MPa, a value considered unlikely.

Finally, the net torques may individually be important in magnitude, but may cancel each other out to produce no

significant true polar wander at present. The net trench pull torque would, tend to produce a polar wander directly opposite (within the precision of the calculation) in direction to that associated with the net ridge-push torque. If these are the only important net torques driving the and if there is no true polar wander, then the net unbalanced torque associated with each meter of length of trench is 9.0×10^{18} N·m. Assuming that the lithosphere is 100 km thick, then this would suggest that the mean plate-boundary associated stress across the subducting plate is roughly 15 MPa greater than the mean extensional stress induced by the 'trench suction' and transmitted through the back-arc to the overlying plate.

If the present lack of true polar wander is the result of such a fortuitous alignment of driving torques, then measurable true polar wander should be expected for periods with significantly different plate boundaries. The closing of Tethys is an example of an event which could so effect the net torque balance.

FIGURE CAPTIONS

- Fig. 5.1 Azimuthal equidistant projections about the north and south poles of the boundaries of the plates and of present-day shorelines at 25 m.y. intervals for reconstruction model A. The reference frame is one in which there is no net torque due to viscous drag. In the northern hemisphere maps (at left), 0° East longitude is at right, 90° East at top, 180° East at left, and 90° West is at the bottom. In the southern hemisphere maps (at right), 0° East longitude is at right, 90° East at bottom, 180° East at left, and 90° West is at the top.
- Fig. 5.2 Plate boundaries at 25 m.y. intervals for the split-Antarctic model B. Map projections are as for Fig. 5.1.
- Fig. 5.3 Plate boundaries at 25 m.y. intervals for the split-Pacific model C. Map projections are as for Fig. 5.1.
- Fig. 5.4 Root-mean-squared velocity of the major plates at 5 m.y. intervals to 80 m.y. ago for reconstruction model A. North America is assumed fixed. Abbreviations for the plates (see Fig. 5.1) are AFR (African), ANT (Antarctic), AUS (Australian), COC (Cocos), EUR (Eurasian), FAR (Farallon), IND (Indian), KUL (Kula), PAC (Pacific), and SAM (South American).

Fig. 5.5 Rms velocities of the major plates for model A in the reference frame with no net torque due to basal drag. ANE and NAM are the Antarctic and North American plates, respectively.

Fig. 5.6 Rms velocities of the major plates for reconstruction model B in the reference frame with no net torque due to basal drag. ANE and ANW are the East and West Antarctic plates, respectively.

Fig. 5.7 Rms velocities of the major plates for reconstruction model C in the reference frame with no net torque due to basal drag. NPA and PAC are the North and South Pacific plates, respectively.

Fig. 5.8 Rms speed of the lithosphere as a whole since the late Cretaceous for the three models in Figs. 5.5 to 5.7.

Fig. 5.9 Comparison of the range of estimates Rms speeds of (Fig. 5.8) the lithosphere as a whole (the shaded region) with estimates of sea-level changes since the Cretaceous-Tertiary boundary. Sea level estimates are as follows: The heavy dashed line is a smoothed curve after Vail et al. (1977), calibrated by sea level estimates of Pitman (1978) and adapted from Parsons (1982). The heavy solid line is the estimate of Watts and Steckler (1979), and the fine line is an interpolation of the results of Bond (1978). The time scale for the sea level estimates is read at bottom. The time scale

for the range of rms lithosphere speeds (which are encompassed within the shaded band) is at top. Times are offset by a period of 15 m.y., chosen as a reasonable lag-time between changes in the rate at which plate motions take place and the resulting change in sea level. This is intended to make the two curves more directly comparable.

- Fig. 5.10 Three paleomagnetic poles for North America, with error circles (Irving, 1979), compared with the poles predicted according to models A, B, and C under the assumption of no net torque due to drag (i.e., no true polar wander).
- Fig. 5.11 Wander of paleomagnetic poles (Irving, 1979) with respect to no-net-drag-torque poles for models A, B, and C. Coordinates are defined by rotating the present-day pole to the appropriate torque balance pole about a rotation pole at the equator.
- Fig. 5.12 Schematic diagram illustrating the estimation of the ridge-push force due to a segment of lithosphere moving away from the ridge.
- Fig. 5.13 Map of spreading ridges. Note that all major ridges, except those in the East Pacific, are located in the middle of an ocean. The more darkly shaded area indicates the "unbalanced" part of the Pacific ocean younger than 80 m.y. Base map after Sclater et al. (1981).
- Fig. 5.14 Map showing distribution of subduction zones. Base map after Sclater et al. (1981).

Figure 5.1
MODEL A, SINGLE ANT, PAC

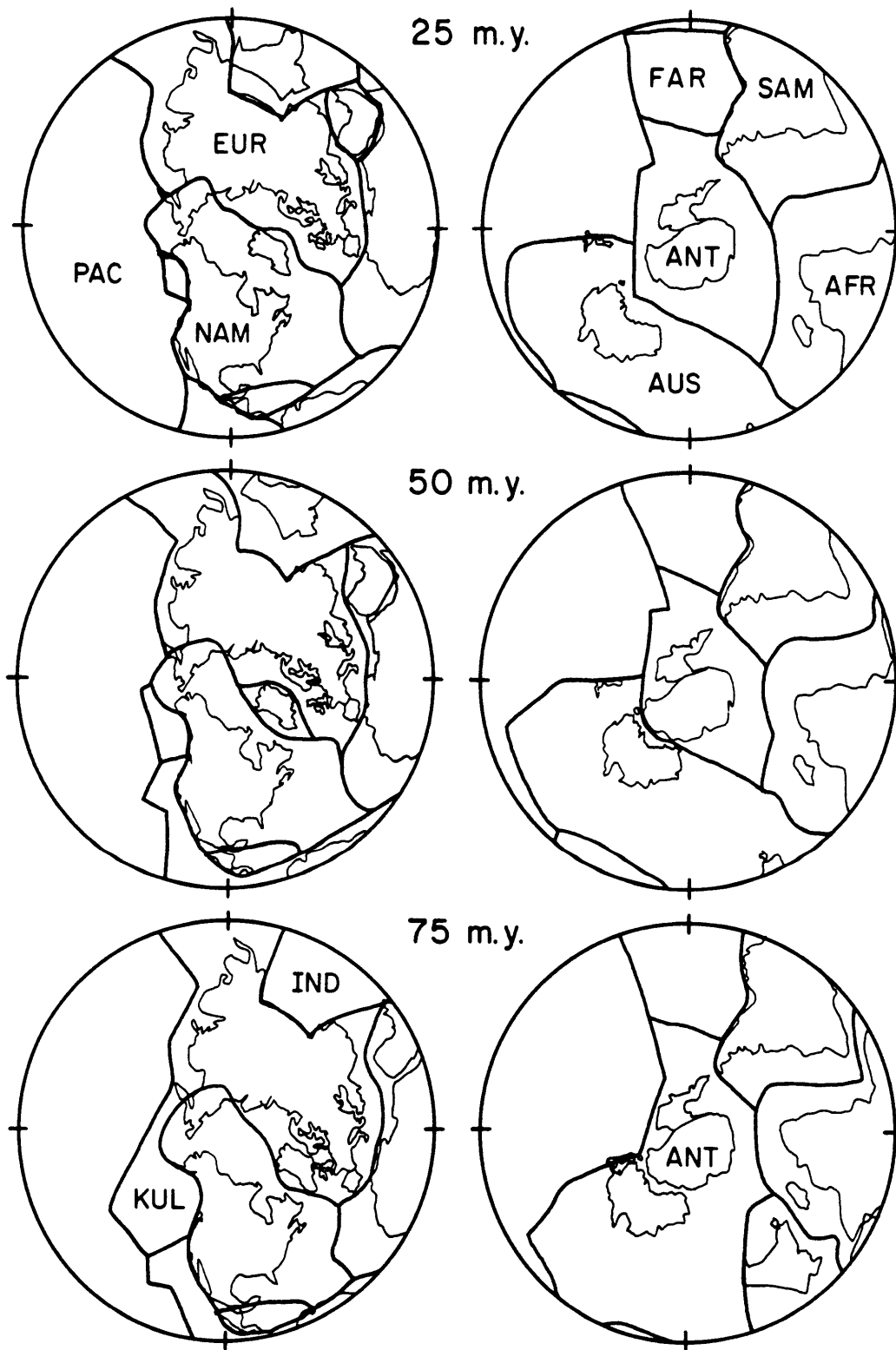


Figure 5.2

MODEL B, SPLIT ANT

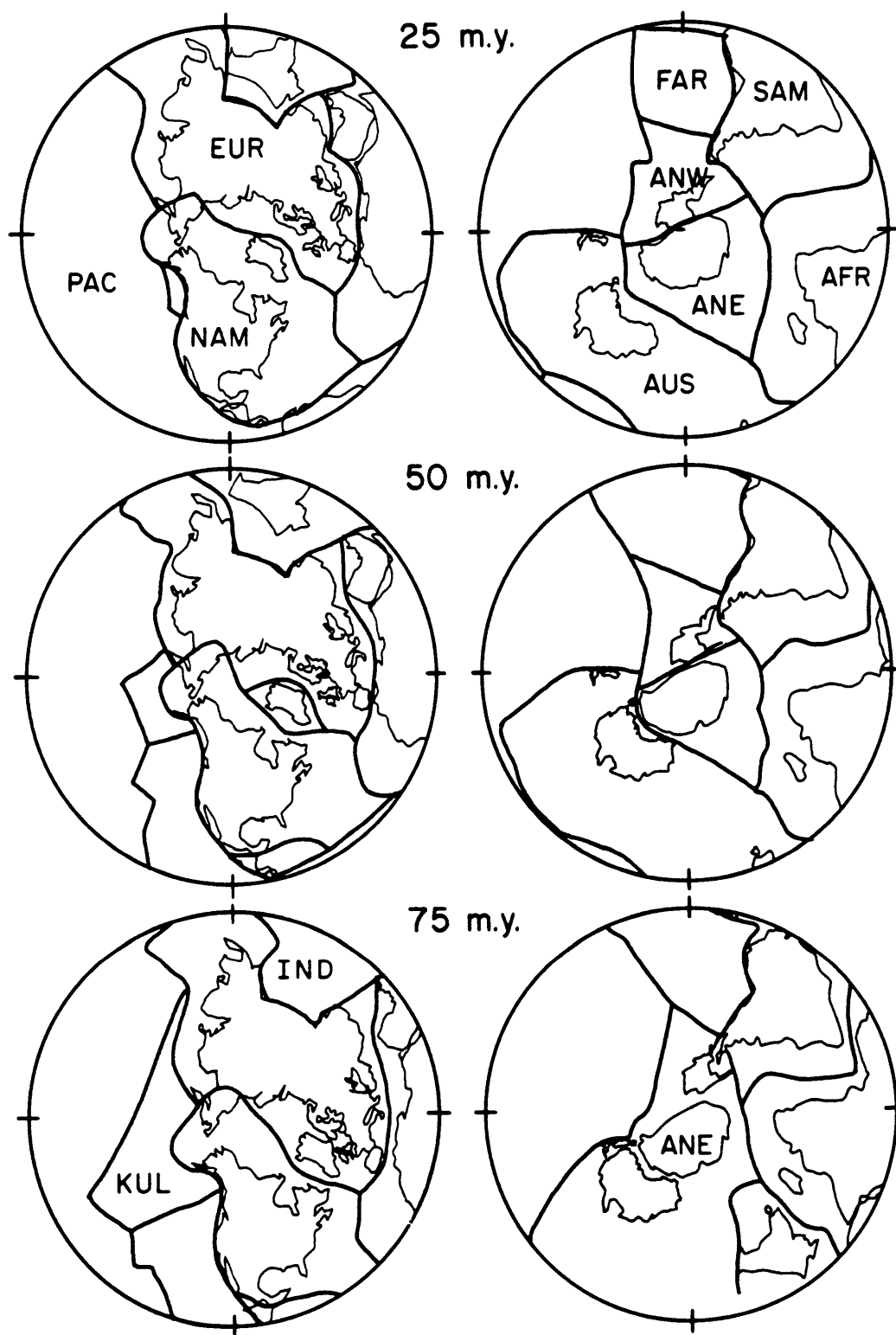


Figure 5.3
MODEL C, SPLIT PAC

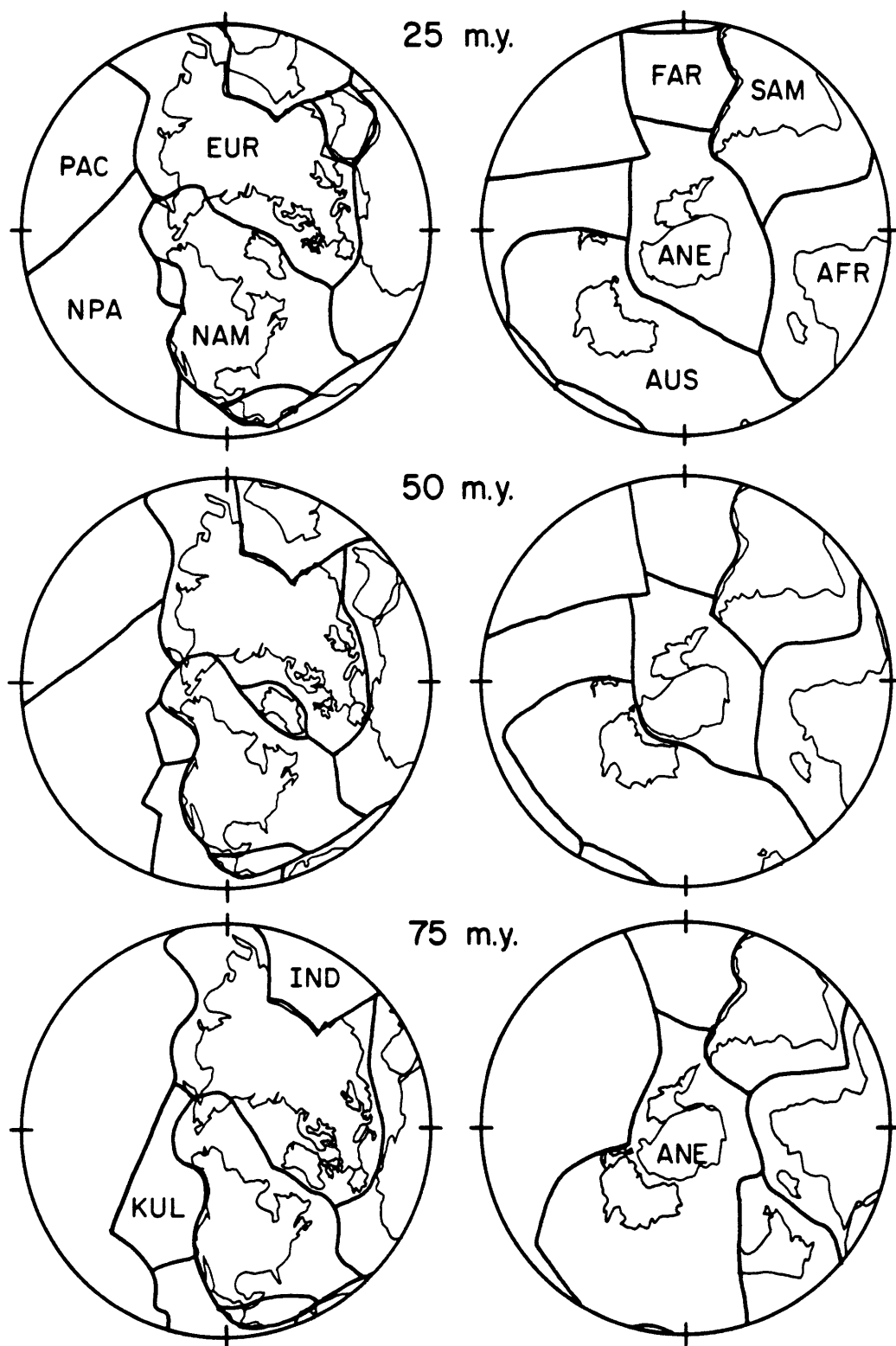


Figure 5.4

MODEL A-SINGLE ANT
NAM=FIXED

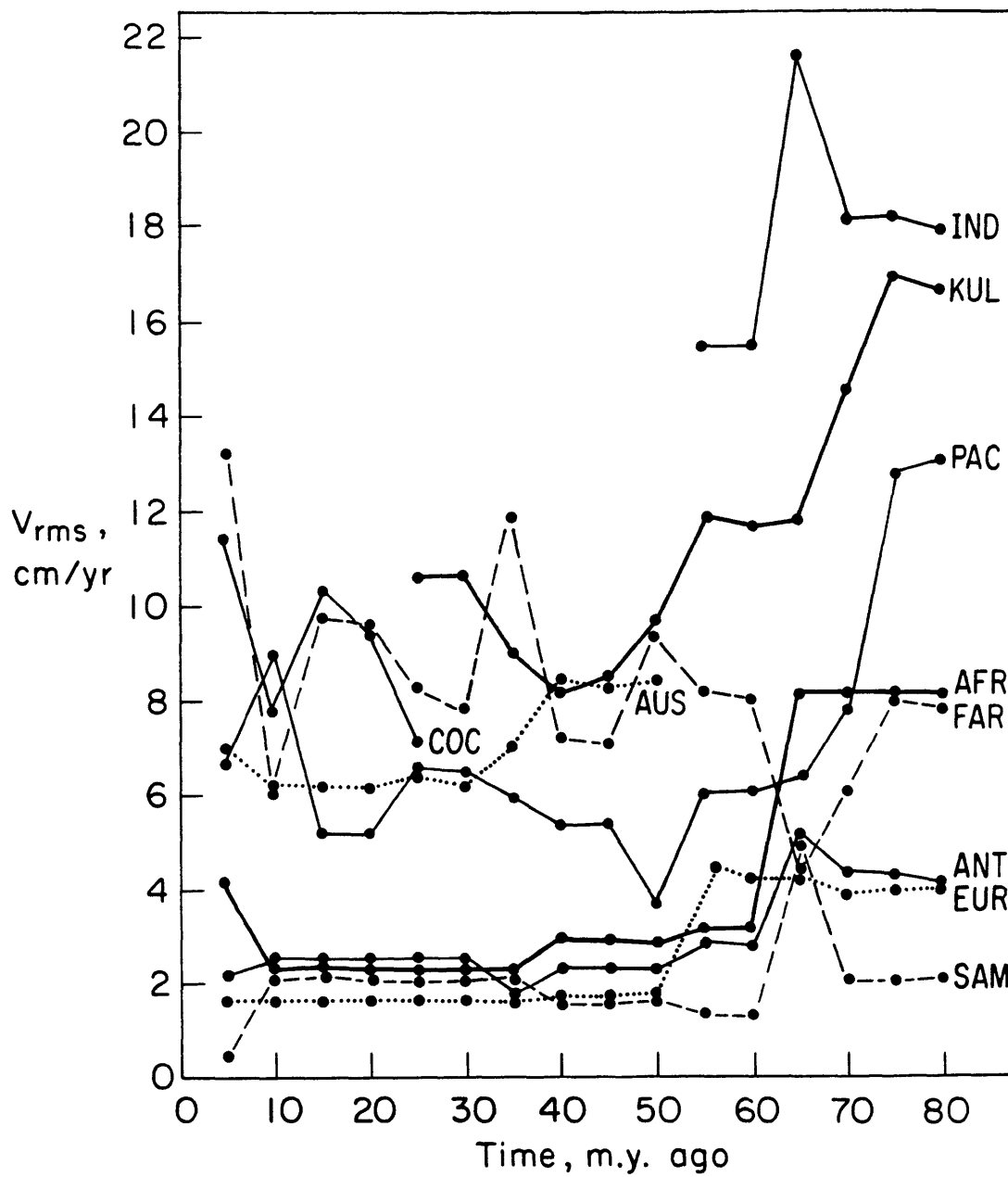


Figure 5.5

MODEL A—SINGLE ANT, SINGLE PAC
No Net Drag Torque

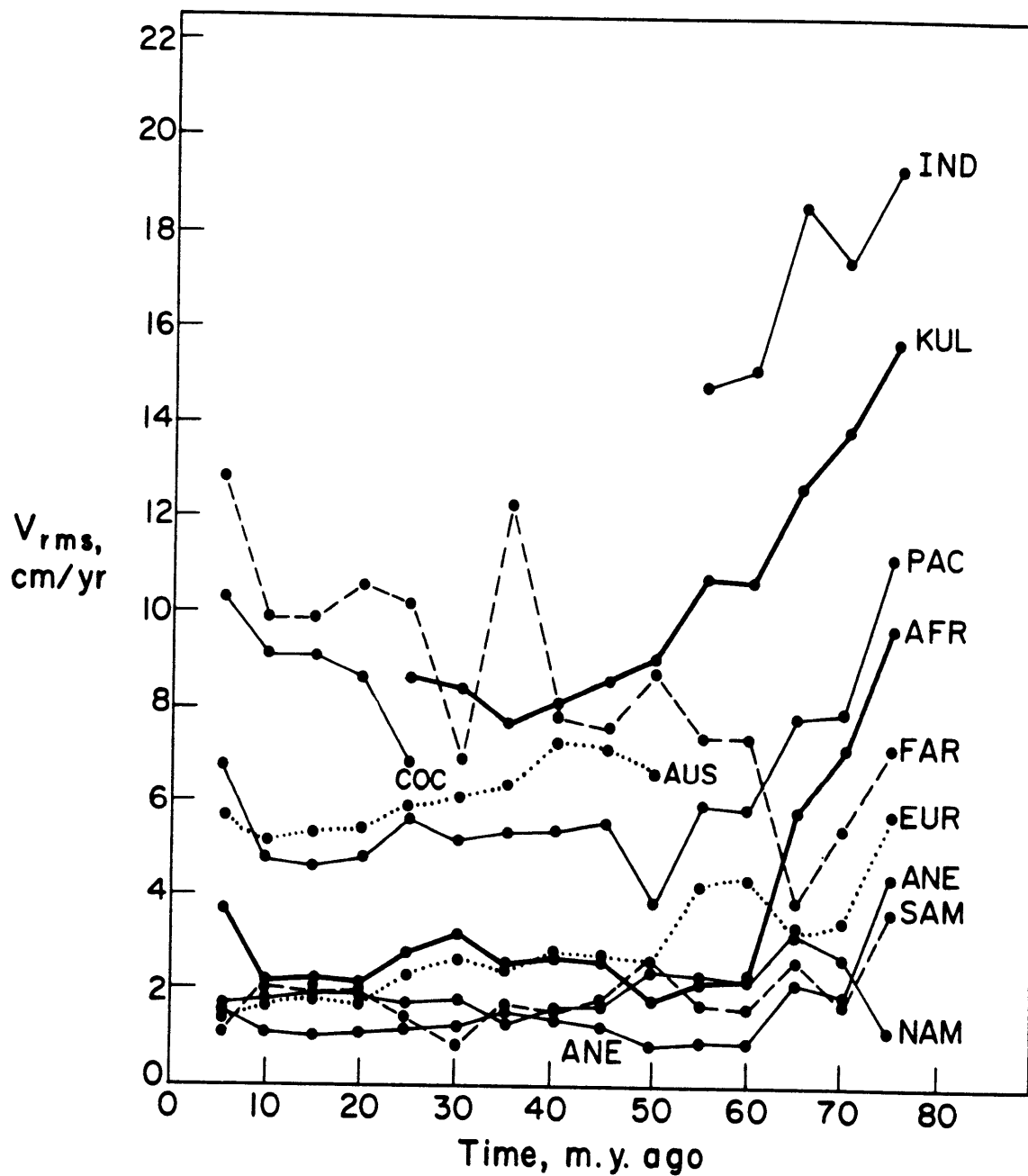


Figure 5.6

MODEL B-SPLIT ANT
No Net Drag Torque

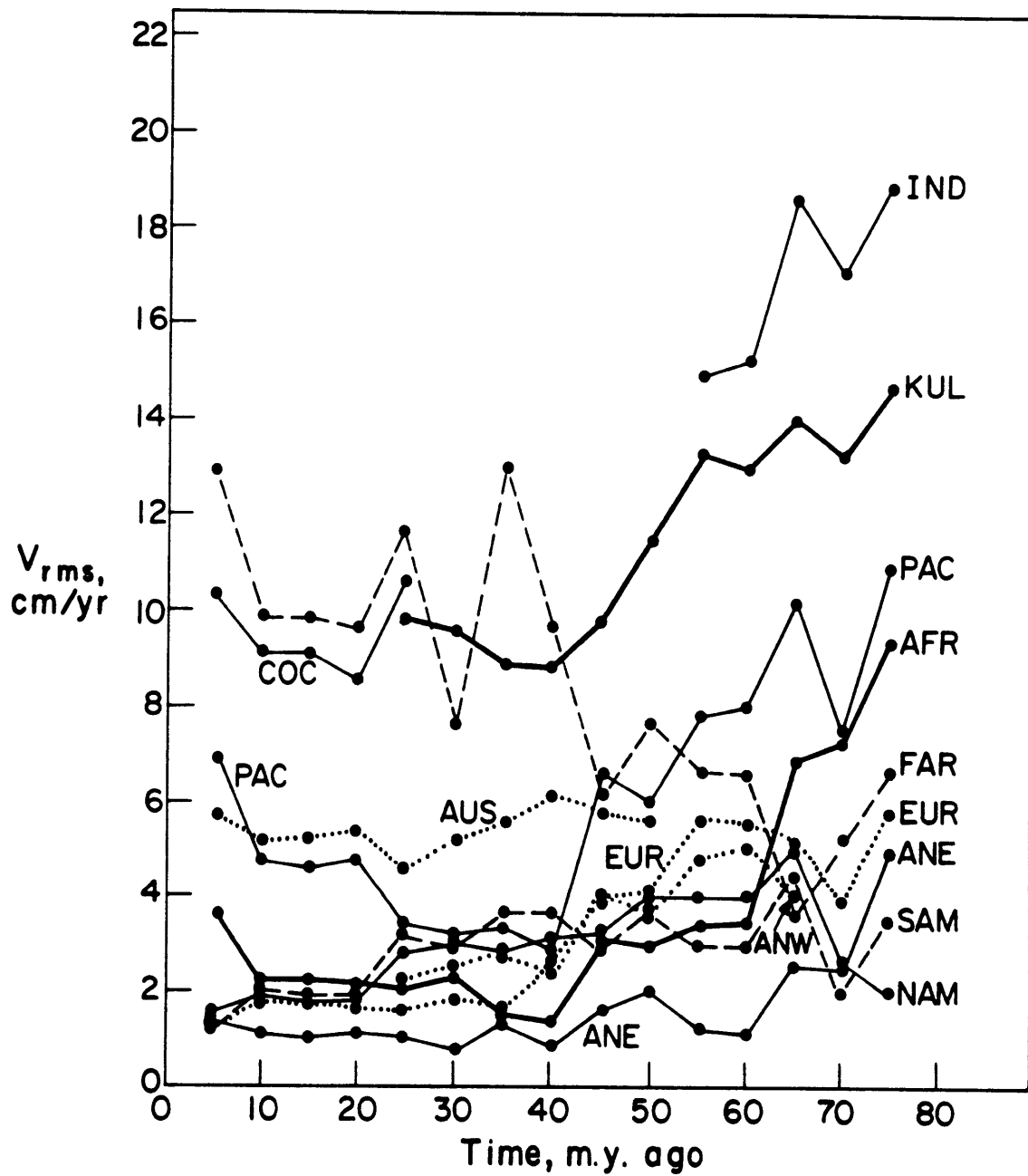


Figure 5.7

MODEL C - SPLIT PAC
No Net Drag Torque

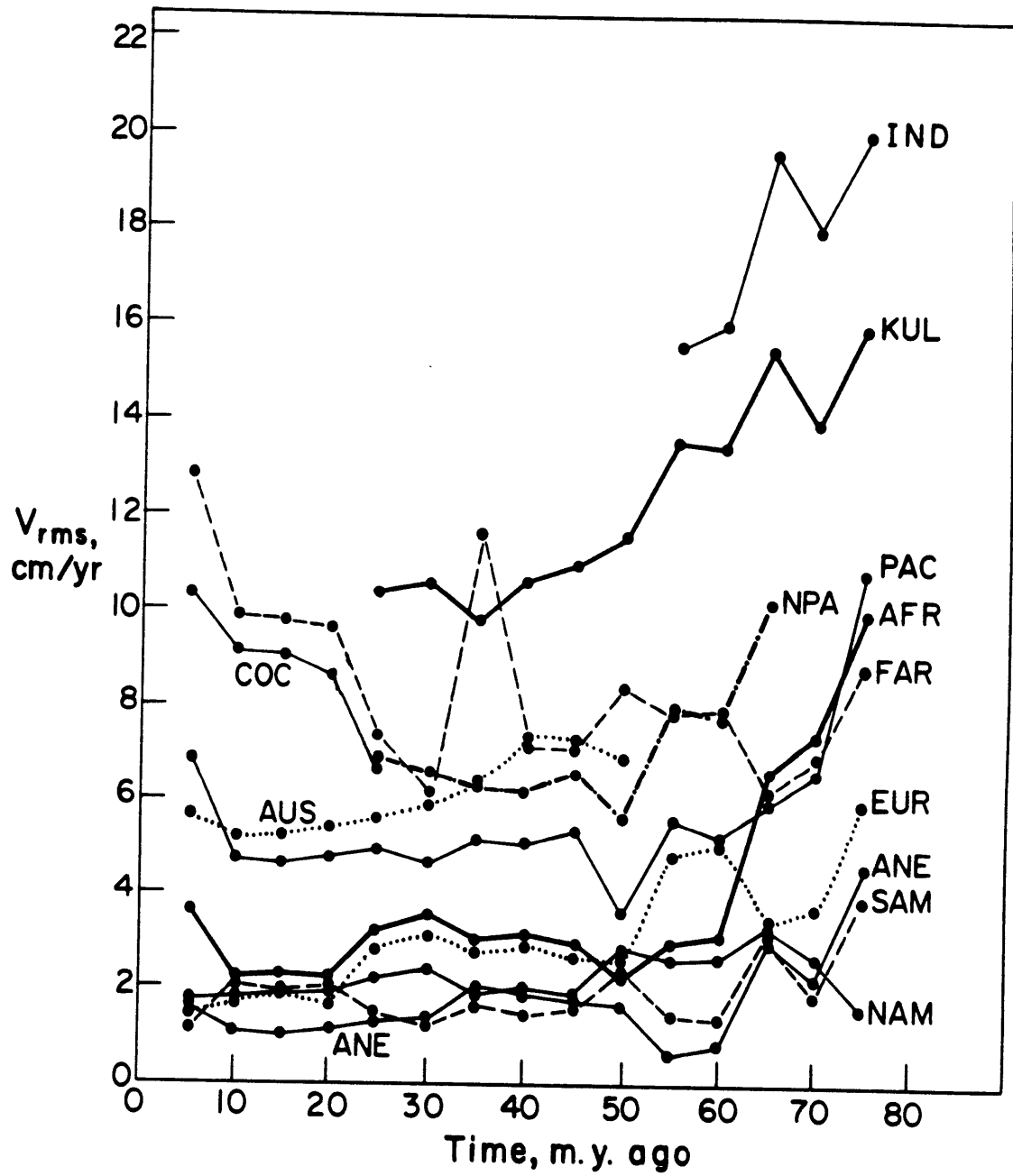


Figure 5.8

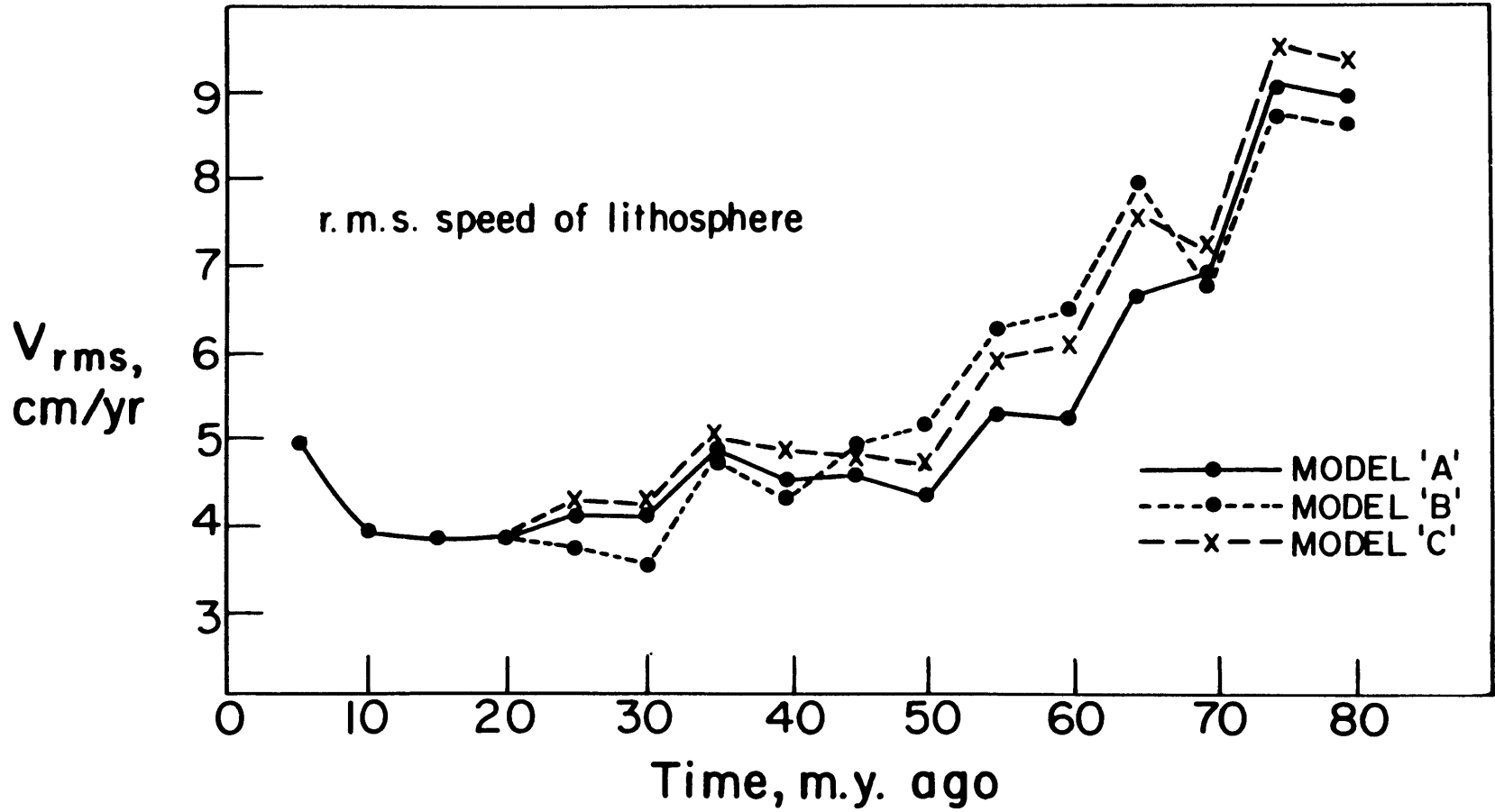


Figure 5.9

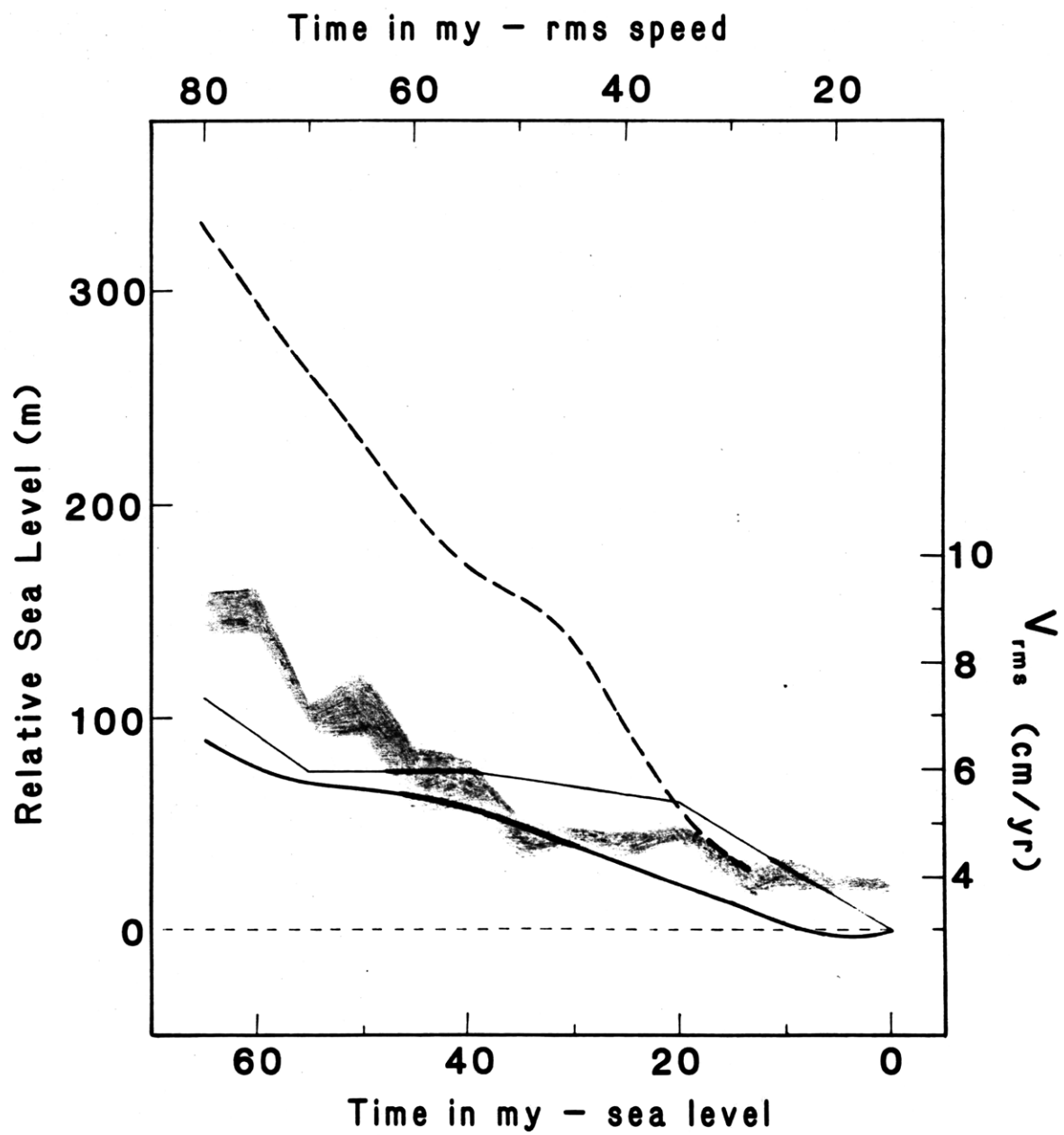


Figure 5.10
NO-NET DRAG TORQUE

CALCULATED NORTH AMERICA POLAR WANDER CURVE

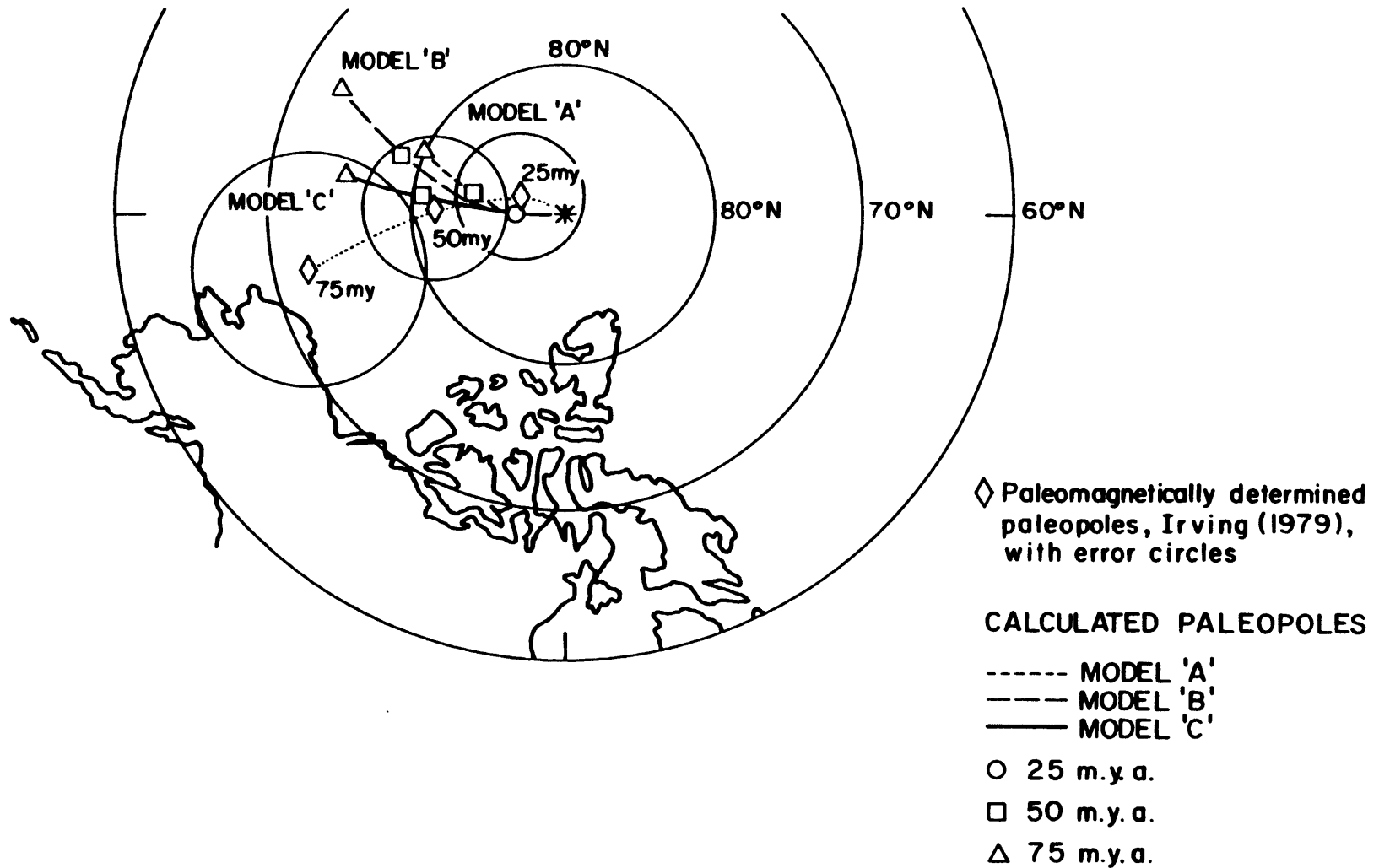


Figure 5.11

TRUE POLAR WANDER FOR 3 NO-NET-TORQUE REFERENCE FRAMES

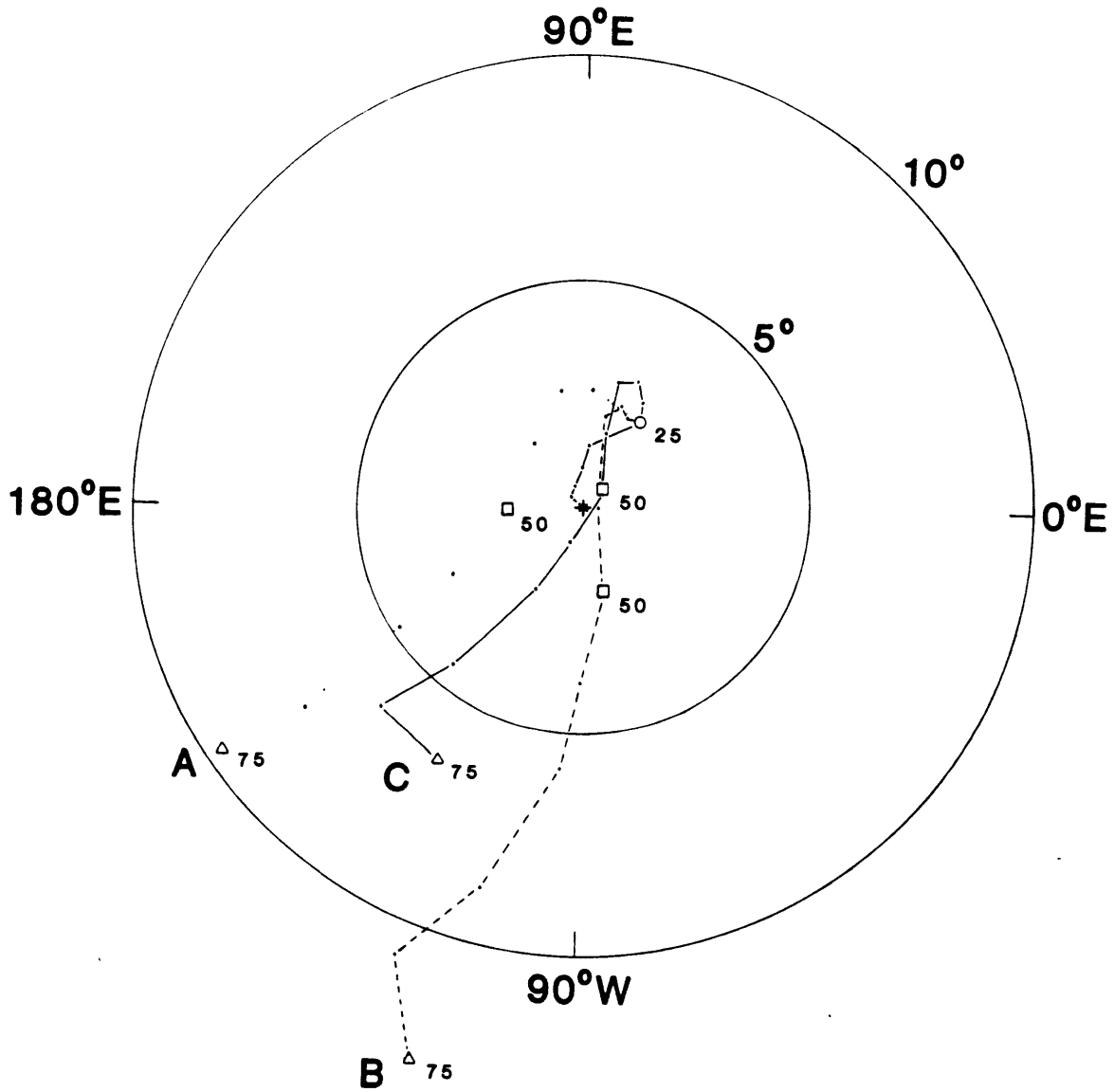


Figure 5.12

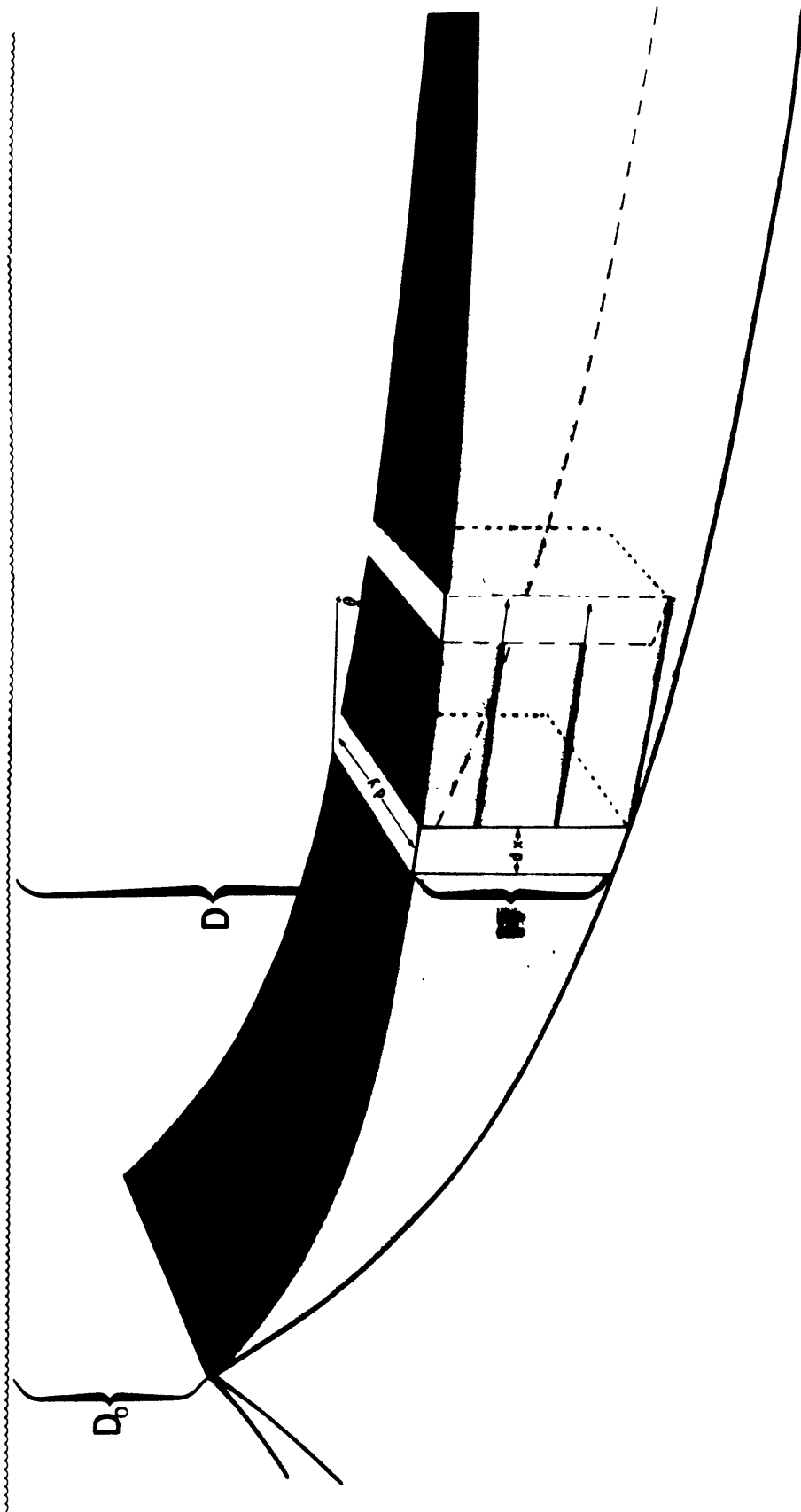


Figure 5.13

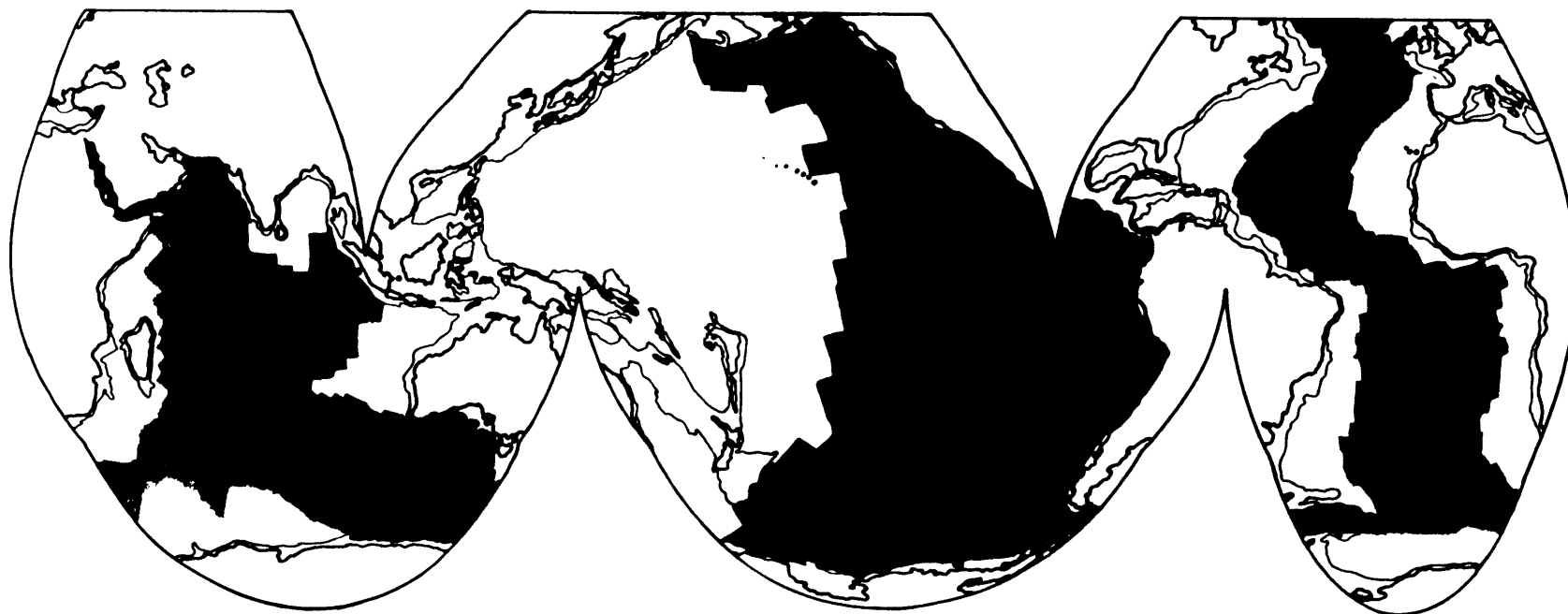
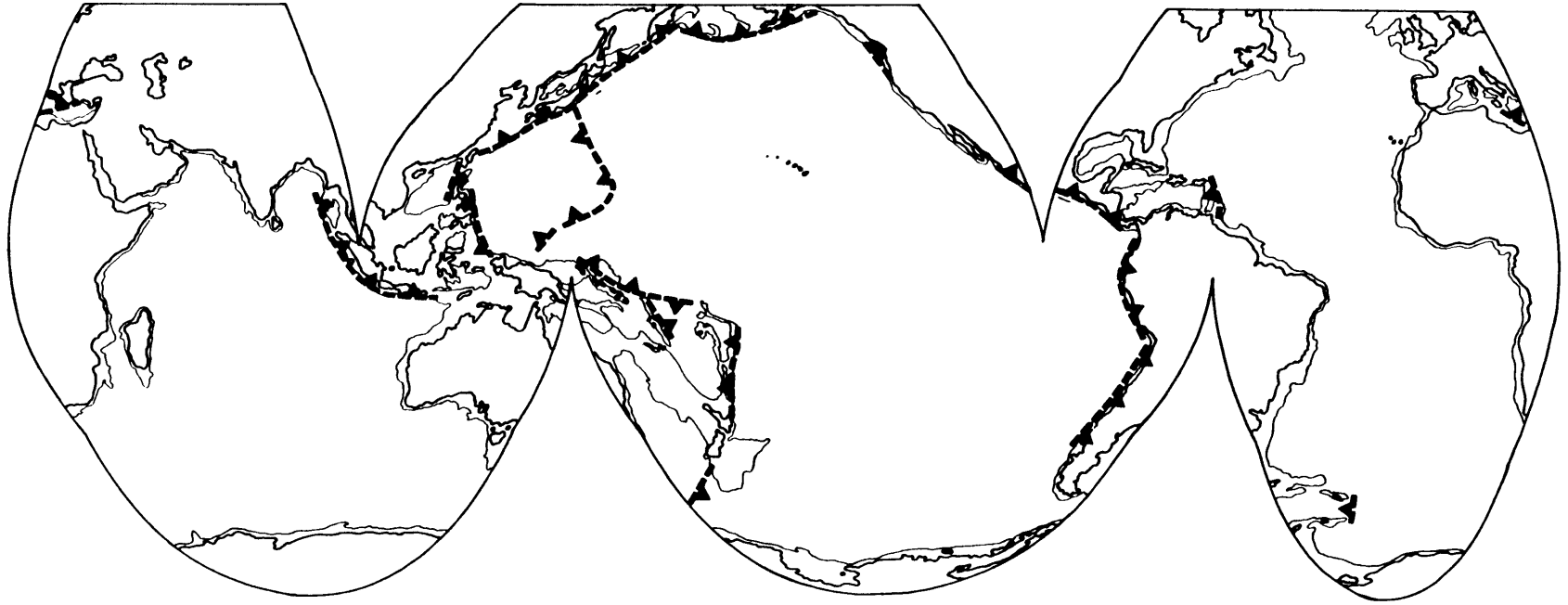


Figure 5.14



CHAPTER 6 SUBDUCTION RESISTANCE AND ANOMALIES

6.1 SHALLOW RESISTANCE TO SUBDUCTION

The analyses of earlier chapters suggest that, with the exception of cases of extremely high overpressures, the overlying plate is subject to a large horizontal compression near the convergent margin. The total length of a subducted slab, down to a depth of 650 km, can approach 1000 km, but the length of underthrusting contact between the overlying and downgoing plates is typically much shorter - on the order of 100 km. The strength of the earth is as much as 2 to 3 orders of magnitude greater along the relatively shallow contact between the two lithospheric plates, however, than at the depths of most of the slab (Brace and Kohlstedt, 1980; Meissner and Strehlau, 1982). The relative strength of this contact zone suggests that a disproportionately large portion of the net resistance to subduction may be concentrated along that relatively small portion of the slab. This statement has implications at two different scales. First, if the collisional resistance is large, then even relatively small changes in that resistance may have significant effects upon the motions of plates as a whole. Second, such changes may have an effect upon the state of stress directly behind the horizontally compressed front.

In this chapter, I shall examine possible mechanisms for variations in subduction resistance with time and suggest ways in which their effects might be observed. Underplating of

sediments at a trench, such as that observed beneath Barbados (Biju-Duval et al., 1981, 1982; Westbrook 1982, Westbrook and Smith, 1983), can be viewed as a result of stratigraphic variations in strength. Such a mechanism for underplating shall also be discussed in some detail.

6.2 STRENGTH ANOMALIES

Extension in back-arc regions provides an interesting opportunity to estimate some of the forces acting near convergent margins. The horizontal compressive stresses near the deformation front at the boundary of the overlying plate are transformed to extension within a distance on the order of only 200 to 400 km. In this section, I shall briefly discuss some of the models which have been proposed to explain this phenomenon. The specific example of the Aegean is discussed in terms of the possible role of salt as a means of weakening the coupling between the plates and therefore the state of compressive stress near the plate boundary. I suggest that the extension is primarily due to asthenospheric counterflow (McKenzie, 1969), and that basal shear stresses of only a few MPa associated with this flow (consistent with the estimates of Töksoz and Hsui, 1978) are required. Additional contributing factors probably include gravitational spreading due to the topographic head of inner Aegea and the intermittent injection of salt into the shallowly dipping plate boundary thrust.

EXTENSION NEAR CONVERGENT MARGINS

Back-arc extension has been recognized to be one of the

most important ways in which the lithosphere violates the simple rigid-plate assumptions usually associated with plate tectonics (Karig, 1971; Uyeda and Kanamori, 1979; Jurdy, 1979). A number of explanations have been offered for the origin of this extension so close to a convergent plate boundary. These include an 'anchored slab' model (Uyeda and Kanamori, 1979) in which the downgoing slab is constrained against sideward movement; an essentially epeirogenic model in which warm, uplifted regions spread gravitationally, as has been proposed for East Africa (Bott, 1982); and a model in which the gravitationally unstable slab sinks downward as well as down dip, causing the trench to migrate oceanward (Forsyth and Uyeda, 1975; Molnar and Atwater, 1978). A model which appears to be applicable to a wide variety of cases is the induced convection model, in which the dipping slab induces convection in a wedge-shaped patch above the slab (McKenzie, 1969; Sleep and Toksoz, 1971; Andrews and Sleep, 1974; Toksöz and Hsui, 1978; Hsui and Toksöz, 1981).

It is not entirely understood what controls the extensional stresses which often exist in the region behind a convergent margin, and the magnitudes of these stresses are not well constrained. However, a gradual transition in stress state appears to exist in a wide range of regions of plate convergence (Nakamura and Uyeda, 1980). Near the trench, the direction of the maximum compressive stress σ_1 is horizontal and perpendicular to the trench, while in the back arc, σ_1 is vertical and σ_3 is horizontal and perpendicular to the trench.

Thus, the styles of faulting progress from thrusting near the trench, occasional strike-slip faulting farther back, and finally normal faulting in the extensional back-arc region (Nakamura and Uyeda, 1980).

AEGEA AS AN EXAMPLE OF EXTENSION

One of the margins examined by Nakamura and Uyeda (1980) was the region of the Hellenic Arc and the Aegean Sea. Behind a narrow band near the plate boundary which is under horizontal compression, there lies a region (Figure 6.1) in which the maximum compressive stress is vertical (McKenzie, 1978; Nakamura and Uyeda, 1980; Shulman and Skala, 1980; Mercier, 1981; Angelier et al., 1982). The margin has apparently extended southward by several hundreds of kilometers since the beginning of extension during the Miocene (Angelier, 1978; LePichon and Angelier, 1981; Mercier, 1981; Le Pichon, 1982). LePichon and Angelier (1979) argued that this extension is a result of gravitational spreading as the higher topography of northern Aegea spreads southward toward the trench, thinning the crust and resulting in the observed high heat flow (Jongsma, 1974; Makris, 1976). Such a model faces the difficult problem of explaining why similar extension does not take place everywhere that a similar or greater degree of topographic relief exists.

The Mediterranean Ridge, which is located south of the Hellenic Trench, has a bathymetric morphology (Ryan et al., 1982; Kenyon et al., 1982) indicative of horizontal compression, suggesting that the Mediterranean Ridge is

actually an accretionary prism analogous to the Barbados Ridge complex. Le Pichon et al. (1982) have suggested that the mechanics of the Mediterranean Ridge may be analogous to those suggested for Taiwan by Davis and Suppe (1980, 1981) and Suppe (1981); (see also Chapter 3). As an aside, I would suggest that their proposed modification to that model (tilting the 'bulldozer blade' to explain landward vergent thrusting) is likely to be ineffective. Because of the very small wedge taper, the orientations of stresses in the wedge (which control the orientation of faults) is governed almost entirely by the upper and lower boundary conditions; the wedge acts like a stress guide.

SLOPE-INDUCED SPREADING

Given the existence of a topographic slope in the overlying plate at a convergent margin, it would seem reasonable to attribute deformation (whether extensional or compressional) to a mechanism related to gravitational spreading off the slope, as proposed for the Aegean by Le Pichon and Angelier (1979). Such models have been proposed in several different ways and for many different regions (Price, 1973; Scholten, 1973; Ramberg, 1973, 1981; Elliott, 1976; Graham, 1981). Spreading can be envisioned as being driven either by shear stresses applied at depth, or by the topographic relief in either of two ways. Either the spreading takes place in response to a local topographic slope, or in response to a regional topographic head.

Let us consider whether spreading can occur in response to

the topographic slope between the overthrust boundary and the back-arc. The theory of mountain belt mechanics presented in Chapter 2 describes a special case of the relation between topographic slope and tectonic deformation, namely, a wedge in compressive failure. Another case which is of interest is the slope at which a wedge will undergo gravitational spreading. Unlike the slope associated with a critical taper (Chapter 2), this slope is very large, unless there is some additional factor which is acting to facilitate gravitational spreading, such as salt or extremely high pore pressures in the basal décollement.

Figure 6.2 illustrates the topographic stability field for a hypothetical wedge which is at its critical taper with a topographic slope $\alpha = 4^\circ$ and basal dip $\beta = 4^\circ$, and pore pressure ratios (as defined in Chapter 2) equal to 0.80. Note (Figure 6.2a) that a reduction of the topographic slope (or, basal dip) pushes the wedge further into the 'compressive failure' regime, which must necessarily require thrust faulting to take place. However, assuming that all other factors are held constant, the wedge can leave this compressive failure regime if the topographic slope is increased. The same effect can be achieved by weakening the basal décollement. This is illustrated in Figure 6.2b for the case of an increase in the pore pressure along the base (the effect of a corresponding weakening of the intrinsic strength of the rock there would be identical). In this case, the topography is stable. However, if the base is significantly weakened, it is possible for such

a modest topographic slope to become unstable, attain extensional failure, and undergo normal faulting (Figure 6.2c). However, note that for the case illustrated in Figure 6.2, this requires that the base be an order of magnitude weaker ($1-\lambda = 0.02$ versus 0.2) than for the case of thrusting in a compressive setting. For a very large region with an extremely small mean topographic slope, such a mechanism is entirely unreasonable. Although the presence of a very weak substance, such as salt, in the décollement may permit such topographic spreading in limited cases, this mechanism clearly is not applicable to spreading such as that of the Aegean.

THE PREFERRED MODEL - THE 'DISTANT TRIGGER'

It is clear from the preceding discussion that some additional factor (such as asthenospheric counterflow or gravitational spreading due to overall topographic relief), must be invoked in order to explain back-arc spreading in Aegea. As we have already seen, such models have been proposed to explain back-arc spreading near many margins around the world (McKenzie, 1969; Töksoz and Hsui, 1978; and others). The Aegean region is somewhat unusual in that there has apparently been a great deal of spreading. This appears to have taken place in a discontinuous, intermittent manner (Angelier, 1978; Mercier, 1981). There is a rather simple way in which we can explain such intermittent normal faulting in Aegea, without requiring that the hypothesized asthenospheric counterflow should have any unreasonable properties. We presume that there is typically a moderately strong

mechanical coupling between the plates, and that the strongly compressive state of stress near the trench is converted to a less compressive or an extensional state of stress in the back-arc primarily by the action of the subduction-induced asthenospheric counterflow. If the aspect ratio of the problem (the ratio of the distance between compressive and extensional regimes divided by the lithospheric thickness) is large, then the magnitude of the basal shear stress required to achieve this state is easily estimated. To go from a mean compressive deviatoric stress on the order of a few tens of MPa to an isotropic stress state requires, with a lithospheric aspect ratio of 10 (Figure 6.3), that a shear stress of magnitude less by a factor of 10 (a few MPa) must be generated at the base of the lithosphere by the asthenospheric counterflow.

I propose that the stress-state in the back-arc is sufficiently close to extensional failure that modest changes in décollement resistance and in the resulting stress state near the plate boundary (Figure 6.4) can initiate back-arc normal faulting. I further postulate that this change in décollement resistance occurs because of the intermittent inclusion of salt rafted in upon the African plate. It has been pointed out by Wang (1981) that the frictional resistance to sliding in a trench could be reduced by the presence of pelagic (deep sea) sediments in the trench. Salt, which has a strength of only 500 kPa at geological strain rates ($10^{-13}/s$) and a temperature of $100^{\circ}C$ (Carter et al., 1982), is even weaker than deep-sea sediments. The magnitude of the coupling

between the overlying and downgoing plates would be therefore greatly reduced as a result of the presence of salt in the décollement. The low density of salt would tend to discourage its subduction, except when it happens to be mixed in with other subducted sediments; this is in agreement with the observations that salt tends to accumulate near the surface instead of being subducted (Le Pichon et al., 1982). These two attributes of salt at a convergent margin present a simple mechanism for the intermittent nature of the extension in the Aegean back-arc region.

The change from a strong décollement to one with salt (and possibly extreme overpressures as well) can reduce the resistance to slip from many tens of MPa to less than 1 MPa. The resulting reduction in the plate boundary force would cause an isotropic stress state in the back-arc region to become extensional, or alternatively, could cause a slightly extensional stress state to become sufficiently extensional to trigger normal faulting. In this way fluctuations in the shallow resistance to subduction can trigger intermittent normal faulting in the back-arc region in response to, among other things, the lithology of sediments being carried into the trench. The presence of a great deal of Messinian salt deposits around the Hellenic trench has been well documented (Cita, 1982; De Benedetti, 1982; Le Pichon, 1982).

To summarize, the underthrust resistance at the plate boundary opposes the combined effects of gravity spreading and asthenospheric counterflow, both of which would, if unopposed,

tend to cause the margin to advance. Removal of the sliding friction along the *décollement* through the introduction of salt into the trench and an increase in pore pressures causes the accretionary prism to become virtually decoupled from the downgoing plate. This reduces the magnitude of the horizontal compression of the lithosphere near the trench and may trigger normal faulting in the back-arc.

6.3 TRENCH SEDIMENT BALANCE

The quantity of sediments in and near a trench is the result of a balance between a number of different phenomena (Figure 6.5). Recent drilling experience (McMillen and Bachman, 1982; Auboin et al, 1982a; Shipley et al., 1982) has made it clear that there are two main sources of sediments in most trench collisional zones. These are the predominantly pelagic sediment cover atop the underthrusting oceanic crust and the flat-lying trench turbidites, which owe their existence to the presence of a great deal of relief along the continental margin. The trench turbidites are not the only sediments which are derived from the overlying plate. A patchy cover of terrigenous sediments are often observed atop the actively deforming mass of accreted sediments, particularly in local depressions (Von Huene et al., 1980a, Westbrook, 1975, 1982; Von Huene, 1979, Von Huene and Arthur, 1982; Moore et al., 1982; and others). A major difference between the mechanical behavior of accretionary wedges and that of subaerial thrust belts is the predominance of sedimentation over erosion along

the upper surface of the accretionary wedge (Chapter 4). Unlike thrust belts, which must remain highly active to maintain their critical taper (Chapter 2) in response to the continuing erosion of their upper surfaces, the sediment balance along the upper surfaces of accretionary wedges will, in the terminology of Chapter 2, tend to make the wedge supercritical. Any erosion of an accretionary wedge is most likely to take place in the form of tectonic erosion along the plane of interface with the downgoing plate (von Huene et al., 1980a, McMillen and Bachman, 1982).

CLIMATE AND TECTONICS

It can be argued that the styles of deformation observed either near a trench or in a subaerial mountain belt should be indirectly related to such variables as the latitude, the hemisphere, the age of subducting lithosphere, and whether the trench is located near the eastern or western end of a major ocean. Let us speculate about how the influence of some of these factors may possibly be observed in the tectonics of convergent margins. We have seen (Chapter 3) the close relationship between erosion and tectonic activity in the fold-and-thrust belt of western Taiwan. Galli-Olivier (1969) has pointed out that observations of the Peru-Chile trench suggest that there is a close relationship between the rate of sedimentation in a trench and the climate in the adjacent land from which sediments are derived. Offshore of particularly arid regions (such as northernmost Chile), the limited activity of erosion leads to a much smaller supply of trench sediments

than offshore of a wet area (such as southern Chile). Ziegler et al. (1981) extend this concept to suggest that continental accretion occurs near rainy zones, while tectonic erosion tends to occur near dry areas, where surface runoff supplies insufficient quantities of trench turbidites. They also use as an example the presence of both tectonic erosion and aridity of the area near the Chile-Peru border, a state of affairs which is related to the position of the Andes in the South American continent with respect to the prevailing winds in the southern hemisphere.

There is a region of the Andes, along the eastern Cordilleran margin from 13° S to 18° S, and to a lesser degree, between 18° and 28° S, which is characterized by relative quiescence in its shallow seismicity compared to the surrounding regions (Suárez, 1982). It is interesting to note that this corresponds surprisingly well with those regions of the Peru-Chile trench which are lacking in trench axis sediments, ranging from 12° S to 17° S and 19° S to 28° S (Schweller et al., 1981), and also with the Atacama desert which is centered on a latitude of 20° S and is one of the driest in the world (Ziegler et al., 1981). The well-known segmentation of the slab subducted beneath South America (Barazangi and Isacks, 1976, 1979; Megard and Philip, 1976) undoubtedly plays a major role in controlling the shallow seismicity in the Andes. However, it may be worthy of note that extreme aridity, leading to reduced erosion, can be expected to result in both a dearth of trench sediments and a

reduction in the amount of thrust faulting. Reduced erosion leads to a reduction in seismicity because less thrusting is required in order to maintain the topography needed in order for stresses within the mountain belt not to greatly exceed the failure criterion (Chapter 2). This latter effect would lead to a reduction in shallow seismicity within the mountain belt, far from the trench.

Given that the quantity and distribution of sediments carried into a trench by the oceanic plate influences the supply of accreted sediments (Moore, 1975) and may influence the mechanics of slip along the *décollement* (Wang, 1981), any factor which influences the distribution of pelagic sediments is likely to affect the tectonics of the collision. The rate of deposition of pelagic sediments is dependent upon latitude, particularly at the equator, where the production of biogenic material increases markedly (Suárez and Molnar, 1980). The depth (and thus the age) of the oceanic lithosphere affects the depth relative to the Carbonate Compensation Depth. This would be expected to alter the distribution of sediments entering the trench, with resulting changes in the magnitude of coupling at the trench.

UNDERPLATING

The accretion of sediments at the trench is a dominant process at many trenches, including the Aleutian (von Huene, 1979; von Huene et al., 1979a; Byrne, 1982) and Barbados accretionary wedges (Westbrook, 1975, 1982; Biju-Duval et al., 1982). However, not all of the sediments at the trench are

necessarily accreted onto the overlying plate. Moore (1975) has pointed out that the choice of stratigraphic horizon separating the accreted and underthrust sediments may be very strongly affected by the mechanical contrast between relatively weak and light clastic deposits and the relatively strong and dense mature biogenic rocks beneath them. In some cases (Westbrook and Smith, 1983) some of the sediments encountered by the overriding plate at the trench are underthrust a great distance. These sediments may either be completely subducted (Shipley et al., 1980, 1982; Karig and Kay, 1981; Wang, 1981) or, at some point well away from the trench, they may be underplated. There is only indirect evidence that underplating actually takes place. Mass-balance arguments and surmised uplift histories at DSDP drilling sites (Watkins et al., 1982; Moore et al., 1982; Shipley, 1982; Moore and Watkins, 1982; McMillen and Bachman, 1982) provide the most important indication that underplating takes place. The mechanism for such underplating is not entirely clear.

Any model for underplating should be able to explain why the stratigraphic horizon which was the mechanically favored site of slip between the plates at a shallow depth is no longer favored when the sediments reach a greater depth. Models have been proposed (Cowan and Silling, 1978; Cloos, 1982) which avoid this whole issue by assuming that the accretionary wedge is a plastically flowing mass bounded by the much stronger buttress of the continental crust of the overlying plate. The specification of such boundary conditions requires that a sort

of circulation take place within the wedge as a whole, with new sediments entering the system being swept under the wedge toward the base of the continental crust, where it is deflected upward. However, such models appear to be directly in conflict with the clearly observed thrust faulting in a wide range of accretionary wedges (Beck and Lehner, 1974; Biju-Duval et al., 1978, 1982; Nasu et al. 1979), and depicted in Figures 4.2, 4.4, and 4.5.

A simple alternative model for the mechanics of underplating is presented in Figure 6.5. Even if the deeper of two stratigraphic horizons is the intrinsically weaker one, it may not be the preferred slip plane at shallow depths, because of the normal-stress (and thus, depth) dependence of resistance to sliding. However, at greater depth, where the dependence of strength upon depth is less important, it is increasingly favored. Thus, sediment packet 2 in Figure 6.5 is underplated at that depth. This model provides a simple way of explaining the different choices of décollement horizon near the surface and at depth. Another factor which should be taken into account is the relative compaction of the different sediment packets, variations in which could change the choice of favored slip horizon with depth.

6.4 SUMMARY

We have seen that changes in the degree of coupling between the plates at a trench may have major effects, not only upon the local tectonics, but also upon deformation in the

back-arc region as well. The relative strength of the rocks of the upper crust magnifies the potential importance of the presence of a weakening factor, such as salt or extremely high overpressures, within the thrust decollement between the two plates. Assuming that intermittent normal faulting in Aegea can be explained by subduction-induced asthenospheric counterflow, plus the effects of periodic infusions of weak salt into the decollement, the magnitude of the basal shear stress associated with the counterflow is estimated to be on the order of a few MPa. Fluctuations of the magnitude of coupling should be given serious consideration as a trigger for a wide range of tectonic processes involving the state of stress in the lithosphere, possibly including major changes in the plate boundary forces.

A major difference between subaerial and submerged wedges lies in the role (or lack thereof) of erosion (Chapter 4), which has important implications for the degree of internal deformation required in order to maintain a critical taper (Chapter 2). The extreme aridity of parts of the Andes (Galli-Olivier, 1969; Ziegler et al., 1981) contributes to the sediment-poverty of the Peru-Chile Trench. This is viewed as the direct converse of the state of affairs in Taiwan (Chapter 3), where a wet climate leads to extremely fast erosion of 5 or 6 mm/yr (Li, 1975), and results in a relatively rapid cycle of destruction of the island as it is rebuilt from its own erosional debris (Suppe, 1981).

There appears to be a strong relationship between sediment

supply and the degree of erosion or accretion at the continental margin. The processes which contribute to the sediment balance near a trench (Figure 6.6) need not be considered mutually exclusive. Instead, geologically extreme cases of tectonic accretion or erosion appear to be the result of an imbalance in the rates of these processes, sometimes due to seemingly unrelated geographical or climatological factors.

Underplating of sediments at a trench may be related to differences between the depth and temperature dependence of their mechanical properties. The slip horizon at any given point is that which permits subduction to proceed in the most energetically favorable manner. If a given horizon is most favored at shallow depths near the trench, it is not necessarily favored at greater depths, where slip elsewhere in the sedimentary column may be favored.

FIGURES

Fig. 6.1 A map of maximum horizontal compressive stress directions in the Aegean region, drawn from Figure 3 of Nakamura and Uyeda (1980). The maximum horizontal stress is σ_1 where the shaded band is dark and σ_2 where it is light. Note the rotation of stress axes away from the case of horizontal compression perpendicular to the trench, which prevails only in a small area. The dashed line and arrows mark location and sense of subduction.

Fig. 6.2 Diagram illustrating the behavior of a hypothetical accretionary wedge with surface slope and basal dip each equal to 4° , with fluid pressure ratios λ equal to a) 0.80, b) 0.90, and c) 0.98. Extremely high pore pressures are needed in order to produce normal faulting in the wedge, but moderately elevated pore pressures can produce a non-accreting supercritical wedge (Davis et al., 1982).

Fig. 6.3 A schematic illustration of the way in which the stress state near a typical margin changes from highly compressive near the front to increasingly extensional in the back-arc region.

Fig. 6.4 A schematic illustration of the effect of a change in the strength of coupling along the decollement. Arrows indicate the magnitude of the horizontal compressive stress. Note that a) the pre-existing

reduction of horizontal compressive stress with distance from the trench is more likely to produce normal faulting in the back-arc if b) there has been a reduction in the strength of the décollement.

Fig. 6.5 Illustration of a simple mechanism for underplating. Although the deeper of two stratigraphic horizons (B) is intrinsically weaker, it is not the preferred slip plane at shallow depths, because of the dependence on normal stress (and thus, depth) of resistance to sliding. However, at greater depth, where the depth-dependence of strength is less important, horizon B is favored. Thus, sediment packet 2 is underplated at that depth.

Fig. 6.6 A schematic diagram illustrating the balance between erosion, accretion, underplating, sediment subduction, and tectonic erosion near a trench.

Figure 6.1

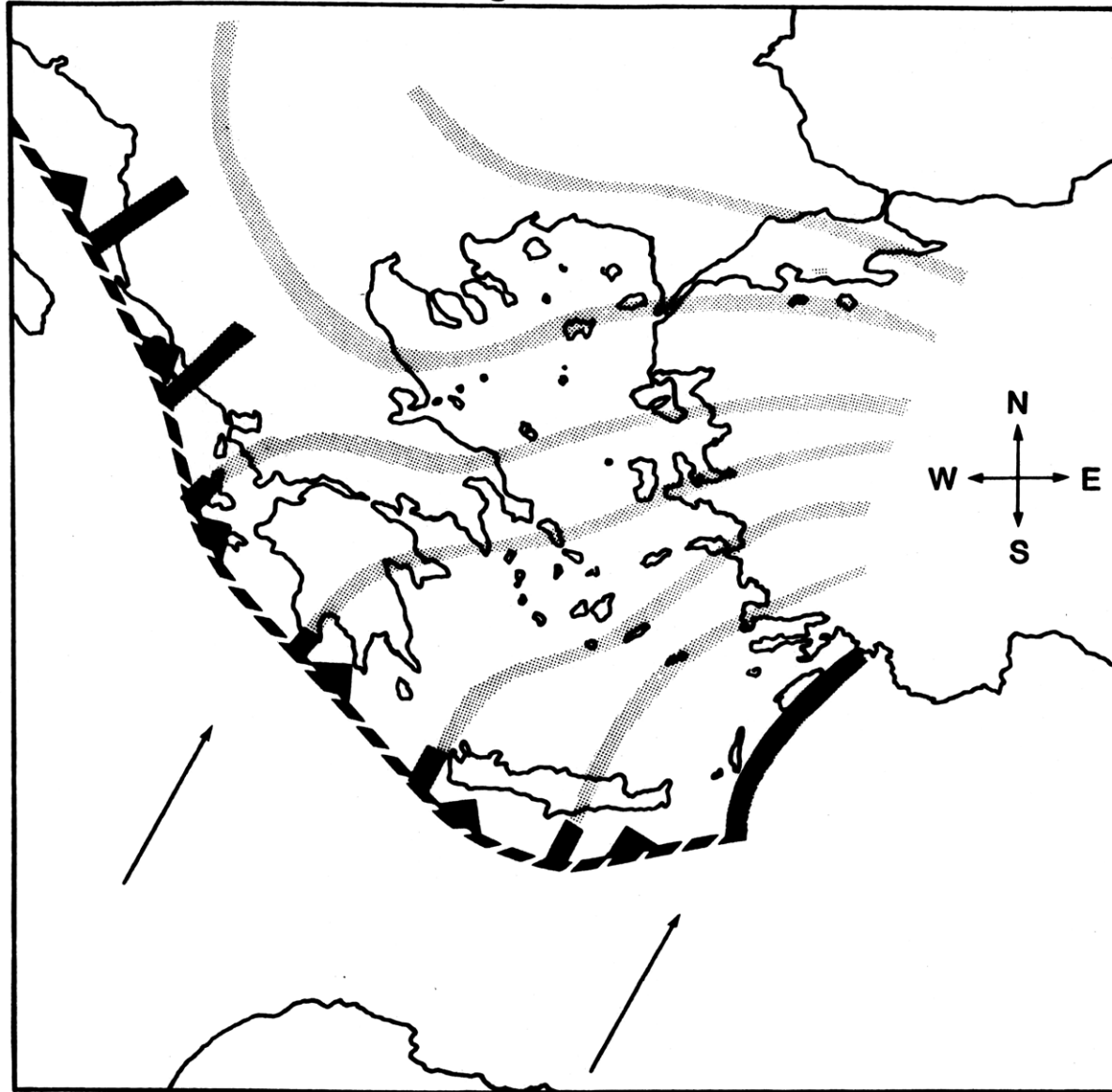


Figure 6.2

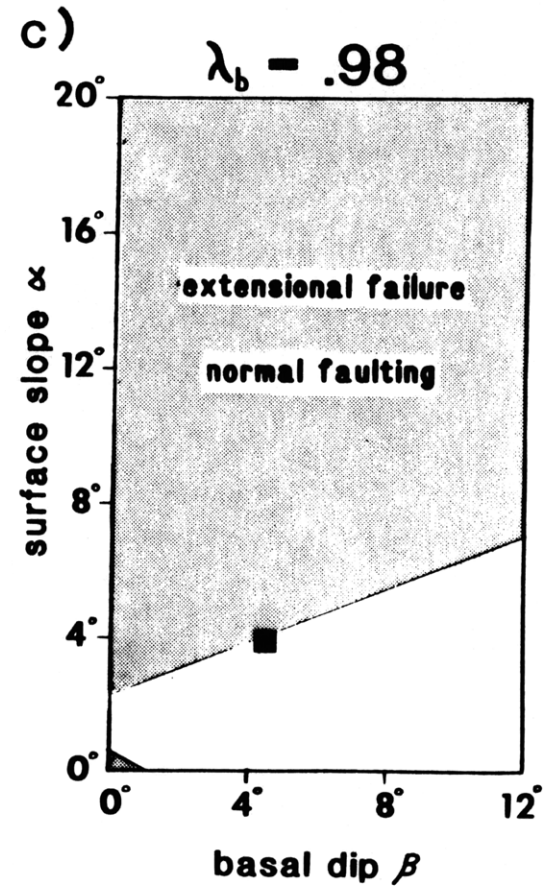
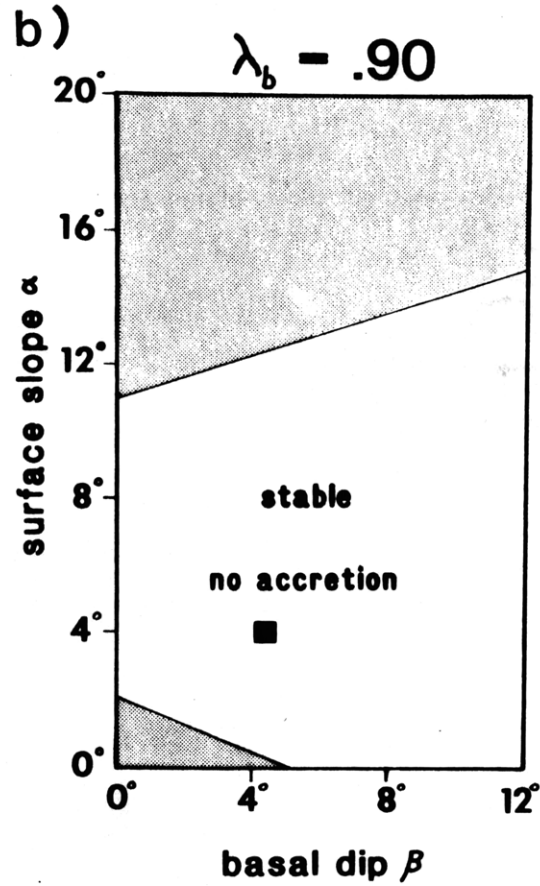
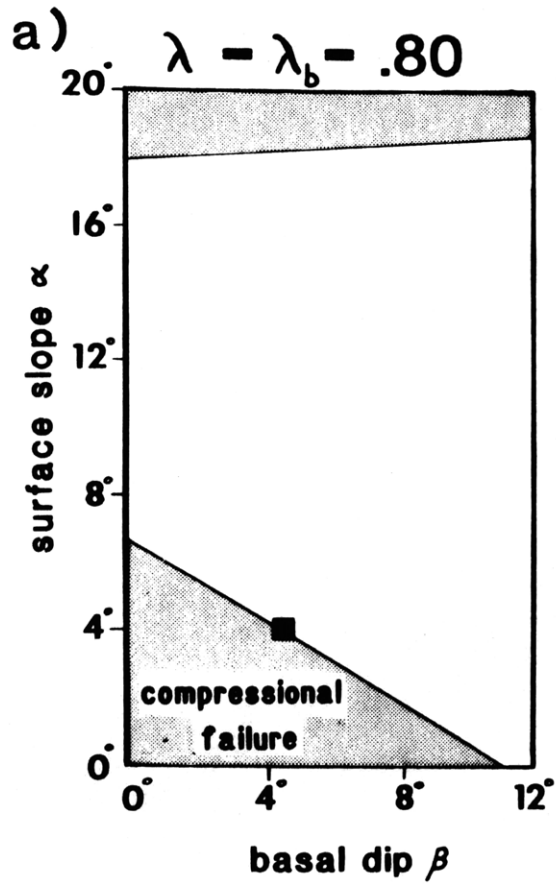


Figure 6.3

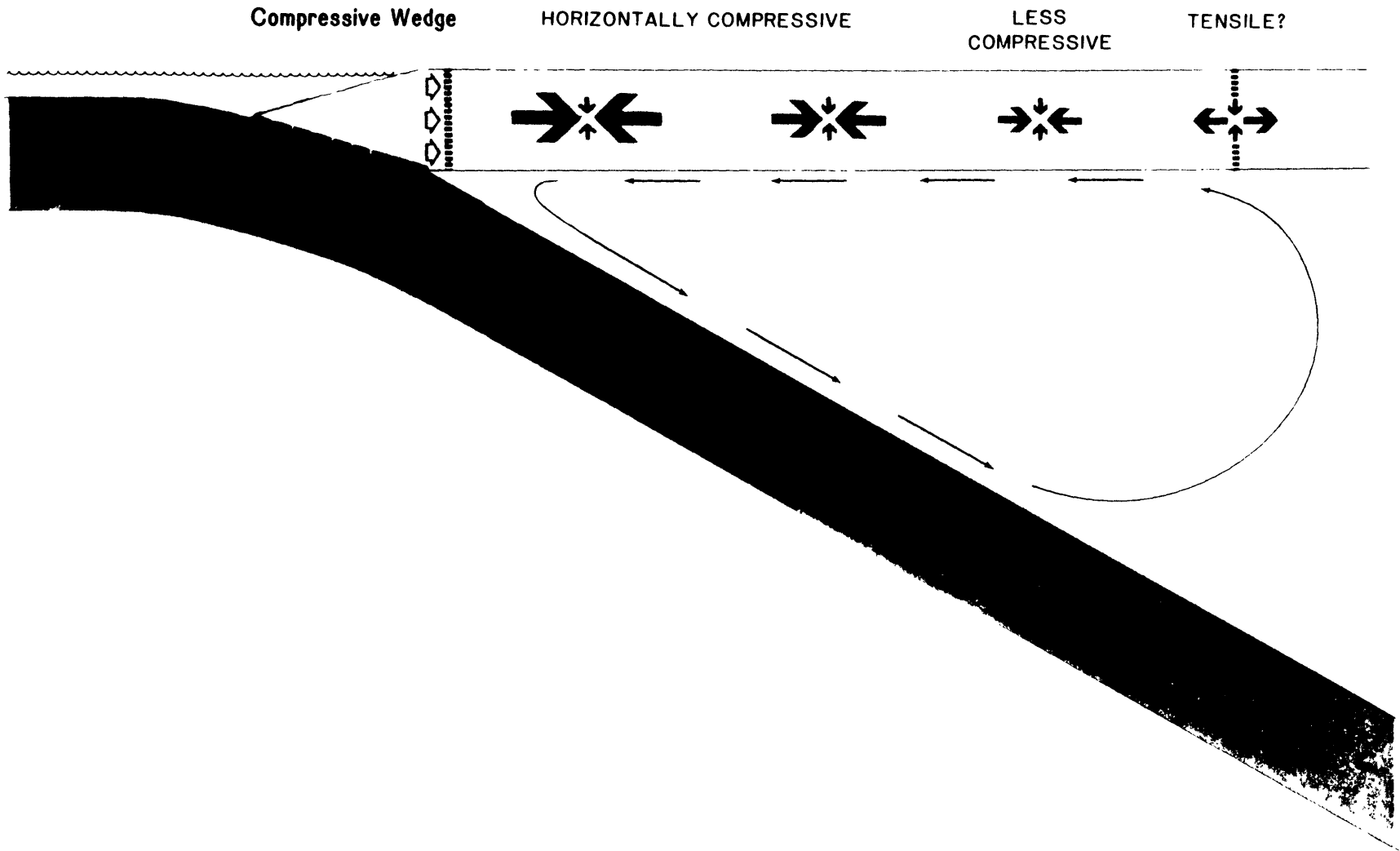


Figure 6.4

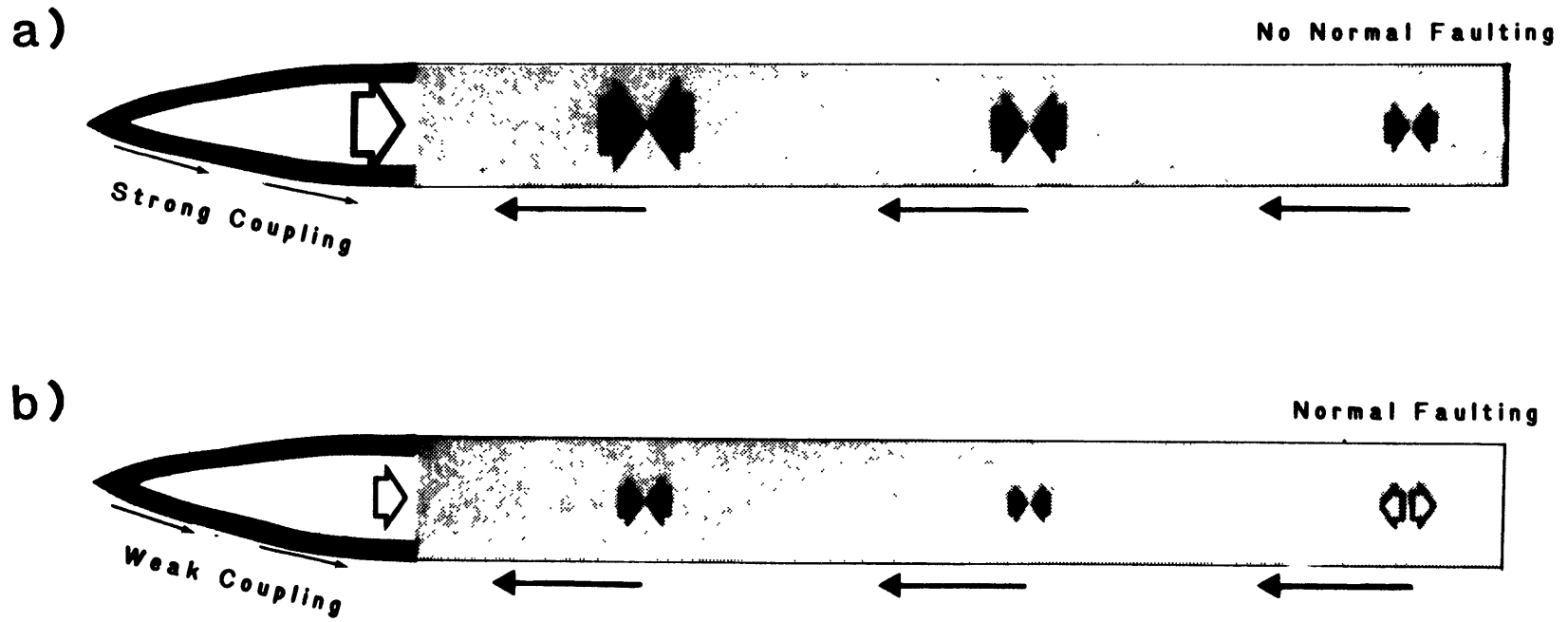


Figure 6.5

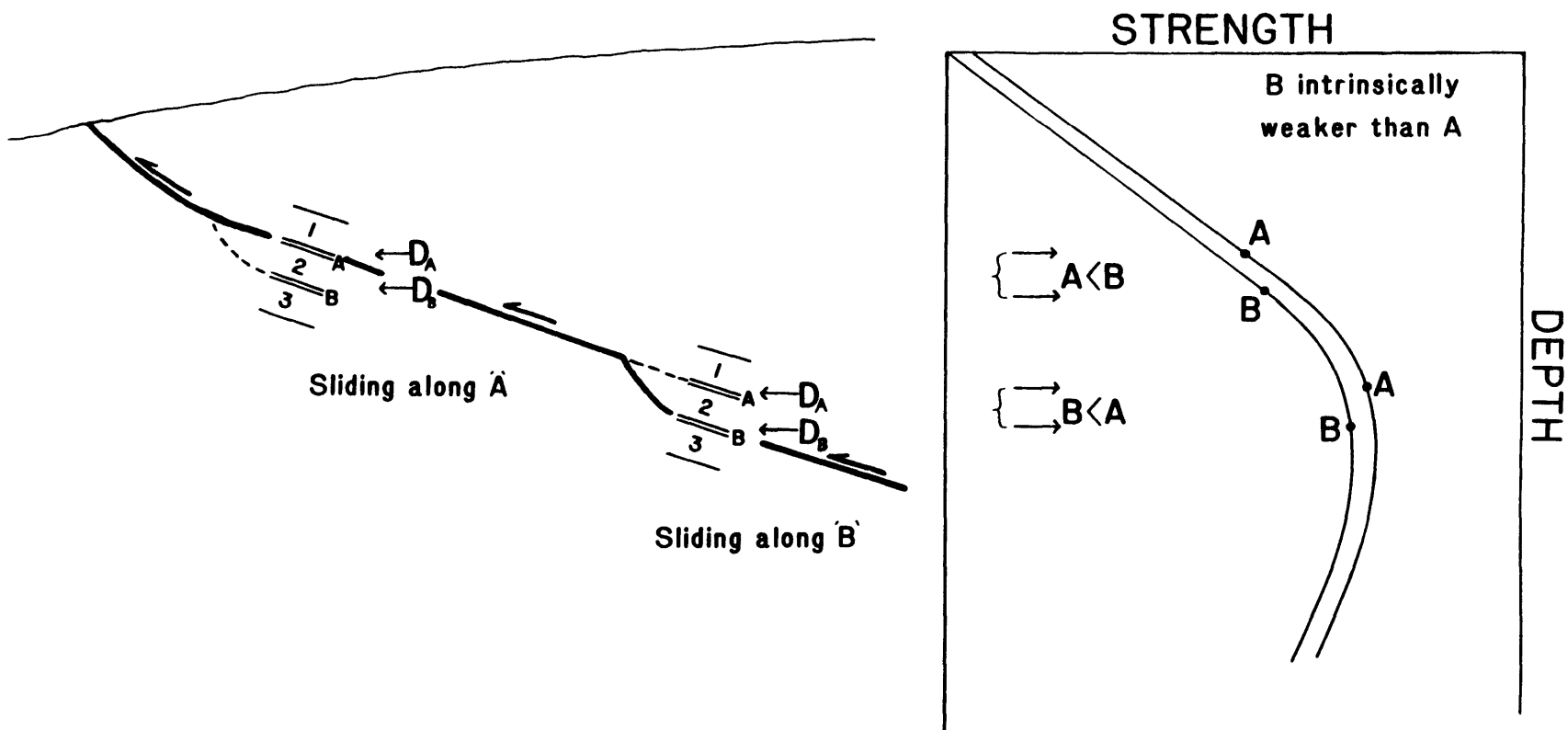
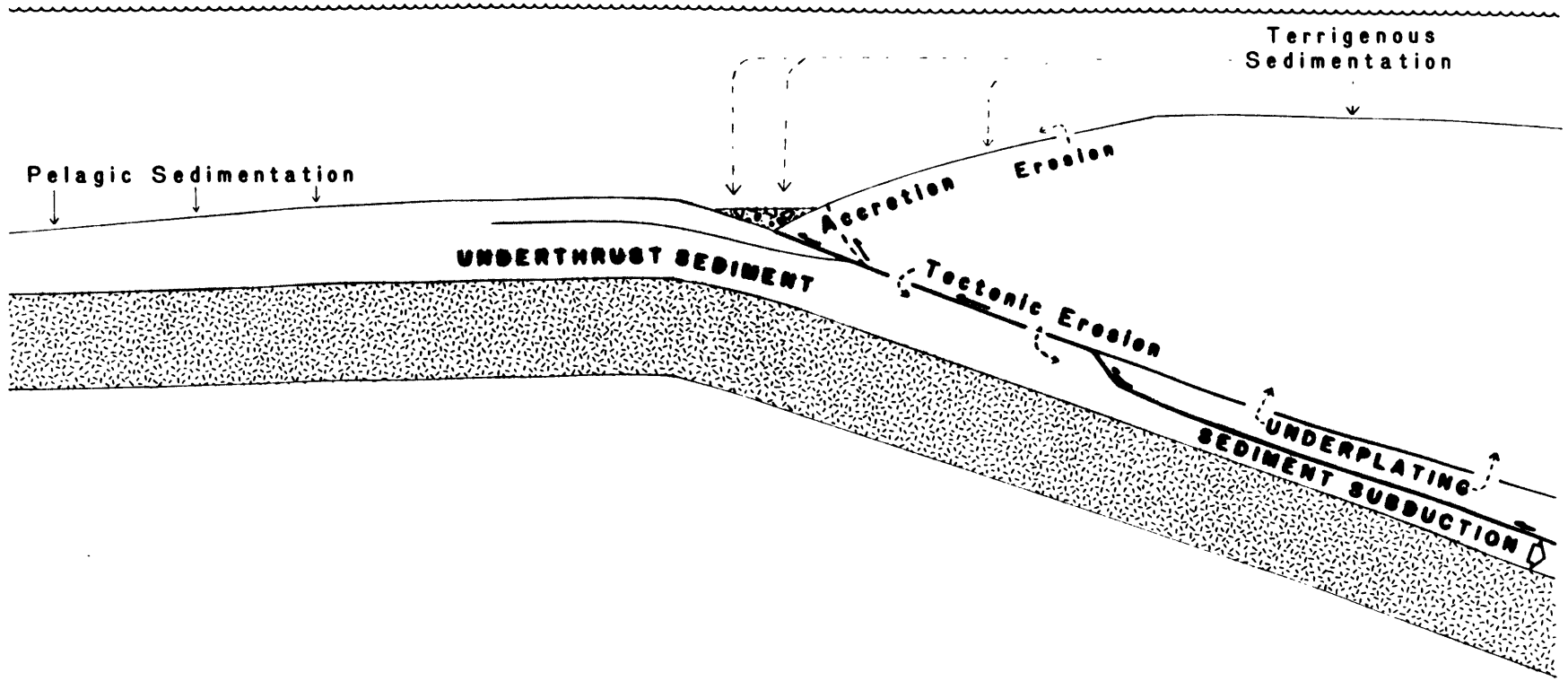


Figure 6.6



CHAPTER 7 DISCUSSION AND CONCLUSIONS

This chapter has two main roles. First, it contains a summary and synthesis of the results of this thesis. Second, it serves as a vehicle for speculations and comments on additional subjects related to the content of the thesis.

7.1 THIN-SKINNED DEFORMATION

In Chapter 2, I presented a simple model for the overall mechanics of fold-and-thrust belts and accretionary wedges, in which they are regarded as being analogous to soil being pushed by a bulldozer. The emphasis of this model upon the compressive nature of thrust belt mechanics is similar to that of Hubbert and Rubey (1959), and the accounting for the importance of topography in the deformation is similar to that of Elliott (1976) and Chapple (1978). The main distinguishing characteristic of this model is the degree to which the overall shape (referred to as the critical taper) can be predicted for actual thrust belts using parameters which are either directly observed or plausibly surmised. The model successfully predicts the overall tapers of many wedges. It appears to be consistent with indirect observations of the stresses (apparently near failure), the kinematics, and the geometry of thrust faulting within both thrust belts and accretionary wedges.

Thin-skinned wedge tectonics can, in principle, exist in the case of crustal extension as well as compression.

However, it is only compressive wedges which are known to be geologically widespread.

In this subsection, we will first examine the differences between the two types of compressive wedges. We explore second the possibility that completely extensional wedges may exist and be of some geologic interest.

DIFFERENCES BETWEEN THRUST BELTS AND ACCRETIONARY WEDGES

A number of differences between thrust belts and accretionary wedges have been pointed out, the most obvious being the total amount of horizontal shortening which has taken place. Shortening in thrust belts is typically by a factor of between 2 and 4, and comprises a net reduction in horizontal distance on the order of 100 of 200 km. However, depending upon how one wishes to define the shortening, the comparable length for accretionary wedges can be many thousands of kilometers. Whereas the entire length of an accretionary wedge overthrusts the downgoing plate at a speed of several cm/yr, thrust belts, as a whole, overthrust the craton at a speed roughly an order of magnitude slower.

The most important differences between the two types of wedge involve their kinematics. The presence of a water overburden increases the critical taper of a subaerial wedge by roughly 1° , as observed along the eastern coast of Taiwan. The presence of rapid erosion on the upper surfaces of thrust belts serves to constantly reduce their taper, with the result that active deformation must

continue to take place throughout. By contrast, the sediment flux atop accretionary wedges is, if anything, positive. Therefore, the process which drives most of the ongoing deformation within subaerial thrust belts simply does not exist for accretionary wedges. This difference explains the otherwise puzzling concentration of accretionary wedge deformation near the toe, in contrast to the more widely dispersed deformation in fold-and-thrust belts. In addition, compared to their counterparts in thrust belts, sediments in accretionary wedges tend to be relatively incompletely lithified, anisotropic, and divided into small thrust slivers. These mechanical differences, along with the absence of erosion, explain the relative seismic quiescence of accretionary wedges discussed by Chen et al. (1982).

THIN-SKINNED EXTENSION

It is interesting to speculate about the mechanics of a wedge which fails in horizontal extension, such that, in effect, the bulldozer has been replaced by a tow truck moving in the opposite direction. The possible importance of low-angle extensional faults in regions undergoing lithospheric extension, such as the Basin and Range province, has been described by Wernicke (1981, 1982) and Wernicke and Burchfiel (1982). Illustrations of such extensional faulting (Wernicke, 1981) depict a very large (tens of kilometers in length), low angle (between 4° and 10° dip) normal fault. This throughgoing fault separates

relatively undisturbed rocks below from a wedge-shaped region above which is described as 'an extensional fault mosaic comprised of listric and planar rotational faults'. The overall geometry of this setting is strikingly similar to that of thin-skinned compressional mountain belts, the mechanics of which have been discussed by Elliott (1976), Chapple (1978), Davis et al. (1983), as well as in in Chapters 2 and 3.

If we assume that the extension is driven by a pull from the side, as well as the direct local effects of gravity (a very reasonable assumption for a setting such as the Basin and Range Province), then it is a simple exercise to adapt the analysis of Chapter 2 to this case. In effect, the only real difference between the problems is a reversal of the direction in which the basal shear traction acts (see eq. 2.8). The definition of the angle ψ , which describes the direction of the greatest principal stress, remains the same, but its magnitude is different. Instead of being located in the quadrant between 0 and $\pi/4$ as for the compressive wedge, ψ is, in this case, between $\pi/2$ and $3\pi/4$, because in an extensional setting it is the least principal stress which is subhorizontal. For such an extensional wedge, the equivalent of the critical taper equation (eq. 2.18) describes the minimum taper of a wedge which can be pulled from behind without undergoing extensional faulting. When the wedge is narrower than this critical taper, the toe cannot be pulled from the thick end

of the wedge, so extensional faulting takes place which separates the toe from the rest of the wedge, thereby increasing the taper of the wedge. The appropriate tensile versions eqs. 2.17, 2.22, and 2.29 for a subaerial wedge yield the following expression:

$$\alpha + \beta = \frac{(1 - \lambda_b) \mu_b - \beta}{1 + (1 - \lambda) K'} \quad (7.1)$$

where all variables are as defined in Chapter 2 and

$$K' = 2H^{-1} \int_0^H \frac{dz}{\csc \phi \sec^2 \psi(z) - 1} \quad (2.22)$$

The magnitude of K' can be approximated by the method of Chapter 2 to be

$$K' \approx \frac{\sin^2 \phi_b + \cos \phi_b (\sin^2 \phi - \sin^2 \phi_b)^{1/2}}{\cos^2 \phi_b - \cos \phi_b (\sin^2 \phi - \sin^2 \phi_b)^{1/2}} - \frac{\sin \phi}{1 + \sin \phi} \quad (7.2)$$

Given the uncertainty of many of the pertinent variables, it would be inappropriate to take too seriously any solution of eq. 7.1 for the examples given by Wernike (1981). However, I would like to suggest that the extensional tectonics described by him may be very closely analogous to that of a thin-skinned thrust belt. If we assume a Byerlee law ($\mu_b = 0.85$) base, with a 20% stronger wedge, then $K' = 0.48$ and the taper ($\alpha \approx 0^\circ$, $\beta \approx 7.5^\circ$) corresponds to $\lambda = \lambda_b = 0.67$, a reasonable (but apparently unconfirmable) value.

7.2 FORCES WHICH DRIVE PLATES

CONSEQUENCES OF NEGLIGIBLE TRUE POLAR WANDER

The results of Chapter 5 indicate that over the past 50 m.y., there has been no measurable deviation between the paleomagnetically observed polar wander curve for North America and the corresponding curve calculated according to an assumption of no net drag torque. This result can be interpreted to mean that during that period there has been no measurable true polar wander. McElhinney, (1973), Jurdy and van der Voo, (1974, 1975) and Jurdy (1981) have concluded there has been little or no true polar wander during that period. Despite the relative unimportance of basal drag forces in the torque balance of individual plates (Forsyth and Uyeda, 1975; Chapple and Tullis, 1977), the negligible true polar wander during the Tertiary suggests otherwise for the lithosphere as a whole. Simple calculations demonstrated in Chapter 5 suggest that the plate driving forces are very inefficient at driving motions of the whole lithosphere. They either apply no net torque whatsoever (as at transform boundaries), nearly cancel themselves out in most cases (ridge-push torques), or (in the case of subduction zones) apply unequal torques to two plates but are so distributed around the world at present that their vector sum is far smaller than their scalar sum. Therefore, for the lithosphere as a whole, unlike individual plates, net driving torques are small enough that the

opposing net torque required of basal drag to achieve balance and the net angular velocity of the lithosphere are also small.

Although plate-boundary forces appear to have a negligible effect upon the motion of the lithosphere as a whole, such forces (particularly the trench-pull force) are nonetheless very important in controlling the velocities of the individual plates (Forsyth and Uyeda, 1975; Chapple and Tullis, 1977). The reconstruction of plate velocity histories since the late Cretaceous given in Chapter 5 indicates that the fastest plates are invariably those which are being subducted over an appreciable fraction of their boundaries, and changes in the velocities of individual plates appear to be related to the initiation and cessation of subduction.

BASAL DRAG

The high speeds of India during the late Cretaceous and earliest Tertiary are a strong argument that plates containing an appreciable amount of continental lithosphere are not always slower than the primarily oceanic plates. This result is in conflict with the conclusion, drawn from present day plate velocities (Forsyth and Uyeda, 1975; Solomon et al., 1975), that drag beneath continents is much greater than beneath oceans. A more likely explanation of the tendency for oceanic plates to be faster is that oceanic plates are more likely to have a subducted boundary.

A comparison of the likely magnitudes of net

lithospheric driving torques with observed (negligible) true polar wander leads to interesting conclusions. In order for the net torques associated with either ridges or subduction zones to result in so little net rotation of the lithosphere, the coefficient of linear drag at the base of the lithosphere must be large enough that shear stresses of 2 or 3 MPa should be exerted at the base of the faster plates. If we accept that this shear stress is too large by roughly an order of magnitude, we are led to conclude that the sum of net driving torques which must be balanced by basal drag is smaller than the calculated net ridge-push torque. A comparison of the probable directions of the net lithospheric torques associated with ridge-push and trench-pull torques around the world suggests that the two net torques could sum in such a manner as to produce negligible polar wander, even though they are individually large enough to drive measureable net rotation of the whole lithosphere.

PLATE BOUNDARY FORCES

If the net trench-pull and ridge-push torques are aligned in such a manner that each one cancels out the tendency of the other to produce true polar wander, then we can estimate their relative magnitudes. Based upon the estimates of the net ridge-push torque in Chapter 5, the net torque associated with a unit length of trench is estimated to be 9×10^{18} N·m per meter. For a 100 km thick lithosphere, this translates to a mean net stress of 15 MPa

extension.

The estimate of the magnitude of the net trench torque developed in Chapter 5 corresponds to the difference between the torques acting upon the two plates, the trench-pull and 'trench suction' torques. The trench-pull force is equivalent to the CONV force of Chapple and Tullis (1977) and the 'trench suction' is equivalent to the difference between their UPPLA and CONV forces. This 'trench suction' torque acting upon the overlying plate, which is large enough to effect the transition between near-trench compression and back-arc extension, is probably of the same order as (though smaller than) the trench-pull torque. The results of Chapple and Tullis (1977) can be expressed in terms of net torque on the lithosphere as a whole associated with the subduction zone (the net trench torque of Chapter 5). For a relative plate velocity of 6 cm/yr, the results listed in their Table 1 yield, on average, a net trench torque of 1.9×10^{19} N·m per meter, roughly a factor of two larger than that calculated in Chapter 5 using a totally different set of assumptions. The most speculative of those assumptions is that of the existence of a rough balance between net worldwide trench-pull and ridge-push torques. The apparently reasonable agreement obtained with the Chapple and Tullis result under the assumption that these major plate-boundary torques come close to cancelling each other out lends some degree of credence to the idea of such a balance.

MECHANISM FOR INTERMITTENT TRUE POLAR WANDER

In Chapter 5, I have suggested that, in a number of different ways, the torques associated with plate boundaries around the world cancel each other out so that their vector sum is much smaller than their scalar sum. Part of this cancelling out is a basic property of the torques. For example, mid-ocean ridges tend to be in the middle of oceans, thereby yielding no net torque. However, to the degree that the present lack of true polar wander is the result of a fortuitous (and possibly transient) relationship between driving torques, then one should expect that this relationship (and the resulting lack of true polar wander) may not have been the case at times sufficiently far into the past that plate boundaries were very different from those at present.

MARINE TRANSGRESSIONS

It appears that the rms velocity of the lithosphere as a whole was significantly greater in the late Cretaceous and earliest Tertiary than at present, although the exact magnitude is uncertain. The timing of this rapid action of plate tectonics appears to support the idea (Hallam, 1971; Hays and Pitman, 1973) that the great Cretaceous marine transgressions are closely related to an increased volume of mid-ocean ridges associated with more rapid plate tectonics.

7.3 LITHOSPHERIC STRENGTH AND STRESSES

STRESSES IN WEDGES

In active thrust belts, shear stresses are, as discussed in Chapters 3 and 4, very close to the yield strength for the material. Therefore, insofar as we can determine the state of stress, we can learn about the strength of the crust as a function of depth. We have seen that the taper of and fault step-up angles in the Taiwan wedge are consistent with friction coefficients in the range $0.2 < \mu < 1.7$, but the range $0.4 < \mu < 0.85$ is favored. This translates to shear tractions along the deeper parts of the basal décollement in the range $30\text{MPa} < \tau_b < 60\text{MPa}$. Such high stresses are not found in all thrust belts, and certainly not in all accretionary wedges. Weak sediments and extremely high pore pressures in many accretionary wedges result in low stresses. Near the toe of the Barbados wedge, shear stresses are on the order of only a few hundred kPa. Thrust belts which ride atop a weak salt horizon, such as the Zagros, can have much lower basal shear stresses, although they are nevertheless near failure, as made clear by the experience of induced seismicity in the thrust belt of western Tadjikstan.

THE BRITTLE-DUCTILE TRANSITION

The depth of transition between strong, brittle rock behavior and weaker, time-dependent deformation is a function of a number of factors. These include the identity

of the minerals present and their deformation mechanisms, the strain rate of deformation, the geothermal gradient, and the friction coefficient and pore pressure ratio which characterize the brittle regime (Brace and Kohlstedt, 1980).

A wide range of thrust belts and accretionary wedges exhibit a reduction in topographic slope where the basal decollement attains a depth of roughly 15 km. This break in slope is interpreted to correspond to the weakening which is expected to be associated with the brittle-ductile transition. This depth is in very good agreement with independent estimates of the depth of this transition, assuming typical geothermal gradients, and a moderately high friction coefficient within the brittle region above 15 km depth.

HIGH STRESS VERSUS LOW STRESS

The work presented within this thesis provides no definitive answers with regard to the high stress/low stress controversy. However, several aspects of this thesis seem to point toward moderately high stresses near subduction zones.

As just mentioned, the depth of the brittle-ductile transition, which appears to be resolvable in terms of a breakdown of the Coulomb-wedge theory of Chapter 2 and Davis et al. (1983), occurs at a depth highly suggestive of a coefficient of friction in the upper part of the crust which is close to that predicted by Byerlee law friction. Analyses of the taper of and fault step-up angles within the

Taiwan fold-and-thrust belt lead to similar conclusions, although the mechanics of the Barbados wedge serve to remind us of the potentially enormous weakening effects of pore fluids.

Estimates of plate-driving torques associated with ridge topography and subduction yield mean stresses across the whole lithosphere on the order of a few tens of MPa. Because that depth range undoubtedly spans a wide range of yield strengths, these results require maximum strengths of several tens of MPa. Taken as a whole, the inference to be drawn from the evidence presented in this thesis is that shear stresses at depth can reach many tens of MPa, and probably attain a maximum value close to the somewhat psychological "kilobar barrier."

7.4 PARTING THOUGHTS

ANCIENT MOUNTAIN BELTS

It is tempting to use the Coulomb-wedge theory to try to estimate the amount of material which has been removed from ancient, currently inactive mountain belts. However, the same sensitivity of the taper to pore pressures which was so useful in the discussion of Chapter 3 makes this a virtually impossible task, in the absence of paleo-pore pressure indicators. However, it would seem to be potentially fruitful to compare the structure of fossil mountain belts, considered as once-deforming wedges, with exposed low-grade metamorphism, which could give an

indication of their burial depths. The relationship between erosion and ongoing wedge deformation might be useful as an additional tool for dating the end of orogeny.

CLIMATE AND TECTONICS

I question whether the intricate relationships between climate and tectonics are adequately appreciated. These relationships extend to the largest of scales. Computer modeling of the Pleistocene in the CLIMAP project indicate that an ice age could not be sustained without the presence of Antarctica at one of the poles, because pole-equator heat exchange would then be too efficient.

Climate and tectonics interact with each other. Orogenic topography alters wind and rain patterns, in a manner dependent upon whether the convergent margin is on the east or west side of the continent. Eroded sediments, whose quantity depends upon topographically controlled climatic conditions, play a major role in the evolution of the trench inner wall, and can affect the direction in which the trench migrates outward or is tectonically eroded away. The quantity of weak ash in a trench depends upon whether the volcanic arc is upwind or downwind.

ABSOLUTE MOTIONS

The whole question of absolute motion reference frames is somewhat ill-defined. Further clarification of the relationship between the various 'absolute' reference frames is desperately needed. One relatively feasible

exercise which would be useful to perform would be the extension into the past of an accounting of net lithospheric torques. Another area which is in need of further examination is the relationship between closely juxtaposed normal faulting and thrust faulting near convergent margins, and how this relates to the overall balance of forces at the plate boundary.

References

- Ahmed, S.S., Tertiary geology of part of South Makran, Baluchistan, West Pakistan, Am. Assoc. Petrol. Geol. Bull., 53, 1480-1499, 1969.
- Anderson, E.M., The Dynamics of Faulting and Dyke Formation with Application to Britain, Oliver C. Boyd, Edinburgh, 1951.
- Andrews, D.J., and N.H. Sleep, Numerical modelling of tectonic flow behind island arcs, Geophys. J. R. Astron. Soc., 38, 237-251, 1974.
- Angelier, J., Tectonic evolution of the Hellenic Arc since the late Miocene, Tectonophysics, 49, 23-36, 1978.
- Angelier, J., N. Lyberis, X. LePichon, E. Barrier, and P. Huchon, The tectonic development of the Hellenic Arc and the Sea of Crete: A synthesis, Tectonophysics, 86, 159-196, 1982.
- Artyushkov, E.V., Stresses in the lithosphere caused by crustal thickness inhomogeneities, J. Geophys. Res., 78, 7675-7708, 1973.
- Aubouin, J., J-F. Stephan, J. Raoup, and V. Renard, The Middle America Trench as an example of a subduction zone, Tectonophysics, 86, 113-132, 1982a.
- Aubouin, J., R. von Huene, M. Baltuck, R. Arnott, J. Bourgois, M. Filewicz, K. Kvenvolden, B. Leinert, J. McDonald, K. McDougall, Y. Ogawa, E. Taylor, and B. Winsborough, Leg 84 of the Deep Sea Drilling Project, Subduction without accretion: Middle America Trench off Guatemala, Nature, 297, 458-460, 1982b.
- Audebaud, E., R. Capdevilla B., Dalmayrac, J. Debelmas, G. Laubacher, C. Lefevre, R. Marocco, C. Martinez, M. Mattauer, F. Megard, J. Paredes and P. Tomasi, Les traits geologiques essentiels des Andes Centrales (Peron-Bolivie): Revue de Geologie Physique Geol. Dynamique, 15, 73-114, 1973.
- Bally, A.W., P.L. Gordy, and G.A. Stewart, Structure, seismic data and orogenic evolution of southern Canadian Rocky Mountains, Bull. Can. Pet. Geol., 14, 337-381, 1966.

- Barazangi, M., and B.L. Isacks, Subduction of the Nazca plate beneath Peru: Evidence from the spatial distribution of earthquakes, Geophys. J. Roy. Astron. Soc., 57, 537-555, 1979
- Barton, N., The shear strength of rock and rock joints, Int. J. Rock Mech. Min. Sci. and Geomech., Abstr., 13, 255-279, 1976.
- Beaumont, C., Foreland basins, Geophys. J. R. Astron. Soc., 65, 291-329, 1981.
- Beck, R.H., and P. Lehner, Oceans, new frontiers in exploration, Am. Assoc. Pet. Geol. Bull., 58, 376-395, 1974.
- Berberian, F., and M. Berberian, Tectono-Plutonic Episodes in Iran, in Zagros-Hindu Kush-Himalaya Geodynamic Evolution, edited by H.K. Gupta and F.M. Delaney, Geodynamics Series volume 3, American Geophysical Union, Washington, D.C., p. 5-32, 1981.
- Berberian, M., Active faulting and tectonics of Iran, in Zagros-Hindu Kush-Himalaya Geodynamic Evolution, edited by H.K. Gupta and F.M. Delaney, Geodynamics Series volume 3, American Geophysical Union, Washington, D.C., p. 33-69, 1981.
- Biju-Duval, B., P. Le Ouellec, A. Mascle, C. Renard, and P. Valery, Multibeam bathymetric survey and high resolution seismic investigations on the Barbados ridge complex (Eastern Caribbean): A key to the knowledge and interpretation of an Accretionary wedge. Tectonophysics, 86, 275-304, 1982.
- Biju-Duval, B., A. Mascle, L. Montadert, and J. Wanneson, Seismic investigations in the Colombia, Venezuela and Grenada Basins, and on the Barbados Ridge for future IPOD drilling in The 8th Caribbean Geological Conference, Geol. Minjbouw, vol. 57, edited by H.J. MacGillavry and D.J. Beets, pp. 105-116, 1978.
- Biju-Duval, B., J.C. Moore, G. Blackington, J.A. Bergen, G.E. Claypool, D.S. Cowen, R.T. Guerra, C.H.J. Hemleben, M.S. Marlow, J.H. Natland, C.J. Pudsey, G.W. Renz, M. Tardy, M.E. Willis, D. Wilson and A. Wright, Premiers resultats des forages IPOD implantes lors de la croisiere 78A du Glomar Challenger aur nord-est de la ride de la Barbade (arc des Petites Antilles): tectonique frontale d'un prisme d'accretion, C.R. Acad. Sc. Paris, 293, 621-628, 1981.
- Bird, P., Initiation of intracontinental subduction in the Himalaya, J. Geophys. Res., 83, 4975-4987, 1978.

- Bond, G., Speculations on real sea-level changes and vertical motions of continents at selected times in the Cretaceous and Tertiary periods, Geology, 6, 247-250, 1978.
- Bott, M.H.P., Origin of the lithospheric tension causing basin formation, Phil. Trans. R. Soc. Lond. A, 205, 319-324, 1982.
- Brace, W.F., and D.L. Kohlstedt, Limits on lithospheric stress imposed by laboratory experiments, J. Geophys. Res., 85, 6248-6252, 1980.
- Brewer, J.A., F.A. Cook, L.D. Brown, J.E. Oliver, S. Kaufman, and D.S. Albaugh, COCORP seismic reflection profiling across thrust faults, in Thrust and Nappe Tectonics, edited by K.R. McClay and N.J. Price, pp. 501-512, Blackwell Scientific Publications, Boston, 1981.
- Brewer, J.A., and D.L. Turcotte, On the stress system that formed the Laramide Wind River Mountains, Wyoming, Geophys. Res. Lett., 7, 449-452, 1980.
- Brown, L.D., P.A. Krumhansl, C.E. Chapin, A.R. Sanford, S. Kaufman, and J.E. Oliver, Deep structure of the Rio Grande rift from seismic reflection profiling, in The Rio Grande Rift: Tectonism and Magmatism, edited by R.E. Riecker, pp. 169-184, Spec. publ. AGU, Washington, D.C., 1979.
- Brune, J.N., T.L. Henyey, and R.F. Roy, Heat flow, stress, and rate of slip along the San Andreas fault, California, J. Geophys. Res., 74, 3821-3827, 1969.
- Burchfiel, B.C., Geology of Romania, Geol. Soc. Am. Spec. Paper, 158, 82 pp., 1976.
- Byerlee, J., Frictional characteristics of granite under high confining pressure, J. Geophys. Res., 72, 3639-3648, 1967.
- Byerlee, J., Friction of rocks, Pure Appl. Geophys., 116, 615-626, 1978.
- Byrne, T., Structural evolution of coherent terranes in the Ghost Rocks formation, Kodiak Island, Alaska, in Trench-Forearc Geology: Sedimentation and Tectonics on Modern and Ancient Active Plate Margins, edited by J.K. Leggett, pp. 229-244, Blackwell Scientific Publications, Boston, 1982.
- Cande, S.C., and Y. Kristoffersen, Late Cretaceous magnetic anomalies in the North Atlantic, Earth Planet. Sci. Lett., 35, 215-224, 1977.

- Caristan, Y., The transition from high-temperature creep to fracture in Maryland diabase, J. Geophys. Res., 87, 6781-6790, 1982.
- Carter, N.L., F.D. Hansen, and P.E. Senseny, Stress magnitudes in natural rock salt, J. Geophys. Res., 87, 9289-9300, 1982.
- Chapman, R.E., Mechanical versus thermal cause of abnormally high pore pressures in shales, Am. Assoc. Petr. Geol. Bull., 64, 2179-2183, 1980.
- Chapple, W.M., Mechanics of thin-skinned fold-and-thrust belts, Geol. Soc. Am. Bull., 89, 1189-1198, 1978.
- Chapple, W.M., and D.W. Forsyth, Earthquakes and the bending of plates at trenches, J. Geophys. Res., 84, 6729-6749, 1979.
- Chapple, W.M. and T.E. Tullis, Evaluation of the forces that drive the plates, J. Geophys. Res., 82, 1969-1984, 1977.
- Chase, C.G., Athenospheric counterflow: A kinematic model, Geophys. J. R. Astron. Soc., 56, 1-18, 1979.
- Chen, A.T., C. Frohlich, and G.V. Latham, Seismicity of the forearc marginal wedge (accretionary prism), J. Geophys. Res., 87, 3679-3690, 1982.
- Chen, W.P., P. Molnar, Focal depths of intracontinental and intraplate earthquakes and their implications for the thermal and mechanical properties of the lithosphere, J. Geophys. Res., 88, 4183-4214, 1983.
- Chi, W.R., J. Namson, and J. Suppe, Stratigraphic record of plate interactions in the Coastal Range of eastern Taiwan, Geol. Soc. China Mem., 4, 491-530, 1981.
- Cita, M.B., The Messian salinity crisis in the Mediterranean: A review, in Alpine-Mediterranean Geodynamics, Geodynamics series 7, edited by H. Berkhemer and K. Hsu, pp. 113-140, AGU, 1982.
- Cloos, M., Flow melanges: Numerical modeling and geologic constraints on their origin in the Franciscan subduction complex, California, Geol. Soc. Am. Bull., 93, 330-345, 1982.
- Comer, R.P., Tsunami generation by earthquakes, Ph.D. thesis, 232pp., Massachusetts Institute of Technology, Cambridge, MA, 1982.

- Cowan, D., and R.M. Silling, A dynamic scaled model of accretion at trenches and its implications for the tectonic evolution of subduction complexes, J. Geophys. Res., 83, 5389-5396, 1978
- Dahlen, F.A., D.M. Davis, and J. Suppe, The state of stress in fold-and-thrust belts and accretionary wedges (abstract), AGU Chapman Conference, Fault Behavior and the Earthquake Generation Process, 1982.
- Dahlen, F.A., W-L Zhao, and D. Davis, The influence of basal cohesion and plasticity on the profiles of fold-and-thrust belts and accretionary wedges (abstract), EOS Trans. AGU, 64, 318, 1983.
- Dalmayric, B., and P. Molnar, Parallel thrust and normal faulting in Peru and constraints on the state of stress, Earth Planet. Sci. Lett., 55, 473-481, 1981.
- Davies, G.F., The roles of boundary friction, basal shear stresses and deep mantle convection in plate tectonics, Geophys. Res. Lett. 5, 161-164, 1978.
- Davis, D.M., The mechanics of thrust faults: A sand box model, A.B. thesis, 53pp., Princeton Univ., Princeton, N.J., 1978.
- Davis, D.M., The mechanics of accretionary wedges applied to the Leg 78A study area near Barbados, Initial Rep. Deep Sea Drill. Proj., Leg 78A, in press, 1983.
- Davis, D.M., F.A. Dahlen, and J. Suppe, Resistance to subduction and normal faulting at convergent margins (abstract), EOS Trans. AGU, 63, 1115, 1982.
- Davis, D.M., and Hussong, D.M., Geothermal observations during DSDP Leg 78A, Initial Rep. Deep Sea Drill. Proj., Leg 78, in press, 1983.
- Davis, D.M., and S.C. Solomon, Variations in the velocities of the major plates since the late Cretaceous, Tectonophysics, 74, 189-208, 1981.
- Davis, D.M., and J. Suppe, Critical taper in mechanics of fold-and-thrust belts (abstract), Geol. Soc. Amer. Abstr. Programs, 12, 410, 1980.
- Davis, D.M., and J. Suppe, The effects of water overburden on the shape of accretionary wedges (abstract), Geol. Soc. Am. Abstr. Program, 13, 436, 1981.
- Davis, D.M., J. Suppe, and F.A. Dahlen, The mechanics of fold-and-thrust belts and accretionary wedges, J. Geophys. Res., 88, 1153-1172, 1983.

- Davis, E.F., and C.R.B. Lister, Fundamentals of ridge crest topography, Earth Planet. Sci. Lett., 21, 405-414, 1974.
- De Benedetti, A., The problem of the origin of the salt deposits in the Mediterranean and of their relations to other salt occurrences in the Neogene formations of contiguous regions, Marine Geol., 49, 91-114, 1982.
- De Cserna, Z., Tectonica de la Sierra Madre Oriental de Mexico, entre Torreon y Monterrey, 87 pp., 10th Internat. Geol. Congress, Mexico, 1956.
- Dewey, J.F., W.C. Pitman III, W.G.F. Ryan, and Bonnin, J., Plate tectonics and the evolution of the Alpine system. Geol. Soc. Am. Bull., 84, 3137-3180, 1973.
- Dickenson, W.R., Widths of modern arc-trench gaps proportional to past durations of igneous activity in associated magmatic arcs, J. Geophys. Res., 78, 3395-3417, 1973.
- Dickinson, W.R., Tectono-stratigraphic evolution of subduction-controlled sediment assemblages, in Island Arcs Deep Sea Trenches and Back-Arc Basins, edited by M. Talwani and W.C. Pitman III, Maurice Ewing Series I, pp 33-40, AGU, Washington DC, 1977.
- Elsasser, W.M., Sea-floor spreading as thermal convection, J. Geophys. Res., 76, 1101-1112, 1971.
- Elliott, D., The motion of thrust sheets, J. Geophys. Res., 81, 949-963, 1976.
- Elliott, D., The strength of rocks in thrust sheets (abstract), EOS Trans. AGU, 62, 397, 1981.
- Engdahl, E.R., Seismicity and plate subduction in the central Aleutians, in Island Arcs Deep Sea Trenches and Back-Arc Basins, edited by M. Talwani and W.C. Pitman III, Maurice Ewing Series I, pp. 259-272, AGU, Washington, D.C., 1977.
- Evamy, B.D., J. Haremboure, P. Kamerling, W.A. Knapp, F.A. Molloy, and P.H. Rowlands, Hydrocarbon habitat of tertiary Niger delta, Am. Assoc. Petr. Geol. Bull., 62, 1-39, 1978.
- Fertl, W.H., Abnormal Formation Pressures, 382 pp., Elsevier, N.Y., 1976.
- Forsyth, D.W., Lithospheric flexure, Rev. Geophys. Space Phys., 17, 1109-1114, 1979.

- Forsyth, D. and S. Uyeda, On the relative importance of the driving forces of plate motion. Geophys. J. R. Astron. Soc., 43, 163-200, 1975.
- Frank, F.C., Plate tectonics, the analogy with glacier flow and isostasy, in Flow and Fracture of Rocks, Geophys. Mon. 16, AGU, 285-292, 1972.
- Fukao, Y., Tsunami earthquakes and subducting processes near deep-sea trenches, J. Geophys. Res., 84, 2303-2314, 1979.
- Fukao, Y. and K. Kanjo, A zone of low frequency earthquakes beneath the inner wall of the Japan Trench, Tectonophysics, 67, 153-162, 1980.
- Galli-Olivier, C., Climate: A primary control of sedimentation in the Peru-Chile Trench, Geol. Soc. Am. Bull., 80, 1849-1852, 1969.
- Gansser, A., Geology of the Himalayas, 289 pp., Interscience-Wiley, London, 1964.
- Goetze, C., The mechanisms of creep in olivine, Phil. Trans. R. Soc. Lond. A., 288, 99-119, 1978.
- Goldburg, B.L., Formation of critical taper wedges by compression in a sand box model, A.B. thesis, 70 pp., Princeton Univ., Princeton, N.J., 1982.
- Gordon, R.G., and A. Cox, Paleomagnetic test of the early Tertiary plate circuit between the Pacific basin plates and the Indian plate, J. Geophys. Res., 85, 6534-6546, 1980.
- Gordon, R.G., M.O. McWilliams, and A. Cox, Pre-Tertiary velocities of the continents: A lower bound from paleomagnetic data. J. Geophys. Res., 84, 5480-5486, 1979.
- Graham, R.H., Gravity sliding in the Maritime Alps, in Thrust and Nappe Tectonics, edited by K.R. McClay and N.J. Price, pp. 335-352, Blackwell Scientific Publications, Boston, 1981.
- Gretnener, P.E., Pore pressure, discontinuities, isostasy and overthrusts, in Thrust and Nappe Tectonics, edited by K.R. McClay and N.J. Price, pp. 33-40, Blackwell Scientific Publications, Boston, 1981.
- Grow, J.A., and T. Atwater, Mid-Tertiary tectonic transition in the Aleutian arc, Geol. Soc. Am. Bull., 81, 3715-3722, 1970.

- Gwinn, V.E., Kinematic patterns and estimates of lateral shortening, Valley and Ridge and Great Valley provinces, central Appalachians, south-central Pennsylvania, in Studies of Appalachian Geology: Central and Southern, edited by G.W. Fischer, F.J. Pettijohn, J.C. Reed, Jr., and K.H. Weaver, pp. 127-146, Interscience, New York, 1970.
- Hafner, W., Stress distribution and faulting, Bull. Geol. Soc. Am., 62, 373-398, 1951.
- Hager, B.H., Oceanic plate motions driven by lithospheric thickening and subducted slabs, Nature, 276, 156-159, 1978.
- Hager, B.H., and R.J. O'Connell, Kinematic models of large-scale flow in the earth's mantle. J. Geophys. Res., 84, 1031-1048, 1979.
- Haimson, B., Hydraulic fracturing in porous and nonporous rock and its potential for determining in-situ stresses at great depth, Ph.D. thesis, Univ. of Minnesota, Minneapolis, 1968.
- Hales, A.L., Gravitational sliding and continental drift, Earth Planet. Sci. Lett., 6, 31-34, 1969.
- Hallam, A., Re-evaluation of the paleogeographic argument for an expanding Earth, Nature, 232, 180-182, 1971.
- Hamilton, W., Tectonics of the Indonesian region, U.S. Geol. Survey Prof. Paper 1078, 345 pp., 1979.
- Hanks, T.C., Deviatoric stress and earthquake occurrence at the outer rise, J. Geophys. Res., 84, 2343-2347, 1979.
- Harper, J.F., On the driving forces of plate tectonics. Geophys. J. R. Astron. Soc., 40, 465-474, 1975.
- Harper, J.F., Asthenospheric flow and plate motions, Geophys. J. R. Astron. Soc., 55, 87-110, 1978.
- Hays, J.D., and W.C. Pitman III, Lithospheric plate motion, sea-level changes and climatic and ecological consequences, Nature, 246, 18-21, 1973.
- Healy, J.H., W.W. Rubey, D.T. Griggs, and C.B. Raleigh, The Denver earthquakes, Science, 161, 1301-1310, 1968.
- Hey, R., Tectonic evolution of the Cocos-Nazca spreading center, Geol. Soc. Am. Bull., 88, 1404-1420, 1977.
- Hoshino, K., H. Koide, K. Inami, S. Iwamura, and S. Mitsui, S., Mechanical properties of Japanese Tertiary sedimentary rocks under high confining pressures, Geol. Survey Japan, Report 244, 200 pp., 1972.

- Hottman, C.E., J.H. Smith, and W.R. Purcell, Relationship among earth stresses, pore pressure, and drilling problems offshore Gulf of Alaska: J. Petroleum Technol., 31, p. 1477-1484, 1979.
- Hsui, A.T., and M.N. Toksoz, Back-arc spreading: Trench migration, continental pull or induced convection?, Tectonophysics, 74, 89-98, 1981.
- Hubbert, M.K., and W.W. Rubey, Role of fluid pressure in mechanics of overthrust faulting: I. Mechanics of fluid-filled solids and its application to overthrust faulting, Geol. Soc. Am. Bull., 70, 115-166, 1959.
- Hubbert, M.K., D.G. Willis, Mechanics of hydraulic fracturing, Trans. AIME, 210, 153-166, 1957.
- Irving, E., Paleopoles and paleolatitudes of North America and speculation about displaced terrains, Can. J. Earth Sci., 16, 669-694, 1979.
- Jacob, K.H., and R.L. Quittmeyer, The Makran region of Pakistan and Iran: Trench-arc system with active plate subduction, in Geodynamics of Pakistan, edited by A. Farah and K.A. DeJong, Geological Survey of Pakistan, Quetta, 1979.
- Jacoby, W., Instability in the upper mantle and global plate movements, J. Geophys. Res., 75, 5671-5680, 1970.
- Jaeger, J.C., The effect of the drilling fluid on temperatures measured in bore holes, J. Geophys. Res., 66, 563-569, 1961.
- Jaeger, J.C., and N.G.W. Cook, Fundamentals of Rock Mechanics, pp. 87-91, Methuen, London, 1969.
- Jongsma, D., Heat Flow in the Aegean Sea, Geophys. J. R. Astron. Soc., 37, 337-346, 1974.
- Jordan, T.E., Thrust loads and foreland basin evolution, cretaceous, western United States, Am. Assoc. Petrol. Geol. Bull. 65, 2506-2520, 1981.
- Jurdy, D.M., A determination of true polar wander since the early Cretaceous, Ph.D. thesis, 88 pp., The Univ. of Michigan, Ann Arbor, MI, 1974.
- Jurdy, D.M., An alternative model for early Tertiary absolute plate motions, Geology, 6, 469-472, 1978.
- Jurdy, D., Relative plate motions and the formation of marginal basins, J. Geophys. Res., 84, 6796-6802, 1979.

- Jurdy, D.M., True polar wander. Tectonophysics, 74, 1-16, 1981.
- Jurdy, D.M., and R. Van der Voo, A method for the separation of true polar wander and continental drift, including results for the last 55 m.y., J. Geophys. Res., 74, 2945-2952, 1974.
- Jurdy, D.M. and R. Van der Voo, True polar wander since the early Cretaceous, Science, 187, 1193-1196, 1975.
- Kadinsky-Cade, K., and M. Barazangi, Seismotectonics of southern Iran: The Oman line, Tectonics, 1, 389-412, 1982.
- Karig, D.E., Origin and development of marginal basins in the western Pacific, J. Geophys. Res., 76, 2542-2561, 1971.
- Karig, D.E., and R.W. Kay, Fate of sediments on the descending plate at convergent margins, Phil. Trans. Roy. Soc. Lond. A, 301, 233-251, 1981.
- Karig, D.E., and Sharman, G.F. III, Subduction and accretion in trenches, Geol. Soc. Am. Bull., 86, 337-389, 1975.
- Kaula, W.M., Absolute plate motions by boundary velocity minimizations, J. Geophys. Res., 80, 244-248, 1975.
- Keller, B., B.T.R. Lewis, C. Meeder, C. Helsey and R.P. Meyer, Explosion seismology studies of active and passive continental margins, in Geological and Geophysical Investigations of Continental Margins, Mem.29, edited by Watkins, J.S., Montadert, L. and Dickerson, P., pp. 443-452, American Association of Petroleum Geology, 1979.
- Kenyon, N.H., R.H. Belderson, and A.H. Stride, Detailed tectonic trends on the central part of the Hellenic outer ridge and in the Hellenic trench system, in Trench-Forearc Geology: Sedimentation and Tectonics on Modern and Ancient Active Plate Margins, edited by J.K. Leggett, pp. 335-343, Geological Society of London, Oxford, 1982.
- Kieckhefer, R.M., G.F. Moore, F.J. Emmel, and W. Sugiarta, Crustal structure of the Sunda forearc region west of central Sumatra from gravity data, J. Geophys. Res., 86, 7003-7012, 1981.
- Kirby, S.H., Tectonic stresses in the lithosphere: Constraints provided by the experimental deformation of rocks, J. Geophys. Res., 85, 6353-6363, 1980.

- Lachenbruch, A.H., Frictional heating, fluid pressure, and the resistance to fault motion, J. Geophys. Res., 85, 6097-6112, 1980.
- Lachenbruch, A.H., and J.H. Sass, Thermomechanical aspects of the San Andreas fault system, in Proceedings of the Conference on Tectonic Problems of the San Andreas Fault System, edited by R.L. Kovach and A. Nur, pp. 192-205, Stanford University Press, Palo Alto, Calif., 1973.
- Lachenbruch, A.H., J.H. Sass, Heat flow and energetics of the San Andreas fault zone, J. Geophys. Res., 85, 6185-6222, 1980.
- Lambe, T.W., and R.V. Whitman, Soil Mechanics, SI Version, p. 69, Wiley, New York, 1979.
- Lambert, W.R., Stress distribution in the Winters Pass thrust plate, M.A. thesis, 97 pp., Rice University, Houston, TX, 1978.
- Langseth, M., and T. Burch, Geothermal observations on the Japan Trench transect, Initial Rep. Deep Sea Drill. Proj. Leg 56-57, pt.2, pp. 1207-1210, 1980.
- LeFort, P., Himalayas: The collided range. Present knowledge of the continental arc, Am. J. Science, 275-A, 1-44, 1975.
- Leith, W., D.W. Simpson, and W. Alvarez, Structure and permeability: Geologic controls on induced seismicity at Nurek reservoir, Tadjikistan, USSR, Geology, 9, 440, 1981.
- Le Pichon, X., Sea-floor spreading and continental drift, J. Geophys. Res., 73, 3661-3697, 1968.
- Le Pichon, X., Land-locked oceanic basins and continental collision: The eastern Mediterranean as a case example, in Mountain Building Processes, edited by K.J. Hsu, pp. 202-211, Academic Press, New York, 1982.
- Le Pichon, X., and J. Angelier, The Hellenic arc and trench system: A key to the neotectonic evolution of the eastern Mediterranean, Tectonophysics, 60, 1-42, 1979.
- Le Pichon, X., and J. Angelier, The Aegean Sea, Phil. Trans. R. Soc. Lond., A, 300, 357-372, 1981.
- Li, Y.H., Denudation of Taiwan island since the Pliocene epoch, Geology, 4, 105-107, 1975.

- Lister, C.R.B., Gravitational drive on oceanic plates caused by thermal contraction, Nature, 257, 663-665, 1975.
- Lyon-Caen, H., and P. Molnar, Constraints on the structure of the Himalaya from an analysis of gravity anomalies and a flexural model of the lithosphere, J. Geophys. Res., in press, 1983.
- Makris, J., A dynamical model of the Hellenic Arc deduced from geophysical data, Tectonophysics, 36, 339-346, 1976.
- Malfait, B.T., and M.G. Dinkleman, Circum-Caribbean tectonic and igneous activity and the evolution of the Caribbean plate, Geol. Soc. Am. Bull., 83, 251-272, 1973.
- Mandl, G., and W. Crans, Gravitational gliding in deltas in Thrust and Nappe Tectonics, edited by K.R. McClay and N.J. Price, pp. 41-54, Blackwell Scientific Publications, Boston, 1981.
- Mandl, G., and G.K. Shippam, Mechanical model of thrust sheet gliding and imbrication, in Thrust and Nappe Tectonics, edited by K.R. McClay and N.J. Price, pp. 79-98, Blackwell Scientific Publications, Boston, 1981.
- Marlow, M., and H. Lee, Physical properties of sediments for the Lesser Antilles margin along the Barbados Ridge: Results for Deep Sea Drilling Project Leg 78A, in Initial Rep. Deep Sea Drill. Proj., 78A, in press, 1983
- McClay, K.R., and N.J. Price, eds., Thrust and Nappe Tectonics, 539 pp., Geological Society of London, Oxford, 1981.
- McElhinny, M.W., Mantle plumes, paleomagnetism and polar wandering, Nature, 241, 523-524, 1973.
- McGarr, A., Some constraints on levels of shear stress in the crust from observations and theory, J. Geophys. Res., 85, 6231-6238, 1980.
- McKenzie, D.P., Speculations on the consequences and causes of plate motions. Geophys. J. R. Astron. Soc., 18, 1-32. 1969.
- McKenzie, D.P., Plate tectonics, in The Nature of the Solid Earth, edited by E.C. Robertson, pp. 323-361, McGraw-Hill, New York, 1972.

- McKenzie, D., Active tectonics of the Alpine-Himalayan belt: The Aegean Sea and surrounding regions, Geophys. J. R. Astr. Soc., 55, 217-254, 1978.
- McKenzie, D.P., and J.G. Sclater, Heat flow in the eastern Pacific and sea-floor spreading, Bull. Volcanol., 33, 101-118, 1969.
- McMillen, K.J., and S.B. Bachman, Bathymetric and tectonic evolution of the southern Mexico active margin, Deep Sea Drilling Project Leg 66, Initial Rept. Deep Sea Drill. Proj., Leg 66, 815-822, 1982.
- McNutt, M., Implications of regional gravity for state of stress in the Earth's crust and upper mantle, J. Geophys. Res., 85, 6377-6396, 1980.
- McPowell, C., A speculative tectonic history of Pakistan and surroundings: Some constraints from the Indian Ocean, in Geodynamics of Pakistan, Geological Survey of Pakistan, Quetta, p. 5-24, 1979.
- Megard, F., and H. Philip, Plio-Quaternary tectono-magmatic zonation and plate tectonics in the Central Andes, Earth Planet Sci. Lett., 33, 231-239, 1976.
- Meissner, R., and J. Strehlau, Limits of stresses in continental crusts and their relation to the depth-frequency distribution of shallow earthquakes, Tectonics, 1, 73-89, 1982.
- Melosh, J., Shear stress on the base of a lithospheric plate, Pure Appl. Geophys., 115, 429-439, 1977.
- Menard, H.W., and L.M. Dorman, Dependence of depth anomalies upon latitude and plate motion, J. Geophys. Res., 82, 5329-5335, 1977.
- Mercier, J.L., Extensional-compressional tectonics associated with the Aegean Arc--comparison with the Andean Cordillera of south Peru-north Bolivia, Phil. Trans. R. Soc. Lond. A, 300, 337-355, 1981.
- Minster, J.B., and T.H. Jordan, Present-day plate motions, J. Geophys. Res., 83, 5331-5354, 1978.
- Minster, J.B., T.H. Jordan, P. Molnar, and E. Haines, Numerical modelling of instantaneous plate tectonics. Geophys. J. R. Astron. Soc., 36, 541-576, 1974.
- Molnar, P., Structure and tectonics of the Himalaya: Constraints and implications of geophysical data, J. Geophys. Res., in press, 1983.

- Molnar, P., and T. Atwater, Interarc spreading and Cordilleran tectonics as alternatives related to the age of subducted oceanic lithosphere, Earth Planet. Sci. Lett., 41, 330-340, 1978.
- Molnar, P., T. Atwater, J. Mammereckx, and S.M. Smith, Magnetic anomalies, bathymetry and the tectonic evolution of the South Pacific since the late Cretaceous, Geophys. J. R. Astron. Soc., 40, 383-420, 1975.
- Molnar, P., and W.P. Chen, Seismicity and mountain building, in Mountain Building Processes, edited by K.J. Hsu, pp. 41-57, Academic Press, New York, 1982.
- Molnar, P., W.P. Chen, T.J. Fitch, P. Tapponier, W.E.K. Warsi, and F.T. Wu, Structure and tectonics of the Himalayas: A brief summary of relevant geophysical observations, Colloques Internationaux du CNRS, Himalaya: Sciences de la Terre, Editions du Centre National de la Recherche Scientifique, Paris, 269-294, 1977.
- Molnar, P., T.J. Fitch, and F.T. Wu, Fault plane solutions of shallow earthquakes and contemporary tectonics in Asia, Earth and Planet. Sci. Lett., 19, 101-112, 1973.
- Moore, J.C., Selective subduction, Geology, 3, 530-532, 1975.
- Moore, J.C., The inadvertant packer experiment, Initial Rept. Deep Sea Drill. Proj., Leg 78A, in press 1983.
- Moore, J.C., and R. von Heune, Abnormal pore pressure and hole instability in forearc regions: A preliminary report, unpublished report for Ocean Margin Drilling Project, 29 pp., 1980.
- Moore, J.C., and J. S. Watkins, Summary of accretionary processes, Deep Sea Drilling Project Leg 66: Offscraping, underplating, and deformation of the slope apron, Initial Rept. Deep Sea Drill. Proj., Leg 66, 825-836, 1982.
- Moore, J.C., J.S. Watkins, T.H. Shipley, K.J. McMillen, S.B. Bachman, and N. Lundberg, Geology and tectonic evolution of a juvenile accretionary terrane along a truncated convergent margin: Synthesis of results from Leg 66 of the Deep Sea Drilling Project, southern Mexico, Geol. Soc. Am. Bull., 93, 847-861, 1982.
- Morgan, W.J., Rises, trenches, great faults, and crustal blocks, J. Geophys. Res., 73, 1959-1982, 1968.
- Morgan, W.J., Convection plumes in the lower mantle, Nature, 230, 42-43, 1971.

- Morgan, W.J., Deep mantle convection plumes and plate motions, Am. Assoc. Petrol. Geol. Bull., 56, 203-213, 1972.
- Morgan, W.J., Hotspot tracks and the opening of the Atlantic and Indian oceans, in The Sea, 7, edited by C. Emiliani, pp. 443-487, John Wiley and Sons, New York, 1981.
- Müller, W.H., and K.J. Hsü, Stress distribution in overthrusting slabs and mechanics of Jura deformation, Rock Mechanics Suppl., 9, 219-232, 1980.
- Nakamura, K., and S. Uyeda, Stress gradients in arc-back arc regions and plate subduction, J. Geophys. Res., 83, 6414-6428, 1980.
- Namson, J.S., Studies of the structure, stratigraphic record of plate interaction and role of pore-fluid pressure in the active fold and thrust belt of Taiwan and a study of manganese deposits from northern California, 302 pp., Ph.D. Thesis, Princeton Univ., Princeton, N.J. 1982.
- Nasu, N., Y. Tomoda, K. Kobayashi, H. Kagami, S. Uyeda, S. Nagumo, I. Kushiro, M. Ozima, K. Nakazawa, Y. Takayanagi, H. Okada, S. Murauchi, Y. Ishiwada, and Y. Ishii, Multi-channel seismic reflection data across the Japan Trench, IPOD-Japan Basic Data Series, No. 3, Ocean Research Institute, Univ. Tokyo, 22 pp., 1979.
- Nishenko, S., and W. McCann, Large thrust earthquakes and tsunamis: Implications for the development of fore arc basins, J. Geophys. Res., 84, 573-584, 1979.
- Norton, I.O., and J.G. Sclater, A model for the evolution of the Indian Ocean and the breakup of Gondwanaland, J. Geophys. Res., 84, 6803-6830, 1979.
- Ohta, Y., and C. Akiba, eds., Geology of the Nepal Himalayas, 286pp., Himalayan Committee of Hokkaido University, Sapporo, Japan, 1973.
- Oliver, J.E., M. Dobrin, S. Kaufman, R. Meyer, and R. Phinney, Continuous seismic reflection profiling of the deep basement, Hardeman County, Texas, Bull. Geol. Soc. Am., 78, 1537-1546, 1976.
- Parsons, B., Causes and consequences of the relation between area and age of the ocean floor J. Geophys. Res., 87, 289-302, 1982.

- Parsons, B., and P. Molnar, The origin of outer topographic rises associated with trenches, Geophys. J.R. Astron. Soc., 45, 707-712, 1976.
- Parsons, B., and J.G. Sclater, An analysis of the variation of ocean floor bathymetry and heat flow with age, J. Geophys. Res., 82, 803-827, 1977.
- Paterson, M.S., Experimental Rock Deformation: The Brittle Field, pp. 16-50, Springer-Verlag, New York, 1978.
- Pfiffner, O.A., and J.G. Ramsay, Constraints on geological strain rates: Arguments from finite strain states of naturally deformed rocks, J. Geophys. Res., 87, 311-321, 1982.
- Pierce, J.W., The northward motion of India since the late Cretaceous, Geophys. J. R. Astron. Soc., 52, 277-311, 1978.
- Pilger, R.H. Jr., A method for finite plate reconstructions, with applications to Pacific-Nazca plate evolution, Geophys. Res. Lett., 5, 469-472, 1978.
- Pitman, W.C. III, Relationship between eustacy and stratigraphic sequences of passive margins, Geol. Soc. Am. Bull., 89, 1389-1403, 1978.
- Pitman, W.C. III, The effect of eustatic sea level changes stratigraphic sequences at Atlantic margins, in Geological and Geophysical Investigations of Continental Margins, Mem. 29, edited by J.S. Watkins, L. Montadert, and P. Dickerson, pp. 453-460, American Association of Petroleum Geology, Tulsa, Oklahoma, 1979.
- Pitman, W.C. III, and M. Talwani, Sea-floor spreading in the North Atlantic, Geol. Soc. Am. Bull., 83, 619-646, 1972.
- Price, R.A., Large-scale gravitational flow of supracrustal rocks, southern Canadian Rockies, in Gravity and Tectonics, edited by K.A. Dejong and R. Scholten, pp. 491-502, John Wiley and Sons, New York, 1973.
- Price, R.A., The Cordilleran foreland thrust and fold belts in the southern Canadian Rocky Mountains, in Thrust and Nappe Tectonics, edited by K.R. McClay and N.J. Price, pp. 427-448, Blackwell Scientific Publications, Boston, 1981.
- Raleigh, B., and J. Evernden, Case for low deviatoric stress in the lithosphere, in Mechanical Behavior of Crustal Rocks, The Handin Volume, edited by N.L. Carter, M. Friedman, J.M. Logan, and D.W. Steanye, pp. 173-186, AGU, Washington, D.C., 1981.

- Ramberg, H., Model studies of gravity-controlled tectonics by the centrifuge technique, in Gravity and Tectonics, edited by K.A. DeJong and R. Scholten, pp. 49-66, John Wiley and Sons, New York, 1973.
- Ramberg, H., The role of gravity in orogenic belts, in Thrust and Nappe Tectonics, edited by K.R. McClay and N.J. Price, pp. 125-140, Blackwell Scientific Publications, Boston, 1981.
- Rich, J.L., Mechanics of low-angle overthrust faulting as illustrated by Cumberland thrust block, Virginia, Kentucky and Tennessee, Am. Assoc. Petrol. Geol. Bull., 18, 1584-1596, 1934.
- Richardson, R.M., Intraplate stress and the driving mechanism for plate tectonics, Ph.D. thesis, Mass. Inst. of Technol., Cambridge, MA, 371 pp., 1978.
- Richardson, R.M., and S.C. Solomon, Apparent stress and stress drop for intraplate earthquakes and tectonic stress in the plates, Pure Appl. Geophys., 115, 317-331, 1977.
- Rodgers, J., Mechanics of Appalachian folding as illustrated by Sequatchie Anticline, Tenn. and Ala., Am. Assoc. Petrol. Geol. Bull., 34, 672-681, 1950.
- Rodgers, J., Evolution of thought on structure of middle and southern Appalachians, second paper, in Appalachian Structures, Origin, Evolution, and Possible Potential for New Exploration, Frontiers, edited by W.H. Kanes, pp. 1-15, West Virginia Geological and Economic Survey, Charleston, 1972.
- Roeder, D., O.E. Gilbert, Jr., and W. D. Witherspoon, Evolution and macroscopic structure of Valley and Ridge thrust belt, Tennessee and Virginia, Dept. Geol. Sci., Univ. Tenn., Studies in Geology 2, 25 pp., 1978.
- Royse, F.J., M.A. Warner, and D.C. Reese, Thrust-belt structural geometry and related stratigraphic problems, Wyoming-Idaho-Northern Utah, Symposium on Deep Drilling Frontiers in the Central Rocky Mountains, p. 41-54, Rocky Mtn. Assoc. Geol., 1975.
- Ryan, W.B.F., K.A. Kastens, and M.B. Cita, Geological evidence concerning compressional tectonics in the eastern Mediterranean, Tectonophysics, 86, 213-242, 1982.
- Scholten R., Gravitational mechanisms in the northern Rocky Mountains of the United States, in Gravity and Tectonics, edited by K.A. DeJong and R. Scholten, pp. 473-490, John Wiley and Sons, New York, 1973.

- Scholz, C.H., J. Beavan, and T.C. Hanks, Frictional metamorphism, argon depletion, and tectonic stresses on the Alpine Fault, New Zealand, J. Geophys. Res., 84, 6770-6782, 1979.
- Scholz, C.H., Shear heating and the state of stress on faults, J. Geophys. Res., 85, 6174-6184, 1980.
- Schubert, G., D.A. Yuen, and D.L. Turcotte, Role of phase transitions in a dynamic mantle, Geophys. J. R. Astr. Soc., 42, 705-735, 1975.
- Schult, F.R., and R.G. Gordon, Velocities of the continents with respect to the hotspots since the early Jurassic: Implications for the driving forces of plate tectonics J. Geophys. Res., in press, 1983.
- Schweller, W.J., L.D. Kulm, and R.A. Prince, Tectonics, structure, and sedimentary framework of the Peru-Chile trench, in Nazca Plate: Crustal Formation and Andean Convergence, edited by L.D. Kulm, J. Dymond, E.J. Dasch, and D.M. Hussong, pp 323-349, Geological Society of America Mem. 154, 1981.
- Scientific Staff, Geochemical Measurements during DSDP Leg 78A, Initial Rept. Deep Sea Drill. Proj., Leg 78A, in press, 1983.
- Sclater, J.G., R.N. Anderson, and M.L. Bell, Elevation of ridges and evolution of the central eastern Pacific, J. Geophys. Res., 76, 7888-7915, 1971.
- Sclater, J.G., Hellinger, S. and Tapscott, C., The paleobathymetry of the Atlantic Ocean from the Jurassic to the present, J. Geol., 85, 509-542, 1977.
- Sclater, J.G., B. Parsons, and C. Jaupart, Oceans and continents: Similarities and differences in the mechanisms of heat loss, J. Geophys. Res., 86, 11535-11552, 1981.
- Seeber, L., and J. Armbruster, Seismicity of the Hazara arc in northern Pakistan: Decollement vs. basement faulting, in Geodynamics of Pakistan, edited by A. Farah and K. DeJong, Geological Survey of Pakistan, Quetta, p. 131-142, 1979.
- Seeber, L., J.G. Armbruster, and R.C. Quittmeyer, Seismicity and continental subduction in the Himalayan arc, in Zagros-Hindu Kush-Himalaya Geodynamic Evolution, edited by H.K. Gupta, and F.M. Delany, pp. 215-242, Amer. Geophys. Union and Geol. Soc. America Geodynamics Series, Vol. 3, 1981.

- Seely, D.R., P.R. Vail, and G.G. Walton, Trench slope model, in The Geology of Continental Margins, edited by C.A. Burk and C.L. Drake, pp. 249-260, Springer-Verlag, New York, 1974.
- Seno, T., The instantaneous rotation vector of the Philippine Sea plate relative to the Eurasian plate, Tectonophysics, 42, 209-226, 1977.
- Shiki, T., and Y. Misawa, Forearc geological structure of the Japanese Islands, in Trench-Forearc Geology: Sedimentation and Tectonics on Modern and Ancient Active Plate Margins, edited by J.K. Leggett, pp. 63-76, Blackwell Scientific Publications, Boston, 1982.
- Shipley, T.H., K.J. McMillen, J.S. Watkins, J.C. Moore, J.H. Sandoval-Ochoa, and J.L. Worzel, Continental margin and lower slope structures of the Middle America Trench near Acapulco (Mexico), Mar. Geol., 35, 65-82, 1980.
- Shipley, T.H., G.F. Moore, and A.M. Volpe, Sediment off-scraping along the Middle America Trench (abstract), EOS Trans. AGU, 63, 1112, 1982.
- Shipley, T.H., and L.E. Shephard, Temperature data from the Mexico drilling area: Report on logging and inhole temperature experiments. in Initial Rept. Deep Sea Drill. Proj. Legs 66-67, pt.1, pp.771-774, 1982.
- Shulman, M. and W. Skala, Reconstruction of stress fields for the Aegean by a finite element method, Rock Mechanics, Suppl. 9, 245-255, 1980.
- Simpson, D.W., and S.K. Negmatullaev, Induced seismicity at Nurek Reservoir, Tadjikistan, USSR, Bull. Seism. Soc. Am., 71, 1561-1586, 1981.
- Sleep, N.H., Sensitivity of heat flow and gravity to the mechanism of sea-floor spreading, J. Geophys. Res., 74, 542-549, 1969.
- Sleep, N.H., and M.N. Toksoz, Evolution of marginal basins, Nature, 33, 548-550, 1971.
- Smithson, G.B., J.A. Brewer, S. Kaufman, J.E. Oliver, and C.A. Hurich, Structure of the Laramide Wind River Uplift, Wyoming, from COCORP deep reflection data and from gravity data, J. Geophys. Res., 84, 5955-5972, 1979.
- Smoluchowski, M.S., Some remarks on the mechanics of overthrusts, Geol. Mag., New ser., V, 6, 204-205, 1909.

- Snavely, P.D., Jr., H.C. Wagner, and D.L. Lander, Geologic cross section of the central Oregon continental margin, Geol. Soc. Am. Map and Chart Ser. MC-28J, 1980.
- Solomon, S.C., and K.-T. Paw U, Elevation of the olivine-spinel transition in subducted lithosphere: Seismic evidence, Phys. Earth Planet. Interiors, 11, 97-108, 1975.
- Solomon, S.C., and N.H. Sleep, Some simple physical models for absolute plate motions, J. Geophys. Res., 79, 2557-2567, 1974.
- Solomon, S.C., N.H. Sleep, and R.M. Richardson, On the forces driving plate tectonics: Inferences from absolute plate velocities and intraplate stress. Geophys. J. R. Astron. Soc., 42, 789-802, 1975.
- Solomon, S.C., N.H. Sleep, and D.M. Jurdy, Mechanical models for absolute plate motions in the early Tertiary, J. Geophys. Res., 82, 203-212, 1977a.
- Solomon, S.C., N.H. Sleep and R.M. Richardson, Implications of absolute plate motions and intraplate stress for mantle rheology, Tectonophysics, 37, 219-231, 1977b.
- Speed, R.C. and D.K. Larue, Barbados: Architecture and implications for accretion, J. Geophys. Res., 87, 3633-3643, 1982.
- Sprague, P., and H.N. Pollack, Heat flow in the Mesozoic and Cenozoic, Nature, 285, 393-395, 1980.
- Stanley, R.S., L.B. Hill, H.C. Chang, and H.N. Hu, A transect through metamorphic core of the Central Mountains, southern Taiwan, Geol. Soc. China Mem. 4, 443-473, 1981.
- Stetsky, R.M., Rock friction-effect of confining pressure, temperature, and pore pressure, Pure Appl. Geophys., 116, 690-704, 1978.
- Stocklin, J., Structural history and tectonics of Iran: A review, Am. Assoc. Pet. Geol. Bull., 52, 1229-1258, 1968.
- Stockmal, G.S, Modeling of large-scale accretionary wedge deformation, J. Geophys. Res., in press, 1983.
- Stockmal, G.S., and W.M. Chapple, Modelling accretionary wedge deformation using a rigid-perfectly plastic rheology (abstract), EOS Trans. AGU, 62, 397-398, 1981.

- Suárez, G., Seismicity, tectonics, and surface wave propagation in the central Andes, Ph.D. thesis, 260pp., Mass. Inst. Technol., Cambridge, MA. 1982.
- Suárez, G., and P. Molnar, Paleomagnetic data and pelagic sediment facies and the motion of the Pacific plate relative to the spin axis since the late Cretaceous, J. Geophys. Res., 85, 5257-5280, 1980.
- Suppe, J., Décollement folding in southwestern Taiwan, Pet. Geol. Taiwan, 13, 25-35, 1976.
- Suppe, J., Fault-bend folding (abstract), Geol. Soc. Amer. Abstr. Programs, 11, 525, 1979.
- Suppe, J., A retrodeformable cross section of northern Taiwan, Geol. Soc. China Proc., 23, 46-55, 1980a.
- Suppe, J., Imbricated structure of western foothills belt, south-central Taiwan, Petroleum Geology of Taiwan, 17, 1-16, 1980b.
- Suppe, J., Mechanics of mountain building and metamorphism in Taiwan, Geol. Soc. China Mem. 4, 67-89, 1981.
- Suppe, J., and J. Namson, Fault-bend origin of frontal folds of the western Taiwan fold-and-thrust belt, Petrol. Geol. Taiwan, 16, 1-18, 1979.
- Suppe, J., J. Namson, and A.M. Pytte, Role of fluid pressure in an active overthrust belt: Taiwan, Geol. Soc. Am. Abstr. Programs, 13, 562, 1981.
- Suppe, J., and J.H. Wittke, Abnormal pore-fluid pressures in relation to stratigraphy and structure in the active fold-and-thrust belt of northwestern Taiwan, Pet. Geol. of Taiwan, 14, 11-24, 1977.
- Tegland, E.R., Seismic investigation of eastern Tennessee, Tenn. Div. Geol. Bull., 78, 68 pp, 1978.
- Tharp, T.M., Material models applied to Pacific trench flexure, Tectonophysics, 69, 123-145, 1980.
- Timoshenko, S., J.N. Goodier, Theory of Elasticity 2nd ed. McGraw-Hill, New York, 506 pp., 1951.
- Toksöz, M.N., and A.T. Hsui, Numerical studies of back-arc convection and the formation of marginal basins, Tectonophysics, 50, 177-196, 1978.

- Toksöz, M.N., J.W. Minear, and B.R. Julian, Temperature field and geophysical effects of a downgoing slab, J. Geophys. Res., 76, 1113-1138, 1971.
- Turcotte, D.L., Driving mechanisms of mountain building, in Mountain Building Processes, edited by K.J. Hsu, pp. 141-146, Academic Press, New York, 1982.
- Turcotte, D.L., and K. Burke, Global sea-level changes and the thermal structure of the earth. Earth Planet. Sci. Lett., 41, 341-346, 1978.
- Turcotte, D.L., D.C. McAdoo, and J.G. Caldwell, An elastic perfectly plastic analysis of the bending lithosphere at a trench, Tectonophysics, 47, 193-205, 1978.
- Turcotte, D.L., and G.C. Schubert, Structure of the olivine-spinel phase boundary in the descending lithosphere, J. Geophys. Res., 76, 7980-7987, 1971.
- Utsu, T., Spatial and temporal distribution of low frequency earthquakes in Japan, J. Phys. Earth, 28, 361-384, 1980.
- Uyeda, S., and K. Horai, Heat flow measurements on Deep Sea Drilling Project Leg 60, Initial Rept. Deep Sea Drill. Proj., Leg 66, 789-800, 1982.
- Uyeda, S., and H. Kanamori, Back-arc opening and the mode of subduction, J. Geophys. Res., 84, 1049-1061, 1979.
- Vail, P.R., and R.M. Mitchum, Jr., Global cycles of relative changes of sea level from seismic stratigraphy, in Geological and Geophysical Investigations of Continental Margins, Mem. 29, edited by J.S. Watkins, L. Montadert and P. Dickerson, pp. 469-472, American Association of Petroleum Geology, Tulsa, Oklahoma, 1979.
- Vail, P.R., R.M. Mitchum, Jr., and S. Thompson, III, Seismic stratigraphy and global changes of sea level, 4, Global cycles of relative changes of sea level, in Seismic Stratigraphy--Application to Hydrocarbon Exploration, Mem. Am. Assoc. Pet. Geol., 26, 83-97, 1977.
- Viele, G.W., Geologic map and cross section, eastern Ouachita Mountains, Arkansas, Geol. Soc. Am. Map Chart Ser. MC-28F, 1979.
- Voight, B., ed., Mechanics of Thrust Faults and Decollement, 471 pp., Dowden, Hutchinson, and Ross, Stroudsburg, PA, 1976.

- von Heune, R., Structure of the outer convergent margin off Kodiak Island, Alaska, from multichannel seismic records, in Geological and Geophysical Investigations of Continental Margins, Mem. 29, edited by J.S. Watkins, L. Montadert, and P. Dickerson, pp. 261-272, American Association of Petroleum Geology, Tulsa, Oklahoma, 1979.
- von Heune, R., and M.A. Arthur, Sedimentation across the Japan Trench off northern Honshu Island, in Trench-Forearc Geology: Sedimentation and Tectonics on Modern and Ancient Active Plate Margins, edited by J.K. Leggett, pp. 27-48, Blackwell Scientific Publications, Boston, 1982.
- von Heune, R., M. Arthur, and B. Carson, Ambiguity in interpretation of seismic data from modern convergent margins: An example from the IPOD Japan Trench transect, in Thrust and Nappe Tectonics, edited by K.R. McClay and N.J. Price, pp. 393-407, Blackwell Scientific Publications, Boston, 1981.
- von Heune, R., J. Aubouin, J. Azema, G. Blackinton, J.A. Carter, W.T. Coulbourn, D.S. Cowan, J.A. Curiale, C.A. Dengo, R.W. Faas, W. Harrison, R. Hesse, D.M. Hussong, J.W. Laad, N. Muzylov, T. Shiki, P.R. Thompson, and J. Westberg, Leg 67: The Deep Sea Drilling Project Mid-America Trench transect of Guatemala, Geol. Soc. Am. Bull., 91, 421-432, 1980a.
- von Huene, R., G.W. Moore, and J.C. Moore, Cross section of Alaska Peninsula-Kodiak Island-Aleutian Trench, Geol. Soc. Am. Map Chart Ser. MC-28A, 1979b.
- von Heune, R., G.G. Shor Jr., and J. Wageman, Continental margins of the eastern Gulf of Alaska, and boundaries of tectonic plates, in Geological and Geophysical Investigations of Continental Margins, Mem. 29, edited by J.S. Watkins, L. Montadert, and P. Dickerson, pp. 273-290, American Association of Petroleum Geology, Tulsa, Oklahoma, 1979a.
- Wang, C.-Y., Sediment subduction and frictional sliding in a subduction zone, Geology, 8, 530-533, 1981.
- Watkins, J.S., K.J. McMillen, S.B. Bachman, T.H. Shipley, J.C. Moore, and C. Angevine, Tectonic synthesis, leg 66: Transect and vicinity, Initial Rept. Deep Sea Drill. Proj., Leg 66, 837-849, 1982.
- Watts, A.B., and M.S. Steckler, Subsidence and eustasy at the continental margin of eastern North America, in Deep Drilling Results in the Atlantic Ocean: Continental Margins and Paleoenvironment, Maurice Ewing Ser., vol. 3, edited by M. Talwani, W. Hay and W.B.F. Ryan, pp. 235-248, AGU, Washington D.C., 1979.

- Watts, A.B., and M. Talwani, Gravity anomalies seaward of deep sea trenches and their tectonic implications, Geophys. J. R. Astron. Soc., 36, 57-90, 1974.
- Weertman, J., The creep strength of the earth's mantle, Rev. Geophys. Space Phys., 8, 145-168, 1970.
- Weissel, J.K., D.E. Hayes, and E.M. Herron, Plate tectonics synthesis: The displacements between Australia, New Zealand and Antarctica since the late Cretaceous, Mar. Geol., 25, 231-277, 1977.
- Wernicke, B., Low-angle normal faults in the Basin and Range province: Nappe tectonics in an extending orogen, Nature, 291, 645-648, 1981.
- Wernicke, B.P., Processes of extensional tectonics, Ph.D. thesis, 169 pp., Mass. Inst. of Technol., Cambridge, MA, 1982.
- Wernicke, B., and B.C. Burchfiel, Modes of extensional tectonics, J. Structural Geol., 4, 105-115, 1982.
- Westbrook, G.K., The structure of the crust and upper mantle in the region of Barbados and the lesser Antilles, Geophys. J. R. Astron. Soc., 48, 201-242, 1975.
- Westbrook, G.K., The Barbados Ridge complex: Tectonics of a mature forearc system, in Trench-forearc Geology: Sedimentation and Tectonics on Modern and Ancient Active Plate Margins, edited by J.K. Leggett, pp. 275-290, Blackwell Scientific Publications, Boston, 1982.
- Westbrook, G.K., and M.J. Smith, Long decollements and mud volcanoes: Evidence from the Barbados Ridge Complex for the role of high pore-fluid pressure in the development of an accretionary complex, Geology, 11, 279-283, 1983.
- White, R.S., Recent fold development in the Gulf of Oman, Earth Planet. Sci. Lett., 36, 85-91, 1977.
- White, R.S., Deformation of the Makran continental margins, in Geodynamics of Pakistan, edited by A. Farah and K. A. DeJong, pp. 295-304, Geological Survey of Pakistan, Quetta, 1979.
- White, R.S., Deformation of the Makran accretionary sediment prism in the Gulf of Oman (north-west Indian Ocean), in Trench-forearc Geology: Sedimentation and Tectonics on Modern and Ancient Active Plate Margins, edited by J.K. Leggett, pp. 357-372, Blackwell Scientific Publications, Boston, 1982.

- White, R.S., and K. Klitgord, Sediment deformation and plate tectonics in the Gulf of Oman, Earth Planet. Sci. Lett., 32, 199-209, 1976.
- White, R.S., and D.A. Ross, Tectonics of the western Gulf of Oman, J. Geophys. Res., 84, 3479-3489, 1979.
- Wiltschko, D.V., Partitioning of energy in a thrust sheet and implications concerning driving forces, J. Geophys. Res., 84, 6050-6058, 1979.
- Wilson, J.T., A new class of faults and their bearing on continental drift, Nature, 207, 343-347, 1965.
- Wu, F.T., Y.H. Yeh, and Y.B. Tsai, Seismicity in the Tsengwen reservoir area, Taiwan, Bull. Seis. Soc. Am., 69, 1783-1796, 1979.
- Yamashina, K., K. Shimazaki, and T. Kato, Aseismic belt along the frontal arc and plate subduction in Japan, J. Phys. Earth, 26, suppl., 447-458, 1978.
- Yoshii, T., A detailed cross-section of the deep seismic zone beneath northeastern Honshu, Japan, Tectonophysics, 55, 349-360, 1979.
- Ziegler, A.M., S.F. Barrett, and C.R. Scotese, Palaeoclimate, sedimentation, and continental accretion, Phil. Trans. Roy. Soc. Lond. A, 301, 253-264, 1981.
- Zoback, M.L., and M.D. Zoback, Faulting patterns in North-Central Nevada and strength of the crust, J. Geophys. Res., 85, 275-284, 1980.

BIOGRAPHICAL NOTE

The author was born in 'The city of gracious living', Yonkers, New York on June 21, 1956. Lacking a telescope, surrounded by city lights, and having uncorrectable double vision, he naturally gravitated toward astronomy. Gratefully rescued from the Yonkers public schools, he attended the Riverdale Country School in the relatively pastoral northern Bronx. At Riverdale, he contracted a particularly severe case of anglophilia. The condition is chronic, and has recently led to an anxiously awaited 3.25 kg complication.

The author spent four intellectually exciting years at Princeton University, known to her sons and daughters as the alma mater of God, class of $-4.6 \cdot 10^9$. Having been told that "Oh, there are jobs in astronomy; after all, people do die", the author came down to earth and switched to geophysics. He found the study of the earth to be so enticing that he elected to spend the next 5 years as a tech tool. Among the diversions which have occupied him during his tenure at the 'tute are the following:

Davis, D.M., and S.C. Solomon, 1981; Variations in the velocities of the major plates since the Late Cretaceous. Tectonophysics, 74, 189-208

Davis, D.M., J. Suppe, and F.A. Dahlen, 1983; Mechanics of Fold-and-Thrust Belts and Accretionary Wedges. J. Geophys. Res., 88, 1153-1172

Davis, D.M., and D.M. Hussong, 1983; Geothermal Observations during DSDP Leg 78A. Init. Repts. DSDP, 78 (in press)

Davis, D.M., 1983; The compressive mechanics of accretionary wedges applied to the Leg 78A study area near Barbados. Init. Repts. DSDP, 78 (in press)